Team 16 Technical Report for the 2025 EuRoC

HyPower Bristol, BristolSEDS of University of Bristol
Queens Building, University Walk, Bristol, United Kingdom

Table of Contents

Do not go gentle into that good night,

Old age should burn and rave at close of day;

Rage, rage against the dying of the light.

Dylan Thomas

Abstract

Project Waxwing is HyPower Bristol's entry into the 3km Liquid category at the European Rocketry Challenge, representing the University of Bristol and BristolSEDS. Waxwing's objective is to serve as a testbed for a fully SRAD liquid bi-propellant launch vehicle, from the propulsion system to aerostructure, avionics, control system, recovery and payload. Waxwing builds on HyPower Bristol's previous entry to EuRoC – Project Feynman, keeping the core design and mission the same while improving on all aspects of design.

The 76.5kg, four-metre-tall rocket uses a regeneratively cooled flight engine, with a novel reinforced coaxial tank design, to propel the launch vehicle. A three-petal airbrake system using a bang-bang controller slows the rocket down accurately to hit a target altitude of 3000m, supported by optimised composite and isotropic structures. SRAD flight avionics control the launch vehicle, from feed system and engine monitoring and control, to hosting controllers to actuate airbrakes. Telemetry is transmitted through a conformal self-developed Blade-IFA structure. A self-developed tender descender system controls a single-separation, dual-deploy recovery system, with a commercial drogue and SRAD main. Waxwing will carry and deploy a quadcopter UAV, which will fly through the rocket plume and measure chemical composition in the atmosphere to monitor rocket emissions.

Acknowledgements

Thank you to the University of Bristol, for providing us support with the faculty, machine shop, technical staff and so many more, to Roxel UK for the incredible support they have provided over the last two years of our development. Thank you to the Manufacturing Technologies Centre for providing us with our three additively manufactured combustion chambers. Thank you to Astron for hosting us at their test site and for the indispensable advice, and to Boeing for contributing to the development and progression of the team. The Range Safety Officers of the United Kingdom Rocketry Association, for the help with our subscale launches. Thank you to Shropshire Stainless & Aluminium for realising our structures into reality, to the Bristol Composites Institute for the time in the lab, technical guidance, and the extra resin when we were in a pinch! Thank you to Texas Instruments for providing us the capability to have a robust avionics system, and for the progression of our team's development. StageGear for giving us all the igniters to get us off the ground, Chell Instruments Limited for providing us with pressure scanners and datalogging software used in our wind tunnel campaign. AMS Composites for providing the COTS pressure vessel for our system. Cameron Ballons for providing the material to produce our main parachute. Ross Handling for donating a set of pneumatic castor wheels for our ground station.

From everyone who has helped us, there are a few individuals that we would like to thank by name. Thank you to Steve Bullock, our faculty advisor, for believing and supporting us every step of the way. Thank you to Natalie Wiggins, who keeps finding ways to let us constantly move forward. Thank you to the University's technical and workshop team, including Jack (Jack) Marsh, Terry Godsmark, Ian Chorley, Matt Richardson, Rob Beazer, Greg Richards and Dominic Hardman. Thank you to Dan Turner and Stuart Wilson at Roxel. And thank you to everyone's who has stopped by the lab, asked questions, and tolerated the multiple-hour lectures from the team about rockets!

1. Introduction

1.1 Project Objectives

I. Following the previous developments of HyPower Bristol, the current design cycle will optimise and develop our systems with a *Test to Inform* objective.

II. To demonstrate a successful launch of a liquid bi-propellant rocket, with coherence between structural, propulsion, avionics and ground system elements.

III. To use a forward integration control system and air brakes to secure accuracy on an apogee of 3000m

IV. To sample atmospheric data in the plume of the launch vehicle with a deployable payload.

V. To successfully recover the vehicle in a re-flyable state using a single separation, dual deployment method.

1.2 Project Organisation

HyPower Bristol, from the University of Bristol, consists of over 60 multidisciplinary students. Founded in 2023, the goal of HyPower Bristol is to educate and teach students beyond standard course structure, on how to think and become better engineers.

HyPower is split into four sub-teams, Propulsion, Launch Vehicle, Electronics and Ground Station. Each sub-team has a team lead, that ensure technical goals are met. Sub-teams are further split up, covering the whole range of operational tasks that are required to design & manufacture a 76.5kg, 4-metre-tall liquid bi-propellant rocket.

1.3 Mission Concept of Operations

The operations are planned as follows; First, secure the rocket onto the launch rail, ensuring it is properly aligned and stable. The ethanol tank is then manually fuelled. The propellant lines are connected, pyrotechnics are armed, and all personnel will move away from the vehicle. Remote fuelling operations will then occur. The nitrogen and then the nitrous oxide tank will be fuelled. The quick disconnects will be released and all systems will be checked for launch. The ignition sequence will then commence, and launch will occur. During the thrust phase, instrumentation will monitor the operating chamber pressure and temperature of the engine. Venting will occur after the burn phase has finished. The coast phase will use the airbrake solver to predict the apogee, and the airbrakes will be actuated to hit a 3000m apogee. At apogee the recovery pyrotechnic charges will fire, and separation will occur to release the drogue parachute, along with the bagged main. At 300m, the tender descender will fire, releasing the main parachute to ensure a safe landing at 7m/s. Upon detecting landing, the system will be recovered.

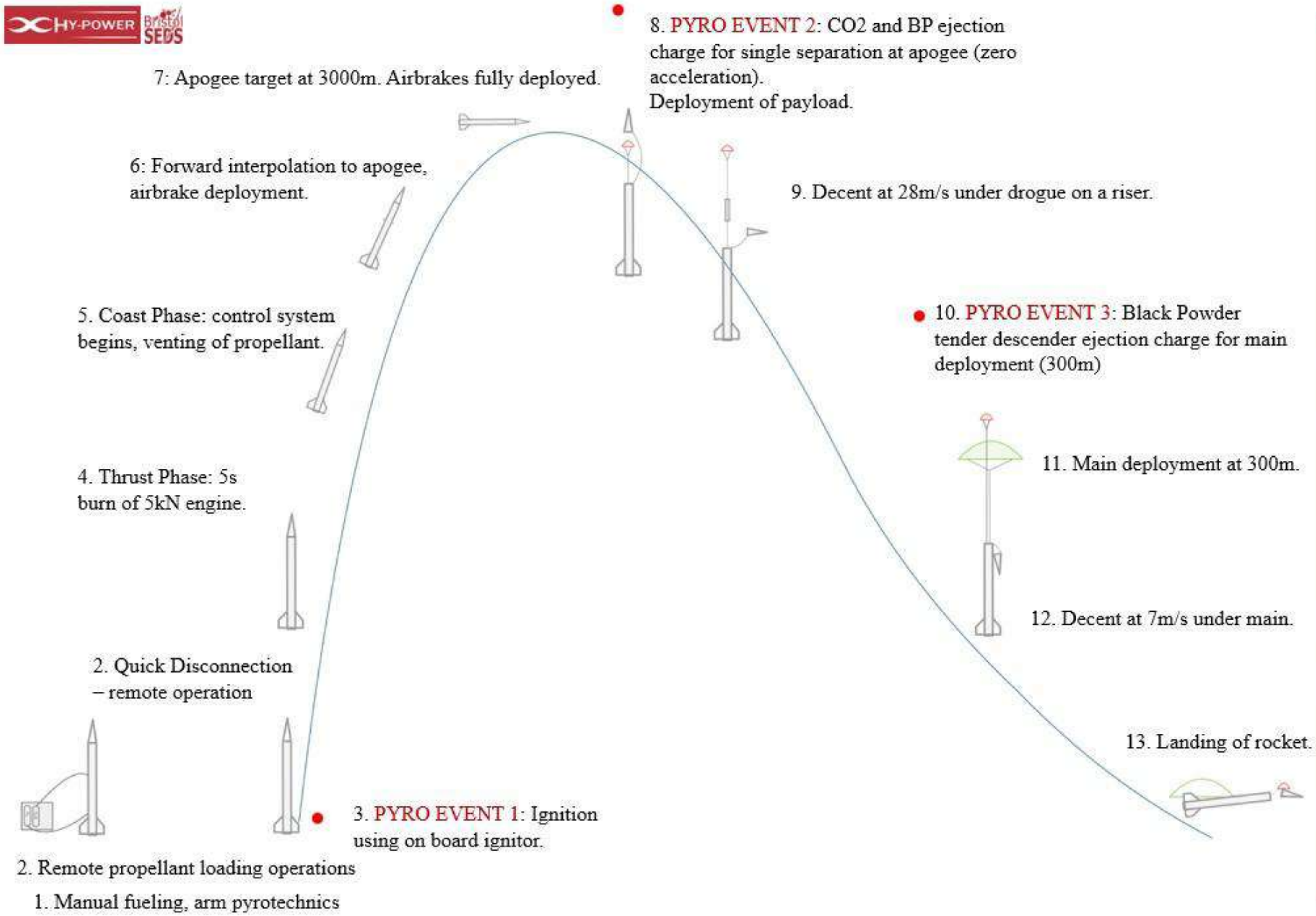

HyPower Bristol ConOps EuRoC'25 L3

Hold Points:

i. Pressures, and fueling duration to be nominal.
ii. Visual verification of Quick Disconnection
iii. Apogee to always be interpolated with intention of 3000m
iv. Ejection charge for drogue must happen at apogee
v. Tender descender to release main.
vi. Confirmation on vent before personnel approach landed rocket.
vii. Rocket to be inspected and decommissioned.

2. System Architecture Overview

Aspect	Value	Unit
Length	3972	mm
External diameter	200	mm
Apogee	3000	m
Maximum velocity	239	m/s
Maximum acceleration	63.2	m/s^2
Velocity off the rail	35.9	m/s
Nominal Thrust	5000	N
Burn duration	5	s
Impulse	25000	Ns
Dry Mass	63.6	kg
Wet Mass	76.5	Kg
Propellants	IPA, Nitrous Oxide C2H5OH, N2O	N/A
Pressurant	Nitrogen	N/A

Nosecone & Recovery

The nosecone is a wet-layup carbon-fibre composite. It features a machined aluminium tip following a Von Kármán profile. The nosecone houses the recovery equipment; a drogue parachute that is deployed at apogee, and a main that is deployed at 420 metres above ground level.

Payload

The rocket will carry an 1000g UAV quadcopter payload, conforming to a 3U CubeSat size. The quadcopter will perform a controlled descent autonomously. It will follow waypoints generated from the rocket's flight path to intercept the exhaust plume.

Airbrakes

An autonomous three-petal airbrake module using an apogee predictor fed into an on off controller to accurately hit the target apogee.

Avionics

The avionics stackup allows full control and measurement over the launch vehicle system, transmitting data in flight over a self- developed antenna array structure.

Aerostructure

Optimised composite aeroshells and panels, as well as isotropic internal couplers and stringers allow for a high strength-to-weight ratio.

Coaxial Propellant Tanks

The coaxial propellant tanks maximise the amount of propellant stored in the diameter, optimising for weight saving and launch vehicle length. The tank is designed to handle the launch vehicle's flight loads.

Fin Can

A three-fin swept trapezoidal configuration allows for low drag at the required stabilisation during all stages of flight, ensuring a nominal ascent.

Engine

Bristol SEDS Experimental Propulsion's Inconel 718 regenerative engine provides 5kN of thrust for a 5 second burn duration, propelling the rocket to an altitude of 3000m.

3. Propulsion System

Figure 1 - Project Waxwing Propulsion System

The propulsion system for Project Waxwing is an SRAD bi-propellant pressure- fed rocket engine with regenerative cooling, as seen in Figure 1. The combustion chamber is additively manufactured from Inconel 718, and the like-like impinging injector is machined from stainless steel. A COTS COPV acts as a high-pressure storage vessel holding the pressurant, and an SRAD coaxial structural propellant tank holds propellants for flight. The system utilizes a propellant combination of isopropyl alcohol and a fuel additive as well as nitrous oxide to generate a nominal 5 kN of thrust.

Property	Value	Unit
Thrust	5	kN
Fuel	IPA 99%– 1% PDMS	[---]
Oxidiser	N_2O	[---]
Burn Time	5	s
Total Impulse	25,000	Ns
Chamber pressure	20	bar
Propellant tank pressure	50	bar

Table 1: Propulsion system overview properties

The propulsion system is designed to offer a trade-off between high thrust and low length. The diameter of the system is constrained to below 200mm to reduce the upfront price of the vehicle. This has an impact in the material need to manufacture the SRAD coaxial tank as well as offering a reduction in material to other subsystems. All the fittings in the feed system are COTS to ensure an acceptable level of safety.
A set of unlike quick disconnects at opposite sides of the coaxial tank offer fuelling points for nitrous oxide and nitrogen.

3.1 Combustion Chamber

Figure 2 - ENGINE-1 Left: as printed on build plate Centre: as assembled with stainless steel injector, Right: photo from bench testing the engine producing 5kN thrust for a 3s burn, results detailed in Appendix B9.

The rocket engine is 3D printed out of heat-treated Inconel 718 and is regeneratively cooled by the fuel propellant. The combustion chamber utilises 56 vertical cooling channels adapted to the chamber geometry. The channels' design was informed by analytical thermal hoop stress calculation based on estimated heat transfer from the software Rocket Propulsion Analysis*,* using the Bartz equation. (Ponomarenko, 2012) A 15% film cooling solution further reduces the heat transfer to the combustion chamber wall with a 1% addition of the additive PDMS, a silicone-based fuel additive like TEOS. (Hyde & Okninski, 2016)

The geometrical design of the cooling channels can be seen below in Table 2 and offers significant cooling effects reducing the peak temperatures experienced by the material. The above cooling strategies have been taken to reduce the inner wall temperatures and thus reduce the thermal gradient stress experienced by the combustion chamber which is an artifact of the low thermal conductivity of Inconel 718 as a material. The resulting thermal conditions of the internal chamber wall are shown in Figure 4(B).

Property	Value
Wall Thickness	0.8
Rib Thickness (Chamber – Throat - Manifold)	2.8 - 0.86 - 2
Channel Width (Chamber – Throat - Manifold)	4 - 2 - 3
Channel Height (Chamber – Throat - Manifold)	1.5 - 2 - 1.5

Table 2: Combustion chamber cooling channel geometries.

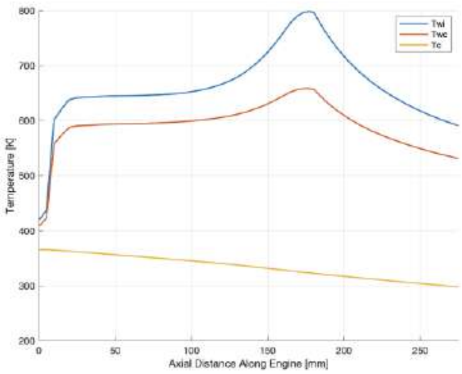

Figure 3, Combustion chamber inner wall (twi), outer wall (twc), and coolant (tc) temperatures relative to position down chamber. These numbers are without factoring in the heat flux reduction of the PDMS

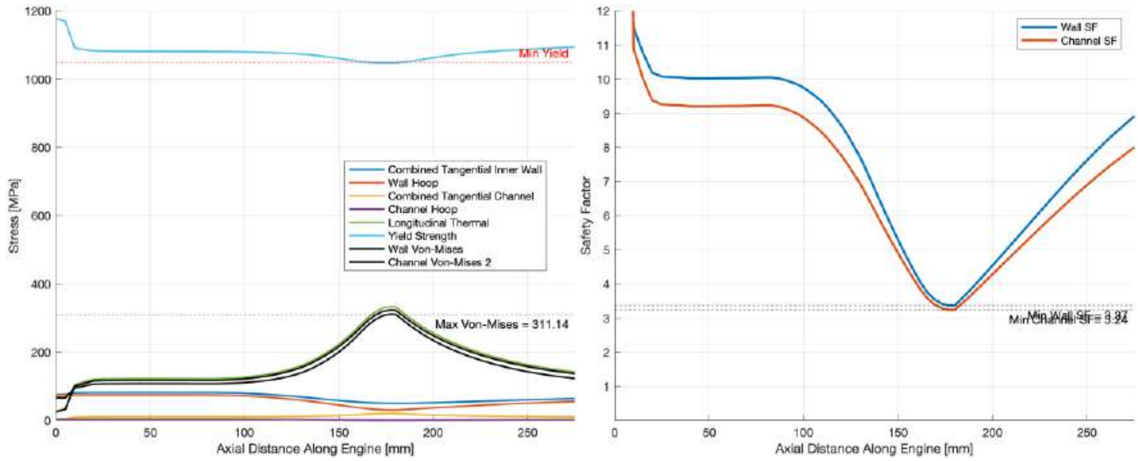

Figure 4 –A graph of pressure and thermal stresses calculated (left) and their associated safety factors (right). Note minimum safety factor of 3.24 for stress at throat compared to the yield stress of Inconel 718 at the temperature of the given point.

A series of analytical calculations were performed to determine the hoop stress under pressure of various key position in the combustion chamber, these were then verified with a simple FEA analysis which produced similar values.

Multiple types of thermal stress equations were then used to estimate the likelihood of potential “doghouse effect,” a phenomenon where the stress experienced by the material between the cooling channels and combustion chamber exceeds the yield strength of the material at which point a breakdown between the coolant and the chamber occurs. (Heister, 2019)

These results were compared to the yield stress of Inconel 718 at the local temperature for every point along the engine. (Saarimäki, 2015) This gave a comfortable safety factor of 3.24 without factoring in the heat-flux reduction of the PDMS.

3.2 Injector Plate

***Authors' Note**: This year the team developed a coaxial swirl injector designed to be machined rather than manufactured using additive methods like many contemporaries and featuring no inter-propellant leak paths. The injector is still in development/testing, with results detailed in H.2 Coaxial Swirl Injector Design*H.2 Coaxial Swirl Injector Design*; as a result, we will be flying the steel injector that we designed last year. The details of this injector are expanded upon below:*

This design impinges streams of fuel and oxidiser with jets of the same type, as depicted below. Upon impingement, the streams disintegrate to form a fan. The primary impingement distance is kept short, at less than 5 x the diameter of the orifice, to avoid streams missing each other – “stream mis-impingement” or stream disintegration which would lead to worse mixing (NASA, 1976). The impinged streams, fuel and oxidiser, are designed to collide on the fans edge and are angled toward each other with a cant angle of 40 degrees to improve mixing (NASA, 1976).

“This is probably the most extensive film cooling (intentional or not) I have ever observed.”

Jacob Sov Larsen (2024)

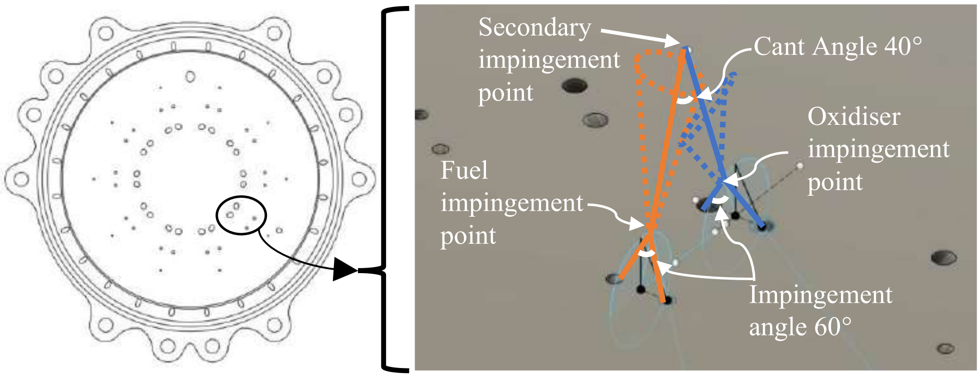

Figure 5 - Operating principle of the like-like impinging doublet

The design features 20 x 2.3mm oxidiser orifices and 20 x 1.1mm fuel orifices with an additional 10 x 0.7mm spray film cooling elements ejecting fuel vertically downward near the combustion chamber lining. The orifices have been sized for a nominal pressure drop of 10 bar across the fuel orifices and 15 bar on the nitrous oxide with a nominal oxidiser flow rate of 1.93 kg/s and 0.64 kg/s fuel resulting in an OF ratio of 3. The discharge coefficients are approximately 0.77 for IPA and 0.51 for N2O, calculated from hot-fire data on a bench test detailed in January hot fire appendix.

Nitrous oxide behaves as a two-phase liquid at room temperature and feed pressures (ESDU, 1991); this behaviour was accounted for when sizing the oxidiser orifices by using non-homogenous non-equilibrium flow equations.

The injector plate design is a three-part assembly comprising of the main injector plate, an oxidiser sealing cap and a fuel sealing plate, see Figure 6 below. The oxidiser sealing cap is threaded and utilises a radial O-ring seal, the cap is tightened through use of a custom pin spanner. The fuel sealing plate is clamped with M4 bolts and will have radial O-rings sealing to the main plate. Angled ports are used to for fuel to flow from the regenerative cooling channels into the fuel manifold. An O-ring face seal is used to seal the fuel to atmosphere leakage path, and a radial O-ring is used to seal the fuel to chamber. In general, radial seals were selected due to them being more immune to part flex creating leakage paths and more compact radially. The O-ring grooves were sized using the Parker O-Ring Handbook (Parker, 2024). To aid disassembly M4 eye bolts were added to the fuel manifold cap, these features may be vital for disassembly if the O-rings are thermally compromised under thermal soak back.

The even distribution of orifices should ensure even combustion within the chamber. Oxidiser elements are placed in the central manifold, as shown in Figure 6 below, to increase the distance between the injection point and the walls. Combined with nitrous oxides low vaporisation pressure concerns of hotspots on the chamber walls can be mitigated.

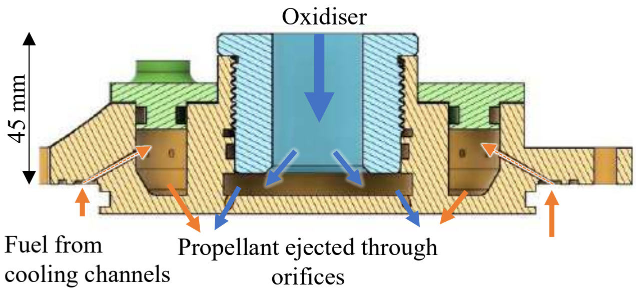

Figure 6 - Cross-section of injector plate assembly. The main injector plate is shown in yellow, oxidiser sealing cap in blue and fuel sealing plate in green.

The injector plate has two additional angled ports for a pressure transducer to measure combustion pressure and a torch igniter; these can be seen in the centre of Figure 7 below at 12 o'clock and 4 o'clock respectively.

Figure 7 – (A) Assembled injector plate. (B) Deposits on injector plate following hotfire. (C) Cleaned injector plate following hotfire.

3.3 Ignitor

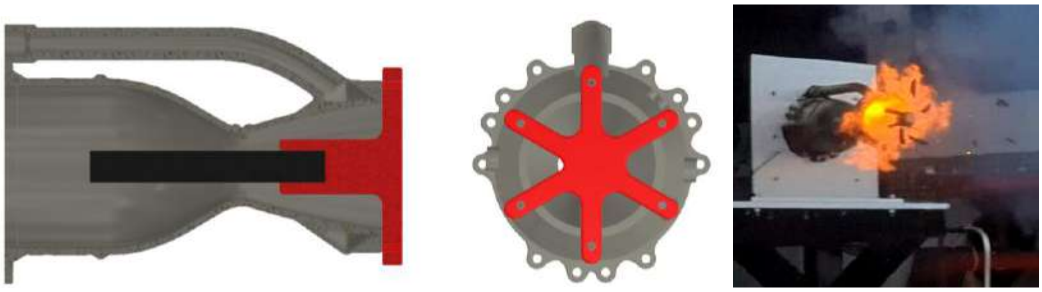

Figure 8 - Left: Half section and Centre: nozzle frontal view of ignitor mount (red) and sparkler (black), Right last years igniter being ejected from the combustion chamber from Appendix B.6 - Oct 2024 Full Stack Testing Summary.

The engine will be ignited by a StageGear Le Maitre PP050 sparkler inserted into the combustion chamber nozzle and secured by a PLA 3D-printed mount, see above. The igniter is ejected post ignition. A steel deflector disk will be mounted in front of the sparkler to protect the injector face. This is improved upon last year's design with a more powerful sparkler and a stronger mount design.

3.4 Feed System

3.4.1 Plumbing

Project Waxwing's feed system has been designed to provide high pressure propellants to the injector plate using a pressure fed system. The P&ID, in Figure 9, demonstrates this implementation. Within the rocket propellants are pressurised via blowdown with a 3L COTS COPV nitrogen tank (TK-N2 in diagram). Pressurant feed is controlled via a COTS regulator (Aqua Environment 873-1500-NV-NA).

The propellant tanks are custom designed co-axial tanks described in section 3.5 Coaxial Propellant Tank. The propellant flow rate into the engine is controlled using servo valves, described in section 3.4.2 Flow Control Valves. High-pressure Swagelok and other compatible parts have been used through the system with burst pressure in all cases of >3x MEOP. All lines are ¼" diameter, except the main inlets to the fuel and oxidiser ports on the engine, which are ½" and ¾" respectively.

A full BOM is listed in H.3 Plumbing Bill of Materials. COTS pressure transducers relay system values to ground control and onboard software for controlling fuelling and flight control. Fittings are typically imperial BSPP, sealed with a Dowty washer, however some components such as the dip tube present in the N2O fuel tank and the pressure regulator were only available in NPT varieties. The system is filled via remotely operatable quick disconnects.

Two COTS Electron-Beam Welded Assembly Burst discs manufactured by Wehberg Safety are placed directly on each compartment of the propellant tank, with a MEOP pressure of 50 bar these burst disks have a burst pressure of 65 bar ±10% and are connected to run tees through an NPT connection. The N_2O tank has the addition of a dip tube for the visual cue of a change in vent colour to indicate when the propellant tank is full. A 5% ullage space is allowed.

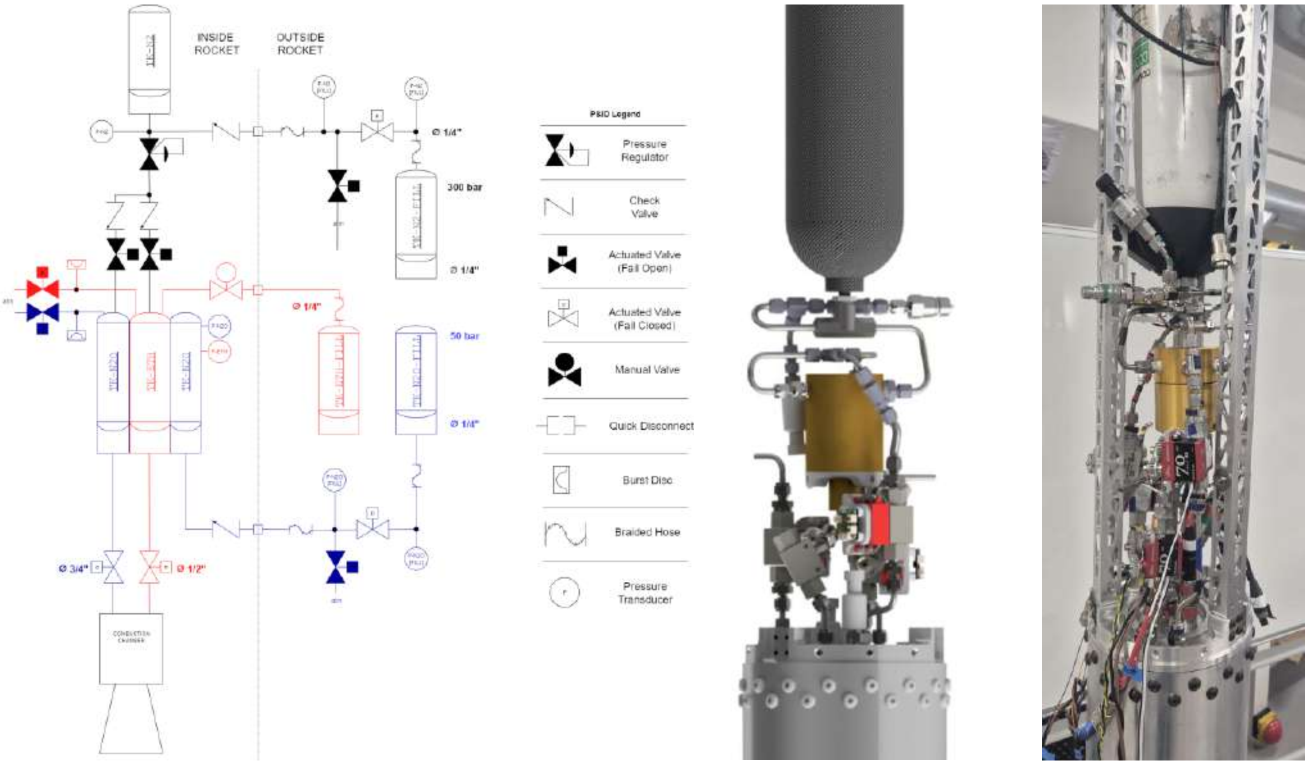

Figure 9 - Left: Feed system P&ID Centre: Top plumbing render Right: Top plumbing assembled in the lab

3.4.2 Flow Control Valves

To control the flow of propellant three servo-control valve variants have been designed; a ¼”, ½”, and ¾”, for the fuelling lines, the engine fuel and oxidiser control valves respectively. Commercial full-bore stainless steel ball valves were selected.

A ¼” servo bracket has been designed and machined from stock aluminium (see Figure 10); gears have been cut using a wire EDM. The ¼” COTS Delta-P valve was chosen due to its ease to design around, as well as availability from the previous design cycle. The design features a double ended rod ball bearing tie to ensure tooth engagement. This is a result of previous issues with gear alignment due to the slop (or “wobble”) in the valve’s head socket. A gear ratio of 1.7 was chosen as a balance between servo gear size, servo range of motion and overall mechanical advantage. A drawback of the chosen COTS ball valves is that of previously overheating the servo motors due the valves propensity to resist their positioning. All ¼” valves utilise 70kgcm 180° servos which helps mitigate this issue due to the greater torque overhead. A further mitigation is that of back driving the servo a couple of degrees from its set position. This releases the “spring” tension and the static torque that comes with it.

Figure 10 - 1/4" geared servo-valve

Additionally, geared ¾" and ½" run valves have been designed. These utilise COTS 3-piece valves. The design consists of two machined aluminium arms attached on the exterior top bolts of the 3-piece valves. This allows for both in-situ mounting, and ease of overall plumbing assembly. The design features a hall-effect sensor aligned with the valve head axis and mounted via a bracket.

The ¾" and ½" main engine valves feature 70 kgcm 360° servos with a hall effect angle sensor for feedback control. Servos of this type are controlled through rotational speed and direction. This allows for more precise valve angular control and a timed startup sequence as well as being much more resistant to stall and hence overheating.

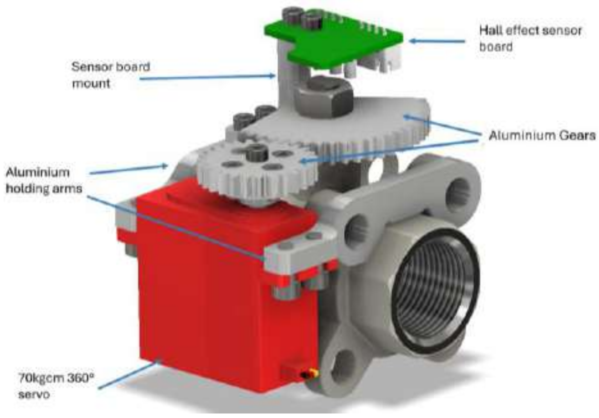

Figure 11 – Left: 3/4" geared servo-vale design in CAD Right: Assembled on the workbench.

3.5 Coaxial Propellant Tank

3.5.1 Tank Design

The primary aim of this year's tank was to prevent the failure case seen in the previous year's tank where a pressure differential between the inner and outer tank caused the inner tank to implode (See Appendix B.7). This resulted in a design which included stiffening rings (See appendix) however during the hydrostatic testing of our tank it was found that the design changes were insufficient to prevent failure. To undoubtably protect against this failure mode, an inner tank with significantly greater wall thickness of 8.5mm was designed to survive the buckling with a conservative safety factor of 10. Shown below is a full CAD render of the revised final tank design with a thicker inner tank.

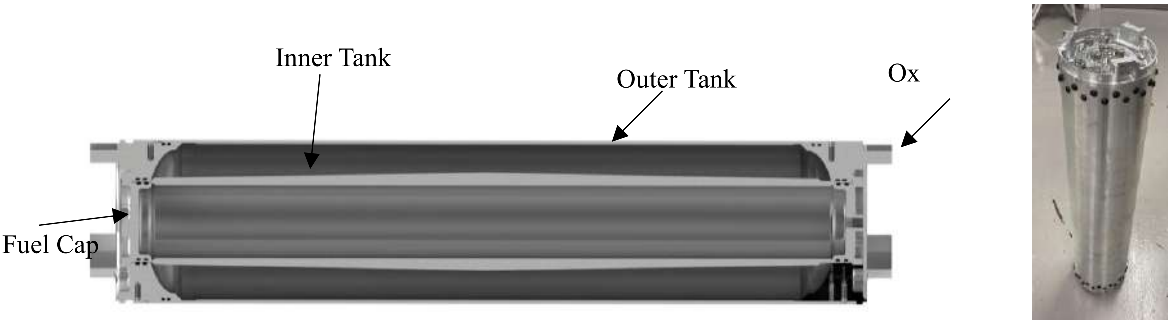

Figure 12 - Left: Half-section view of the full tank assembly Right: A picture of the assembled tank

The tank endcaps were the simplest part to redesign, as last year's caps were designed with multiple flaws, including:

- Varying fillet radii throughout the cap – changed to just a few radii, approved by the machine shop.
- Uneven, and inefficient weight-saving cutouts – improved by increasing the radius of cutouts, and cutting out more sections, saving mass.

Shown below are the fittings used on the bottom and top bulkheads.

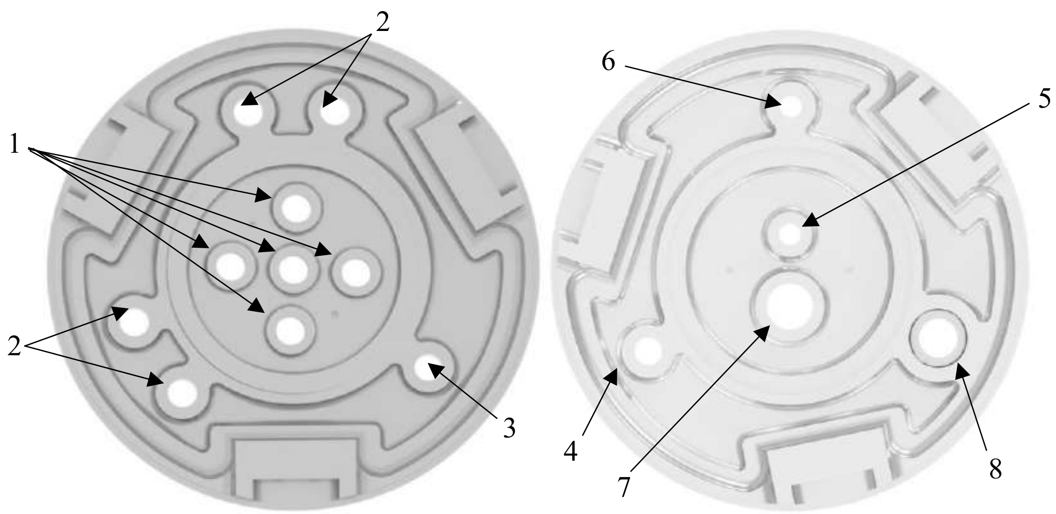

Figure 13 - CAD Renderings of Tank Endcaps

Table 3 - Table Supporting Figure 13 showing the nature of ports on the tank bulkheads

Label	Port size	Port function
1	5x1/4 BSPP	Pressure in, Fill, Transducer, Vent, Burst Disc
2	3x1/4 BSPP	Pressure In, Transducer
3	1x1/4 NPT	Diptube/Vent
4	1x1/4 BSPP	Fill
5	1x1/8 BSPP	Ignitor Fuel Line
6	1x1/8 BSPP	Ignitor Ox Line
7	1x1/2 BSPP	Fuel Flow out
8	1x3/4 BSPP	Ox Flow out

3.5.2 Design and Analysis

Following the first hydrostatic testing campaign, the inner tank was redesigned to prevent the buckling failure seen previously. The stiffening rings were most likely detached from the inner walls of the tube, due to insufficient adhesive application or human error. This led to the pressure acting solely on the wall thickness, which was not enough to resist the pressures, which went up to 85 bar.

To eliminate this failure mode, the tank was redesigned with a significantly greater wall thickness. This design involved removing the stiffening rings, meaning any human error in applying the adhesive was removed entirely. FEA simulations in ABAQUS were carried out for inner wall thicknesses of 6.5mm, 7.5mm, and 8.5mm, which can be found in appendix H.4. These were carried out using a non-linear buckling step, and solved using the Lanczos method, with 25 eigenvalues requested, with the force applied a uniform pressure of 50 bar. Finally, to ensure that the tank did not fail by this buckling mode, the tank design was altered to have a higher thickness near the centre of the tank of 15.5 mm being the thickest 8.5 mm, being the thinnest. From the pressure of 50 bar applied, this had an eigenvalue of 41.864, which meant the inner tank could withstand 2500 bar, over 41x the MEOP.

3.5.3 Inner Tank Simulation

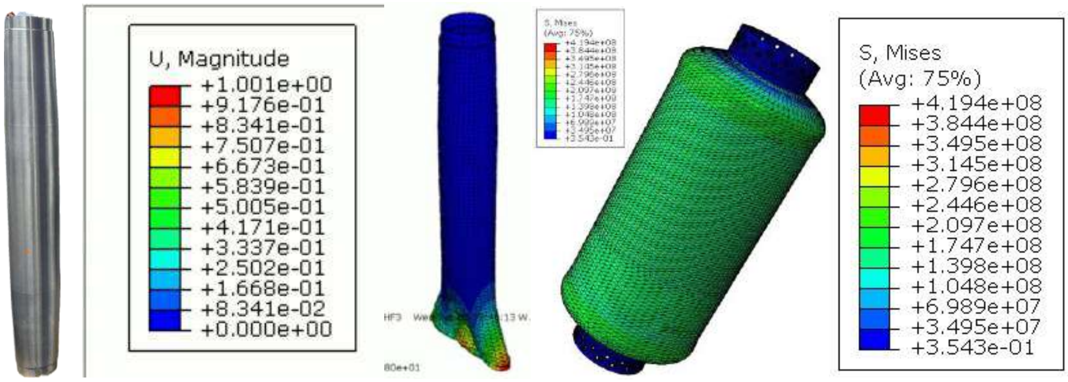

Figure 14 (L): FEA buckling simulations for the final tank iteration, with thickness concentrated at the middle portion (R): FEA simulation of a 100 bar pressure inside the outer tank

3.5.4 Outer Tank Simulation

FEA simulations in ABAQUS were carried out for inner wall thicknesses of 8.5mm. These were carried out using a non-linear buckling step, and solved using the Lanczos method, with 25 eigenvalues requested, with the force applied a uniform pressure of 50 bar.

From the pressure of 50 bar applied, this had an eigenvalue of 44.258, which meant the inner tank could withstand 514.6, over 10x the MEOP.

The outer tank is made of Aluminium-6082 and is designed to survive 2x MEOP internal pressure load. Peak stress at boundary conditions is due to unrealistic pinning. True stress in material seen at the central positions.

3.5.3 Testing

Hydrostatic testing was completed at Astron Systems, the inner, outer, and combined tank(s) being taken up to a pressure 1.5x MEOP (75 bar) and held there for a period of 15 minutes for the formers and 30 minutes for the latter, in accordance with the EuRoC Regulations.

4. Launch Vehicle

4.1 Structures

4.1.1 Nosecone

The nosecone follows a Von Kármán profile from the Haack series, selected for its low-drag characteristics across the vehicle's operating speed range. To maintain a consistent outer diameter of 200mm, the profile was extended by 370mm beyond the taper point, resulting in a total length of 770mm. Previous iterations exhibited an excessively high safety factor, prompting a mass-optimised redesign. The final design utilises three plies of 600gsm CFRP in a [-45/0/45] lay-up, with an aluminium 6082-T6 tip for added structural integrity. The completed assembly weighs 0.829kg—1.78kg lighter than in Project Feynman.

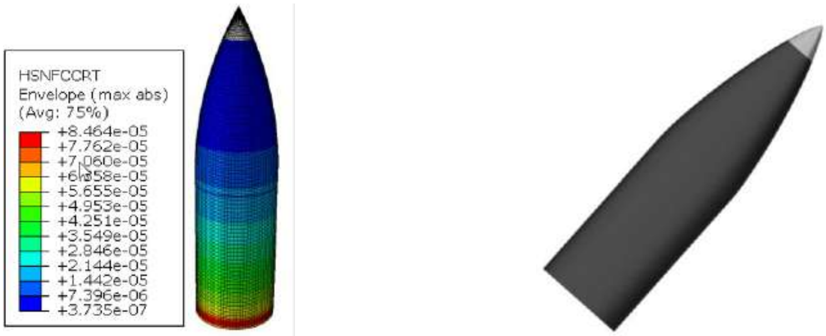

Figure 15 - (Left) Simulation of Hashin's Fibre Compression Failure Criteria (HSNFCCRT) under same conditions. (BCs: fixed bottom circumference. Main load is axial compression.) / (Right) A CAD render of the Nosecone

FEA simulations confirmed that the reduced-mass design still meets all structural performance requirements. The resulting Hashin fibre compression failure index is 8.5×10^{-5}, and buckling occurs at 18kN, corresponding to a safety factor of 27.8. While these values remain higher than strictly necessary, a degree of redundancy has been intentionally preserved due to imperfect manufacturing techniques.

4.1.2 Avionics Bay

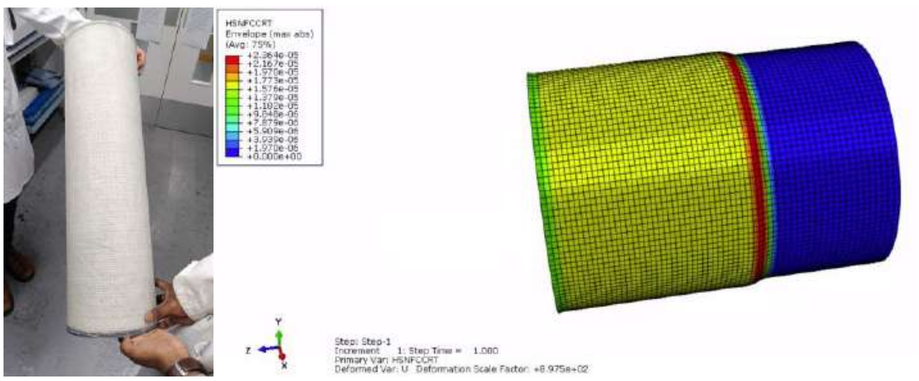

Figure 16 - Left: A picture of the Avionics Bay pre-post-processing Right: A FEA simulation of the AV Bay

The avionics bay is a GFRP tube made up of three 820 gsm triaxial plies with a [-45,45,0] layup. The avionics bay houses the payload, top stack electronics, and recovery equipment. An FEA study was conducted on it with the main priority load case being the thrust from the engine, has shown a HSNFCCRT of 2.4e-5. The avionics bay weighs 950 grams, with a length of 640mm.

4.1.3 Fins & Fin canister

The Fins are swept & trapezoidal to follow a hybrid profile with a NACA leading edge and a sharp wedge trailing edge. Fins uses 3 triaxial CFRP plies in a [-45,0,45] layup, the main loading criteria is the 1kN deflection on the tip. The FEA shows a 0.8mm deflection from the fin root.

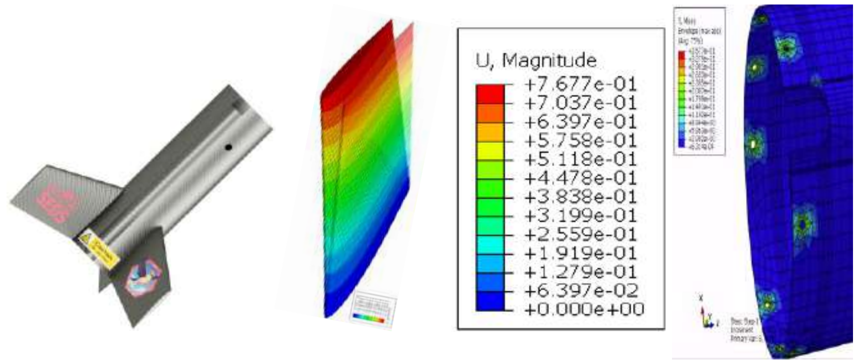

Figure 17 - Render of Fin Can (Left), FEA results of Displacement (Middle), FEA results of Fin canister (Right)

The Fins are attached to the Fin canister using 'Tip to Tip' i.e. using CFRP layers tip to tip of the fin to bond it to the Fin canister and helping with lateral loading. The Fincanister uses 3 triaxial CFRP plies in a [-45,0,45] layup, the main loading criteria is the stress concentration caused from the lower bulkhead's bolts. FEA resulted in a maximum Von Mises stress of 35.7 MPa (2.6 safety factor based on a minimum composite yield strength of 64 MPa).

4.1.4 Metallic Frame (Stringers & Bulkheads)

Figure 18 - A CAD render of the metallic frame

The rocket's primary load-bearing structure consists of a metallic frame, including thrust and feed system support structures, comprised of two bulkheads connected by three c-section stringers, and the coaxial tank. The design was an iteration of Project Feynman's structure, with the primary objective of reducing mass while maintaining the required load-bearing capability. Additional constraints and objectives were also identified during the design process:

- Reducing the flange of the thrust stringers to increase access to the plumbing.
- Increasing the lengths of the thrust and feed system stringers by 74 mm and 65 mm, respectively, to accommodate expanded plumbing requirements.
- Continuing the use of the same C-section stock dimensions (1½ × 1½ × 3/16 × 3/16 inches) due to its superior stiffness-to-weight ratio and structural efficiency compared to flat bar alternatives.
- Maintaining the same material: aluminium 6082-T6, with a yield strength of 255 MPa.
- Including mounting points for internal electronics and external composite aero panels.

Analyses were performed on both individual stringers and sub-structures (thrust and feed system supports), using load cases extracted from OpenRocket simulations, with a conservative 1.5× safety factor applied. The primary load cases analysed included:

- Axial compression due to thrust at launch: 4309.4 N
- Bending moments from aerodynamic forces and thrust misalignment: 26.06 kNmm
- Shear and bending from high dynamic pressure: 4.51 kN
- Deceleration forces at parachute deployment: 1282 N

Preliminary FEA revealed that the previous year's design was significantly overengineered, indicating potential for substantial material reduction. To preserve the interface design while improving access to internal components, the flange depths were reduced to 19mm for the feed system stringers and 20mm for the thrust structure stringers.

Mass optimisation was then achieved by introducing triangular cutouts aligned in a truss-like configuration on the flat faces of the stringers. The feed system stringers were able to accommodate cutouts on all three faces. However, in the thrust stringers, the combination of flange reduction and cutouts led to buckling due to a reduction in the second moment of area. As a result, cutouts were applied only to the web of the thrust stringers. The final designs for both stringer types are summarised in Table 4, with both achieving a significant mass reduction despite the increased lengths.

Table 4 - Summary of stringer design changes and mass reduction.

Sub-structure	Location of triangular cut-outs	Stringer length increase (mm)	Stringer mass (kg)	Stringer mass reduction (%)
Feed system	All faces	65	0.567	67.7
Thrust	Web only	74	0.317	26

The key results of the FEA on the new designs are given in Table 5 below, considering Von Mises (VM) stress and buckling for the most severe load case of axial compression due to 4.5kN of thrust at launch, with 6.5kN applied during FEA when including the 1.5x factor. As expected, the stress is concentrated at bolt holes and contact surfaces, as shown below. However, the large safety factors in buckling loads and low stress on the flanges suggests there is room for further mass reduction in future iterations.

Table 5 - Summary of FEA results for the sub-structures of the metal skeleton.

Sub-structure	Max VM Stress (MPa)	VM Stress Safety factor	Buckle Load (kN)	Buckle Safety Factor
Feed system	77.18	3.3	95.9	14.8
Thrust	144.1	1.77	33.8	5.2

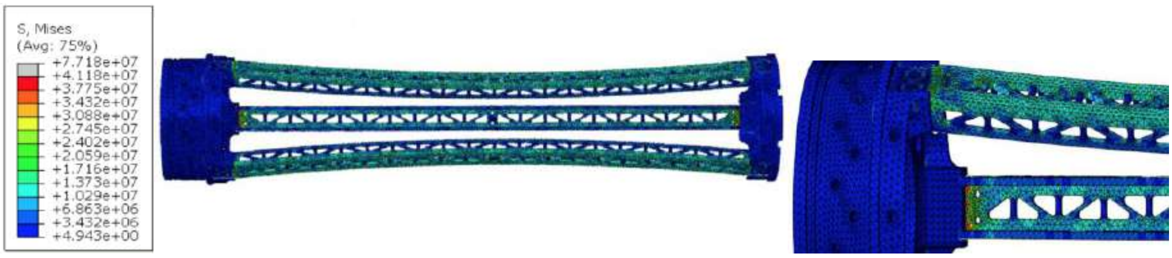

Figure 19 - Feed system support structure max Von Mises stress (BC: fixed top bulkhead, main load: axial compression); Deformation scale factor: 75 (note colour scale is shifted for visual purposes)

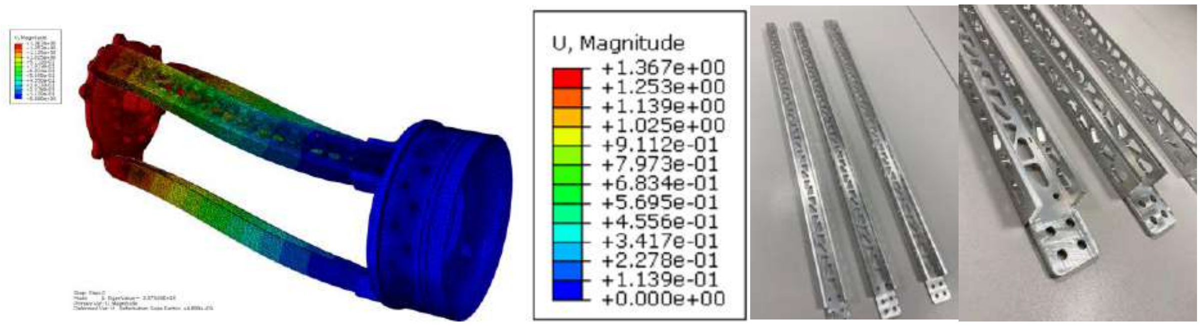

Figure 20: Left thrust structure buckling simulation, right manufactured stringers.

4.1.5 Nosecone Coupler

A metallic coupler has been introduced for this year's design to improve load paths and reduce local stresses of the avionics bay and nosecone. Mass reduction through triangular cutouts was implemented since they give excellent shear load paths along their sides, with fillets used to avoid high stress concentrations at corners. The design uses an isogrid structure to spread load on multiple paths, avoiding single-ligament overload and raising local bending stiffness, for it being a thin-walled cylinder. Loads were used from OpenRocket and applied to FEA, taking the highest priority load case, and simulating accurate boundary conditions in each step. Mass estimates were calculated to maximise strength to weight ratio, with a safety factor of 3.25.

shows the FEA results under the most severe loading case: bending moments induced by aerodynamic forces and thrust misalignment. The analysis considers a thrust load of 6.5kN and a 39kNmm moment with a full fixed Encastre boundary condition on the isogrid. The coupler material is again Aluminium 6082-T6, with yield strength 260MPa.

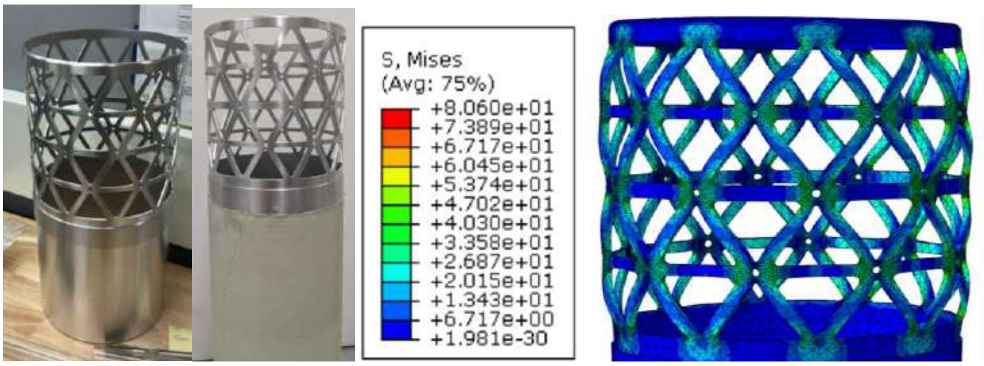

Figure 21- Nosecone Coupler FE results of Von- Mises

4.1.6 Strake

The strake, Figure 22, has been designed to house wires running from forward avbay to the aft fin can and sits on the coaxial tank, with 10mm of clearance for wires to pass through. The forward face is tapered to match the Von Kármán profile of the nosecone.

Figure 22 - A CAD Render of the Strake

4.1.7 Airbrakes

The airbrakes present an iteration on Project Feynman's design, drastically reducing weight while resolving key integration issues. An upper and lower casing house three airbrake "petals", which are actuated by a single 180-degree servo with a stall torque of 40 kg/cm. Each air brake deploys radially from the body. Each petal and gear are supported by pairs of radial and thrust bearings.

A mechanical locking system is implemented as our first fail safe. This pin will remain in place until an altitude of 1500m has been surpassed, and the velocity of the rocket is within 10m/s of the maximum safe velocity for the deployment of the petals. The mechanical locking pin is retained by a rack and pinion gear system and actuated by a 180 degree servo with a stall torque of 40kg/cm. Cutouts in the airbrake design have been included to allow wires for electronics to pass through.

Figure 23 shows the results of FEA on the final airbrake system when considering the most severe load case of 6.5kN of axial compression due to thrust. The system is made from Aluminium 6082-T6 with a yield strength of 260MPa, with a resulting safety factor of 3.5 for the axial compression load case.

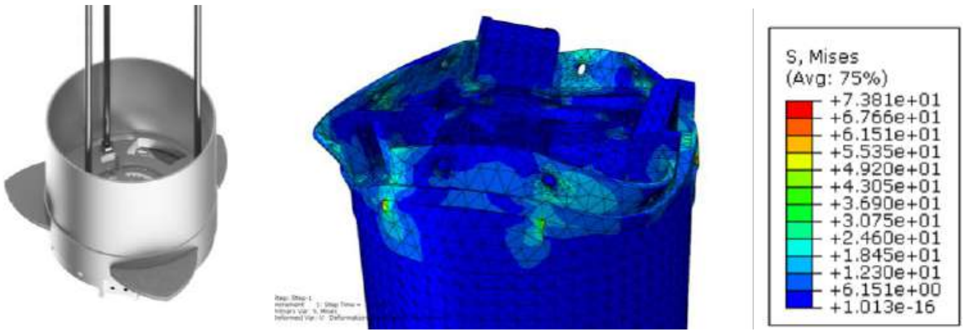

Figure 23: Airbrake system CAD (L), Von Mises stress results (R)

4.1.8 Panels

There are 3 removable panels, each equally sized to 120 degrees of the circumference, and 865mm long. The panel design aim to provide an aero shell for feed system access, and to reinforce the metallic frame, particularly against torsion. Each panel is made from a carbon fibre-reinforced polymer composite with an epoxy matrix at a 3 ply [–45/0/45] fibre layup. They are attached to the metallic frame via three M6 bolts at the forward and aft edges each, and 6 M6 bolts on the port and starboard edges of the panel. Given each panel is secured onto the metallic frame, the primary expected load is from shear traction on the surface due to aerodynamic effects & the stress concentration on the bolt holes from the load transfer from the metallic frame. FEA resulted in a maximum Von Mises stress of 35.4 MPa (2.6 safety factor based on a minimum composite yield strength of 64 MPa).

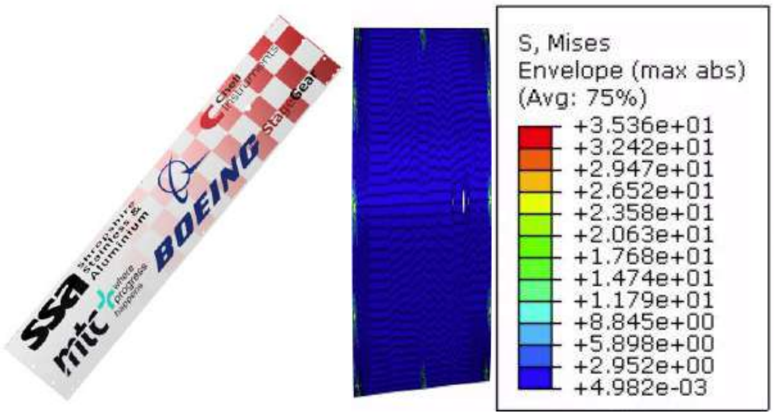

Figure 24: (A) CFRP Panel render (B) FEA analysis right.

4.1.9 Thrust Clamp

The thrust clamp acts as a break-away system to restrain the launch vehicle after sufficient thrust has been reached. This is achieved using shear bolts inserted into three 2-plate interfaces attached directly to the engine mounts, 120 degrees apart. The launch vehicle itself is held down by M10 rods connecting into a 2-plate interface that is attached onto the launch rail directly. The 2-plate interface provides a single shear of the bolt shank. An M3 PEEK bolt demonstrates a shear strength of 100 MPa. This allows for 0.6-0.8kN on each interface to reach a shear stress of 99MPa at 0.7kN. FEA was conducted on the entire thrust clamp assembly to see the exact failure mode and stress distribution on the bolt. The results in Figure 25 show the calculated stress around the interface, showing failure at 95MPa. This has validated in testing by using a hydraulic press to simulate shear, this resulted in a clean shear of the bolt failure, with the main thrust clamp interface holding to the tension.

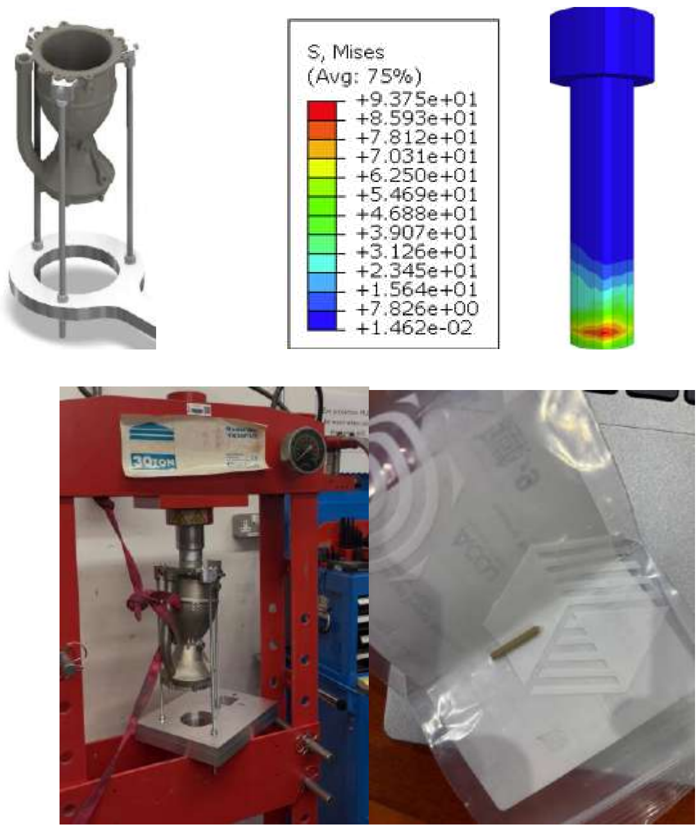

Figure 25 - Thrust mount render (Top-left), Bolt FEA (Top-Right), Test setup (Bottom-Left) & Post-Test (Bottom-Right)

4.1.10 Rail Buttons

Rail buttons constrain the rocket onto the launch rail during the initial phase of flight, until it reaches enough speed to ensure the correct stability margin. The rail buttons are machined out of nylon, to fit onto the standard EuRoC 50x50mm launch rail aluminium profile. An aerofoil profile is incorporated to improve drag characteristics and is attached via an M6 bolt that is tapped and bonded into the stringer structure.

Figure 26 - A CAD render of the Rail Button

4.2 Aerodynamics

4.2.1 Numerical Simulation

The aircraft will be flying at speeds up to Mach 0.8 meaning both subsonic and transonic flow will act on the body of the aircraft. Thus, a K-Omega and K-Epsilon solver was used on Star CCM+ to model boundary layer flow close and far from the surface, ensuring an accurate solving of the simulation. Such solvers helped model and account for compressibility of the flow alongside shockwaves or behaviour in transonic flow. Details of the mesh sizing and model selection can be found in

Two designs for the airbrakes were considered using theoretical reasoning to maximise drag and stability during braking. Two factors were considered for stability: brake geometry as well as interaction between fins and the wake shed from the air brakes during braking. The number of airbrake flaps had to match the number of fins for them to be perfectly displaced with each other, minimising interactions between the two flows. The two flap geometries that were tested are shown in Figure 27:

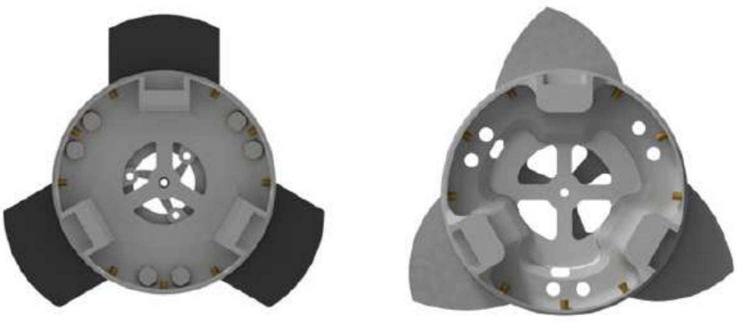

Figure 27 - a) Slot airbrake design b) Petal airbrake design

It was concluded through Computational Flow Dynamics (CFD) that the rounded petal design, provided greater braking force and stability. However, a greater separation from the body alongside possible interaction with the fins. Contrarily, a petal shape, provided less drag and a more predictable separation for a constant petal base length. Thus, a compromise between the two geometries achieved the desired performance. To determine the airbrake design, Project Feynman's fin configuration was used as the new fins would have had a similar geometry. Simulations were re-run with the new fin configuration to verify they would not cause significant changes upstream.

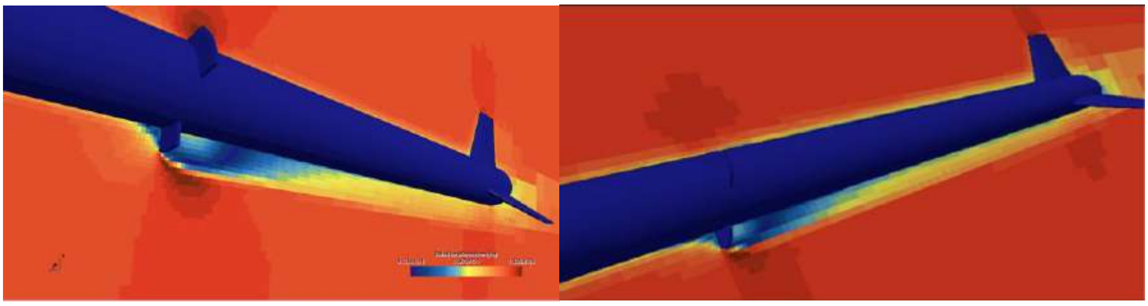

Figure 28 - Comparison between the separation of flows between the two geometries during the braking phase

A partial interaction with the turbulent boundary layer would bring to high instabilities and/or stall. Therefore, the axis-symmetric simulation in Figure 26 was sliced along the z axis to view the flow's interaction with the fins.

4.2.2 Fin Design

The aim of the overall design was to achieve a configuration which minimizes drag and maximizes stability with a minimum mass penalty. The fin aerofoil was tailored to achieve minimal drag in subsonic flight. According to the RocketPy simulations, the maximum Mach Number is 0.8, meaning the fins will be subject to both subsonic and transonic flows. This means shock formation would have to be considered between altitudes of 500-1000m.

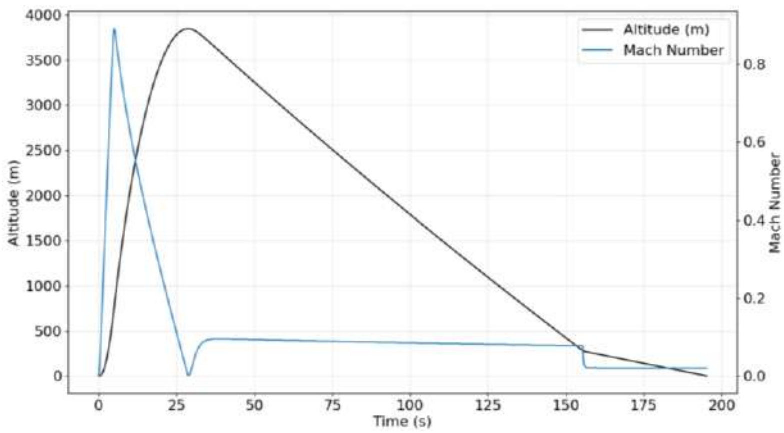

Figure 29 - Illustration of Mach Number variation throughout trajectory

Since the fin will be subject to both subsonic and transonic flows a novel hybrid fin design was considered. The hybrid fin consisted of a NACA leading edge, and a sharp-wedge trailing edge as shown in figure [28]. The reasoning behind this new design is that the leading edge NACA profile will minimise flow separation at subsonic speeds. Additionally, the sharp-wedge trailing edge will minimise flow separation as the air leaves the fin, since the stagnation point will pin itself to the sharp tip of the wedge. In the transonic regime, the sharp wedge trailing edge reduces shock-induced separation which reduces wave drag and the leading edge NACA profile helps delay shock-induced separation.

Standard 2D NACA profiles were compared against the new hybrid fin design using the Computational Fluid Dynamics (CFD) software, Star CCM+. It was demonstrated that the hybrid fin profile produced the optimum drag coefficient values. The performance of three different standard NACA fin profiles were tested at thicknesses 10%, 12% and 14%. Initially the profiles were tested at the trajectory's average conditions to ensure the best performance throughout the whole mission. The drag coefficient from the CFD analysis are reported in Table 9 and were computed by the considering the average conditions during the rocket's launch (). It was found that the Hybrid with 10% thickness gave the least amount of drag, and therefore it was chosen as the selected profile with the scale show in Figure 30.

Table 6 - Drag data on different profiles under investigation

Hybrid (% thickness)	Drag Coefficient	Normal NACA (% thickness)	Drag Coefficient
10	0.0661	10	0.0670
12	0.0687	12	0.0691
14	0.0703	14	0.0715

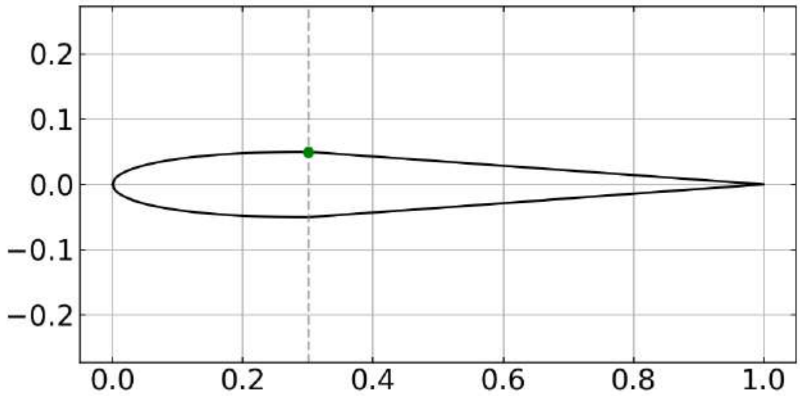

Figure 30: Non-dimensional schematic showing the scale of hybrid fin design. Vertical dashed line at x = 0.3 shows the transition point when the NACA0010 Aerofoil leading edge transitions into the sharp wedge.

A simple MATLAB code which iterated the panel method for any given geometry was used to compare drag data achieved through CFD on Star CCM+.

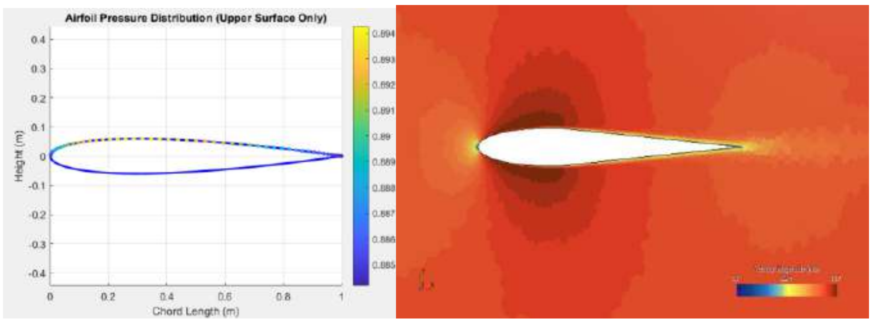

Figure 31 - Example of MATLAB Code and Star CCM+ usage to down select aerofoil geometry.

Figure : Example of MATLAB Code and Star CCM+ usage to down select aerofoil geometry.

Table 7 - Fin Design Specifications

Root Chord (cm)	Tip Chord (cm)	Height (cm)	Sweep length (cm)	Sweep angle (degrees)
23	17	23	12.7	28.9

Three fins provided sufficient stability, and acceptable weight for the vehicle. Four fins may increase the likelihood of the turbulent flow from the airbrakes interacting with the fins downstream, putting stability at risk.

Trapezoidal swept wings were determined to be optimal for a subsonic flight [8]. Ellipsoid fins were considered adequate too, however, the performance given did not outweigh the implementation difficulty of manufacturing such geometry in composite material. The formal selection process using an MCDA matrix is shown in . Open Rocket [9] was used to test the performance of different fin configurations throughout the trajectory. This was done by inserting the BoM of each fundamental component in the application as well as the rocket's engine performance. Hence, achieving a graph of stability over time. A target stability margin of 1.5 to 2.5 was set to ensure enough stability during the mission. As seen in the Figure 32 below a stability margin of 2.6 to 3.1 was achieved with the configuration seen in Table 9. The chosen higher stability margin will maintain stability during the braking phase of the mission.

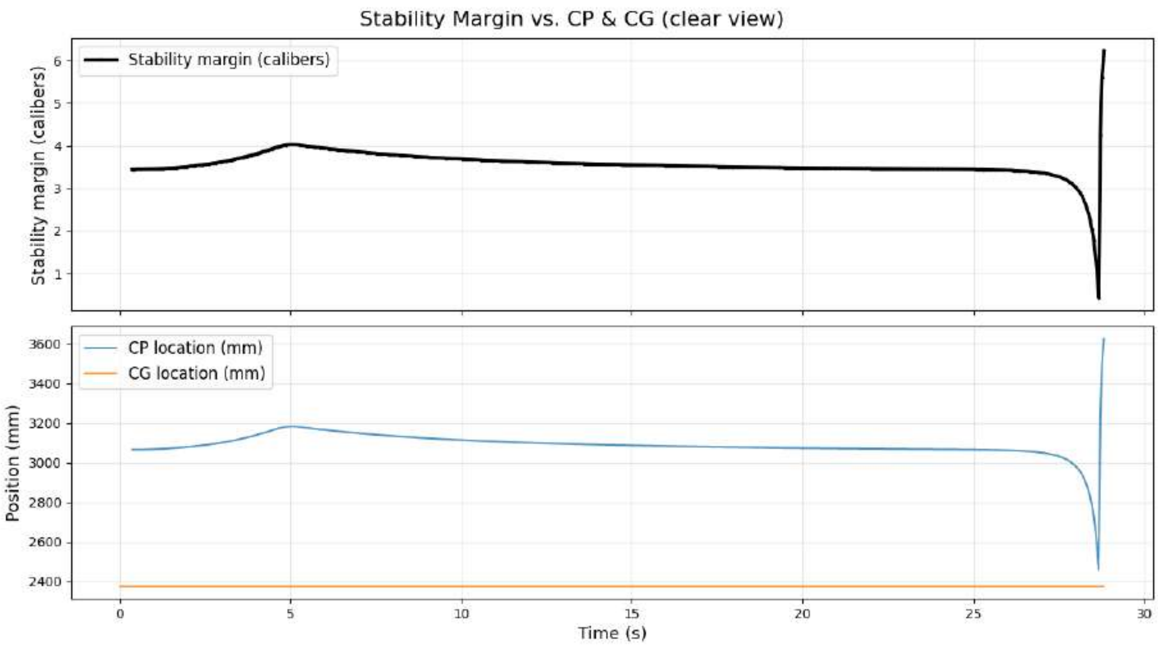

Figure 32: Graphs describing the stability of the aircraft during the mission

4.2.4 Wind Tunnel Model Design

The wind tunnel model was conceived as a scaled aerodynamic demonstrator, enabling controlled experimental validation of computational fluid dynamics (CFD) predictions for launch conditions. The data pathway was built in successive layers. Full-scale CFD established the design framework and baseline performance expectations. Wind tunnel testing then provided experimental measurements under controlled but Reynolds-limited conditions. A dedicated WT-specific CFD bridged the two by replicating the test geometry and conditions, which enabled compressibility corrections and calibration. Finally, launch simulations delivered the ultimate reference under true flight conditions. This inter-correlation ensured that discrepancies could be traced and systematically resolved with CFD informed design, WT validated CFD trends, WT-specific CFD corrected for scale effects, and closing the loop with real-world data. An in-depth analysis can be found in Appendix I.1.

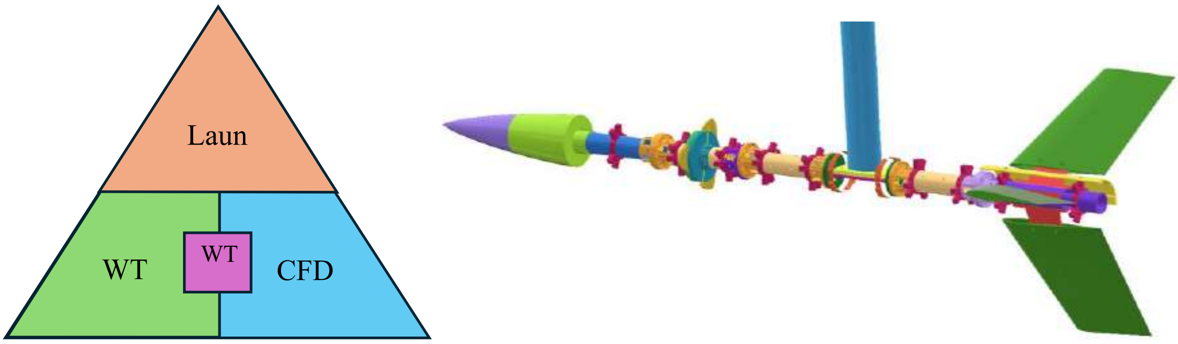

Figure 33: (A) Data/Information hierarchy (B) Wind Tunnel CAD Model

Current progress so far includes a completed CAD design (Figure 26B) and a main frame skeleton assembly. Testing procedure and planning has been completed, with testing scheduled for the first 2 weeks in November of this year.

4.3 Controller Design

4.3.2 High Level Overview

High level control is necessary to avoid failure cases. This is further split into different logic in a main and backup airbrake controller to provide a level of redundancy.

To avoid the airbrake being actuated when the locking pin is in, only one PWM channel for the servo is initialized and active at any moment in time.

Upon power on, the airbrake lock servo is actuated to lock in the airbrake. This lock is maintained until the rocket is detected launching. The launch detection is provided by a CAN message and the CAN heartbeat from the ground station to be lost. A timer is then activated for. At T+12s after launch detection, the locking servo PWM channel is de-initialized, and the main airbrake deployment servo is initialized. The airbrake is then actuated according to the low-level controller.

At T+30s after launch detection and the rocket has reached apogee, the controller then deploys the airbrake to maximum and locks it in place. It remains in this state until end of mission.

The main controller also listens for a “main controller failure” CAN message from the backup controller. Upon receiving such a CAN message, the main controller stops sending any PWM signal and hands it over to backup controller.

Operating in parallel to the main system, the Backup controller is in place for situations where the main controller fails. Upon power on, just like the main controller, it initializes its peripherals, including the locking PWM channels and SPI bus for communication. However, its primary function at this stage is to continuously monitor the main controller’s servo channels. By continuously checking the PWM channels, it is able to detect if the main controller is not deploying the airbrakes when it should be. By continuously checking the PWM channels, it is able to detect if the main controller’s locking signal becomes inactive prematurely or if the main servo begins to receive an active command, allowing the backup system to autonomously switch into an active role at the first sign of a primary system failure.

Once the launch CAN message is received and the subsequent loss of the heartbeat signal is detected, the Backup controller starts its own timer that runs in parallel with the main controller. At the timer’s designated 150 m/s mark (T+12.5s after launch detection), the backup system begins observing that the main controller’s lock is inactive or its servo is commanded to move. If the states of PWM signals does not match the expected states, the backup controller initiates its own takeover sequence. It sends a “main airbrake controller failure” signal on the CAN bus and deploys the airbrake to full.

The time-based lockout is to provide dissimilar redundancy against a barometer failure which could lead to airbrake deploying at speeds above 150m/s or below 1500m.

4.3.3 Low-level Controller

The low-level controller is made by 3 parts. Sensor filters, apogee estimator, and a bang-bang controller.

A barometer measures current altitude, which is then differentiated to measure the rocket vertical velocity. To eliminate noise, the altitude measurement is passed through a low-pass filter. The rocket vertical velocity is filtered by a low-pass filter and a moving average filter.

The apogee predictor solves for the estimated apogee given the current altitude, vertical speed and airbrake deployment angle. In the predictor, it is assumed that the airbrake deployment angle does not change, and air density is constant. Therefore, the drag force scales quadratically with airspeed, and a simple equation can be used to predict the final apogee (NASA Glenn Research Center, 2025). This output is further filtered with another low-pass filter to remove high-frequency noise.

After an estimated apogee is produced, it is compared to the target apogee. This output is converted by a bang-bang controller into a target angle, which is then fed to the airbrake servo via PWM signal.

Figure below shows the architecture of the controller.

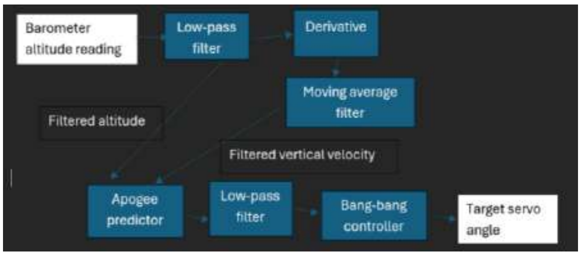

Figure 34 - A graph showing the architecture and filter of the low-level controller

Simulation in MATLAB Simulink indicates that the controller has an approximate error of about 10m. It can correct the apogee if it lies between 3km and 3.1km.

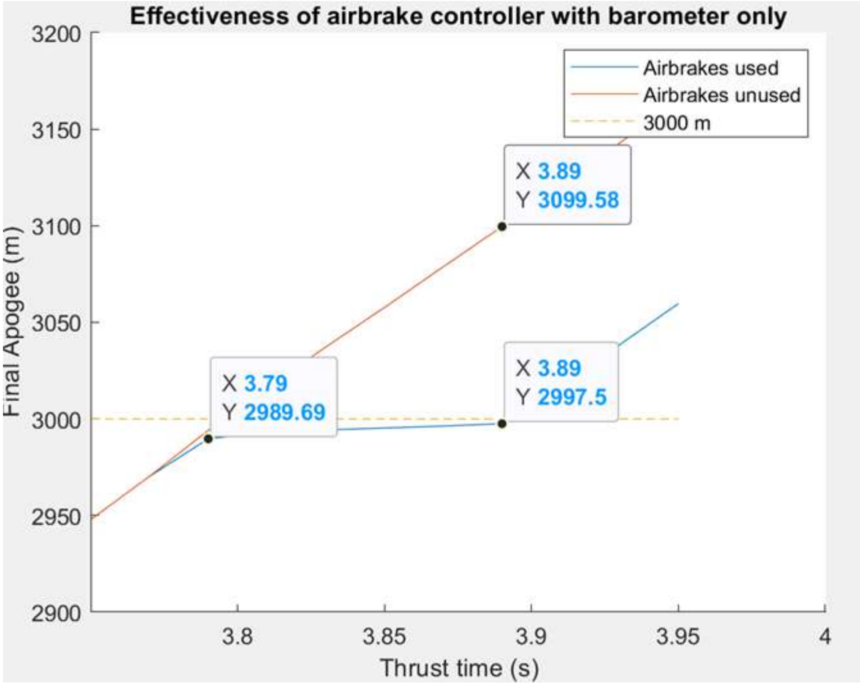

Software for the airbrake controller was generated using Simulink embedded coder. A Software-in-the-loop test was carried out to ensure that the software matched the design models.

4.3.4. Failure Analysis

- To address requirements EuRoC-LV-RQT-0670 and EuRoC-LV-RQT-0680, Fault Tree Analysis was completed. The scenarios of the failure modes were labelled with the common severity categories – Catastrophic, Critical, Major, Negligible. (ECSS-Q-30-02A Failure modes, effects, and criticality analysis, 2001) System Failure

At a high system level, two failure cases were considered – airbrake deployment at a velocity higher than 150 m/s, which is identified as a catastrophic failure, and failure to reach the target apogee, which is labelled as minor/negligible. The table below presents the actions taken for each case, with the catastrophic failure mode being the design driver.

Table 8 - A table showing the failure cases of the airbrake controller.

Fault Tree	Actions
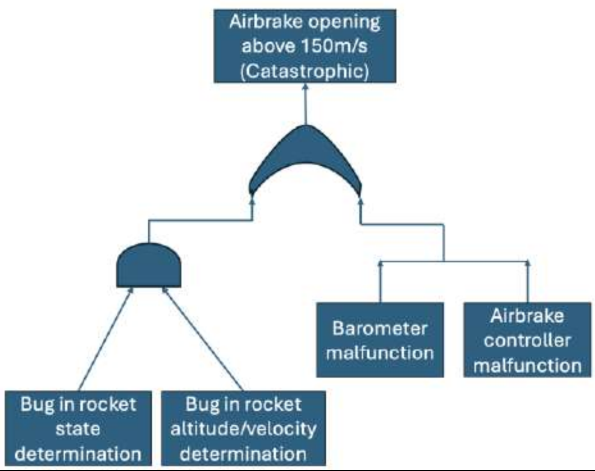	• Secondary barometer in warm redundancy. • Backup Airbrake controller in warm redundancy. • Time-based airbrakes deployment system that "lock-out' PWM signal to airbrake deployment servo.

<table>
<tr>
<td>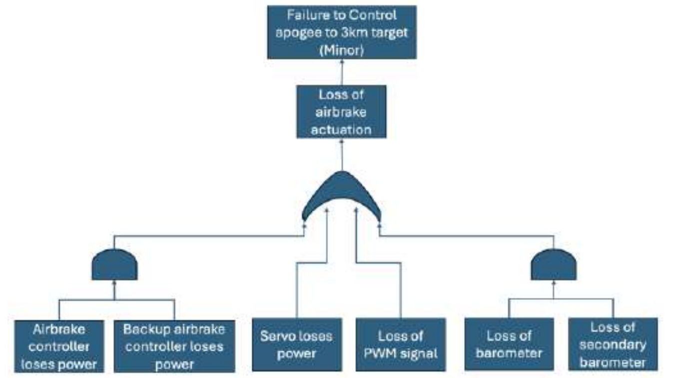
</td>
<td>

- Secondary barometer in warm redundancy.
- Backup Airbrake controller in warm redundancy.
- Time-based airbrakes deployment system.

</td>
</tr>
</table>

For failure management a secondary barometer is introduced in warm redundancy. It is connected to the flight computer on the same CAN bus. During thrust phase, when the airbrakes are inactive, five readings from the two sensors are cross-checked - if the readings are within 50 Pa the primary barometer is kept and the controller logic implemented. Otherwise, a time-based system of full airbrake deployment is activated. A Backup Airbrake controller is introduced in warm redundancy as well.

- Unit Failure

The Figure below shows the fault tree analysis for the unit failure case, specifically the barometer.

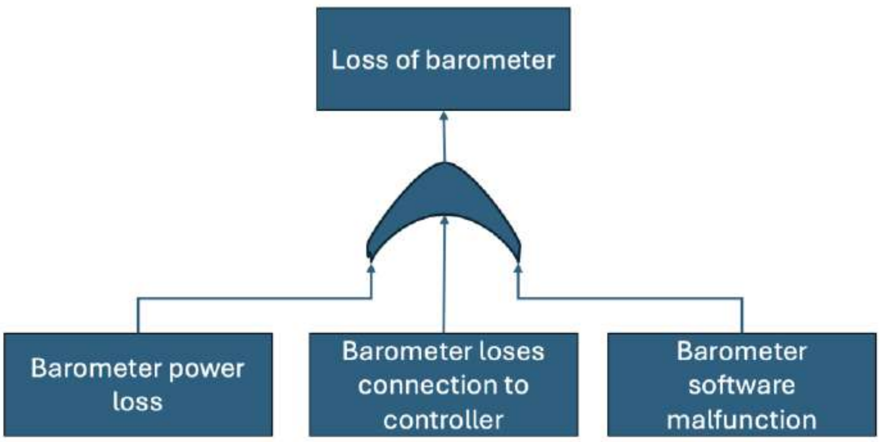

Figure 35 - A Figure showing how the barometer can fail

5 Recovery Systems

5.1 Single Separation Dual Deployment

To keep a minimum number of separation points on the rocket, a single separation, dual deployment event is used. The drogue is released in the first separation event, along with a bagged main parachute. This bag is released at a later stage of the descent, allowing the main parachute to inflate and bring the vehicle down to 8m/s to land.

The first recovery event, in which the nosecone separates and the recovery systems is deployed, will be triggered by a CO2 canister. A redundant black powder charge, and multiple e-matches attached to separate computers ensure a successful separation. All COTS flight computers used (6.2.1) have demonstrated successful recovery over multiple flights.

The second recovery event involves a tender descender to release the bagged main, which is stored under tension. The separation of the tender descender is forced by black powder ignited by e-matches. These e-matches are triggered by the flight computer, with a redundant cup included in the design.

To ensure that the proposed recovery method works, two separate test flights have been conducted, shown in Appendix B.2 and B.3.

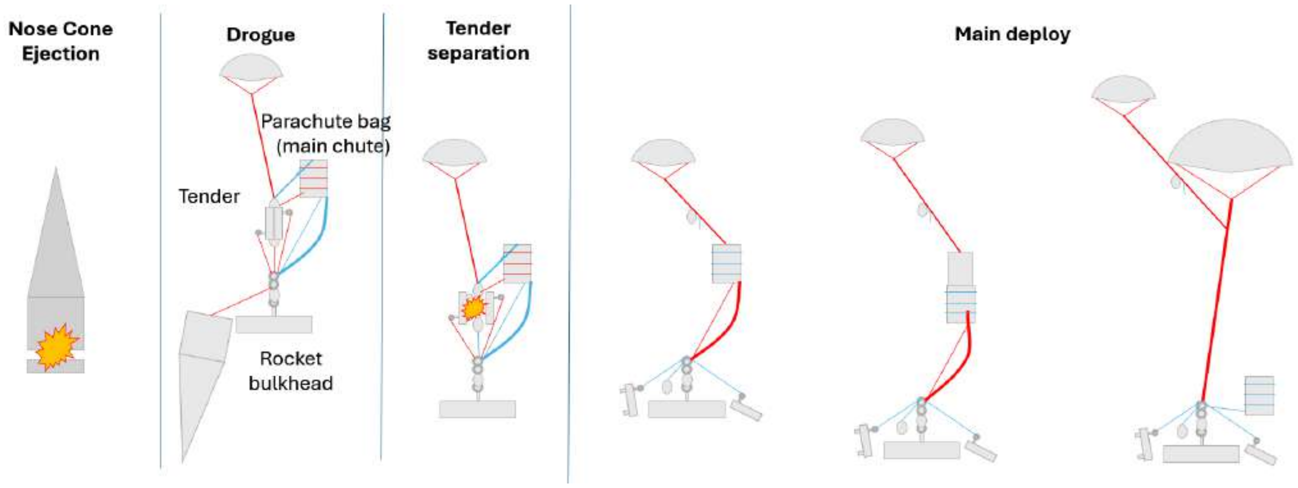

Figure 36 - A Figure Showing Parachute and Payload Deployment

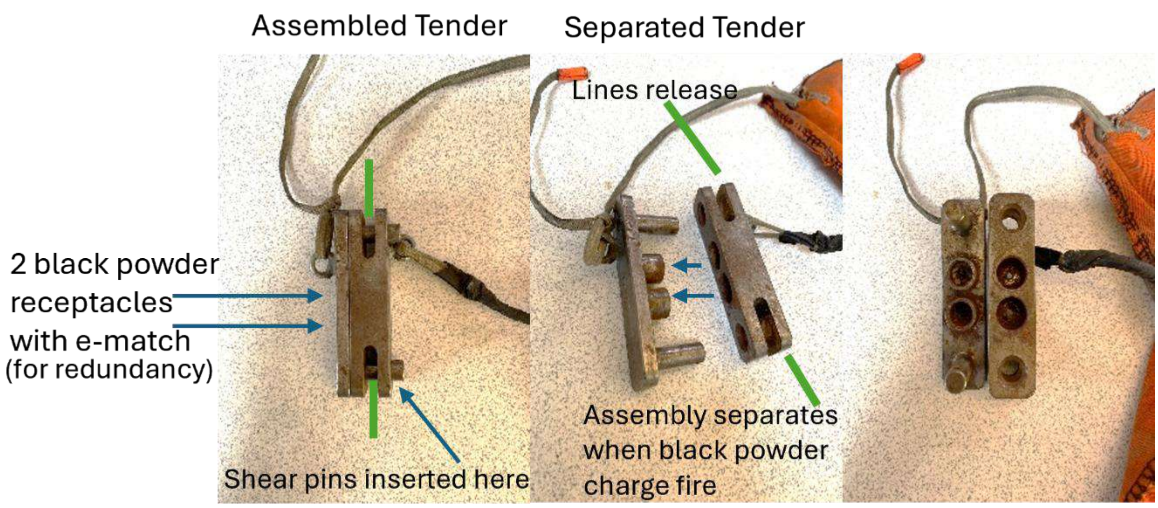

Tender separation device operated by e-matches in black powder charges.

5.2 Parachutes

Due to the higher weight of the rocket, comparing to historical launch vehicles flown by University of Bristol students, purchasing the required size of parachute would have the allocated budget for recovery. This has led to the development of our SRAD main parachute.

The drogue parachute will be a COTS 60-inch Black Cat parachute. On deployment, this will slow the rocket down to a descent speed of 28 m/s, and upon main parachute deploy, will slow the rocket down to 7 m/s.

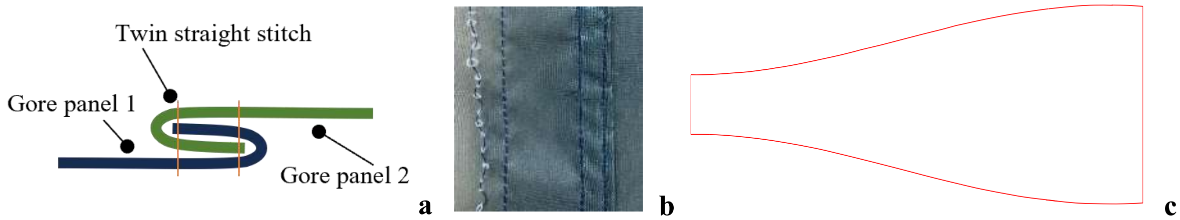

Figure 37 - a) diagram of a French fell seam, to ensure a strong join between gores. b) left to right, tension and stitch length testing on ripstop nylon, along with a practice French fell seam. c) pattern piece for one gore of twelve, for the main parachute

The main parachute has been designed to maximise the coefficient of drag, with the minimum amount of fabric. This goal resulted in the choice of a toroidal, or pull-down apex, parachute shape [13]. This canopy consists of a single radially symmetrical skirt, with a spill hole at the centre, which is "pulled down" using the lines. To maintain both good curvature and simplicity of design, the shape was divided into 12 gores. The panel shape shown in Figure 37 was then developed from open-source code, to suit the skirt and spill diameters required for this project. The fabric was chosen as 90gsm ripstop nylon as a low porosity fabric, with proven use cases for flight in hot air balloons, provided by Cameron Balloons. Literature recommended using French fell seams with straight stitch to ensure proper load transfer between gores [15]. The drag required from the parachute, and that the gores are each made from a continuous piece of fabric, meant there was no requirement to introduce a structural skeleton of tape in the seams. The load path is directed from the lines through webbing and into a stressed homogenous shell of the parachute skirt.

Figure 38 Left main chute packed into deployment bag, right demonstration of main parachute.

5.3 CO2 Subsystem

CO2 ejection is a novel separation technique being explored by BristolSEDS. This system has flown successfully on BristolSEDS' first two-stage rocket, Project Tempest producing a successful separation of the rocket on CO2 activation.

The change from black powder-based ejection to CO2 is to eliminate hot gases produced from combusting black powder during airframe pressurisation, which would otherwise damage recovery lines, even with the use of Nomex sheets and wadding. The mechanism functions by puncturing a CO2 canister with a piston to release cool gas to pressurise the airframe. A cross section of the mechanism can be seen in Figure 39.

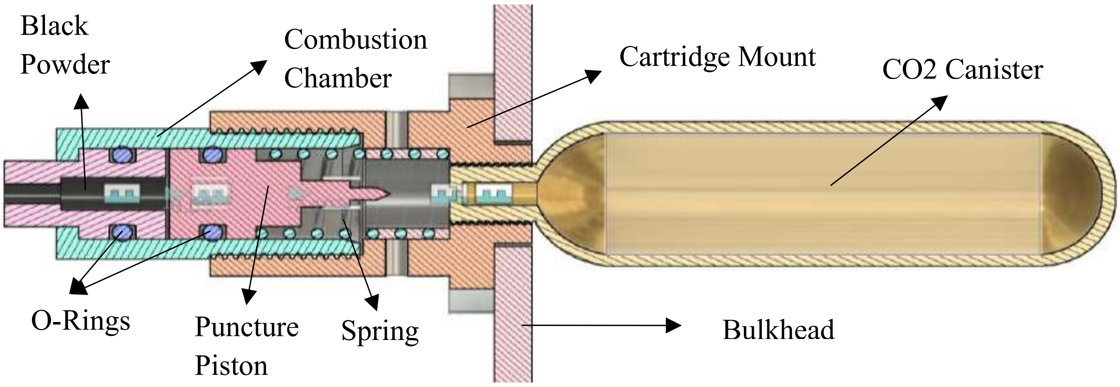

Figure 39 - Cross Section of the CO2 Ejection System

The mechanism operates when an E-match ignites, and increases the pressure inside the e-match housing, causing the puncture piston to move towards and puncture the CO2 canister. Pressure from the CO2 canister escapes using the four holes in the cartridge mount, to pressurise the airframe for separation.

The combustion chamber and cartridge mount are designed to thread together, which allows for housings to be prepared before launch day, allowing for quicker integration when compared to black powder housings. A black powder ejection charge will be flown for redundancy, and timed to ignite two seconds after CO2 ignition, to reduce damage to the parachutes and shock cords if the CO2 is successful.

Nose cone ejection via black powder charge:

6. Ground Operations

6.1 Mission Control

The connection between the fuelling cabinet and mission control is facilitated through point-to-point Wi-Fi (PTP), which last year has been successfully tested up to 800m. There are two communication links between mission control and the vehicle: a LoRa link predominantly used during flight, and an indirect CAN channel interfaced through a local area network via ethernet. This redundancy enhances the resilience of mission control communications.

6.1.1 Electronics Software

Mission control serves as the central hub where all data feeds converge, allowing for the control and monitoring of sub-systems on both the rocket and the fuelling station. Building upon the design from Project Feynman, it hosts two primary services, packaged as Docker containers for ease of interchangeability and initialization: a user interface and a backend API. These services enable the team to view live data through a streaming service and provide remote-control capabilities for fuelling operations.

A Raspberry Pi, hosting the backend, provides a REST API for commanding the rocket, and MQTT sockets for streaming data from the rocket. This is received by a frontend Grafana user interface, running on a laptop. The Grafana UI makes requests to the REST API for controls and visualises the MQTT data sent by the Raspberry Pi.

Prototypes for the new UI and the necessary WebSocket wrappers around the brokers are currently being developed. Figure 38 below, from the last design cycle, is undergoing updates to reflect these changes.

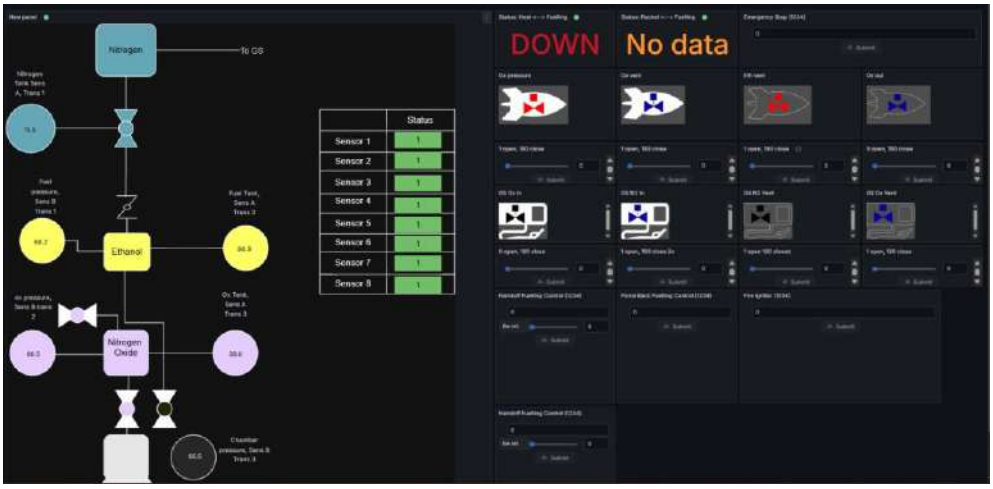

Figure 40 - Mission Control User Interface

6.1.2 Electronics Hardware

The electronic system for ground systems is divided into two main cabinets. The first houses the power sources: a backup battery and a 230VAC mains to 15VDC PSU. The two power sources are connected through ideal diodes, which enable seamless power transfer in case of a mains power loss. Since the mains PSU voltage is higher than the battery (15V vs 13Vmax), power will not be drawn from the battery during normal mains operations.

The second (main) cabinet contains the ground system control electronics and power regulation components required to create the necessary power rails. Panel mount connectors facilitate the transfer of power and data through the cabinet. A Raspberry Pi and Ground Station Control Unit form the main control electronics of the ground station. The Pi manages ground operations and communicates over CAN and connects to mission control through an Ethernet link to the PTP Wi-Fi network. The GSCU communicates with the Pi over CAN and control servos, and senses current draw and pressure transducers. 5V rails power the exhaust fan, GSCU, and Pi. A BEC creates the 7.4V needed for the servo valves, and a buck-boost converter generates 12V to power the pressure transducers. A 24V converter is used for the PoE Wi-Fi injector, and 18V is generated to charge the on-board batteries in the rocket and provide ground power. Additionally, there is a weather resistance air inlet to allow airflow over electronics. Component power loss and reliability were prioritised over size and weight.

6.2 Remote Fuelling Operations

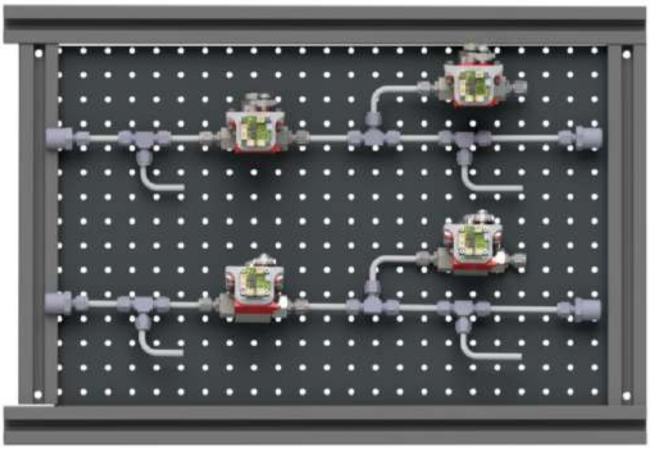

Figure 41 - CAD of the Fuelling Station and Feed Systems Panel

The fuelling station consists of a frame structure of extruded aluminium with rubber puncture-proof castor wheels for easy movement and secure movement to the launch rail. It is composed of three major parts: the panel holding the feed systems components, the electronics cabinet and the backup battery.

6.2.1 Feed Systems

The Ground Station Feed System comprises two separate lines (Figure 41): one designated for nitrogen and the other for nitrous oxide. At one end, each line interfaces with its respective gas cylinder, while the opposite end terminates at a pair of quick-disconnect fittings that interface with the rocket via flexible hoses. The System P&ID is shown in Figure 9 (feed system).

The lines are mounted onto a perforated base panel, providing a modular and reconfigurable structure to facilitate system modifications. Custom 3D-printed PLA brackets are strategically positioned along each line, enabling secure attachment to the panel using M5 fasteners. Each line consists of a pair of valves which are used to regulate flow and vent the flow if necessary. The automated valves employed in the system are identical in design to those integrated within the rocket. Each fill line is instrumented with two pressure transducers to enable real-time pressure monitoring and redundancy.

6.2.2 Fuelling Operations

	Stages	GS N2 Fill	GS N2 Vent	GS N2O Fill	GS N2O Vent	LV Eth Fill	LV N2O Vent	LV Eth Vent	LV N2O Pressure	LV Eth Pressure	LV N2O Run	LV Eth Run
Initial stage (10x)	1	OPEN	OPEN	OPEN	OPEN	OPEN	OPEN	OPEN	OPEN	OPEN	OPEN	OPEN
Verification (10x)	1.1	CLOSED	CLOSED	CLOSED	CLOSED	CLOSED	CLOSED	CLOSED	CLOSED	CLOSED	CLOSED	CLOSED
Safe system	1.3	CLOSED	OPEN	CLOSED	OPEN	CLOSED	OPEN	OPEN	CLOSED	CLOSED	CLOSED	CLOSED
Connect		Connect fuelling lines										
Fuelling	2.1	CLOSED	OPEN	CLOSED	OPEN	OPEN	OPEN	OPEN	CLOSED	CLOSED	CLOSED	CLOSED
End Fuelling	2.2	CLOSED	OPEN	CLOSED	OPEN	CLOSED	OPEN	CLOSED	CLOSED	CLOSED	CLOSED	CLOSED
Pre Press Load	3.1	CLOSED	CLOSED	CLOSED	OPEN	CLOSED	OPEN	CLOSED	CLOSED	CLOSED	CLOSED	CLOSED
Press Load	3.2	OPEN	CLOSED	CLOSED	OPEN	CLOSED	OPEN	CLOSED	CLOSED	CLOSED	CLOSED	CLOSED
End Press Load	3.3	CLOSED	CLOSED	CLOSED	OPEN	CLOSED	OPEN	CLOSED	CLOSED	CLOSED	CLOSED	CLOSED
Pre-Oxidiser	4.1	CLOSED	CLOSED	CLOSED	CLOSED	CLOSED	CLOSED	CLOSED	CLOSED	CLOSED	CLOSED	CLOSED
Ox-Load	4.2	CLOSED	CLOSED	OPEN	CLOSED	CLOSED	VENT 1sec	CLOSED	CLOSED	CLOSED	CLOSED	CLOSED
Post Ox	4.3	CLOSED	CLOSED	CLOSED	CLOSED	CLOSED	VENT 1sec	CLOSED	CLOSED	CLOSED	CLOSED	CLOSED
Pre press	5.1	CLOSED	CLOSED	CLOSED	CLOSED	CLOSED	CLOSED	CLOSED	CLOSED	CLOSED	CLOSED	CLOSED
Press	5.2	CLOSED	CLOSED	CLOSED	CLOSED	CLOSED	CLOSED	CLOSED	OPEN	OPEN	CLOSED	CLOSED
End Press	5.3	CLOSED	CLOSED	CLOSED	CLOSED	CLOSED	CLOSED	CLOSED	CLOSED	CLOSED	CLOSED	CLOSED
Pre-Launch	7	CLOSED	CLOSED	CLOSED	CLOSED	CLOSED	VENT 1sec	CLOSED	CLOSED	CLOSED	CLOSED	CLOSED
Disconnect		Disconnect fuelling lines										
GS safe	8	CLOSED	OPEN	COSED	OPEN	CLOSED	CLOSED	CLOSED	CLOSED	CLOSED	CLOSED	CLOSED
Hand-Over		Ground Station hands control of LV valves to rocket										
Launch	9	CLOSED	OPEN	COSED	OPEN							
E STOP	E	CLOSED	OPEN	CLOSED	OPEN	CLOSED	OPEN	OPEN	OPEN	OPEN	CLOSED	CLOSED
Safe Unload - Ox	U-LV-OX	CLOSED	OPEN	CLOSED	OPEN	CLOSED	CLOSED	CLOSED	CLOSED	CLOSED	OPEN	CLOSED
Safe Unload - Fuel	U-LV-F	CLOSED	OPEN	CLOSED	OPEN	CLOSED	OPEN	OPEN	CLOSED	OPEN	CLOSED	OPEN
Safe GS - Press	U-GS-N2	OPEN	OPEN	CLOSED	OPEN							
Safe GS - Ox	U-GS-OX	CLOSED	OPEN	OPEN	OPEN							

Figure 42 - Valve Operation Sequence

Figure 42 shows the operation sequence of each actuated valve during the fuelling process. The initial stage is a control stage to verify that valves are operational, before moving to a safe state for propellant loading. Valve commands will be sent individually, except during a pre-programmed emergency stop, which returns all valves to a pre-determined safe position. This vents all the tanks to make the launch vehicle safe to approach. The initial “safe” state is with all vents open, which then enables fuelling. Before launch, the propellant lines are disconnected from the launch vehicle, and the ground station hands control to the rocket once countdown is initiated. An emergency stop is accessible by both a physical button, as well as a software panel where a simple passcode is required to prevent accidental clicks.

6.2.3 Quick Disconnect Mechanism

A quick-disconnect mechanism is utilised to remotely disconnect the fuel hoses from the Launch Vehicle. This is achieved by using a pair of servo-driven cams to pull back a sleeve on the ’female side’ which then decouples the quick-disconnect fitting. The system has been tested to ensure actuation occurs even in the case of a single servo failing. To avoid the risk of ‘servo burn’, the servos are not under any loading and are de-activated when the fitting is coupled.

To avoid inadvertent misconnections, a pair of dissimilar quick disconnect fittings are used. (DTEG : 2.6.3). Furthermore, a 2mm steel cable is used as a back-up manual "Emergency Release” to actuate the mechanism in case of electronic failure. (DTEG 2.)

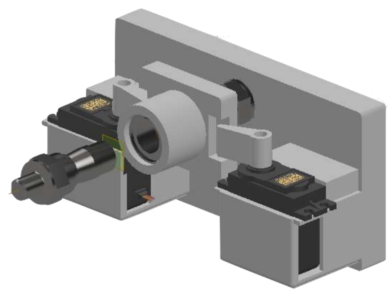

Figure 43 - CAD Render of QD Mechanism

7. Avionics

7.1 Avionics Overview

Project Waxwing's avionics system iterates on Feynman's architecture, prioritizing redundancy, reliability and efficiency. The avionics system has capability to control all aspects of the launch vehicle, from controlling the propulsion system, actuating airbrakes, and activating pyrotechnics for recovery deployment.

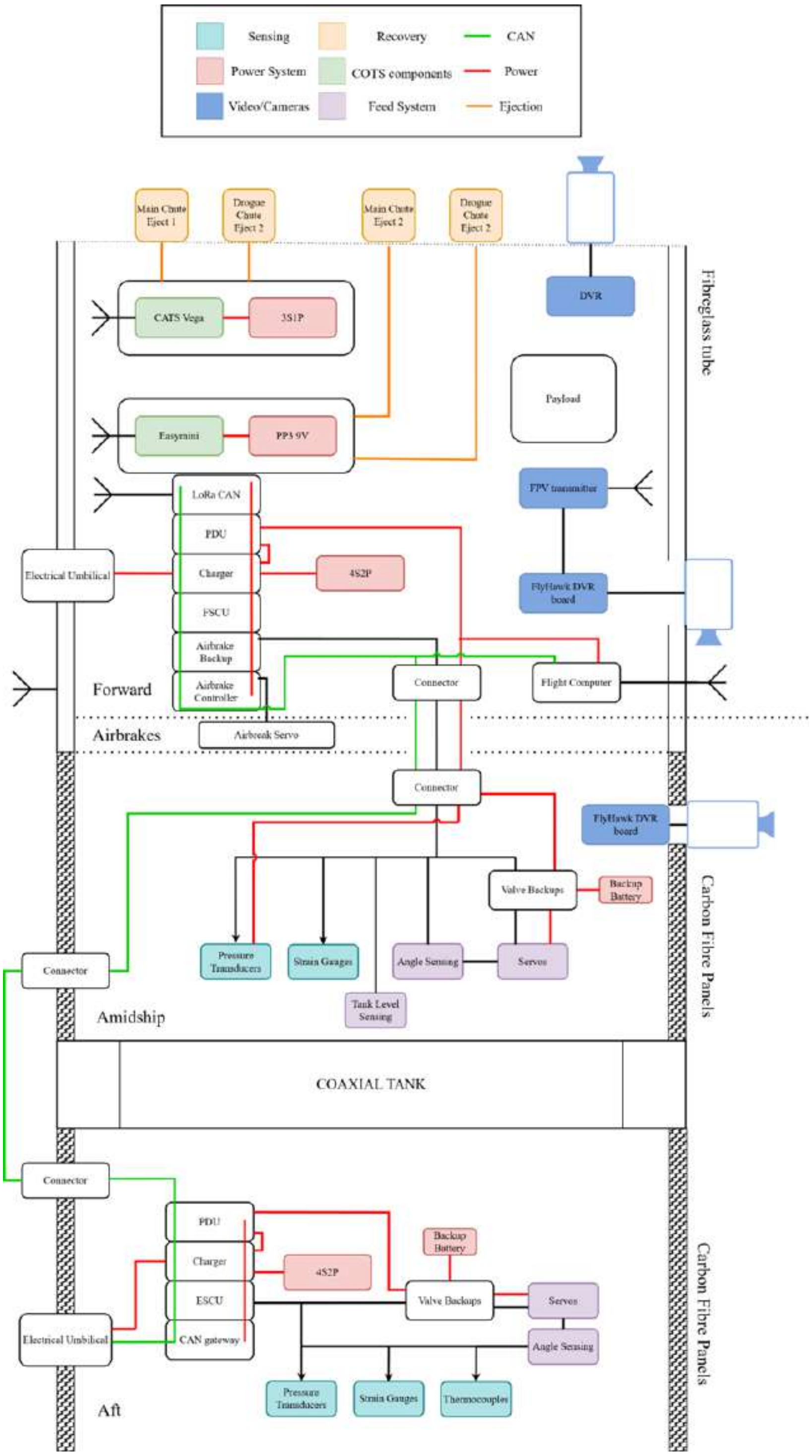

Figure 44 - Avionics Overview

7.2 COTS Avionics System

7.2.1 Recovery

Table 9: COTS avionics overview

Component	Max current consumption (mA)	Voltage input (V)	Calculated battery life (h)
CATS Vega	1000	7-24	36
Altus Metrum EasyMini	20	3.7-12	25
3S1P 18650 Battery Pack	3600	9.6-12.6	n/a
PP3	500	9	n/a

The system uses a CATS Vega and an Altus Metrum EasyMini to ensure a redundant recovery system. The CATS Vega is powered by an isolated 3S1P 18650 battery pack, which allows for 36 hours of operation time. The EasyMini is powered by a PP3 9V battery, which has been proven on multiple test flights to be a reliable power source for e-match ignition. This battery allows for 25 hours of operation time.

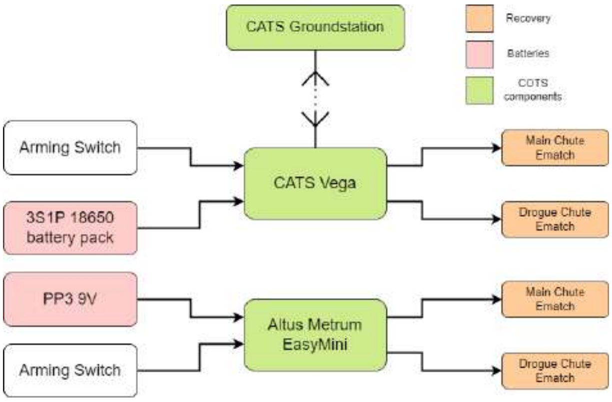

Figure 45: COTS avionics diagram

7.2.2 Camera System

Table 10: Camera overview

Component	Max current consumption (mA)	Voltage input (V)
Hawkeye Split	300	7-28
RunCam Mini DVR	250	3.3-5.5
HolyBro Atlatl FPV transmitter	300	5-23

The camera system utilises two Hawkeye Split V5 4K FPV camera systems, one RunCam Mini FPV DVR and a Holybro Atlatl HV Micro video transmitter. These are wired onto the main power bus, and give footage of stage separation, airbreak actuation, and a side view.

7.3 SRAD Hardware

The SRAD avionics system is developed around the STM32 series of microcontrollers (MCUs). This was chosen for the versatility of these chips, vast documentation and support, and previous experience with software development and debugging.

The boards are concentrated in two flight stacks to reduce the amount of wiring, complexity in mounting, and to assist testing without the launch vehicle. The forward stack is responsible for LoRa transmission, airbrake control, and feed systems control. The aft stack is responsible for Controller Area Network (CAN) transmission to the ground station, and engine control. Both stacks rely on their own four-series, two-parallel (4S2P) battery source.

7.3.1 [unnamed] Avionics Module Template

Figure 47: Avionics Stack Module Render

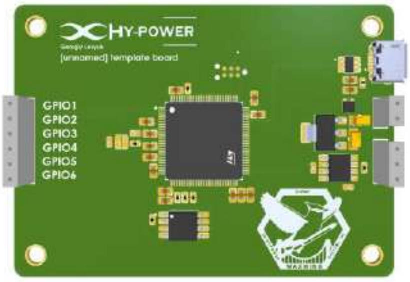

Figure 46: [unnamed] avionics module template

Table 11: [unnamed] Avionics Module Template Design

Dimensions [mm]	50x70
GPIO pins	6
Voltage Input	5V
CAN Channels	1

All boards use the [unnamed] schematic and layout template for use within the system. This template standardises key components used in the system as well as layout positions for the headers.

Standard parts include Low Dropout Regulators for power conversion to the MCU's 3V3 required voltage, a CAN transceiver for the launch vehicle's CAN 2.0 bus, W25Q128x 16Mb flash memory for data logging, connector footprint for debugging, headers, USB connections and peripherals. This assists the team by ensuring that there is a strong foundation to build upon, and to keep back up stock of common components in case of board failures. Six GPIO pins were included in the system to aid various external functions which were desired in the previous cycle, such camera control.

7.3.2 Feed Systems Control Unit (FSCU)

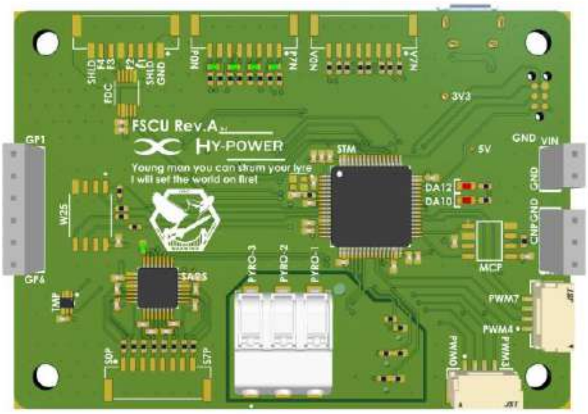

Figure 48: Feed Systems Control Unit Board

Table 12: FSCU Design

Spec	Quantity
PWM Control Channels	8
External Shunt 15A Ammeters	8
On-board Shunt 30Ma Ammeters	16
I2C Interfaces	2
Farad Meter Channels	4
Ambient Thermometer	1
6A Pyrotechnic Relays	3
Thermocouple / Misc Voltmeter Channels	8

The Feed Systems Control Unit (FSCU) provides plumbing control and monitoring capabilities throughout the launch vehicle and ground station. The FSCU makes use of the Texas Instruments ADS131 and FDC1004 to take voltage and capacitance readings which are combined with shunt resistors, ambient thermometers and AC shields to form ammeters, thermocouple interfaces and farad meters.

It is also equipped with supplementary Pyrotechnic Relays, Thermocouple interfaces to service additional feed system related systems. There are three variations of the FSCU, with the other two being the Engine Control Unit (ECU), located in the Aft Stack, and the Ground Station Control Unit (GSCU). The FSCU makes use of the Texas Instruments ADS131 and FDC1004 to take voltage and capacitance readings which are combined with shunt resistors, ambient thermometers and AC shields to form ammeters, thermocouple interfaces and farad meters.

The FSCU makes use of the Texas Instruments ADS131 and FDC1004 to take voltage and capacitance readings which are combined with shunt resistors, ambient thermometers and AC shields to form ammeters, thermocouple interfaces and farad meters.

7.3.3 Strain Gauge Monitor

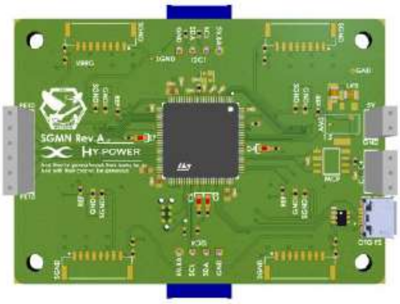

Figure 49: Strain Gauge Monitor Board

Table 13: Strain gauge Monitor Design

I2C Interfaces	2
On-board Shunt 30Ma Ammeters	32
Flash chips	4
Storage types	Flash

The Strain Gauge Monitor allows for reading up to 32 strain gauges, for the analysis of stringer sections, airbrake structures and the tank. Each strain gauge channels can be configured between on-board or external bridge circuits depending on assembly configuration and the Monitor provides two I2C buses to allow for expansion with additional digital sensors in future design cycles.

7.3.4 Hall Effect Angle Sensing

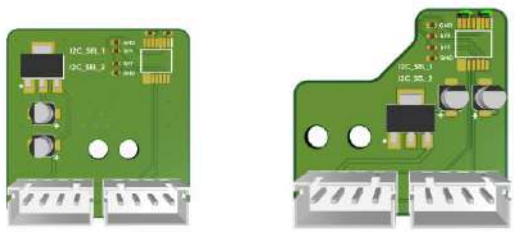

Figure 50:(L) 1/2 inch hall effect board, (R) ¾ inch hall effect board

Table 14: Hall Effect Angle Sensing Design

Input Voltage [V]	5V (12V MAX)
Sensing method	Hall-effect
Inputs/Outputs	I2C, angle of valve
Dimensions	

The hall effect angle sensor uses a hall effect sensor to measure the angle of a diametric magnet that is mounted to the valve control gear. The sensor ideally should be mounted on the axis of rotation of the magnet, but due to space constraints, an off-axis alignment will be used. This will not diminish performance significantly. The board uses the A1335 hall effect sensor to detect the rotation of the magnetic field lines. The sensor provides a digital signal that is transmitted using the I2C protocol. Mechanism to manually set-up the I2C address of the sensor is available on the board, allowing 4 different pre-programmed addresses to be used. A voltage regulator and decoupling capacitors ensure a stable 5V power supply.

7.3.5 Valve Backup Board

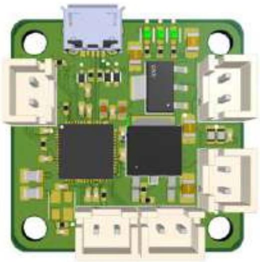

Figure 51: Valve Backup Board

Table 15: Valve Backup Board Design

Input Voltage [V]	7V4, Bat
Output Voltage [V]	7V4
Inputs	PWM, I2C
Outputs	PWM, 7V4
Dimensions [mm]	30x30

All feed system valves will have an electronic backup board. The valve backup board has two preventable failure cases: losing either main 7V4 power or losing main PWM signal. In the case of main 7V4 power failing, the backup board automatically switches to backup battery power. This is controlled by a MOSFET logic gate, with no input from an MCU. The valve backup board operates PWM by receiving the PWM signal from the FSCU/ECU, monitoring the signal exists, then parsing it through. If at any point the valve backup board does not receive a PWM signal for a set amount of time, the board will revert to its fail-state, which will be pre-programmed in to be fail open or close depending on the valve location.

7.3.6 Charging Board

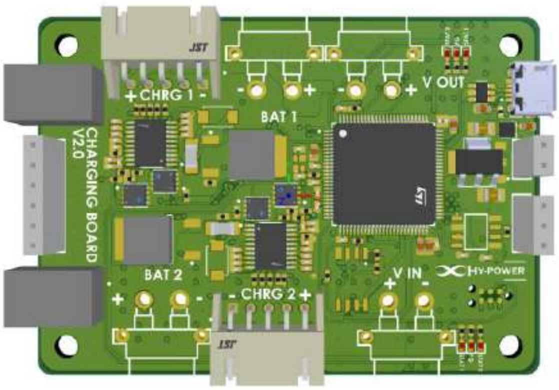

Figure 52: Charging Board

Table 16: Charging Board Design

Input Voltage [V]	18
Output Voltage [V]	12.8-16.8
Battery Charging	4S2P
Sensing	Voltage, Temperature, Current

The Charging Board is based around the Texas Instruments BQ24616RGER chip, which has capability to charge a 1-6S li-ion battery pack, and offers input overvoltage protection, temperature control, battery overcurrent and overvoltage protection. The BQ2461 has power path switching to ensure that the batteries are not getting discharged simultaneously while charging. The Texas Instruments BQ7692006PWR acts as a Battery Monitoring System (BMS) which ensures that all the cells in the battery pack are uniformly charged by regulating the current flow in each cell. The charging board receives 18V from the ground station and supplies 16.8V to the BMS to charge the 4S battery pack. The board sends voltage measurements and charging control via CAN. The batteries used are Panasonic NCR 18650B 3.4Ah Li-ion cells, in a 4S2P configuration, which provide a 16.8V 6.8Ah battery pack. This provides of approximately 3 hours after lift-off.

7.3.7 Power Distribution Unit (PDU)

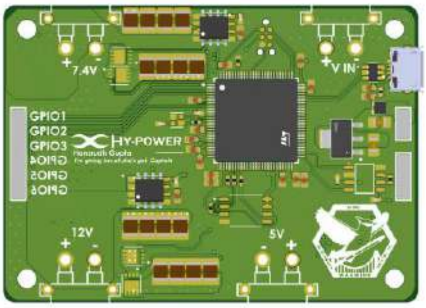

Figure 53: Power Distribution Unit Board

Table 17: Power Distribution Unit Design

Input Voltage [V]	12.8-16.8
Output Voltage [V]	5V, 7V4, 12V
Max Current	4S2P
Sensing	Voltage, Temperature, Current

The Power Distribution Unit (PDU) board is designed to manage and regulate power to ensure stable and efficient power to all connected subsystems (valves, servos and other PCBs). It is powered by a 4S2P Li-ion battery pack. For matching the varying required voltage requirements, the PDU uses two LM25145 buck converters to step down the voltage to 12V and 7.4V and one TPS56637 buck converters to generate 5V output. This setup provides different voltages from 4S2P battery input.

For current monitoring the board incorporates the ASC712 Hall Effect current sensors on each output rail which can measure currents in 20 Amps. These sensors provide accurate measurements to track power consumption. By integrating hall effect sensors, the board reduces the use of resistors which ensures thermal efficiency.

7.3.8 LoRa

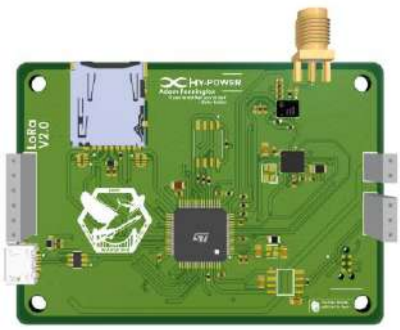

Figure 54: LoRa Board

Table 18: LoRa board Design

Inputs	2.4 GHz LoRa
Outputs	2.4 GHz LoRa
Storage types	SD/Flash

Long-Range (LoRa) communication is handled by two boards: LoRa onboard and LoRa ground. The LoRa onboard utilises an STM32F412RET6 MCU to enable interfacing between LoRa and external systems, using a 2.4GHz SX1280 LoRa transceiver and an SE2431L front-end module. The LoRa transceiver communicates with the MCU via SPI. FreeRTOS is used to perform tasks at consisten intervals, relaying messages from the ground station to the CAN bus, transmitting heartbeats, and logging all data to an SD card.

7.3.9 CAN Gateway

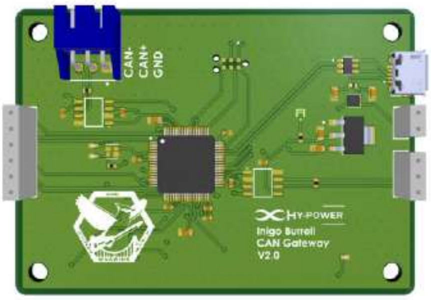

Figure 55: CAN Gateway board

Table 19: CAN Gateway Design

CAN I/O buses	2
Flash chips	4
Storage types	SD/Flash

The CAN gateway is a common node on the Ground System and Launch Vehicle CAN buses. The board is based around the STM32H523RCT7 microcontroller, selected for the necessary CAN FD, SDMMC and QSPI connectivity options. There are two CAN ports, to provide CAN communication at up to 1Mbps. The board contains four W25Q128JVSIQ flash chips, providing a total of 64MB of flash storage. These are for storing network history while the rocket is in flight, which is then written to a microSD on touchdown. During ground operations, it facilitates bi-directional communication across the two separate networks. Once a message is received in a reception FIFO queue, the interrupt-triggered callback function is immediately called, re-transmitting the frame with a higher priority CAN ID. This combination of higher priority IDs and configuration of interrupts prevents any buffer overflow/ data loss. During flight, the 'gateway' aspect is terminated, and the board acts as a data logger for the Launch Vehicle. This board also monitors the heartbeat of all other connected boards, recording offline if an interval greater than the specified maximum threshold has elapsed since the last time a message originating from a node has been detected. This threshold has provisionally been set to 1 second. All data logged is initially stored to flash chips, then transferred to an SD card after parachute deployment.

7.3.10 Flight Computer

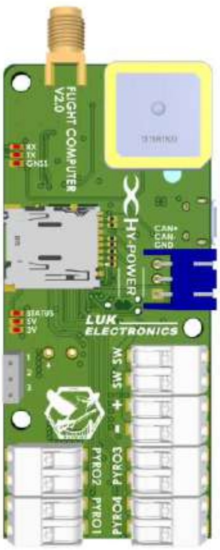

Figure 56: Flight Computer Board

Table 20: Flight Computer Design

Input Voltage [V]	3.7-29V
Pyro Channels	4
Storage	32MB flash, SD card interface
Peripherals	CAN bus, I2C, 3x PWM outputs
Sensors	32G 6DOF IMU, 200G 3DOF IMU, 0-30km Barometer
RF communication	868/915 MHz LoRa, 1Mm theoretical range GNSS telemetry
Dimensions [mm]	35x80

The flight computer is based around the STM32H523RCT7 microcontroller. The flight computer is intended to function as a computer for current and future HyPower projects, building into it abilities for multiple pyrotechnic outputs, the ability to communicate on multiple protocols, redundant sensors specified for high acceleration and altitude flights, with long-range communication and tracking.

7.3.11 Flight Computer Ground Station

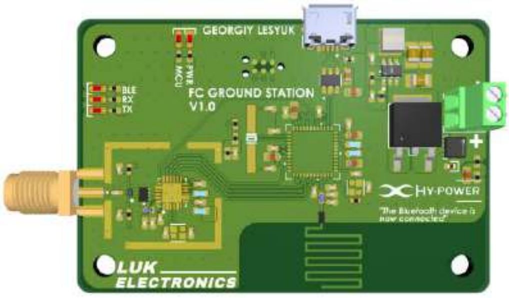

Figure 57: Flight Computer Ground Station Board

Table 21: Flight Computer Ground Station Design

Voltage Input [V]	3.7-29V
RF communication	868/915 MHz LoRa, BLE
Dimensions [mm]	40x60

The ground station is based around the STM32WB55CGU6, chosen for its integrated Bluetooth Low Energy (BLE) capability. The ground station will connect to a mobile phone via BLE, and use mobile sensors such as GNSS and IMU data to correlate with rocket-supplied data. Data is received from the flight computer and relayed to the user. Minimal processing power is required, as all intensive tasks can be delegated to the user's mobile. The board will track the rocket using two methods, receiving GNSS data from the rocket, and pinging the flight computer through LoRa to measure distance by acknowledgement time. This ensures the launch vehicle can be tracked even if GNSS signal is lost.

7.3.11 Airbrake Controller

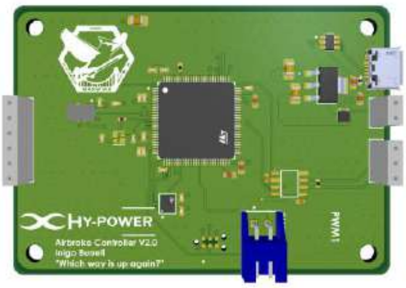

Figure 58: Airbrake Controller Board

Table 22: Airbrake Controller Design

Outputs	PWM
Sensing chips	32G 6DOF IMU, 0-30km Barometer
Storage types	SD/Flash

The airbrake controller reads sensor data from the MCP2562 barometer and LSM6DSO32TR 32G, 6DOF digital accelerometer and gyroscope. Each is interfaced via its own SPI channel alongside an additional dedicated EXTI pin to allow interrupt-based handling of the barometer. Sensor noise is mitigated using digital filters on each IC and further low-pass filters. Two PWM channels individually control the airbrake locking and actuating servos. Locking servos are actuated upon system power-up.

7.3.12 Airbrake Backup

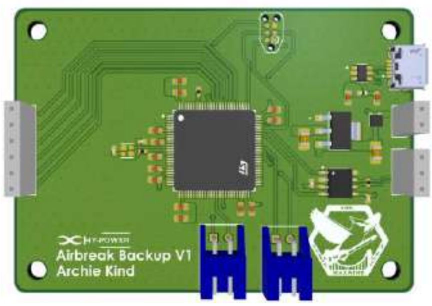

Figure 59: Airbrake Backup Board

Table 23: Airbrake Backup Design

Inputs	PWM
Outputs	PWM
Storage types	Flash

The airbrake backup board monitors PWM generation from the locking and actuating servo channels on the airbrake controller. If the correct signal is not detected for the relevant flight phase, it generates the correct output and/ or transmits a CAN message to the airbrake controller to halt further PWM operations.

7.4 RF System

7.4.1 Blade-IFA antenna array

EuRoC requirements dictate an omnidirectional antenna window for all transmission lines form a launch vehicle. Typically, this means replacing a section of carbon fibre airframe with glass fibre, which reduces the strength-to weight of the structure. The blade-IFA antennas designed are intended to conform to the exterior of the launch vehicle's airframe and is compatible with carbon fibre section without compromising strength or weight. A preliminary design for a wraparound microstrip patch antenna design was attempted, but complications with bandwidth, cost and simulation difficulties required an alternate antenna design.

The antenna array is designed or the 915 MHz band, with three individual blade-IFA antennas positioned 120 degrees around the rocket, giving an omnidirectional gain pattern. The array has a simulated bandwidth of 50 MHz, and a simulated gain of 1.855 dBi at 915 MHz. The antenna has an aluminium 6082 structure, with PTFE insulation for the feed line.

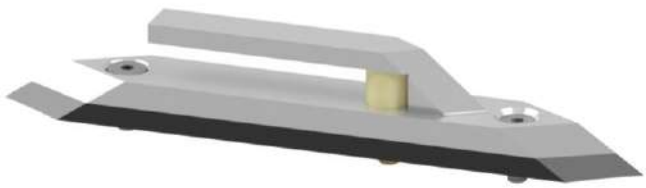

Figure 60: Blade-IFA antenna element

7.4.2 Four-way Wilkinson Power Divider

To realise an antenna array, a power splitter is necessary to use the system from one input port. This requires a minimum of a 1 to 3 power splitter. Wilkinson Power Dividers are a class of power divider circuits that can split signals into two equal phase outputs signals, or work in the opposite direction to combine two equal phase signals.

The Wilkinson divider (Fig 2a) was designed to JLCPCB's 2-layer board stack-up, for the frequency band of 915 MHz. A four-way splitter was designed to reduce complexity and improve isolation, when compared to a 3-way splitter, with a termination cap used on one of the output ports. The board interfaces with standard SMA components and SMD resistors to achieve a simulated useable bandwidth of 1000 MHz centering on 915 MHz, which is acceptable for this use case.

Table 24: Waxwing Antenna Table

Component	Antenna	Voltage (V)	Use
CATS Vega	ExpressLRS Moxon	2.4 GHz	LoRa Transmission
CATS Vega	APAE1575R1820ABDC1-T Ceramic Patch	1.575 GHz	Receive GNSS
LoRa board	ExpressLRS Moxon	2.4 GHz	LoRa Communication
FPV Transmitter	Monopole	5.8 GHz	Video Transmission
Flight Computer	Blade IFA Antenna Array	915 MHz	LoRa Communication
Flight Computer	ATPG1590R2540A Ceramic Patch	1.575 GHz	Receive GNSS

7.5 Software Overview

7.5.1 RTOS and DMA

Both RTOS (Real-Time Operating System) and DMA (Direct Memory Access) are technologies that attempt to ensure the processor is able to execute critical transactions as much as required, without being blocked by other processes.

DMA enables communication with peripherals to occur in the background, freeing up the processor for other tasks in the meantime. The use of interrupts allows customisation of what occurs before the read or write begins and once it has finished.

RTOS allows high priority processes to interrupt those with a lower priority preventing critical processes being blocked by non-critical ones. Built-in support for RTOS within STM32IDE makes it easy to implement. However, not all boards will find its use beneficial, particularly simpler ones with fewer potentially blocking processes. Decisions are being made on a board-by-board basis regarding its use.

7.5.2 CAN Bus

A CAN bus is used for communication between the boards, both onboard the rocket and the ground. This protocol was chosen due to its widespread use and support onboard STM32 microcontrollers. Its vast documentation and support makes development easier and faster, as well as being simpler than other protocols used in aerospace.

The CAN bus has been discussed at length with the obvious intricacy being the CAN gateway, and the best way to ensure reliable transmission of data between busses. The primary concern with this board was the possibility of having either the FIFO-queues that store received messages for processing or the mailboxes that store messages to be transmitted fill up, therefore resulting in the loss of data. Many solutions were discussed, including creating larger buffers to store messages in among others. Eventually we decided on assigning each message a high-priority CAN ID which would result in the messages being immediately moved from the transmission mailbox to the bus. Careful attention is being paid to the assignment of CAN IDs and therefore the prioritisation of different devices on the bus.

7.5.3 Memory Management

Writing code in C, rather a memory-safe language, opens up many vulnerabilities. Care is taken throughout the software, as well as best practices taken, to avoid memory issues. The easiest way to prevent such issues is to avoid dynamically allocating memory and statically allocating memory at the start of the program. This not only means garbage collectors are needed, but also increases performance, and makes the code far more predictable. Aside from FreeRTOS, which has its own memory management

7.6 Avionics Integration

7.6.1 Forward Avionics Bay

The forward stack is designed for vertical mounting of all components shown in figure [x], which include the recovery flight computers, forward stack, magnetic arming switches, SRAD flight computer, cameras and the Wilkinson power divider. These components are distributed across three panels. A central cut out and horizontal mounting structure have been made to house the forward stack. Boards requiring radio transmission, i.e. the forward stack containing the LoRa board, Flight Computer and CATS Vega, have been placed in a vertically central position to maintain distance from metallic couplers, and antennas are separated . Flutes were added to the bottom for ease in assembly onto 3 M8 rods that run through the length of the avionics bay, connecting the sled to the blast bulkhead and airbrake assembly. Cutouts are included along the spine to allow wiring between components on different panels.

7.6.2 Aft Avionics Stack

In the aft avionics stack, the boards are slotted onto each other and secured using spacers and bolts (not shown). This will ensure that, during flight, vibrations do not cause the boards to lose contact, which would be fatal to the entire system. The aft stack-up is shown mounted to the feed system in figure [x]. This design achieves the original objective of creating a robust board structure that optimizes space utilisation and minimises wiring.

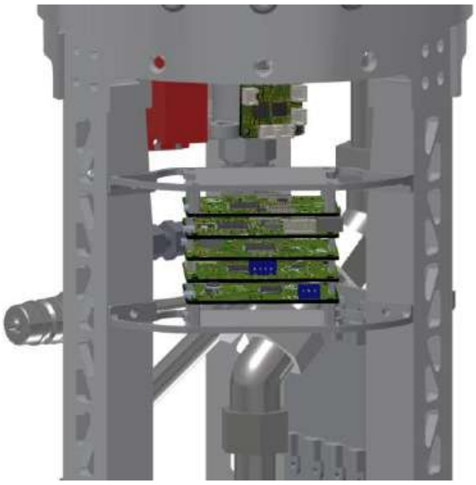

Figure 61: L, Avionics Bay with forward stack. R, aft stack mounted in the aft plumbing

7.6.3 Umbilical Connection

The umbilical connection provides power and a CAN to the launch vehicle while in ground operation. These connections are based on 4-pin magnetic pogo pin connectors. The aft umbilical provides power and CAN to the aft stack for the gateway. The forward umbilical only provides power. Power is supplied at 18V from the ground station and is fed into the charging boards. Each pin is rated for 4A, allowing up to 8A of power to flow through a single connector. This high current budget allows for simultaneous charging and reliable valve operation.

The umbilical connection provides power and a CAN to the launch vehicle while in ground operation. These connections are based on 4-pin magnetic pogo pin connectors. The aft umbilical provides power and CAN to the aft stack for the gateway. The forward umbilical only provides power. Power is supplied at 18V from the ground station and is fed into the charging boards. Each pin is rated for 4A, allowing up to 8A of power to flow through a single connector. This high current budget allows for simultaneous charging and reliable valve operation.

7.6.4 Arming Switches

Previous projects in HyPower designed for screw switches to arm the avionics, and thus the recovery pyrotechnics, of the launch system. Screw switches have been found through testing to be difficult to operate reliably. Project Waxwing's arming system uses XT-60 plugs to complete the switch circuits of all three flight computers. The XT-60 plugs are located in the aft of the launch vehicle, running wires through the strake, to ensure the launch vehicle can easily be safely de-armed.

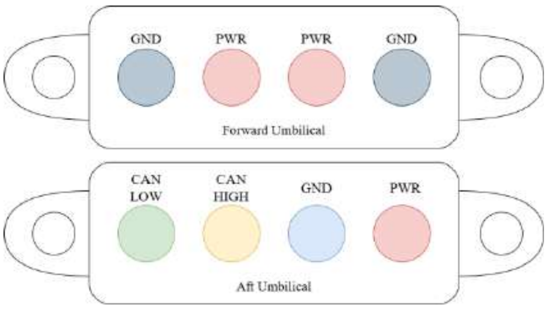

Figure 62: Avionics Umbilical Connector Pinouts

8. Payload – The RAINDROP

This section introduces the folding drone payload, named the RAINDROP - a compact system designed to operate after release from a rocket. It provides a lightweight and versatile platform capable of tracing rocket trajectories and conducting atmospheric measurements.

The objectives of this design are to follow the rocket's trajectory after deployment, collect environmental data, and serve as a proof of concept for future missions with more advanced instrumentation. A key goal is to measure and analyse the impacts of rocket emissions on the atmosphere, providing critical insights into their environmental effects. Folding drones like this example offer portability, rapid deployment, and adaptability, making them promising tools for scientific research, reusable launch vehicle development, and long-term atmospheric monitoring.

Table 25 - Payload Subsystem Table

Subsystem	Description
Flight Controller	CubePilot flight controller for stabilization, waypoint navigation,
Mission Computer	Raspberry Pi Zero for mission, payload data handling, and camera control.
Folding Mechanism	Slider actuated by a servo and belt to unfold propeller arms with a limit switch to confirm full deployment and a locking mechanism.
Deployment Detection	Hall effect sensor triggers initial sequence on release from the payload bay.
Parachute System	90 cm drogue parachute to reduce descent speed to approximately 5 m/s.
Payload Sensors	Camera for visual recording and gas sensor (MQ-135) for measuring combustion byproducts.
Communications	CATS Vega module for radio broadcasting of telemetry and mission data to the ground station.

Table 26 - Payload Material Specification

Component	Specification
Frame Material	FDM-printed PLA parts and carbon fibre tubing
Propellers	8-inch folding
Folding Mechanism	Belt-driven with limit switch and locking arm and various metal fixtures
Payload Securing	Foam inserts in nose cone housing the payload and its parachute

8.1 Mechanical Design and Structure

The payload is a folding drone designed to fit within a 3U CubeSat volume with a total mass of 1000g. The frame combines FDM-printed components with carbon fibre tubing. Foam inserts secure the payload inside the rocket nose cone to prevent movement during launch and ensure safe deployment. Folding 8-inch propeller blades are used for compact storage and efficient flight. The folding mechanism uses a belt with a limit switch and locking arm.

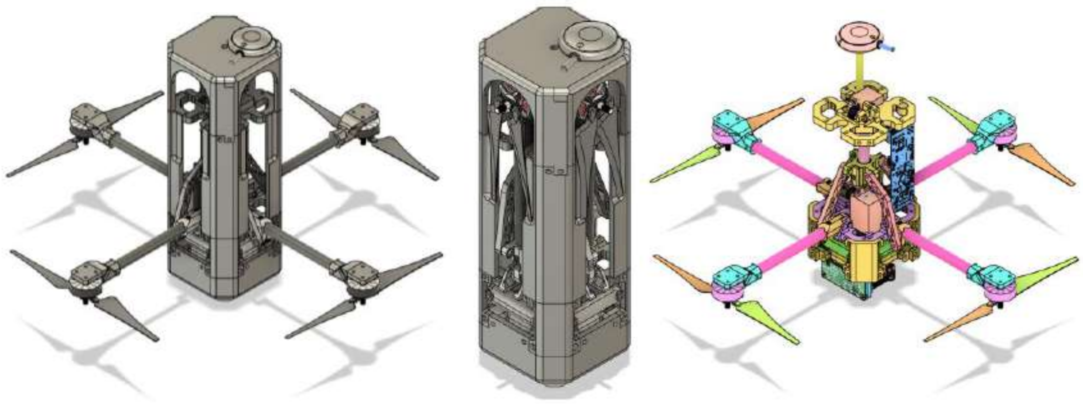

Figure 63 - CAD Renders of the Drone Payload

8.2 Power System

Powered by a 14.8V 3200 mAh Li-ion battery. A buck converters supply the Raspberry Pi and servos, and other powers the CubePilot Cube Orange+. Runtime estimates and safety considerations are included.

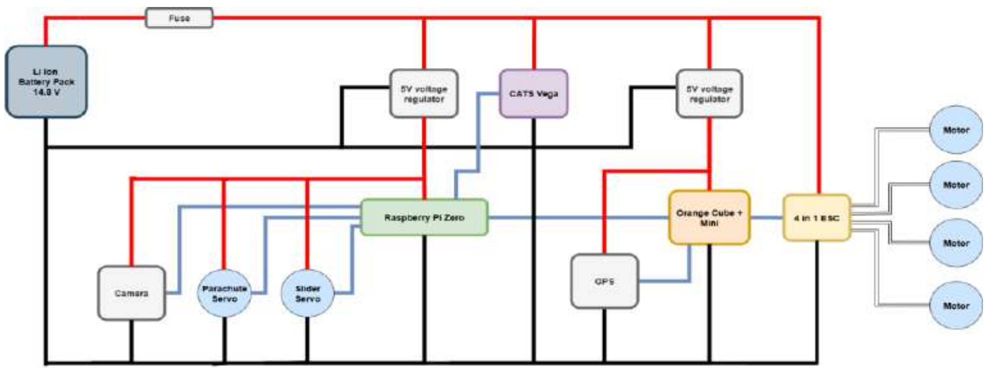

Figure 64 - Payload Drone Internals

8.3 Communications and Control

Raspberry Pi Zero running Linux calculates waypoints and communicates with the CubePilot Cube Orange+ via MAVLink. CATS Vega broadcasts telemetry signal. Payload includes a 1-inch LCD display and buttons for configuring the mission and testing subsystems before launch.

8.4 Sensors

Camera and MQ-135 gas sensor for measuring combustion byproducts. The MQ-135 detects ammonia (NH_3), carbon dioxide (CO_2), alcohol vapours (ethanol, isopropanol), toluene, acetone, and smoke, enabling air quality and emission assessment. As more rockets are launched in the future, this project serves as a proof of concept and platform for sophisticated testing equipment to study the effects of rocket emissions on the atmosphere at high altitudes.

Table 27 - Drone Sensors

Sensor	Function
MQ-135	NH_3, CO_2, alcohols, toluene, acetone, smoke, measures in ppm
Raspberry Pi Camera Module 3	Visual recording of flight

8.6 Deployment and Parachute System

Deployment is detected using a Hall effect sensor, which triggers the initial sequence upon release from the payload bay. Upon payload deployment, a 90 cm drogue parachute is passively released to reduce descent speed to approximately 5 m/s. This combined system ensures reliable activation of the descent phase and safe stabilisation of the payload before powered flight operations begin.

8.7 Flight Stages

The drone's flight operation is divided into three primary phases following deployment from the rocket nose cone, with deployment detection and sensors active throughout:

- **Deployment:** Hall effect sensor detects release from the payload bay, triggering parachute deployment and sensor activation.
- **Align Phase:** Drone stabilizes and aligns toward the trajectory while descending gently.
- **Drop Phase:** Drone follows waypoints along a defined 3D path, actively controlling movement to trace the rocket's trajectory.
- **Land Phase:** Controlled vertical descent toward the landing site, with motors modulating descent speed and telemetry recording until landing.

If propeller arms fail to unfold (detected by an end limit switch), the parachute will remain attached to prevent uncontrolled descent. In the case of a GPS lock failure, a direct land from deployment location would be performed.

8.8 Testing and Validation

8.8.1 Simulation Tests

The first stage of testing was a Python-based simulation has modelled the drone's powered descent and parachute phases. The simulation included simplified rocket trajectory to 3 km altitude with horizontal drift, quadcopter payload deployment at apogee, passive parachute-controlled descent, and powered descent phases.

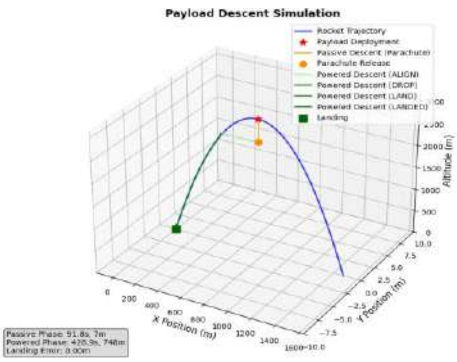

Figure 37: Payload Simulation Results

8.8.2 Hardware Tests

Hardware testing will verify the full functionality of the drone under realistic conditions. These tests include static deployment, hover tests, waypoint navigation, sensor verification, full powered descent, battery endurance flight test to verify expected runtime, telemetry and communication checks, and safety evaluations.

9. Conclusions and Outlook

Project Waxwing represents the most technologically advanced launch vehicle ever produced by BristolSEDS. It stands as a marker of the technical ability and the perseverance of our 60 team members.

Waxwing has served as a learning platform for all aspects of our launch vehicle, iterating on Project Feynman's design.

In propulsion, the team has demonstrated a novel coaxial swirl injector design, paired with the first ever CP-1 aluminium rocket engine. While the engine achieved a partially successful hot fire, it marked a significant milestone demonstrating our capabilities and laying the groundwork for future propulsion systems. Waxwing has also marked the first integrated hotfire of a liquid rocket engine by the University of Bristol.

Improvements have been seen in our manufacturing techniques, as well as the application of analysis for structural isotropic and composite optimisation. This has been applied to parts such as the stringers, tank and airbrakes. The fins have been optimised even further through numerical analysis, down selecting the aerofoil shape to improve stability while reducing drag and weight. The avionics have seen a complete architectural consolidation, redefining how the avionics are integrated through a new stackup structure, as well as exploring completely new areas such as antennas.

10. References

Bayvel, L. a. (2019). *Liquid atomization.* Abingdon: Routledge.

Bazarov, V. Y. (2004). Design and dynamics of jet and swirl injectors. In *Liquid rocket thrust chambers: aspects of modeling, analysis, and design* (pp. 19-103). Reston, VA: AIAA.

Bell, Ian H. , Wronski, Jorrit , & Quoilin, Sylv. (2014). Pure and Pseudo-pure Fluid Thermophysical Property Evaluation and the Open-Source Thermophysical Property Library CoolProp. *Industrial & Engineering Chemistry Research*, 2498--2508.

ECSS-Q-30-02A Failure modes, effects, and criticality analysis. (2001, September 7). ESA.

ESDU. (1991). *ESDU 91022 - Thermophysical Properties of Nitrous Oxide.* ESDU.

Heister, S. D. (2019). *Rocket Propulsion.* Cambridge University Press.

Hyde, S., & Okninski, A. (2016). *Silicon Oil Thermal Barrier System for in Space Applications.* Space Propulsion.

NASA. (1976). *Liquid rocket engine injectors - NASA SP-8089.* Cleveland, Ohio: NASA.

NASA. (1976). SP-8089 Liquid Rocket Engine Injectors . *NASA Technical Reports Server*.

NASA Glenn Research Center. (2025, September 4). *Flight Equations with Drag*. Retrieved from https://www1.grc.nasa.gov/beginners-guide-to-aeronautics/flight-equations-with-drag/

Parker. (2024, 09). *Parker O -Ring Handbook*. Retrieved from Parker: https://www.parker.com/content/dam/Parker-com/Literature/O-Ring-Division-Literature/ORD-5700.pdf

Pedersen, T. (2018, 6 4). *copenhagensuborbitals.com*. (copenhagen suborbitals) Retrieved 09 16, 2024, from https://copenhagensuborbitals.com/a-few-%ce%bcm-of-sio2-please/

Ponomarenko, A. (2012). *Thermal Analysis of Thrust Chambers.* Rocket Propulsion Analysis.

Rohdenburg, F. H. (2020). Experimental lifetime study of regeneratively cooled rocket chamber walls. *International Journal of Fatigue, 138*, 105649.

Saarimäki, J. (2015). *Effect of Dwell-times on Crack Propagation in Superalloys.* Linköping University .

Trident Racing Supplies. (n.d.). *Bolts-Commercial grade*. (Tident Racing Supplies) Retrieved 04 12, 2024, from https://tridentracing.co.uk/product/bolts-commercial-grade/

Yasuda, K, Nakata, D, Okada, K, Uchiumi, M., Higashino, K. , & Imai, R. (2018). N2O tank emptying characteristics on a running rocket sled. *Joint Propulsion Conference*, 4596.

Zimmerman, J. &. (2013). Review and Evaluation of Models for Self-Pressurizing Propellant Tank Dynamics. *Zimmerman, Jonah & Waxman, Benjamin & Cantwell, Brian & Zilliac, Gregory. (2013)49th AIAA/ASME/SAE/ASEE Joint Propulsion Conference.*

11. Appendices

A. System Data

A.1. Propulsion Overview

Table 28 - Table Showing an Overview of the Technical Specifications of the Propulsion System

Metric (unit)	Value	Notes
Engine & Injector Mass (kg)	6.2	
Nominal Thrust (kN)	5.0	
Burn Time (s)	5.0	
Nominal Impulse (kNs)	20.0	
Designed Fuel Type	IPA	Isopropyl Alcohol *(Ethanol as a substitute provides the same performance)*
Oxidiser Type	N2O	Nitrous Oxide
Nominal ISP (s)	190	Achieved at Sea Level during hotfire test at Airborne Engineering
Tank Mass (kg)	23.5	
Oxidiser Volume (l)	14.4	
Fuel Volume (l)	5.28	
Nitrogen Tank Mass (kg)	1.93	
Forward Plumbing Mass (kg)	5.4	
Aft Plumbing Mass (kg)	2.2	
Ignitor Type	StageGear Le Maitre PP050	
Ignitor Duration (s)	10	
Ignitor Burn Height (ft)	20	

A.2 Launch Vehicle Overview

Table 29 - Table Showing an Overview of the Technical Specification of the Launch Vehicle

Metric (unit)	Value
Length (mm)	3972
External diameter (mm)	200
Apogee (m)	3000
Maximum velocity (m/s)	239
Maximum acceleration (m/s^2)	63.2
Weight (kg)	63.6
Velocity off the rail (m/s)	36.1

A.3 Length Breakdown

Table 30 - A Table Breaking Down the Length of the Launch Vehicle

Component	Length (mm)
Fin spillage	67
Fin can	691
Coaxial Tank	884
Panels/forward stringers	865
Airbrakes	25
Avionics Bay	640
Nosecone Coupler	30
Nosecone shoulder	370
Nosecone	400
Total	3972

A.4 Weight Breakdown

Table 31 - A Table Breaking Down the Masses of the Launch Vehicle

Section	Weight (kg)
Aft propulsion	8.2
Fin can	1
Aft Stringers	1.2
Aft Avionics	0.75
Tank	23.5
Forward Plumbing	7.75
Forward Stringers	2.1
Panels	1.2
Antennas	0.3
Airbrakes	4.4
Forward Avionics	5
Avionics Bay	1.3
Nosecone Coupler	1.7
Nosecone	0.8
Payload	1
Recovery	3.4
Total	63.6

B. Detailed Testing Reports

B.1 Ground Recovery Testing

Initially, pull out tests of the system were conducted to ensure that the lines and chute could deploy smoothly. The team then tested the ejection charges, including sufficient separation and tender descender deployment. This was then incorporated into a combined test, in which the ejection charges were fired, a pull out of the chutes was done and then the tender descender fired. The team then approached the vehicle and continued the pull-out test to ensure that the full recovery operation could be successful. Once each of these testing stages was passed the recovery method was approved for flight by UK Rocketry Association RSOs.

Figure 65 - Pictures Showing Ground Recovery Testing

B.2 Flight Recovery Testing – Subscale Flight 1

HYPOWER BRISTOL – POST FLIGHT REPORT FOR EuRoC'24 SUB-SCALE VEHICLE TEST 1

Authors: ***L. Macbeth, J. Cox*** University of Bristol, Bristol, U.K.

ABSTRACT: This document reports on the sounding rocket HyPower Bristol are using to test for EuRoC'24, and its flight. The Subscale launch vehicle was designed and built to reach a range of apogees above ground level with a commercial off-the-shelf solid motor and recover with a single separation, dual deployment method. The achieved apogee was 621m AGL, with successful deployment of the launch vehicle drogue. The launch vehicle was recovered with some damage. This paper discusses the flight, recovery and the faults encountered.

KEYWORDS: Rocketry, Solid COTS Motor, Apogee.

1. INTRODUCTION

EuRoC is the Annual European High Power Rocketry Competition hosted by the Portuguese Space Agency. HyPower Bristol as a University of Bristol and Bristol SEDS team entered the S3-c category, meaning that the flight was powered by a solid grain off-the-shelf COTS motor, with a target apogee of 3km.

Following the success of the EuRoC'23 competition under a solid COTS motor, HyPower Bristol is exploring liquid propulsion as their next challenge and have successfully entered the L3 category of EuRoC'24. The target apogee for the competition is 3km and the following tests

The team who attended the test launch consisted of the following persons:

Name	Course	HyPower Discipline
Jacob Cox	Yr 4 Engineering Design	Launch Vehicle
Lillian Macbeth	Yr 4 Civil Engineering	
Izzy Popiolek	Yr 4 Engineering Design	Ground Station
Laurence Jackson	Yr 4 Aerospace Engineering	Electronics
Jake Fitzgerald	Yr 4 Mechanical Engineering	Launch Vehicle

Jordan Brass	MSci Electronic Engineering	Ground Station
Georgiy Lesyuk	Yr 1 Electrical Engineering	Launch Vehicle
Arnav Peehal	Yr 3 Aerospace Engineering	Aerodynamics
Purva Doolani	Yr 2 Aerospace Engineering	Aerodynamics
Bryn Fergeson	Yr 1 Aerospace Engineering	Electronics (Propulsion)

2. DESIGN & BUILD

The design for the subscale has been underway since February, with manufacturing beginning in earnest in May. The bulkheads and tender descender were machined by the University of Bristol Faculty of Engineering Machine workshop. The C-channel aluminium made up the stringers and was machined by the University of Bristol Faculty

3. PRE-FLIGHT OPERATIONS

The motor was integrated on site, at Midlands Rocketry Club under the supervision of an RSO. The motor used was an Aerotech J800T-14A with a 1280Ns total impulse.

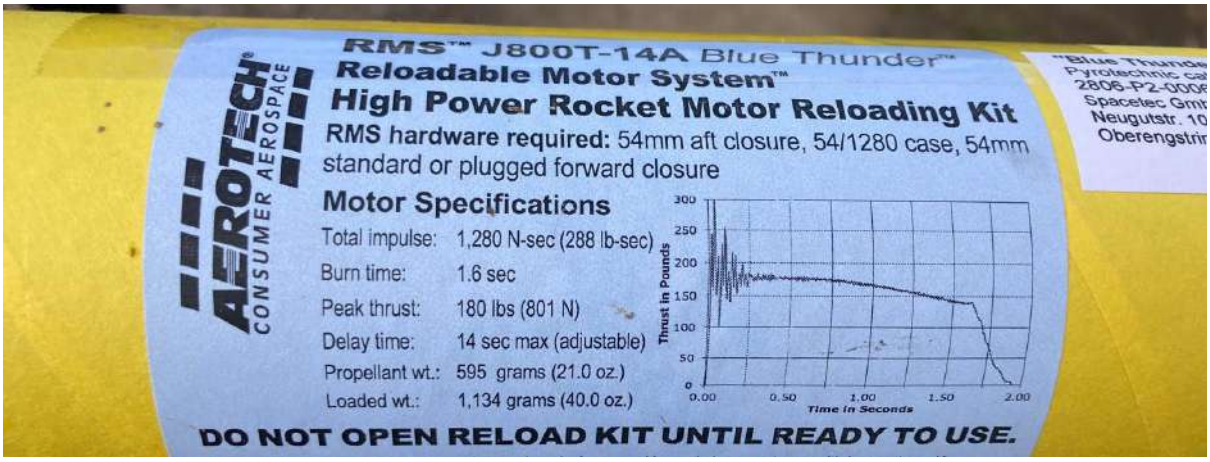

Figure 66 - Subscale Rocket Motor Specifications

Advisories were discussed during the Flight Readiness Review, but we were able to quickly resolved them and progressed to be able to book a launch slot with no comments on our flight card.

- List of advisories discussed in FRR:
- Responsible person to be added to checklist
- Column for notes on checklists
- Add acceptance boundaries on checklists
- Tape to be used for access hatches, not screws
- Make sure no conductive parts are exposed on
- Need PPE for arming rocket

4. FLIGHT SUMMARY

At 15:50 the rocket was launched, reaching an apogee of 619m after a 13.1 seconds. The flight was observed to be stable and consistent; this is shown both in flight data and photographic evidence.

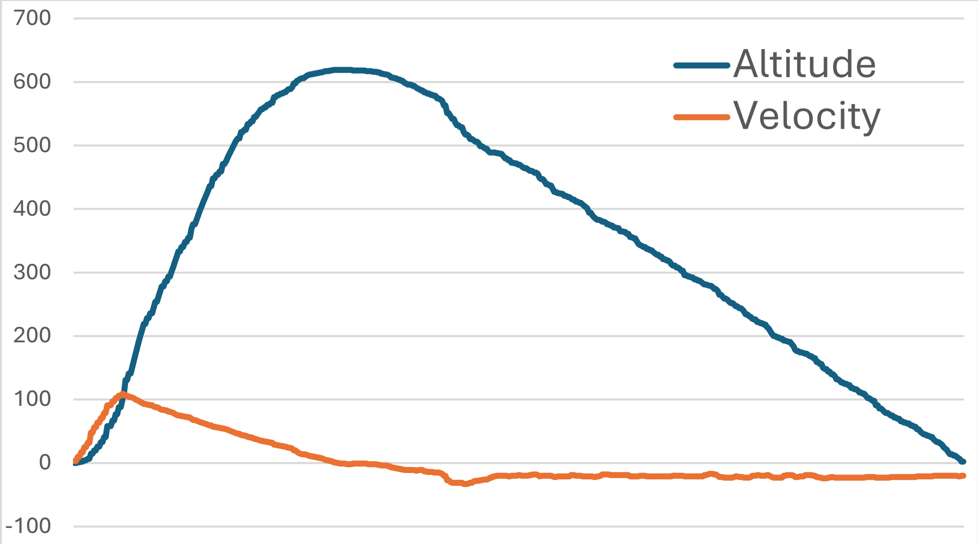

Figure 67 - Graph generated from CATS Vega data

Figure 68 - Image of J800 burn off of launch rail.

5. RECOVERY

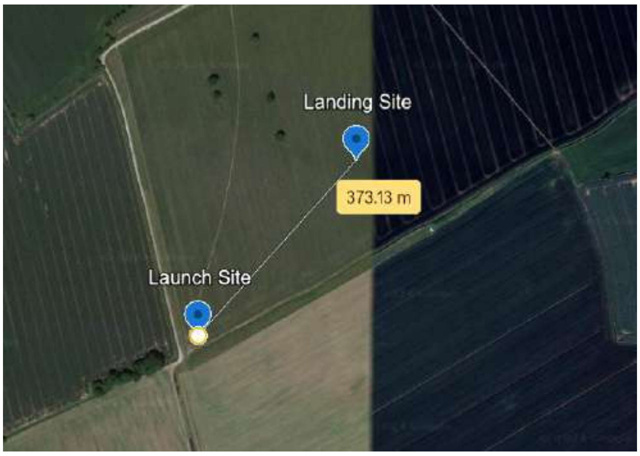

Figure 69 - Map of key locations

5.1 Launch Vehicle Recovery

The launch vehicle drogue chute was deployed from the forward body at apogee. Both ejection charges powered by the CATS Vega and Altus Metrum, respectively, successfully fired the ejection charges. The Launch Vehicle was recovered 373.13m from the launch site.

6. GROUND STATION

This test launch saw good development of ground systems operations. A livestream of the launch with two camera feeds were run. Additionally, live graphing of data from the SRAD flight computer was streamed alongside the camera feeds. This will be improved at future launches, with better calculations between data and shown graphs.

Figure 70 - Launch Livestream

6. DISCUSSION OF FAILURES

6.1 Engineering Cameras

Due to the time and stress pressure on the launch pad, compounded with sunlight obscuring the LEDs inside the rocket, the engineering cameras were not turned on, and therefore there is no in-flight footage. We will resolve this by turning the engineering cameras on in the paddock – the batteries and memory are sufficient, and this is to be incorporated into the sequencing in future checklists.

6.2 Coding and calibration on SRAD flight computer

The equation within the coding on the SRAD flight computer was not used correctly. This can be rectified in the lab and will be verified on future launches. The additional problem with the SRAD flight computer is that the calibration of the onboard sensors needs further work.

6.3 Drogue scorching

The drogue experienced damage from scorching, this could have been mitigated with better packing of the chutes and a better covering with the fire blankets.

6.4 Load paths through recovery lines

All ejection charges were successful, however the load path did not transfer correctly due to tangled lines.

6.5 CATS transmission lost upon landing

Ground station file shows full descent of vehicle. Telemetry must have been lost upon impact landing as a wire at the back of the JST-XH 2 connector broke. Descent under the intended recovery system should not incur this issue.

6.6 Tender descender eyebolt shearing

One tender descender eyebolt sheared, as it was only one out of two it is believed that the failure mode was through becoming tangled in the lines. We will up to M4 bolts

6.7 No FPV link on launch pad

A successful FPV link was practiced in the lab and prior to the launch multiple times, but was not achieved on the launch pad. This meant that we were not able to livestream any of the onboard footage and had to wait until disassembly of the av-bay to recover the SD card.

6.8 Bulkhead becoming wedged due to ejection charge

The ejection charge bulkhead in this vehicle is seated against a thin ring of fiberglass. It was challenging to remove the bulkhead after the launch and ejection charges as the bulkhead has become wedged due to the impulse loading. In the fullscale, this will not be an issue as we will seat metal to metal.

6.9 Looms

Looms in previous rockets have been much tidier and therefore easier to follow. Time constraints, as well as learning curves meant that the looms in this rocket were not able to be quite as tidy but this will be improved for subsequent launches.

6.10 SRAD flight computer power down upon landing

In 18650 battery holder terminal has been dislodged under impact. This is impacted by the introduction of battery spacers. This caused a power discontinuity and the board to shut down.

6.11 Damage to launch vehicle upon landing

Upon landing, the fin-can hit a rock (Figure X). This caused the plywood centre of the fin to fail, though the fibreglass lay-up remained in-tact. For future projects we will use only composites to construct the fins, as this will keep them lightweight, but increase the durability.

B.3 Flight Recovery Testing – Subscale Flight 2

Authors: ***L. Macbeth, G. Lesyuk*** University of Bristol, Bristol, U.K.

ABSTRACT: This document reports on the sounding rocket HyPower Bristol are using to test for EuRoC'24, and its second flight. The Subscale launch vehicle was designed and built to reach a range of apogees above ground level with a commercial off-the-shelf solid motor and recover with a single separation, dual deployment method. The achieved apogee was 621m AGL, with successful deployment of the launch vehicle drogue. The launch vehicle was recovered with some damage. This paper discusses the flight, recovery and the faults encountered.

KEYWORDS: Rocketry, Solid COTS Motor, Apogee, Air Brakes.

1. INTRODUCTION

EuRoC is the Annual European High Power Rocketry Competition hosted by the Portuguese Space Agency. HyPower Bristol as a University of Bristol and Bristol SEDS team entered the S3-c category, meaning that the flight was powered by a solid grain off-the-shelf COTS motor, with a target apogee of 3km.

Following the success of the EuRoC'23 competition under a solid COTS motor, HyPower Bristol is exploring liquid propulsion as their next challenge and have successfully entered the L3 category of EuRoC'24. The target apogee for the competition is 3km and the following tests

The team who attended the test launch consisted of the following persons:

Name	Course	HyPower Discipline
Jacob Cox	Yr 4 Engineering Design	Launch Vehicle
Lillian Macbeth	Yr 4 Civil Engineering	
Izzy Popiolek	Yr 4 Engineering Design	Ground Station
Angeline Pang	Yr 4 Engineering Design	Ground Station
Tom McKeague	Yr 4 Mechanical and Electrical	Ground Station
Laurence Jackson	Yr 4 Aerospace Engineering	Electronics
Jake Fitzgerald	Yr 4 Mechanical Engineering	Launch Vehicle
Jordan Brass	MSci Com Sci	Ground Station
Georgiy Lesyuk	Yr 1 Electrical Engineering	Launch Vehicle
Bryn Fergeson	Yr 1 Aerospace Engineering	Electronics (Propulsion)
Ethan Sheehan	Yr 1 Aerospace Engineering	Propulsion

2. DESIGN & BUILD

Following the damage sustained on the previous method, a new fincan was manufactured and tested for deflection. A set of airbrakes was also tested and built. The aluminum housing and nylon petals were manufactured by the University of Bristol machine shop. These interface in a simple manner with the stringers, where the stringers sit in impressions and are bolted directly to the airbrake unit.

Much more development was put into the avionics bay, to ensure that all flight computers and connections were secure thorugh flight and high impulse events.

Figure 471: Improved avionics bay for the subscale vehicle

3. PRE-FLIGHT OPERATIONS

The motor was integrated on site, at Midlands Rocketry Club under the supervision of an RSO. To help with consistency the same motor was used, an Aerotech J800T-14A with a 1280Ns total impulse.

Figure 572: J-800 moto packaging with specifications

The ejection charges were then loaded with black powder and the recovery system. This was held at 15:45, and UKRA RSOs were satisfied that the rocket was safe to fly. The team carried the rocket down to the launch rail and successfully armed the rocket. Advisories from the previous flight readiness review were checked against and passed. The RSOs also required additional testing and proof that the airbrakes would remain mechanically locked.

4. FLIGHT SUMMARY

At 16:15 the rocket was launched, reaching an apogee of 621m after a 10.3 seconds. The flight was observed to be stable and consistent; this is shown both in flight data and photographic evidence.

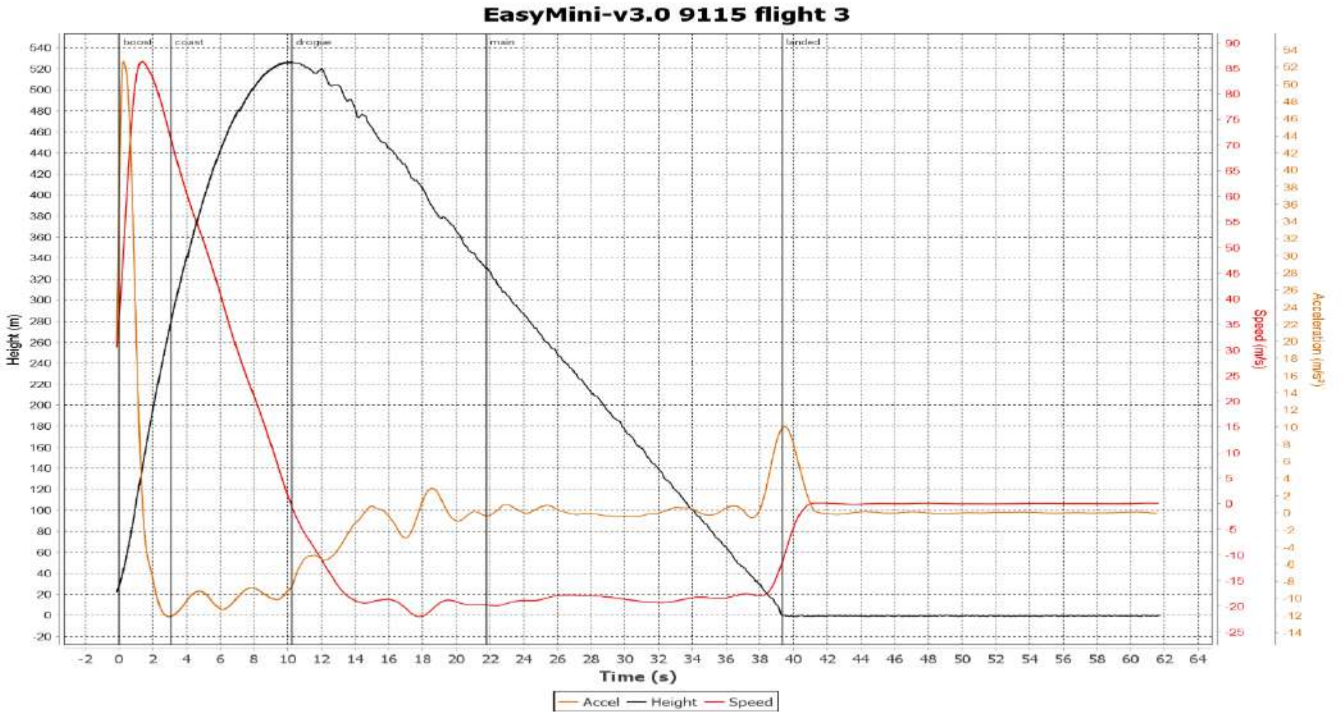

Figure 5: Graph generated from Altus Metrum

4.1 Air Brakes

The airbrakes were successful at effecting the acceleration of the graph, as they were deployed to 50 and 100% before apogee. This can be seen in the orange acceleration against time line on Figure 3.

Figure 673: Image of J800 burn off of launch rail.

5. RECOVERY

5.1 Launch Vehicle Recovery

The launch vehicle drogue chute was deployed from the forward body at apogee. Both ejection charges powered by the CATS Vega and Altus Metrum, respectively, successfully fired the ejection charges. All charges on the tender descender also fired. It was evident that as in testing, the first ejection charge on the tender descender separated the two halves. This was shown by no soot being on the front of the second cup.

The lines of tension were much improved to the first test launch and the line around the bag containing the main was undone.

6. DISCUSSION OF IMPROVEMENTS ON SUBSCALE TEST LAUNCH 1

6.1 Engineering Cameras

In the first test launch, the engineering cameras could not be activated. In this second test they were activated and managed to stream to the ground station. This was a vast improvement and was likely impacted by improved connections throughout the electronics architecture.

6.2 Coding and calibration on SRAD flight computer

The coding on the SRAD flight computer meant that graphs on the livestream provided much better data, giving the ground station team a better idea of the computer performance as well as rocket position.

6.3 Drogue scorching

No parachutes experienced scorching on this test launch, due to better placed Nomex. This protected the parachutes from the ejection charges.

6.4 Load paths through recovery lines

In the first test, all ejection charges were successful, however the load path did not transfer correctly due to tangled lines. This was resolved by conducting many more tests, and an improved bagging method.

6.5 CATS transmission lost upon landing

No connections were lost during the flight and recovery on the second launch. This is due to improved electronic connections throughout the vehicle.

6.6 Tender descender eyebolt shearing

M4 bolts were used in the second test launch, no shearing was experienced.

6.7 No FPV link on launch pad

A successful FPV link was practiced in the lab and prior to the launch multiple times, but was not achieved on the launch pad in the first launch. It was not perfect on this second launch, but connection was achieved.

6.8 Bulkhead becoming wedged due to ejection charge

As stated in the previous report, this issue will be mitigated by providing a greater seat for the blast bulkhead.

6.9 Looms

As shown in Figure 2, the looms were vastly improved on this launch.

6.10 SRAD flight computer power down upon landing

No terminals, power sources or flight computers were damaged in the second test launch.

10.1.4. Proof Pressure Testing Pressure Vessels (SRAD, Modified COTS) (if applicable)

The strain gauge data from the tests is shown in graphs below:

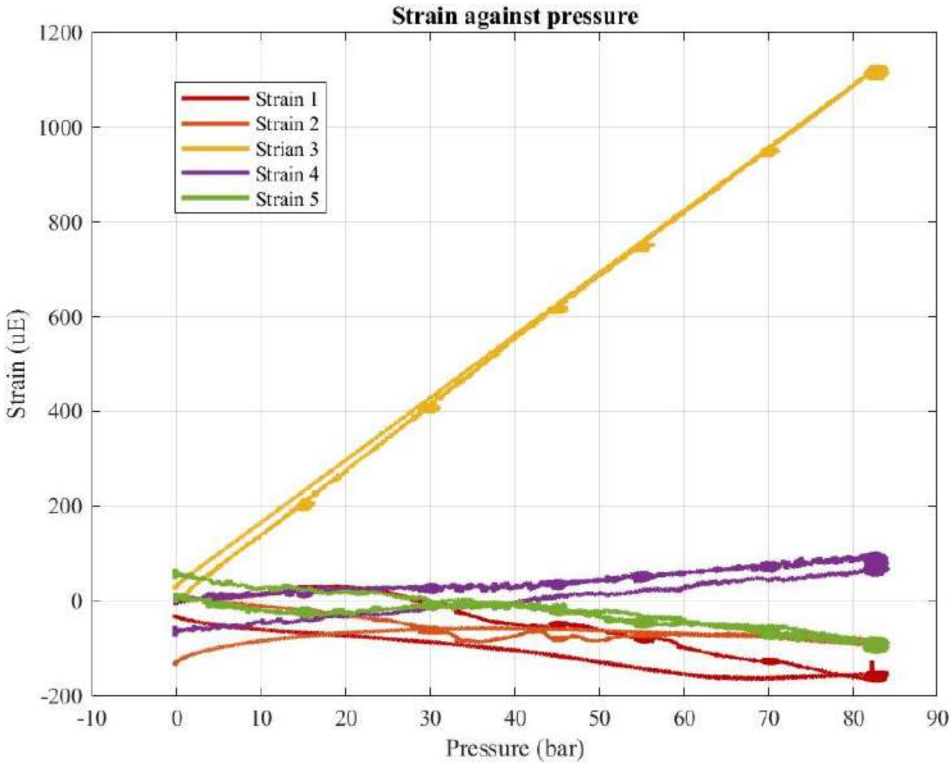

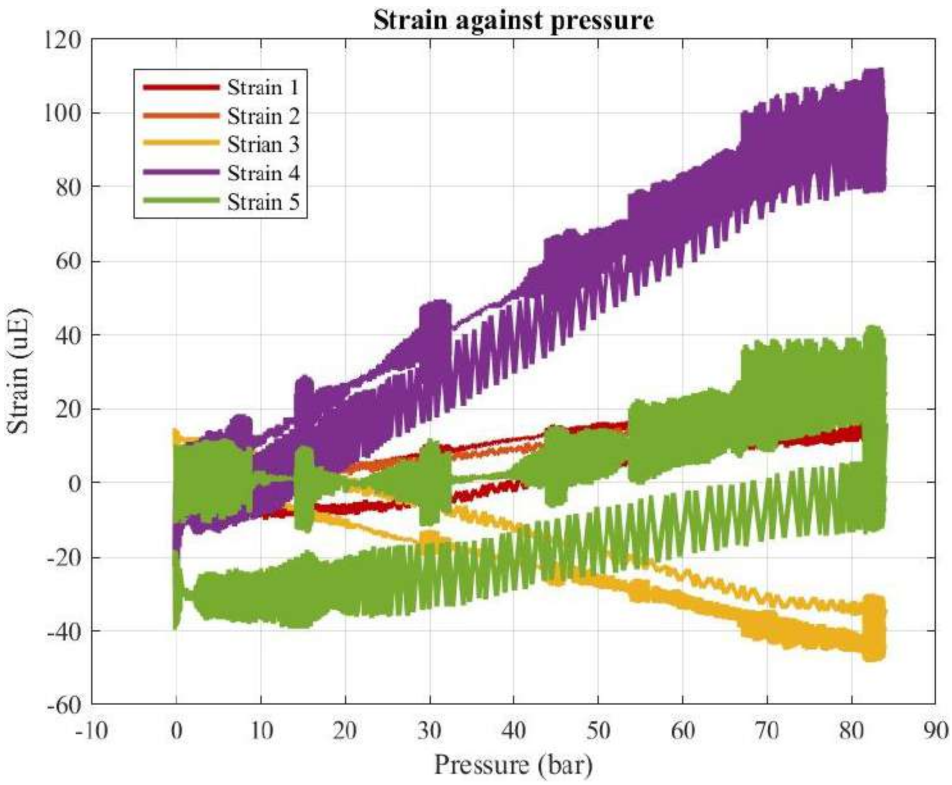

10.2.8. Test of SRAD flight computers with capability of actuating the recovery systems

B.4 Coaxial Tank Hydrostatic Testing

Test No.	4	Asset	Feed Systems
Risk Assessment No.	n/a	Sub Team	Propulsion
ITP No.	2	Date	28/08/2025

<u>Test Outcome: Success</u>

<table>
<tr><th colspan="3">Item 3: 1.5x MEOP Testing of Coaxial Tank</th><th>Initial</th><th>Time</th><th>Pass</th></tr>
<tr><td>3.1</td><td>Ensure that systems are as expected.</td><td>No damage to SRAD system in transport.
No dismantling of system.
Confirmation from Astron that system is nominal.</td><td>GL</td><td>10:49</td><td>Yes</td></tr>
<tr><td>3.2</td><td>Integrate systems.</td><td>Ensure that fittings are flush, no threads have been crossed.</td><td>GL</td><td>10:49</td><td>Yes</td></tr>
<tr><td>3.4</td><td>Depressurise system.</td><td></td><td>GL</td><td>10:50</td><td>Yes</td></tr>
<tr><td>3.5</td><td>Inspect tank and system for signs of fatigue.</td><td></td><td>GL</td><td>10:50</td><td>Yes</td></tr>
<tr><td>3.6</td><td>Bring vessel and outer tank to 1.5x MEOP in 10 bar increments, holding at each interval of 10 bar for 2 minutes.</td><td><table>
<tr><th>Pressure</th><th>No Pressure Drop for 2 min</th></tr>
<tr><td>15</td><td>pass</td></tr>
<tr><td>25</td><td>pass</td></tr>
<tr><td>35</td><td>Pass</td></tr>
<tr><td>45</td><td>pass</td></tr>
<tr><td>55</td><td>pass</td></tr>
<tr><td>65</td><td>pass</td></tr>
<tr><td>75</td><td>pass</td></tr>
</table></td><td>GL</td><td>11:00
Start</td><td>Pass</td></tr>
<tr><td>3.7</td><td>Hold 1.5x MEOP for 15 minutes.</td><td>Less than 10% pressure drop seen.</td><td>GL</td><td>11:20</td><td>Pass</td></tr>
<tr><td>3.8</td><td>Depressurise system.</td><td></td><td>GL</td><td>11:37</td><td>Pass</td></tr>
<tr><td>3.9</td><td>Inspect tank and system for signs of fatigue.</td><td></td><td>GL</td><td>11:50</td><td>Pass</td></tr>
<tr><td>3.10</td><td>Bring inner coaxial tank to 1.5x MEOP in 10 bar increments, holding at each interval of 10 bar for 2 minutes.</td><td><table>
<tr><th>Pressure</th><th>No Pressure Drop for 2 min</th></tr>
<tr><td>15</td><td>Pass</td></tr>
<tr><td>25</td><td>Pass</td></tr>
<tr><td>35</td><td>Pass</td></tr>
<tr><td>45</td><td>Pass</td></tr>
<tr><td>55</td><td>Pass</td></tr>
<tr><td>65</td><td>Pass</td></tr>
</table></td><td>GL</td><td>11:55</td><td>Pass</td></tr>
</table>

		75 — Pass			
3.11	Hold 1.5x MEOP for 15 minutes	Less than 10% pressure drop seen.	GL	12:26	Pass
3.12	Bring both inner and outer coaxial tank to 1.5x MEOP in 10 bar increments, holding at each interval of 10 bar for 2 minutes.	Pressure — No Pressure Drop for 2 min 15 — Pass 25 — Pass 35 — Pass 45 — Pass 55 — Pass 65 — Pass 75 — Pass	GL	12:48	Pass
3.13	Hold 1.5x MEOP for 60 minutes.	Less than 10% pressure drop seen.	GL	13:05	Pass
3.14	Depressurise system.		GL	13:35	Pass
3.15	inspect tank and system for signs of fatigue.		GL	13:46	Pass

Witnesses:

Tom Wormald

Georgiy Lesyuk

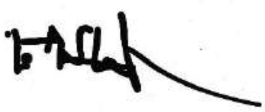

Ethan Sheehan

Result and Conclusions:

The due to the structural improvements made on the inner coaxial tank, it has held up to all possible failure cases. This has improved on previous designs and has withstood buckling when the inner fuel tank is depressurised, and the outer fuel tank is pressurised. The result of this test can be deemed a success.

B.5 SRAD Avionics Thermal Testing

Test Title	Avionics Thermal Testing	**Asset**	PDU
Risk Assessment No.	n/a	**Sub Team**	Electronics
ITP No.	2	**Date**	06/09/2025

Test outcome: Success

PDU thermal load testing			Initials	Time	Pass
3.1	Verify power supply voltage	Power supply is at 16V	SSK GL	20:23	Yes
3.2	Ensure that PDU is set up correctly. The PDU is powered by a power supply rated up to 10A, with an Ammeter and Chassis Resistor on the 7V4 rail	Setup is correct	SSK GL	20:27	Yes
3.4	Monitor initial temperature readings with a thermal gun	 	SSK GL	20:28	Yes
3.5	Turn on power supply	Voltage is displayed currently, power supply is drawing current and ammeter is reading 10A Load	SSK GL	20:28	Yes
3.6	Monitor temperatures on the IC and MOSFETs after power supply is turned on	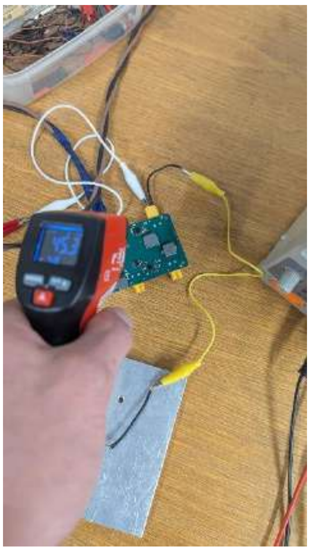	SSK GL	20:29	Yes

3.7	Wait 20 minutes, measure temperatures on the IC and MOSFETs	 	GL	20:50	Yes
3.8	Wait a further 10 minutes, measure temperatures on the IC and MOSFETS	 	GL	20:62	Yes

Yes

Witnesses:

Georgiy Lesyuk

Sara Shabbir Khan

Hansrudh Gupta

Results and Conclusions:

The PDU after 30 continuous minutes of drawing a 10A load has not reached higher than 54 degrees Celsius. This is well within the temperature range of all components on the board, and a comfortable temperature for the electronics. Since the PDU will not be expected to draw high current continuously for this period of time, this test can be considered a success.

B.6 September 2025 Full Stack Testing Report

Analysis of Full Stack Testing of HyPower Bristol's 2025 5kN Launch Vehicle

Georgiy Lesyuk, Tom Wormald, Ethan Sheehan

This report documents HyPower Bristol's test campaign at Astron Systems from the 16th to the 20th September 2025.

Contents

Testing Timeline

The testing campaign took the following form:

Day 1:

- Setup
- Leak Testing

Day 2:

- Nitrogen Purge and Ignitor Test
- Hot Fire 1

Day 3:

- Nitrogen Purge
- Hot Fire 2

Day 4:

- Propellant Loading & Offloading test
- Hot Fire 3

Procedure

The checklists and procedures followed were modified versions of those found in the Technical Report for Team 16. This was necessary due to the differences in the nature of the systems present for launch, and those available at the test site. As a result, our checklists were modified by Astron Systems to allow us to integrate effectively with their hardware (e.g. the attachment of our nitrogen COPV to their own run tanks to increase pressurant volume due to their bottle regulators only going up to 100 bar).

Other features included were the attaching of one of Astron's valves to allow for the removal of fuel to the ground of the test cell, rather than through the run valves, in the event of equipment failure and the removal of check valves from the Nitrogen and Nitrous fill lines to allow it to be vented through their ground systems if necessary.

Test Setup for Integrated Hot Fire

Figure 74 - General Configuration of the Test

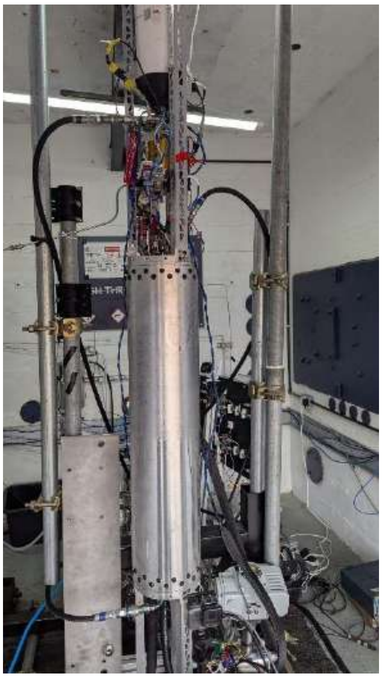

Figure 75 - Close Up of the Tank

Figure 76 - Side View of the Configuration

The test campaign was conducted at Astron Systems in their high thrust test cell. The tank was set up vertically, with the engine mounted horizontally. Thrust was measured using a load cell, and pressure and temperature data were captured using Pressure Transducers and Thermocouples.
The ignitor was a sparkler attached to the engine via a 3D print, reenforced by a laser cut piece of plywood to increase the residence time.

Figure 77 - A Picture of the Ignitor Set Up

Figure 78 - A Downrange Picture of the Test Site

Ground System

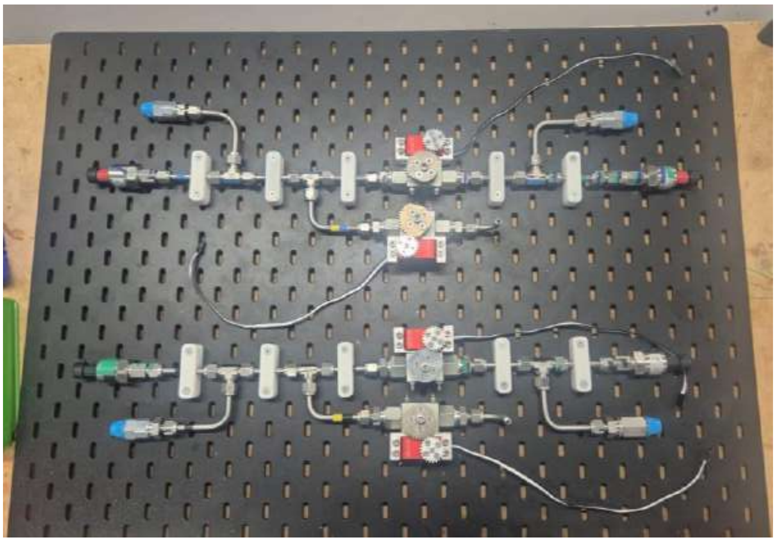

Figure 79 - The plumbing section of the Ground Station

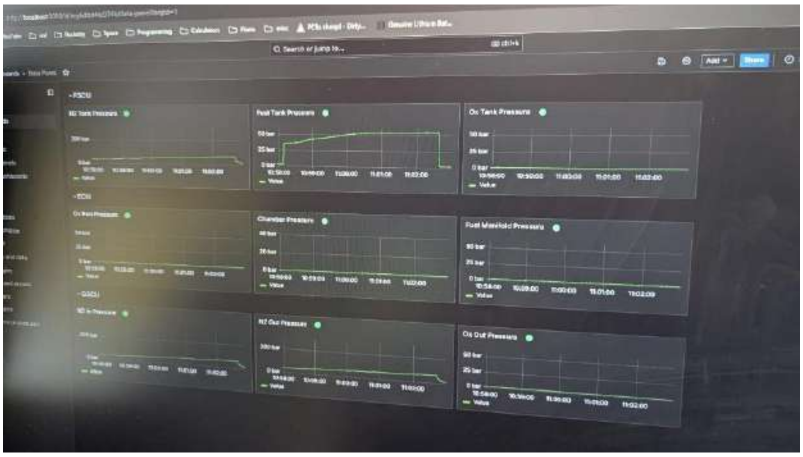

Figure 80 - The Control Room Pressure Readouts

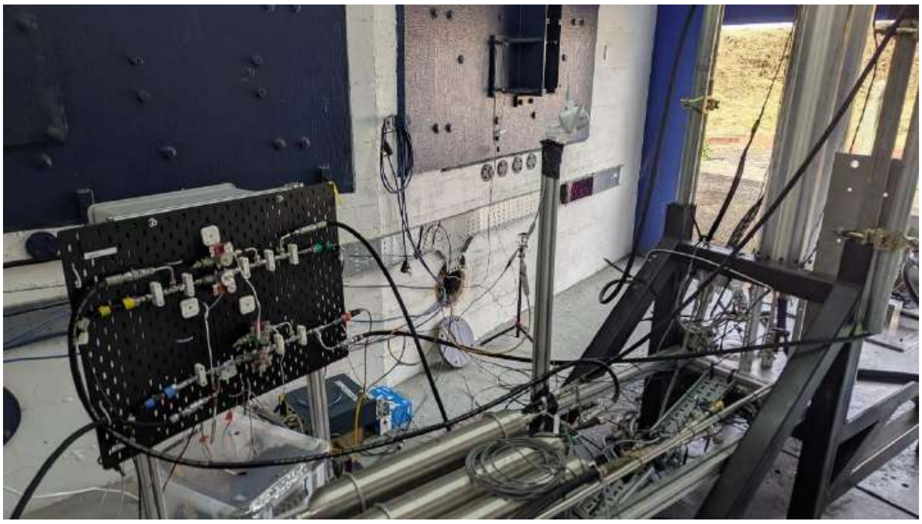

Figure 81 - A View of the Ground Station in the Test Cell

Propellant Bay

Figure 82 - Image of the Propellant Bay from the 2023/24 Testing Campaign

Control Room

Figure 83 - The Control Room

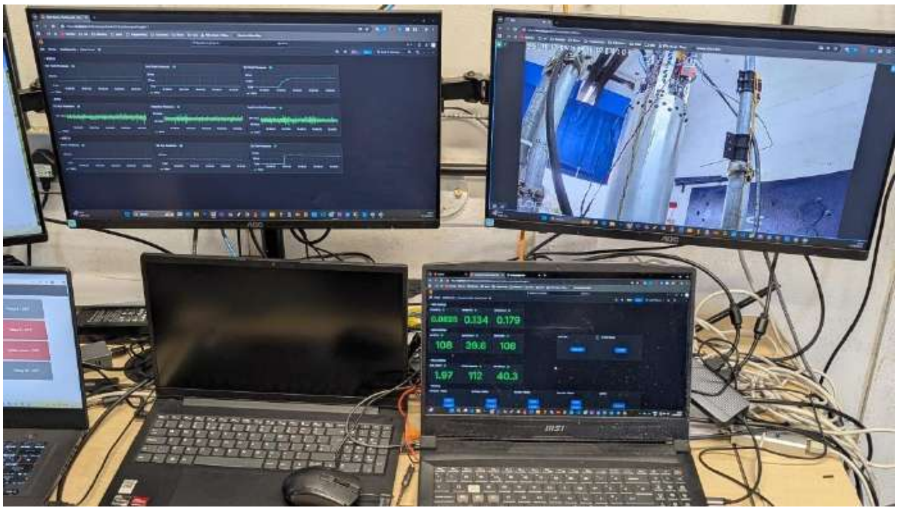

Figure 84 - A Close Up of the Control Room Displays

Leak Test

A leak test was performed on the first day of testing to validate that the system was not venting large amounts of pressure. Slow leaks were deliberately left in the Nitrous Oxide and Nitrogen lines in the unlikely event of power and battery failure. This means that the pressure would slowly vent over the course of several hours.

Nitrogen Flow & Ignitor Test

A Nitrogen cold flow and Ignition test was performed to certify the system before firing. This consisted of loading the LV with approximately 100 bar of nitrogen and then starting the ignition sequence (Fuel run valve leads Ox run valve by 0.3s with 2 seconds of sparkler burn time before either are opened.).

This sequence was performed nominally, and the rocket was then vented of all remaining nitrogen.

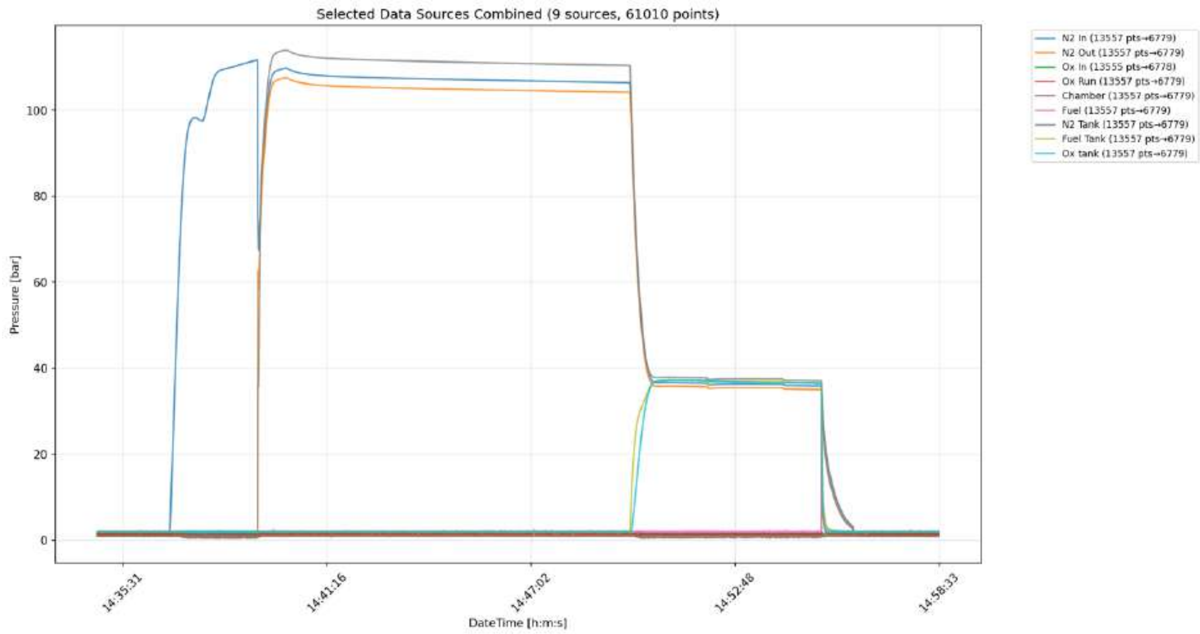

Figure 85, Day 2 test 1: '2025-09-16 14:34:48' - '2025-09-16 14:58:33', Nitrogen flow data

Hot Fire Tests

Hot Fire 1 – Partial Duration & Low Thrust

Due to a loose fitting that was missed during pre-fire inspections there was a leak of Nitrous Oxide during fueling. This leak was isolated quickly, to ensure no additional nitrous was lost. The Nitrous tank had been fueled slightly; due to the time it took to notice the leak. The team and test site decided to continue with the launch checklist and fired the engine with the partially fuelled Nitrous tnak. This resulted in a short burn of 1s, with a peak thrust of 3.7kN.

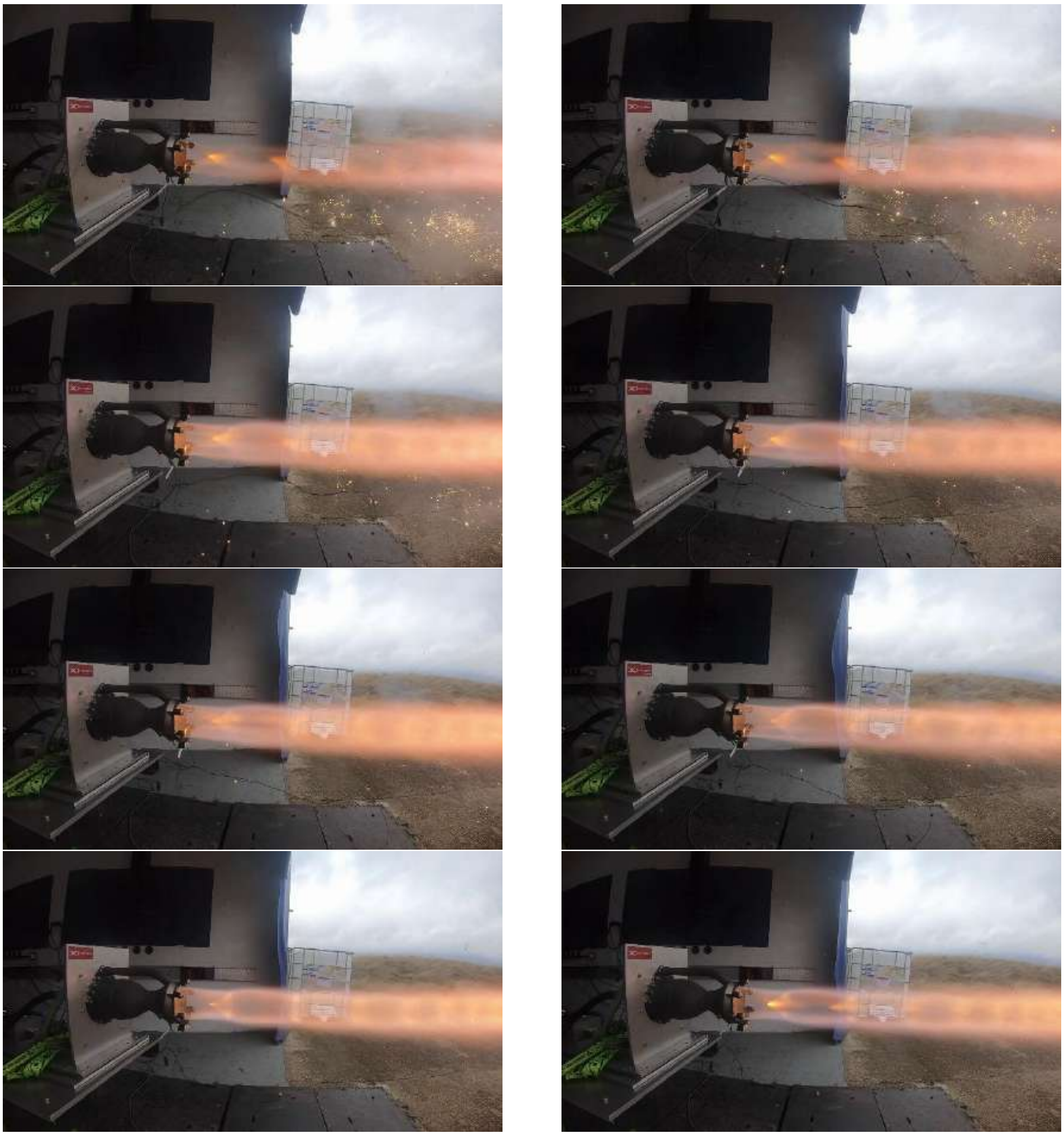

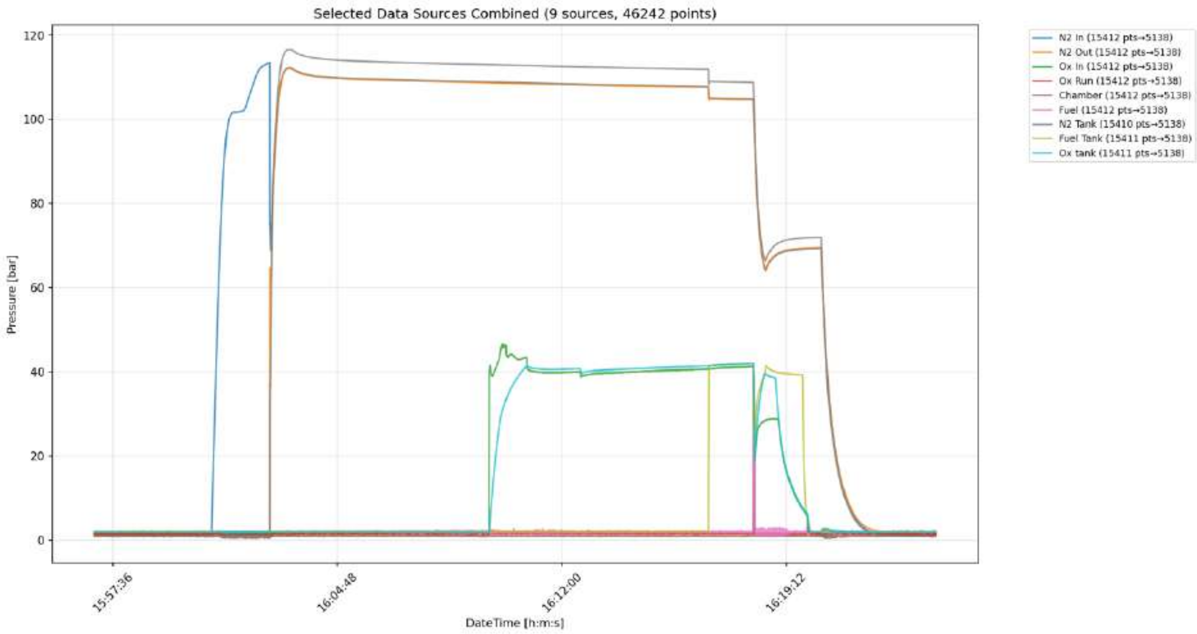

Figure 86, '2025-09-16 15:57:00' - '2025-09-16 16:24:00', Hotfire 1 full pressure data

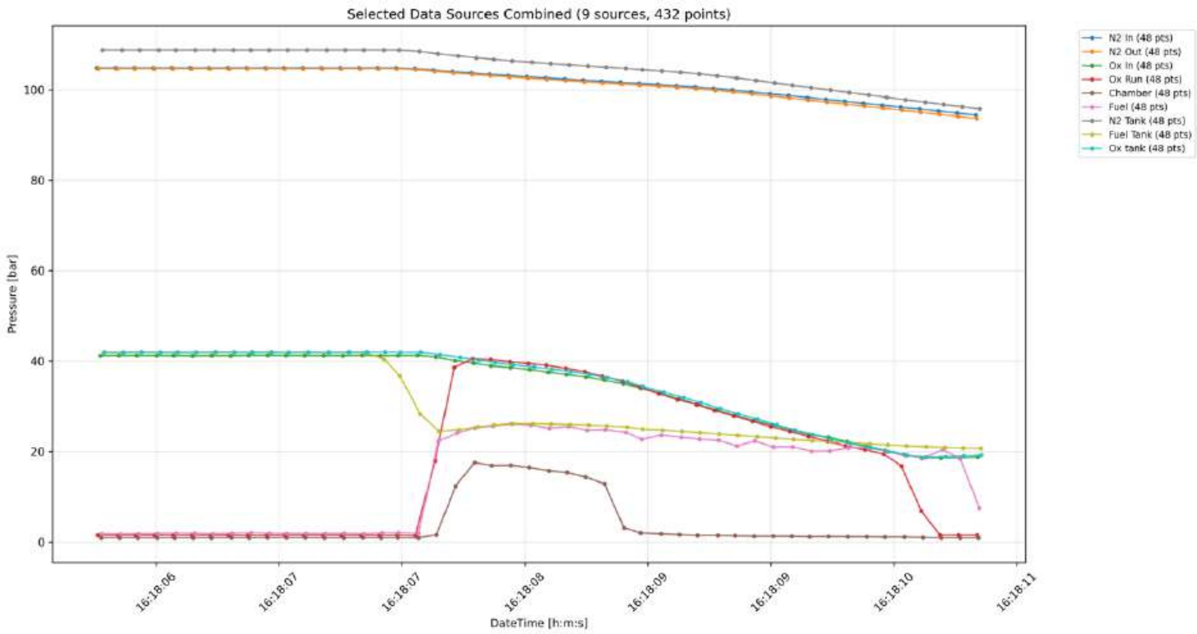

Figure 87, '2025-09-16 16:18:06' - 2025-09-16 16:18:11', Hotfire 1 burn time pressure data

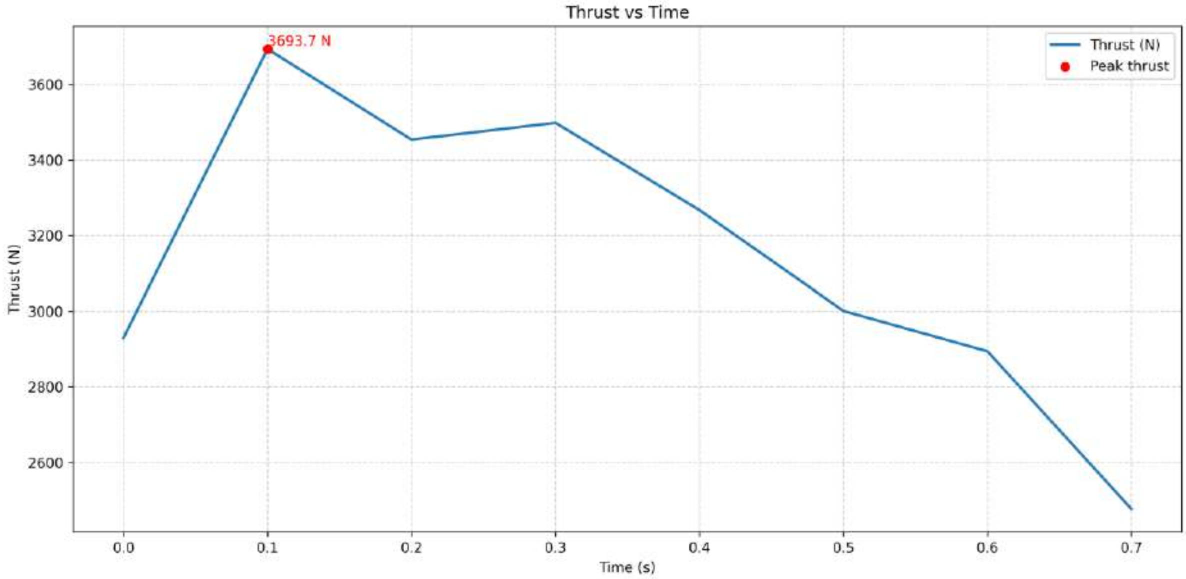

Figure 88, Thrust vs Time Graph for the First Hot Fire

Hot Fire 2 – Full Duration & Low Thrust

During hot fire 2, suitable preparations were taken to ensure the propellant loading was conducted nominally. With full nitrous and IPA tanks, we demonstrated a 7 second burn, with a peak thrust of 4kN, linearly dropping to 3.6kN over the course of the burn.

Despite changes to our ignition timings, increasing the sparkler burn time to 5 seconds before valve actuation, we see that ignition happens almost instantly after the oxidizer valve is opened.

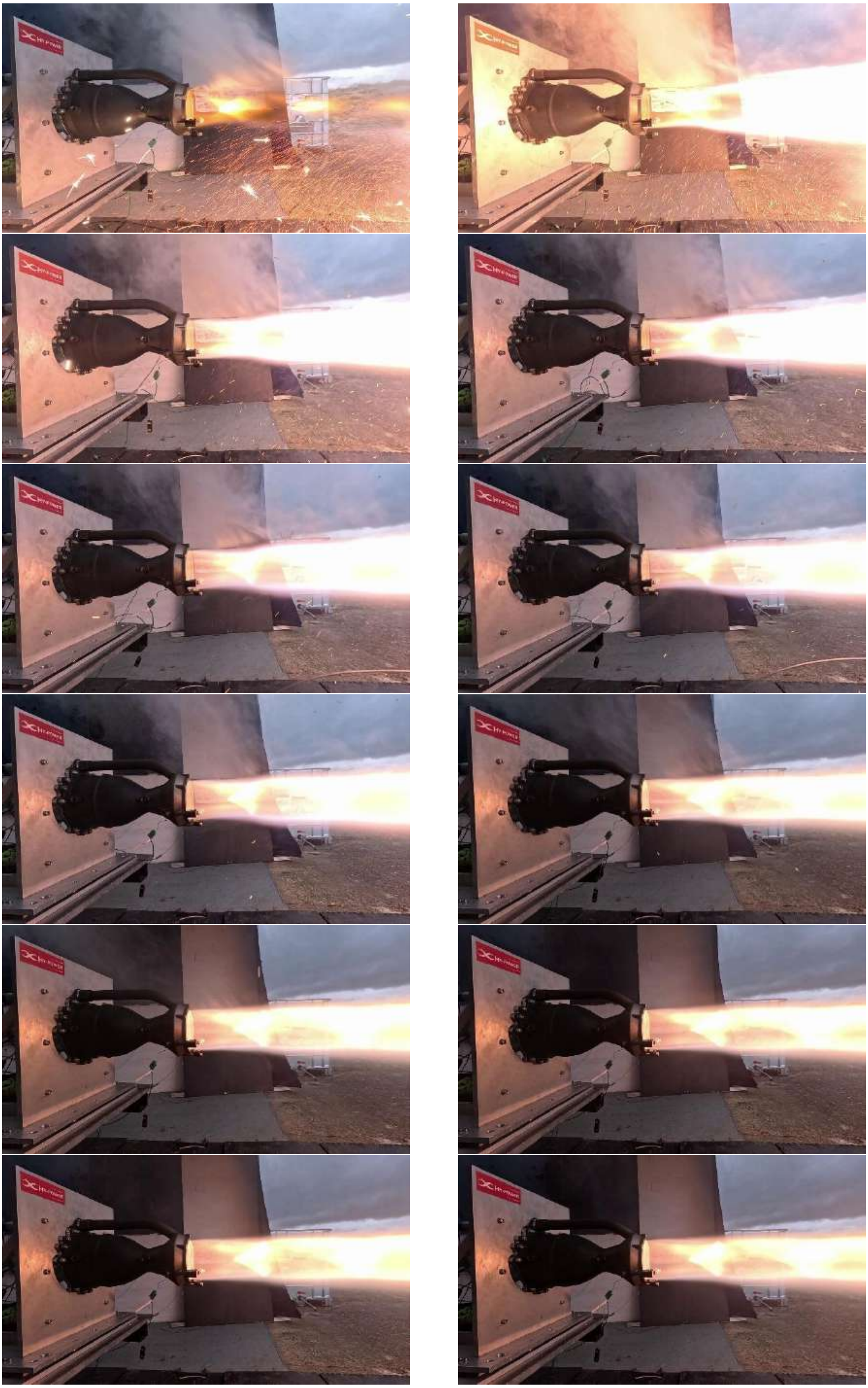

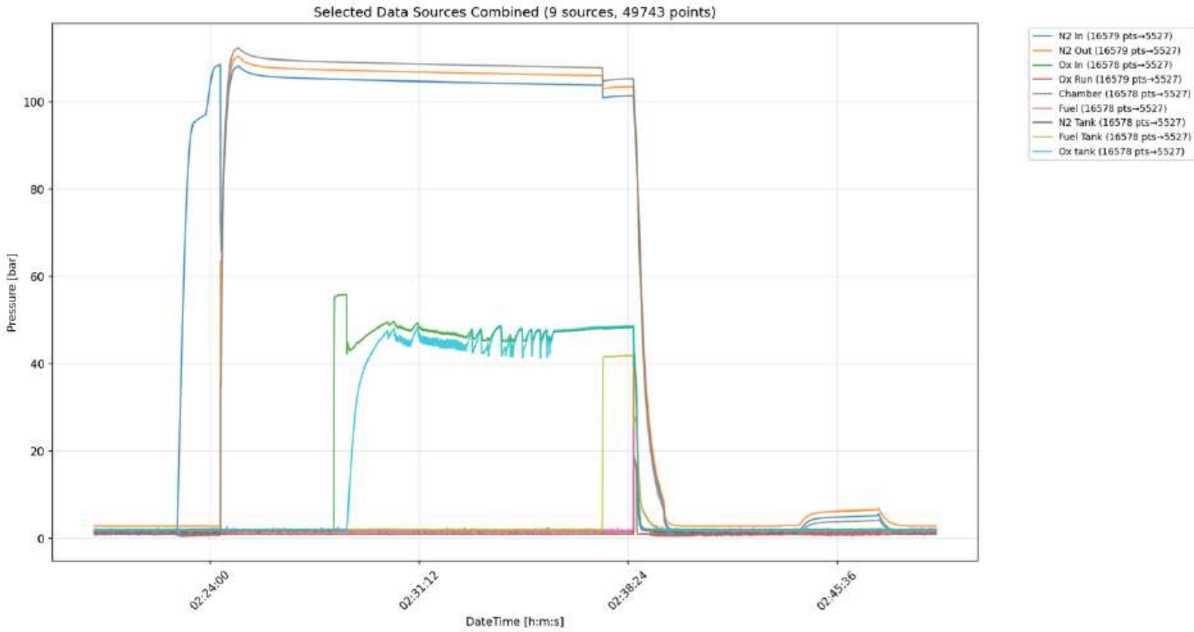

Figure 89, Day 3 Test 3: '2025-09-17 2:20:00' - '2025-09-17 2:49:00, Hotfire 2 full pressure data'

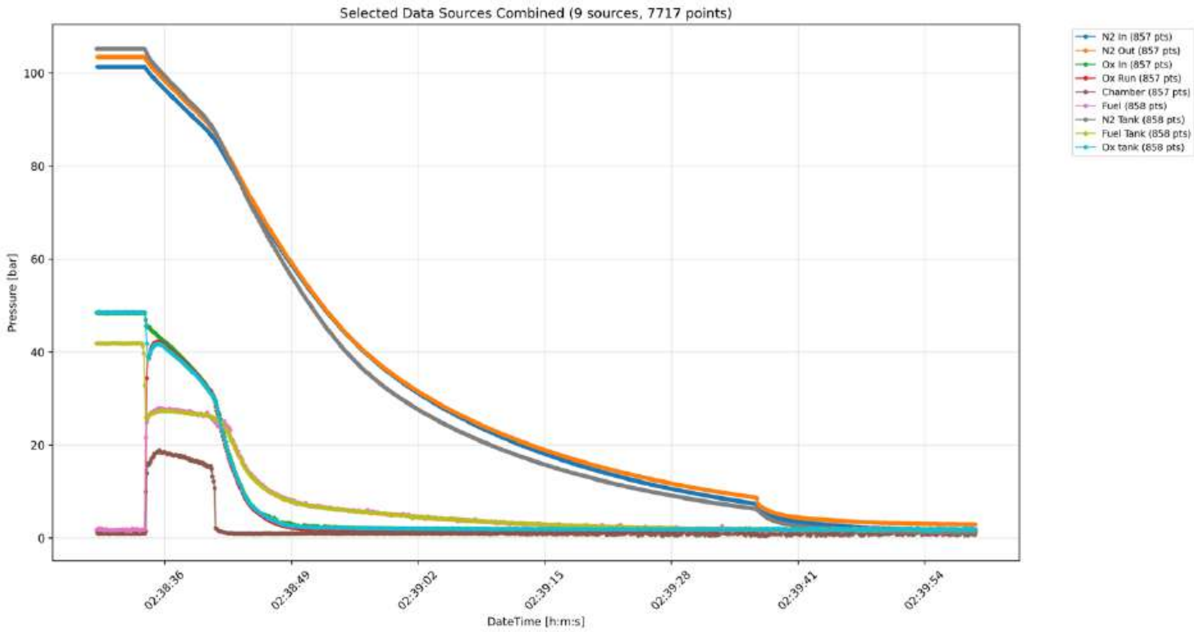

Figure 90, Day 3 Test 3: '2025-09-17 02:38:30' - '2025-09-17 02:40:00', hotfire 2 burn time pressure data

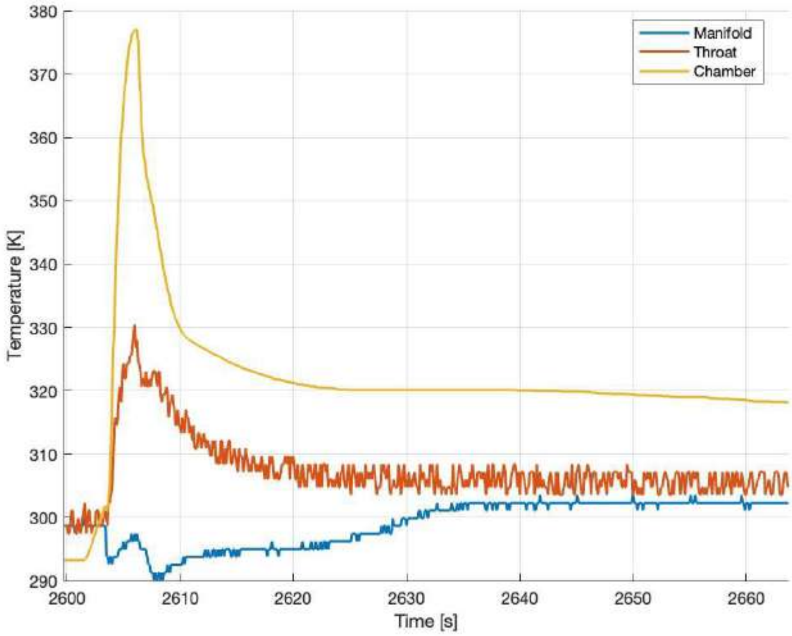

Figure 91, Hotfire 2 Combustion chamber thermocouple data

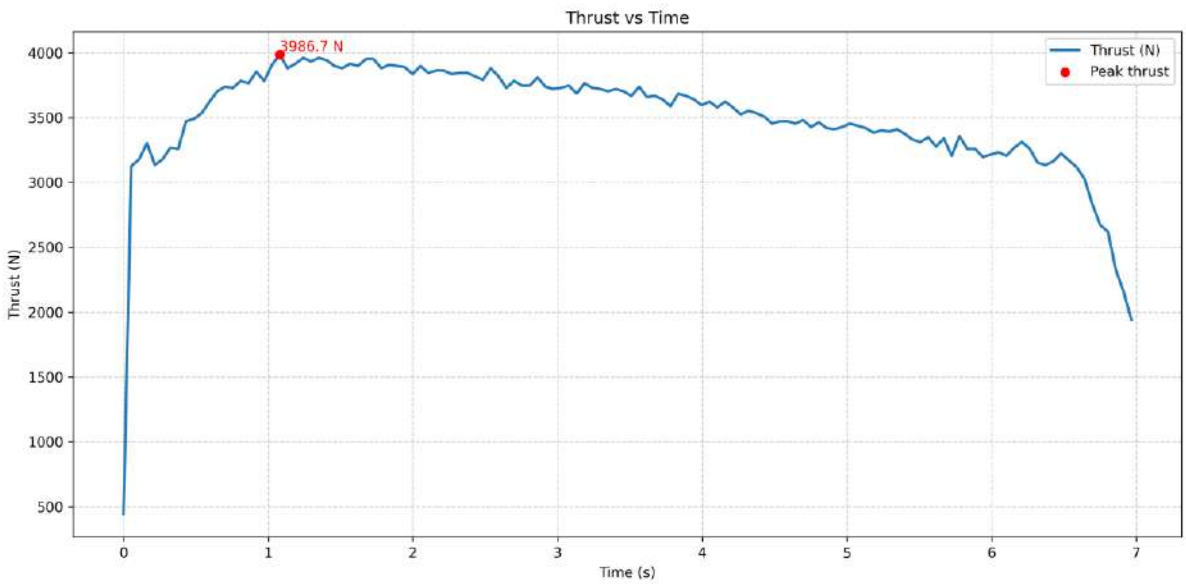

Figure 92 - Thrust vs Time Graph for the Second Hot Fire

	Name	Configuration	Velocity off rod	Apogee	
!	4kN 7sec	[E-1.2-0]	30.7 m/s	2350 m	2

Velocity at deploym...	Optimum delay	Max. velocity	Max. acceleration	Time to apogee	Flight time	Ground hit velocity
27.4 m/s	16.9 s	214 m/s	43.4 m/s²	23.8 s	148 s	7.05 m/s

Figure 93 - OpenRocket Simulation for Hot Fire 2 Thrust Data

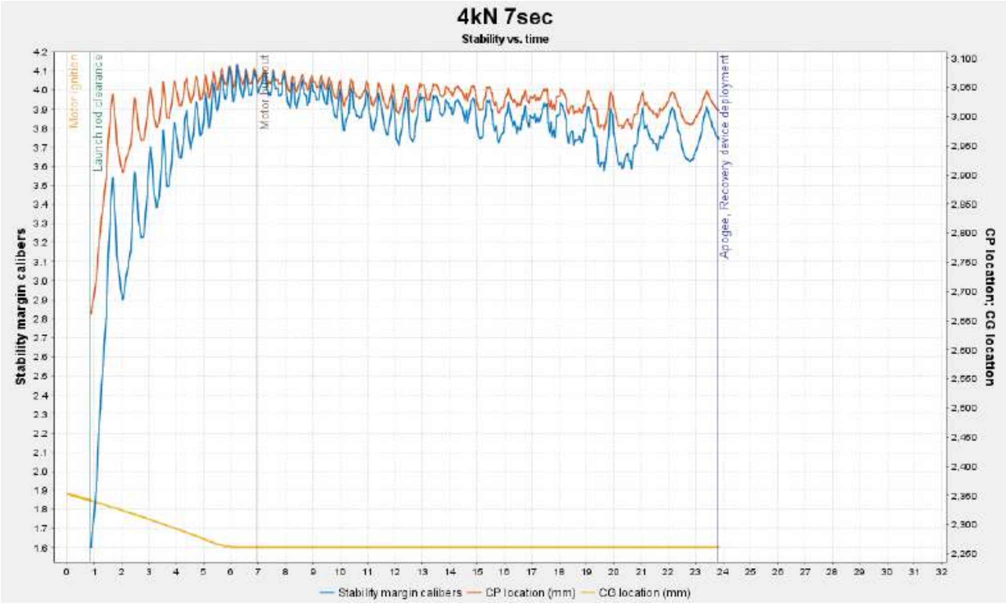

Figure 94 - A Graph of Stability vs Time for Hot Fire 2 Thrust Data

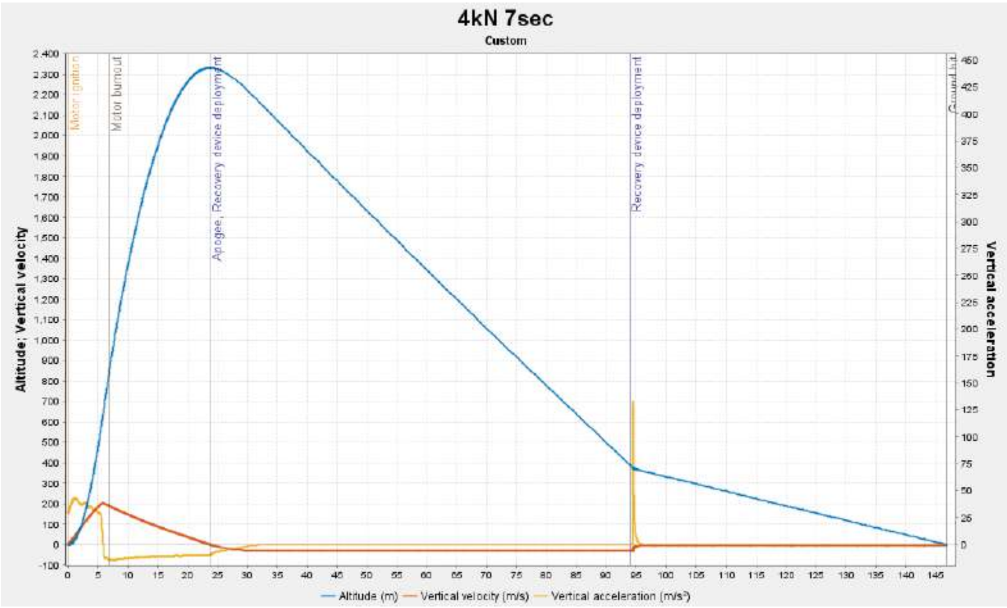

Figure 95 - A Graph of Altitude vs Time for the Hot Fire 2 Thrust Data

Using the data collected from the load cell in an OpenRocket simulation of the launch vehicle (Figure 19), a velocity of 30.7 m/s can be observed off the rail, using the EuRoC provided launch rails. This conforms with EuRoC-LV-RQT-1100, where the vehicle shall be capable of achieving a rail departure speed higher than 30 m/s on the intended launch rail's length. The launch vehicle has a stability of 1.52 at the moment of leaving the launch rail, which complies with EuRoC-LV-RQT-1030.

Hot Fire 3 – Partial Duration & Full Thrust

After the previous Hot Fire and the desire for a higher safety factor for launch rail velocity the regulator on the rocket was increased to give a downstream pressure of 50 (the original design pressure of the tank). This was in hopes of increasing the mass flow rates and chamber pressure to give us greater thrust at lift off.

Due to the pre-fire checklists being incorrectly followed there was a venting of a large amount of Nitrous Oxide, meaning that there was very little left in the external tank to reach optimum LV tank pressure. Consequently, we could not fill the tank to a sufficient degree to obtain a full duration burn (much like with Hot Fire 1) meaning that the engine only fired for 0.86 seconds.

Despite this, due to our fast start up, we were able to reach a peak thrust of 5.58kN

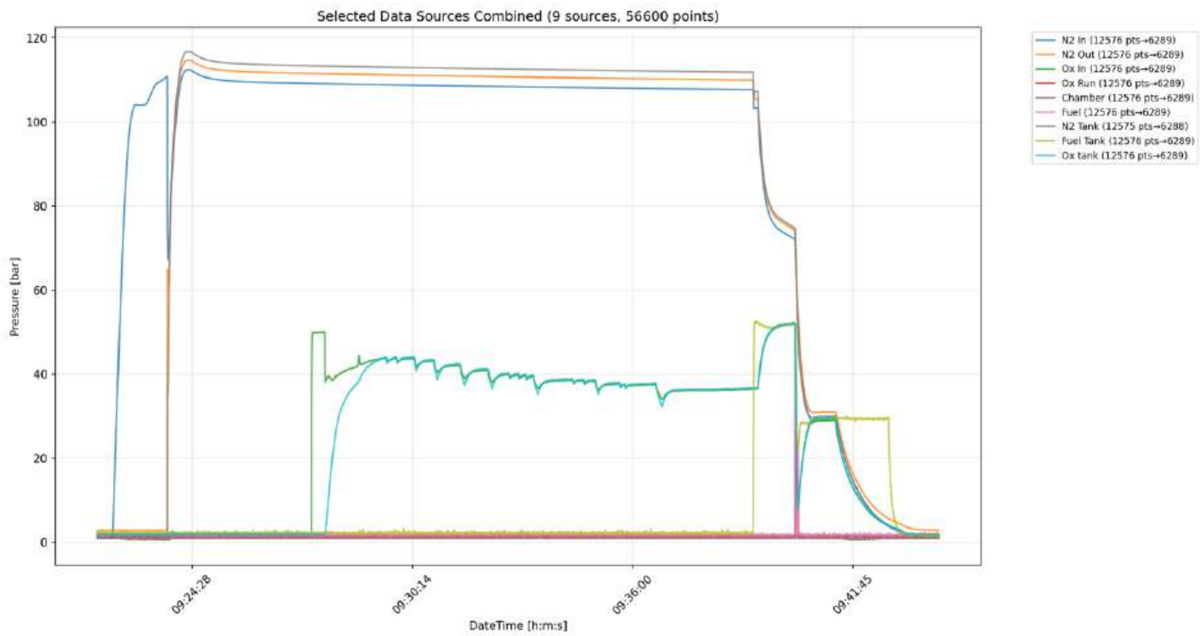

Figure 96, '2025-09-17 09:22:00' - '2025-09 -17 09:44:00', Hotfire 3 full pressure data

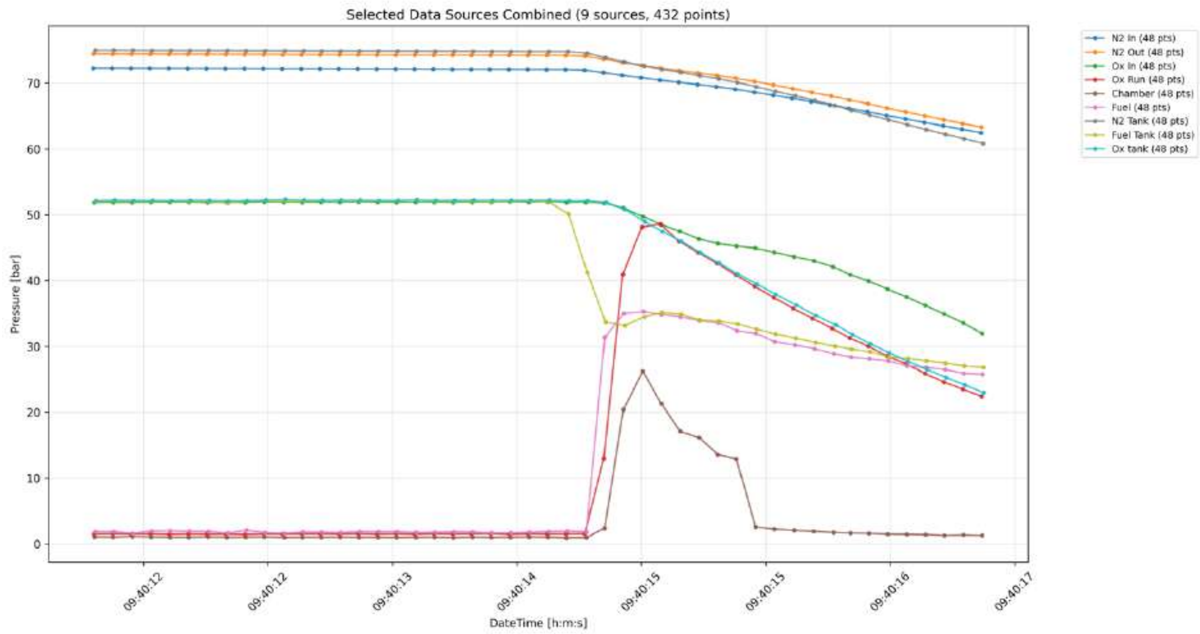

Figure 97 - '2025-09-17 09:40:12' - '2025-09-17 09:40:17', Hotfire 3 burn time pressure data

Figure 98 - Thrust vs Time Graph for the Third Hot Fire

	Name	Configuration	Velocity off rod	Apogee	Velocity at deploym...	Optimum delay
	5.5kN 0.86sec	[E-1.4-0]	34.9 m/s	82.2 m	2.32 m/s	3.72 s

Optimum delay	Max. velocity	Max. acceleration	Time to apogee	Flight time	Ground hit velocity
3.72 s	36.5 m/s	67.2 m/s²	4.58 s	9.42 s	25.9 m/s

Figure 99 - OpenRocket Simulation for Hot Fire 3 Data

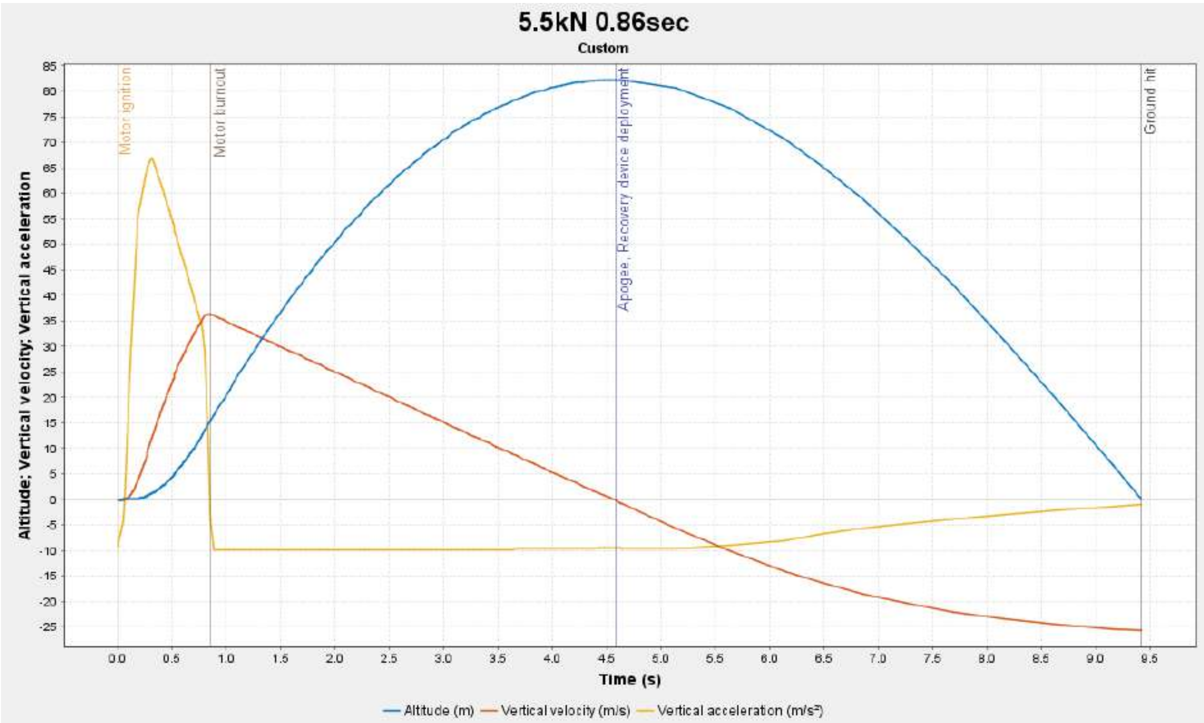

Figure 100 - A Graph of Altitude vs Time for Hot Fire 3 Thrust Data

Figure 101 - A Graph of Stability of Time for Hot Fire 3 Thrust Data

Using the load cell data from the 5.5kN burn for the OpenRocket simulation, a velocity of 34.9 m/s can be observed from the rocket leaving the launch rail. This fully complies with EuRoC-LV-RQT-1100 with a large margin. A stability margin of 2 is observed from leaving the launch rail, with stability dropping to 1calibre at apogee. This is partially compliant with EuRoC-LV-RQT-1030, but this effect will not be reproduced on a full-duration burn.

Propellant Loading & Offloading testing

Loading Leak – Nitrous Loading & Offloading test

As alluded to in the Hot Fire 3 description, on the 4th day we experienced a nitrous leak in our ground station mid fueling process. Since the leak could not be isolated, this meant it was unsafe to hotfire. We used this as an opportunity to demonstrate our propellant offloading sequence. The remaining Nitrous Oxide in the tank was all vented and then the Nitrogen was also successfully vented from both tanks, leaving only the inert IPA and PDMS fuel mixture in the central tank. The IPA was not offloaded to recycle the fuel for the next hot fire attempt.

Procedure:

Once the leak was detected, the following steps were demonstrated

1. Manually fill fuel tank
2. Fill Nitrogen tank
3. Begin filling Nitrous tank
4. Observe Nitrous tank pressure loss
5. Close ground station Nitrous fill valves
6. Still observe Nitrous tank pressure loss
7. Conclude there is a Nitrous leak – No go for firing

8. Vent Nitrous out of tank
9. Observe ambient pressure in the Nitrous Tank
10. Open Nitrous Pressurization valve
11. Vent Nitrogen through empty Nitrous Tank

Pressure Regulator Tuning – Fuel Loading & Offloading test

The pressure regulator needed to be tuned up from 40 bar to 50 bar so we took this as an opportunity to demonstrate fuel loading and offloading.

1. Manually tune pressure regulator to estimated desired point
2. Manually fill fuel tank
3. Slowly remotely fill nitrogen tank to slightly above 50 bar
4. Observe pressure difference across the regulator
5. Close Fuel tank pressurization valve
6. Vent nitrogen out of nitrogen tank
7. Open fiel tank vent valve and vent pressure
8. Open fuel run valve to evacuate fuel

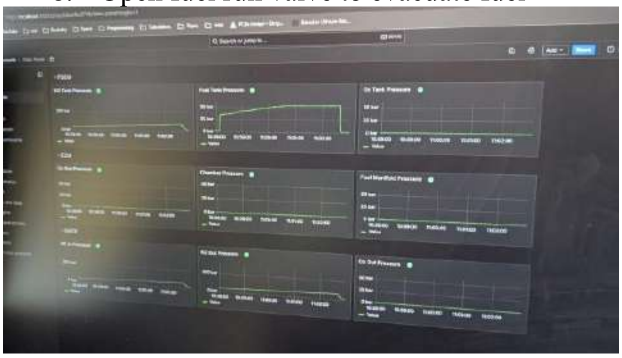

Conclusion

We believe that this testing campaign demonstrates the ability of our propulsion system to achieve the requirements set out in the EuRoC SRD. Despite not achieving a combined design thrust and full duration hot fire, the data we have presented within this report shows our capability to complete a full duration burn with sufficient thrust to exit the rail with sufficient velocity, as well as the fact that we have demonstrated we can produce more thrust with a new system configuration to ensure a margin of safety in rail speed. We have also demonstrated that our sparkler ignitor is a reliable ignition source, having successfully ignited the engine 3 times in a row under varying conditions with no hard starts, demonstrating rapid smooth ramp up.

Signatures:

Tom Wormald Georgiy Lesyuk Ethan Sheehan

B.7 2024/2025 Tank Failure Analysis

The testing carried out over the 2024/25 design cycle saw a failure in the propellant tank because of an ignition failure that led to a valve actuation failure and ultimately a tank failure. Focus lies on the tank failure as it is the only part of the system which could not be easily and quickly fixed. Ultimately the tank failure led to the end of the testing campaign. An attempt to mitigate this failure going forwards must be supported by full appreciation and analysis of the observed failure conditions. To this end a revaluation of the simulations of the failure was conducted. We observed in practice an outer tank pressure of 38 Bar acting on an empty inner tank. This pressure gradient is thus the value in which failure occurs. The strategy for simulations was that of simplification. By simply modelling the inner tank with pinned constraints on either end and a force of 30 bar acting in a buckling analysis, a failure pressure of ~40 bar was observed. This is in good correspondence with the observed buckling result.

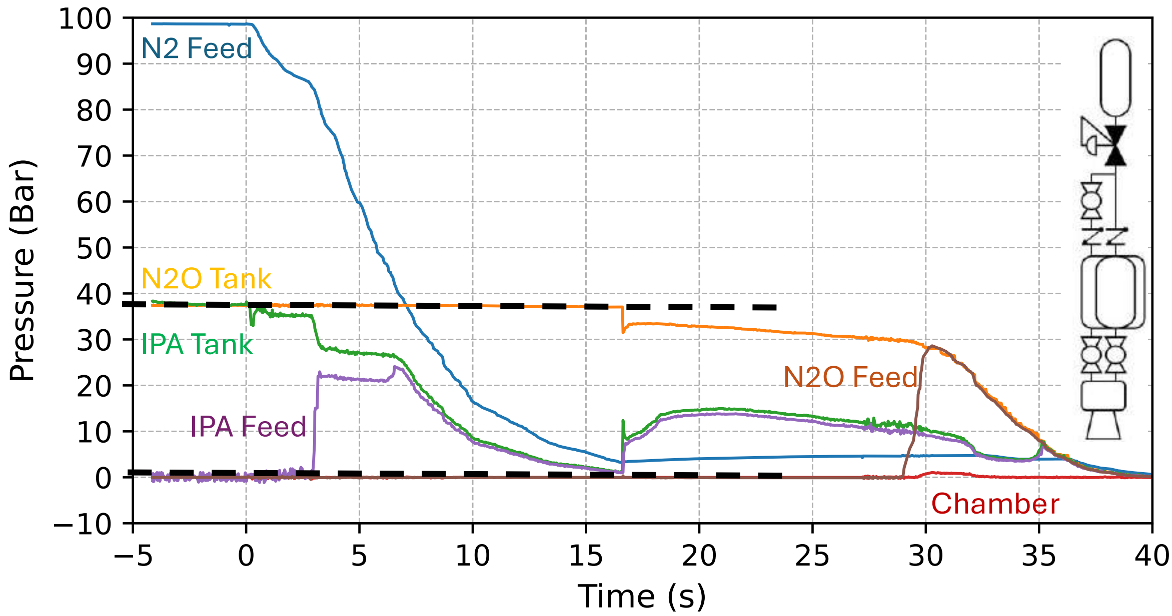

Figure 14, pressure breakdown from Second Star testing

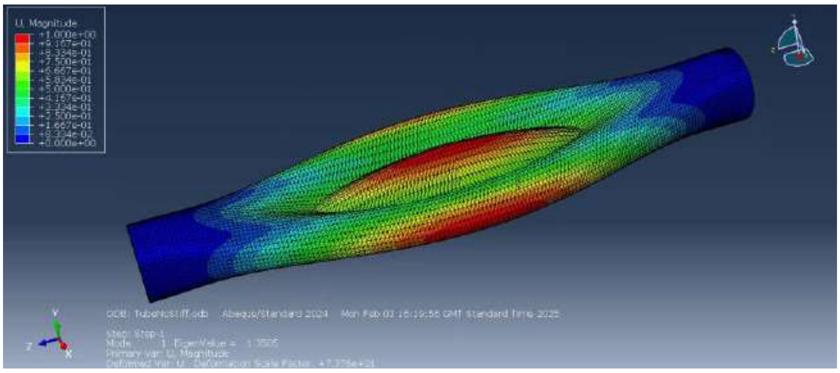

Figure 15, simulated inner tank buckling. Buckling in sim occurs at the exactly the same pressure that the tank buckled at during testing

B.8 2025 Initial tank Hydrostatic Testing



Tank before hydro testing View of tank buckling Axial view of tank buckling

Following our initial hydrostatic test campaign at Astron Systems the inner tank had buckled, as seen in the Figures above. We believe this to be as a result of the incorrect placement of the stiffening rings and improper adherence to the walls of the tank itself; in addition to problems in simulating a non-homogeneous structure using our FEA methods. This was further complicated by limitations in manufacturing (specifically the length of the lathe bed) meaning that the inside of the tank could not be bored to a specific diameter – rather the internal diameter of the stock (and hence the imperfections of it) was utilised resulting in a poor fit for the stiffening rings.

The testing consisted of three main phases – 1) An outer tank pressurisation test up to 85 bar 2) An inner tank pressurisation test up to 85 bar 3) Both tanks being pressurised to 75 bar. Following the first test we attempted to complete the second, however we noticed a build up in pressure in the outer tank in direct proportion to the pressure in the inner tank, this indicated to us that there was a breach between the tanks and hence a redesign was necessary.

Following our initial hydrostatic test campaign at Astron Systems the inner tank had buckled, as seen in the figures above.

B.9 Chamber Hydro-static Pressure Test

- Identical engine design to the flight engine tested during out 2024 integrated test campaign
- Hydro-statically tested for 10 minutes to 30 bar
- 20 bar is nominal chamber pressure for 5 s burn duration

Setup

1. A blanking plate, with an internal o-ring seal, was applied to the nozzle outlet of the combustion chamber.
2. The system filled with water and pressurised with nitrogen to 30 bar.
3. The system held pressure for greater than 10 minutes.
4. The system was then vented.

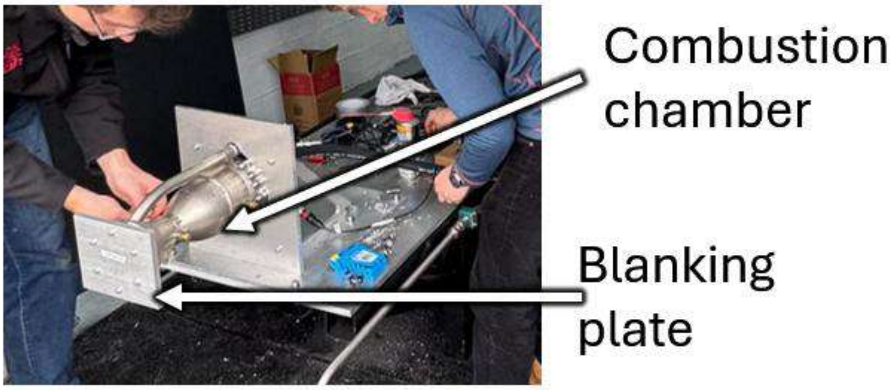

Results

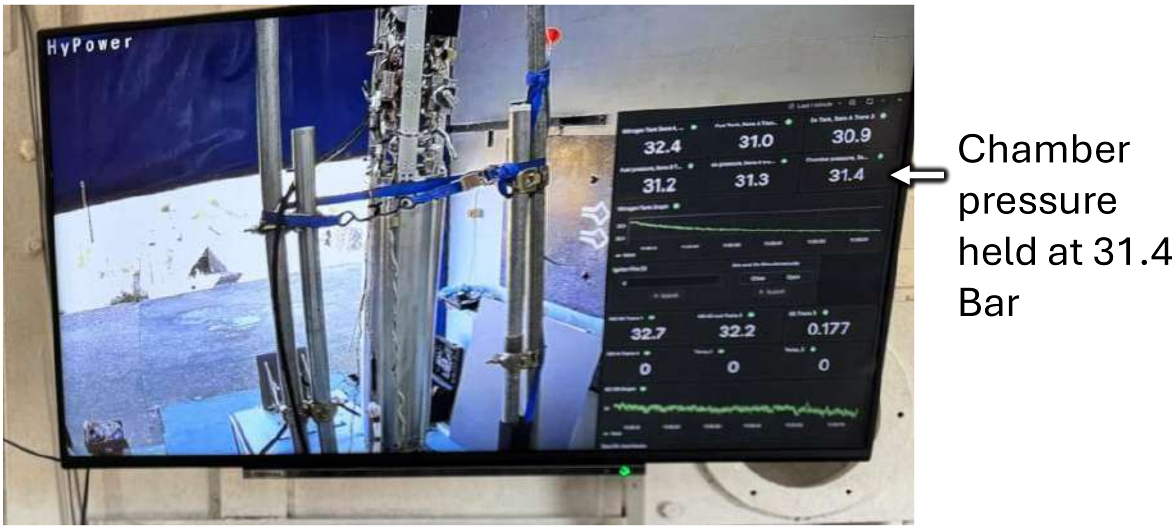

No damage observed in chamber or injector. No leaks observed from engine seals.

Signatures

B.10 January 2025 Engine Testing

On 10th January the engine and injector plate described above was hot fire tested at Airborne Engineering Ltd.

Property	Design Value	Test 1	Test 2 Matching chamber pressures	Test 3 Capability demonstrator	Unit

			Matching design flow rates			
Nominal thrust		5.0	4.35	4.96	5.94	kN
Burn duration		5.5	3.0	3.0	3.0	s
Specific Impulse		198.32	177.82	174.80	179.81	s
Fuel		78% IPA 20% Water 2% PDMS	98% IPA 2% PDMS			[-]
Oxidiser		N_2O	N_2O			[-]
Fuel mass flow rate	Target	0.64	0.64	0.74	0.74	kg/s
	Measured		0.64	0.73	0.75	kg/s
Ox mass flow rate	Target	1.93	1.93	2.24	3.50	kg/s
	Measured		1.86	2.16	2.62	kg/s
OF mass ratio (Meas)		3.01	2.92	2.95	3.52	[-]
Chamber Pressure		20	17.48	19.62	23.55	bar

Measurements taken as the mean average between 1.5 – 3 s.

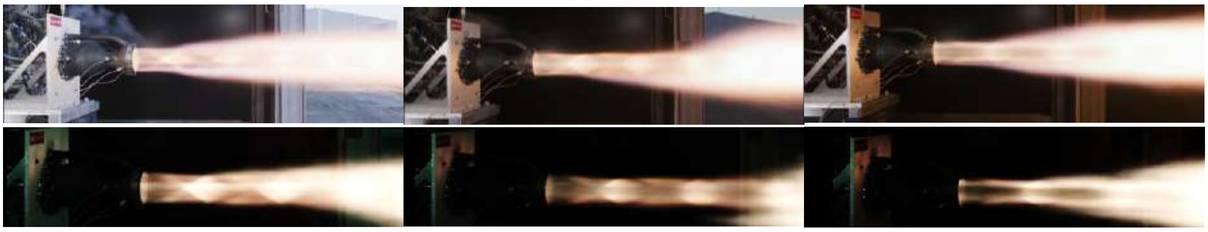

Fig. 1 Photos of steady state nozzle plume from test 1-3. Top: high res camera, bottom: slow motion camera.

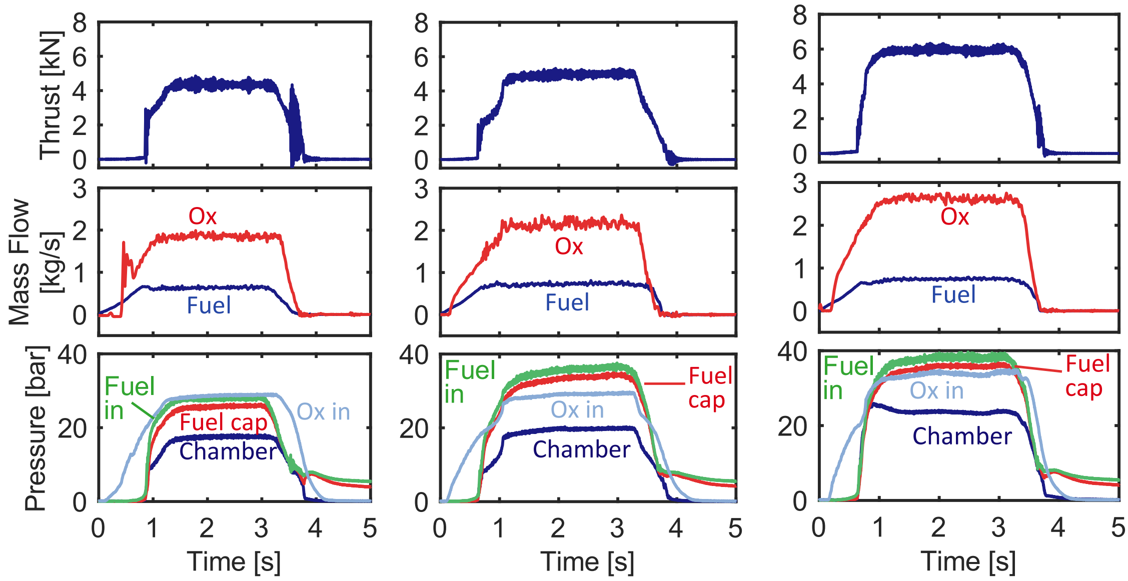

Fig. 2 Time domain plots of hot fires 1-3.

Property	Design Value	Test 1 Matching design flow rates	Test 2 Matching chamber pressures	Test 3 Capability demonstrator	Unit
Regen pressure drop		2.20	2.37	2.37	bar

CdA regen		3.74e3	3.80e3	3.74e3	m^-2
IPA pressure drop		11.06	13.80	12.17	Bar
N2O pressure drop		8.12	9.40	10.27	Bar
Cd IPA Injector		0.7694	0.6880	0.7462	[-]
Cd N2O Injector		0.5149	0.5423	0.6306	[-]

Tear Down

B.11 July 2025 Hot Fire Testing

On the 1st of July the BSEP Engine 2 was hot fire tested at Airborne Engineering Ltd.

<table>
<tr><th colspan="2">Property</th><th>Design Value</th><th>Average</th><th>Peak</th><th>Min</th><th>Unit</th></tr>
<tr><td colspan="2">Nominal thrust</td><td>5.0</td><td>1.59</td><td>3.78</td><td>1.02</td><td>kN</td></tr>
<tr><td colspan="2">Burn duration</td><td>5.0</td><td colspan="3">5.0</td><td>s</td></tr>
<tr><td colspan="2">Specific Impulse</td><td>198.32</td><td>114.13</td><td>249.55</td><td>73.90</td><td>s</td></tr>
<tr><td colspan="2">Fuel</td><td>99% IPA
1% PDMS</td><td colspan="3">99% IPA
1% PDMS</td><td>[-]</td></tr>
<tr><td colspan="2">Oxidiser</td><td>N_2O</td><td colspan="3">N_2O</td><td>[-]</td></tr>
<tr><td>Fuel mass flow rate</td><td>Target</td><td>0.64</td><td>0.36</td><td>0.93</td><td>0.0</td><td>kg/s</td></tr>
<tr><td>Ox mass flow rate</td><td>Target</td><td>1.93</td><td>1.06</td><td>1.14</td><td>0.96</td><td>kg/s</td></tr>
<tr><td colspan="2">OF mass ratio (Meas)</td><td>3.01</td><td>2.96</td><td>inf</td><td>1.19</td><td>[-]</td></tr>
<tr><td colspan="2">Chamber Pressure</td><td>20</td><td>7.02</td><td>10.63</td><td>3.36</td><td>bar</td></tr>
</table>

Measurements taken as the mean average between 1 – 5 s.

The burn can be split into 5 clear segments:

- Ignition: – 0.73
- Low Fuel Burn: 1.04 – 2.10
- Burn-through: 2.10 – 4.16
- High Fuel Burn: 4.16 – 5.21
- Shutdown 5.21 –

Image	Value

Ignition Phase	
	0.27
	0.38
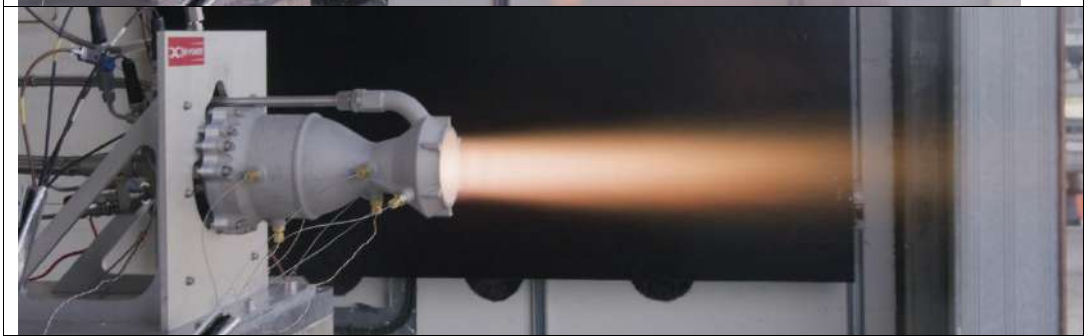	0.48
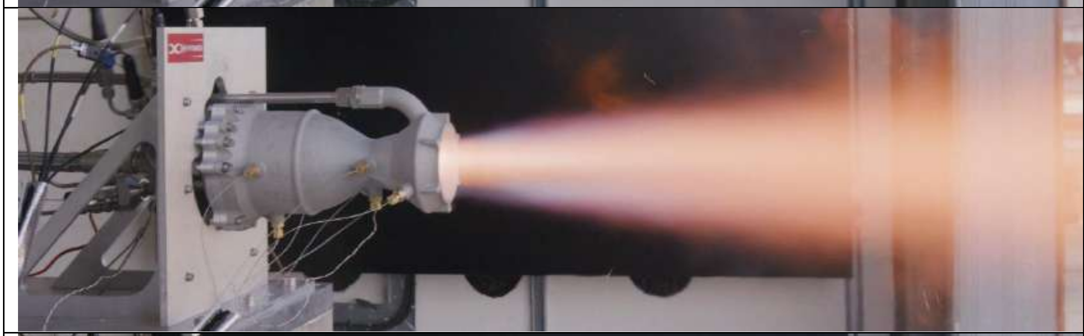	0.49
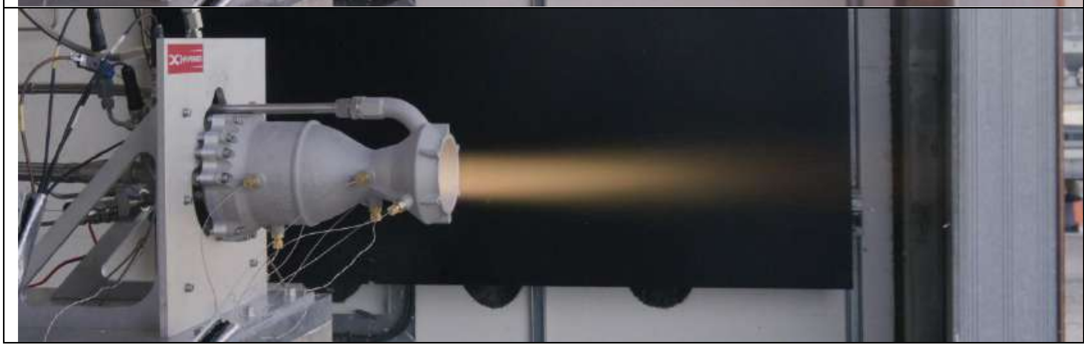	0.57

	0.77
Low Fuel Phase	
	1.18
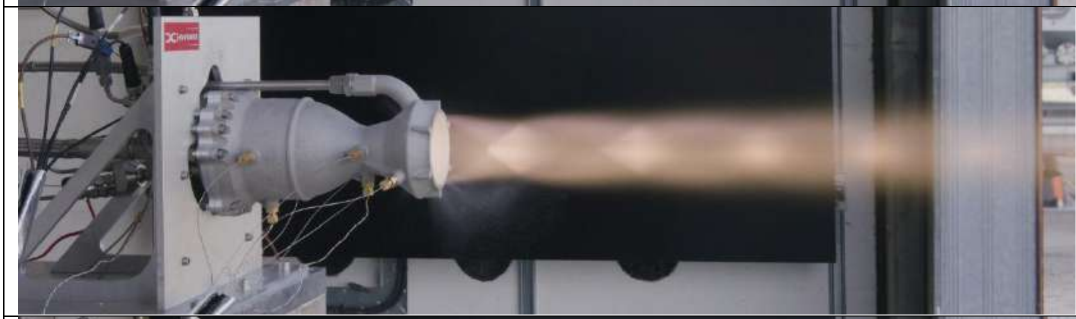	1.20
	1.92
Burn-through Phase	
	2.12

	2.28
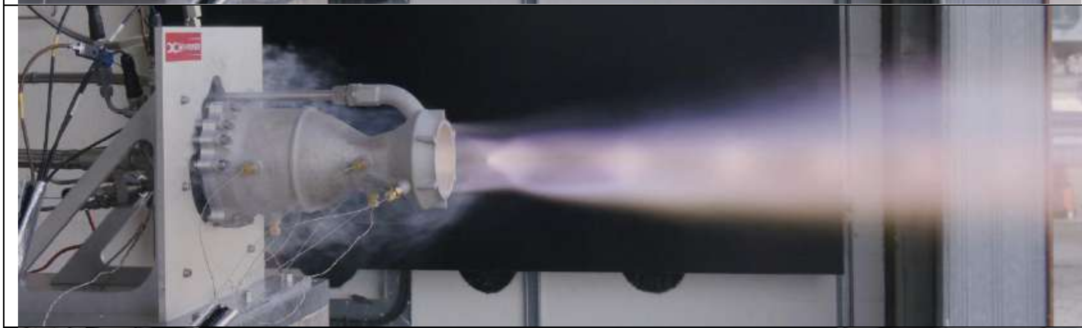	3.09
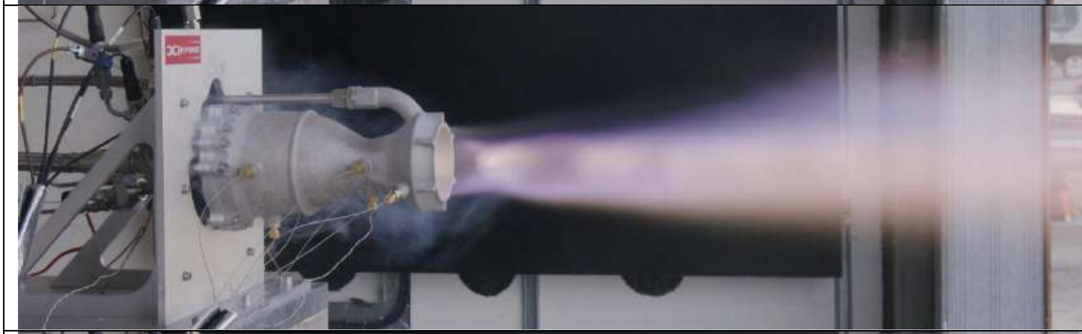	3.49
	3.57
High Fuel Phase	
	4.29

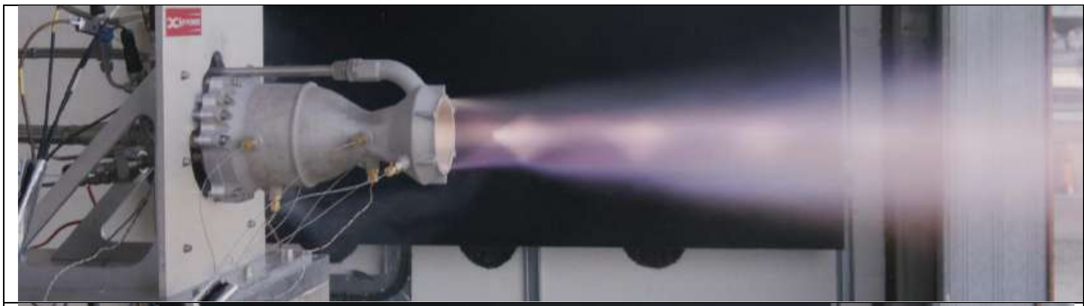	4.72
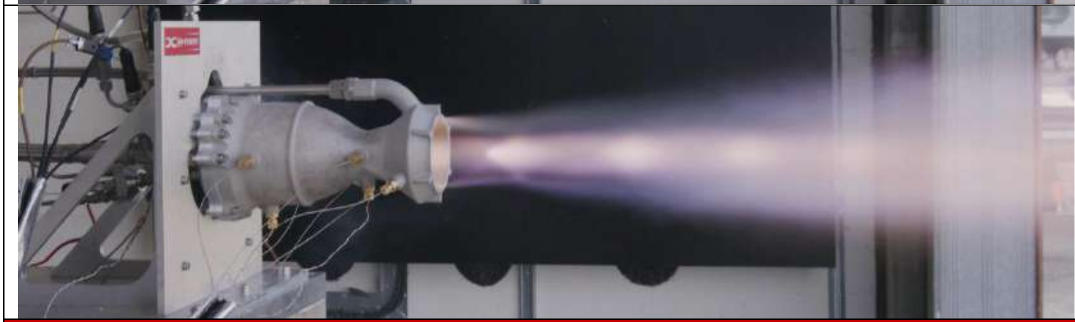	5.05
Shutdown Phase	
	5.42

What we believe happened is illustrated in the images above and the graphs below. After a successful ignition from Airborne's torch igniter, the plume dies down and then fully ignites around T+1.04. Instead of achieving the full 5kN of thrust and bright white plume we were expecting (since it should have been similar to our previous engine), only ~1.5kN of thrust were produced and the plume is weak, hazy and yellow. The IPA mass flow then drops to virtually 0kg/s for ~0.53s and then actually 0kg/s for ~0.39s.

This lack of fuel mass flow is due to swarf, that was inside the regen cooling channels and chamber manifold, being forced into the injector and clogging it. Surprisingly, the flame does not die out, only weakening, until T+2.10 where we believe burn-through occurred.

Since no fuel was flowing, nothing was cooling the chamber. The film cooling holes were completely blocked by the swarf so it effectively did not exist. The PDMS fuel additive cannot deposit if no fuel is flowing, so it effectively did not exist. The regenerative cooling was blocked so we believe the coolant was boiling and stagnant which means it could not absorb heat from the inner wall, so it effectively did not exist. All this combined with the fact that it was burning extremely ox rich makes it extremely unsurprising that the chamber failed.

At T+2.12, the plume begins to turn purple and the IPA mass flow rate begins to increase. This is where the first channel burst, followed by a few more, completely changing the colour of the plume. At this point, Airborne's fuel valve has a stroke trying to keep up with the rapid sudden change in IPA mass flow, leading to weirdness throughout all the data and an unstable burn.

Finally, at T+4.16, the IPA mass flow stabilizes and the engine completes its full duration burn in a relatively steady state.

In conclusion, the chamber performed admirably given its conditions and the fact that the injector worked throughout the chaos and abuse is a promising sign in validating the design.

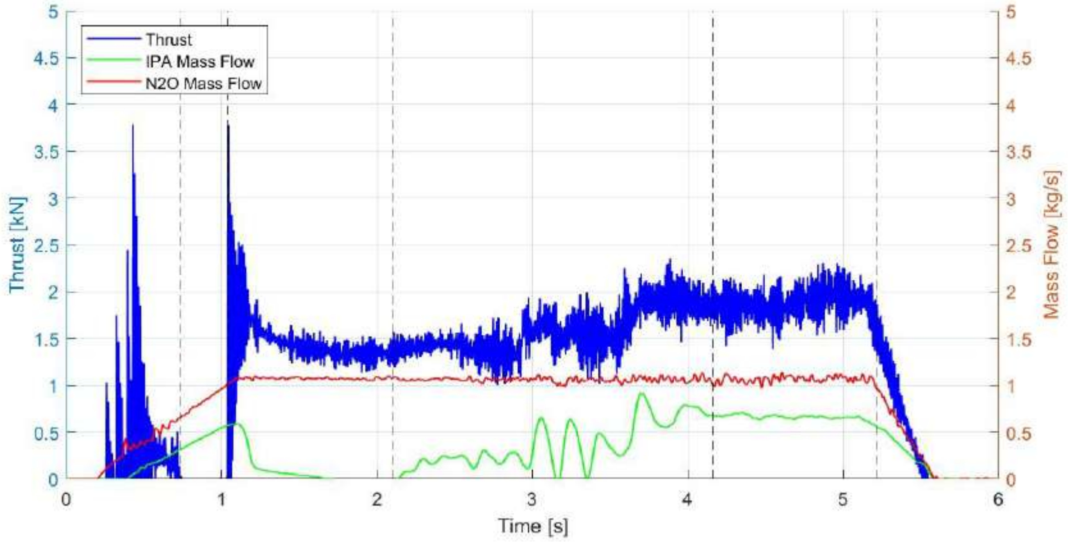

Figure 102, graph showing Thrust and mass flows against Time. The distinct phases of the burn can clearly be seen in the Thrust and IPA mass flow lines while the N2O remains steady but below the desired value. Each spike in the IPA mass flow line could be a channel bursting and Airborne's fuel valve compensating for it.

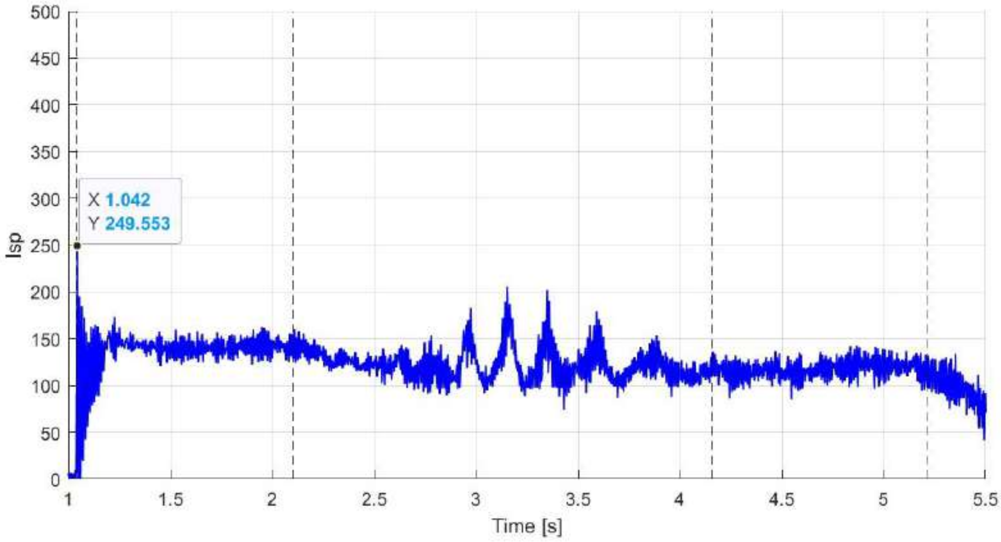

Figure 103, graph showing the Specific Impulse against Time. Clearly peaks and ~250s an gets close to 200s multiple times throughout the burn. Otherwise its really bad so only look at the peaks thanks.

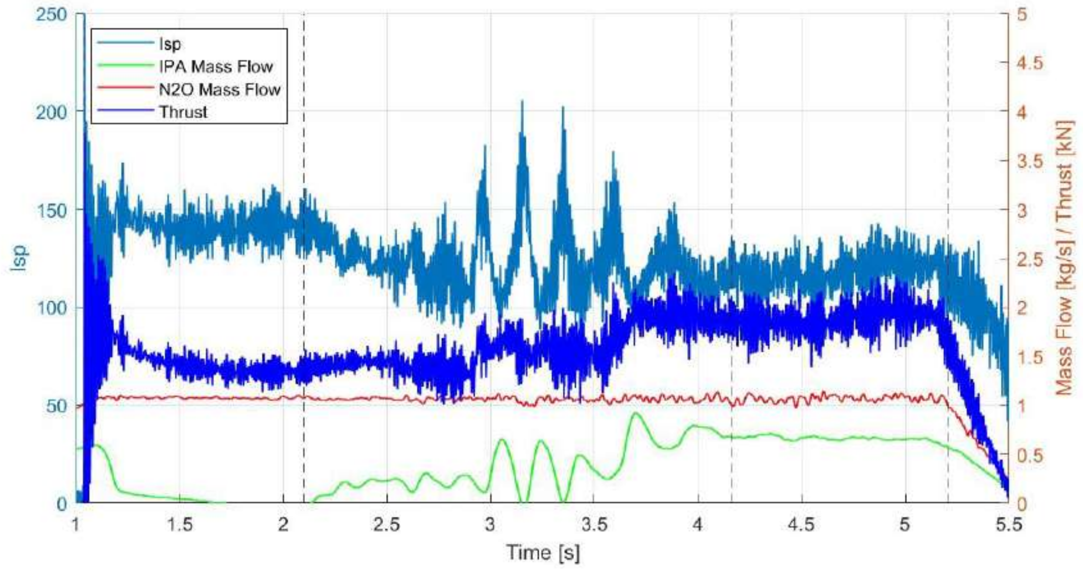

Figure 104, graph combining Figure 1 and Figure 2. Specific Impulse goes crazy when the IPA mass flow has a stroke.

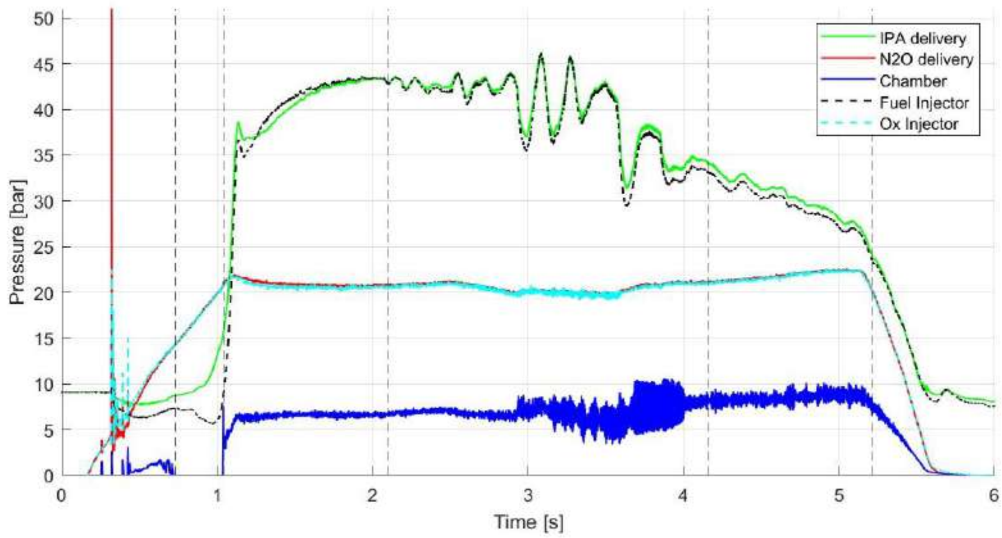

Figure 105, graph showing the pressure data. The pressures inside the injector manifolds can be seen to line up pretty much exactly with the delivery pressures. The chamber pressure remains low throughout the burn, following the pattern of beginning lower, having a stroke, then returning slightly higher. Also worth noting the IPA pressure is ~10 bar higher than expected and the chamber pressure ~10 bar lower than expected, resulting in a net 20 bar greater pressure drop on the inner wall of the chamber between the cooling channels and the combustion area.

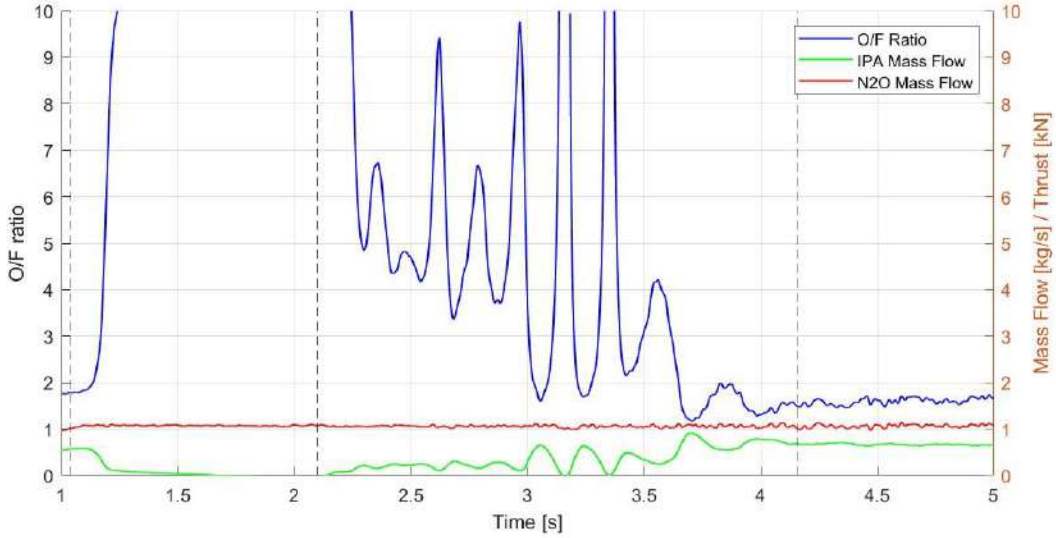

Figure 106, graph showing the mass flows and O/F ratio against Time. As expected, the O/F ratio begins extremely high, most likely abetting the chamber failure. It then swiftly proceeds to have a stroke, and stabilize below the designed ratio.

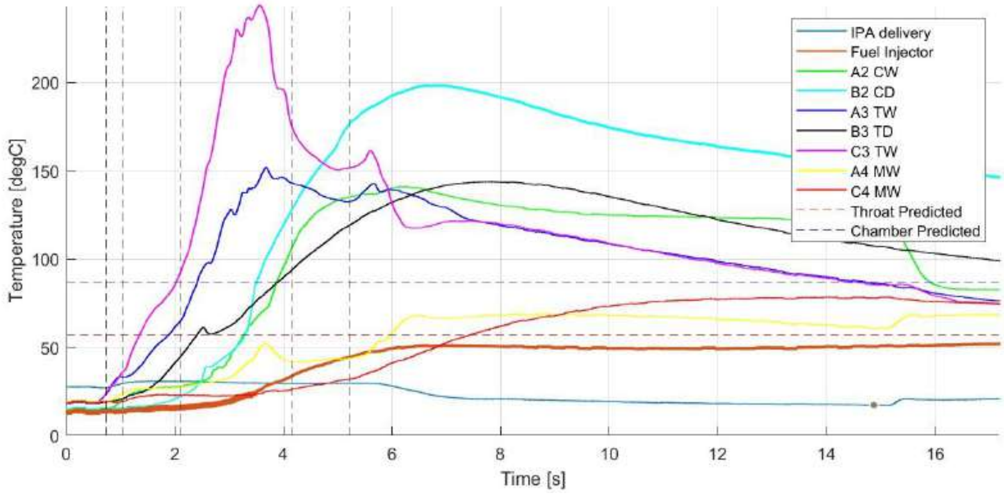

Figure 107, graph showing thermocouple data. See BSEP 2025 CDR for diagram explaining thermocouple placement. A, B, and C run across ¾ of the chamber. 2 is on chamber wall, 3 is at throat, and 4 is in chamber manifold. B thermocouples are dry, the rest are wet. More clear thermal data of specific parts and explanations shown below.

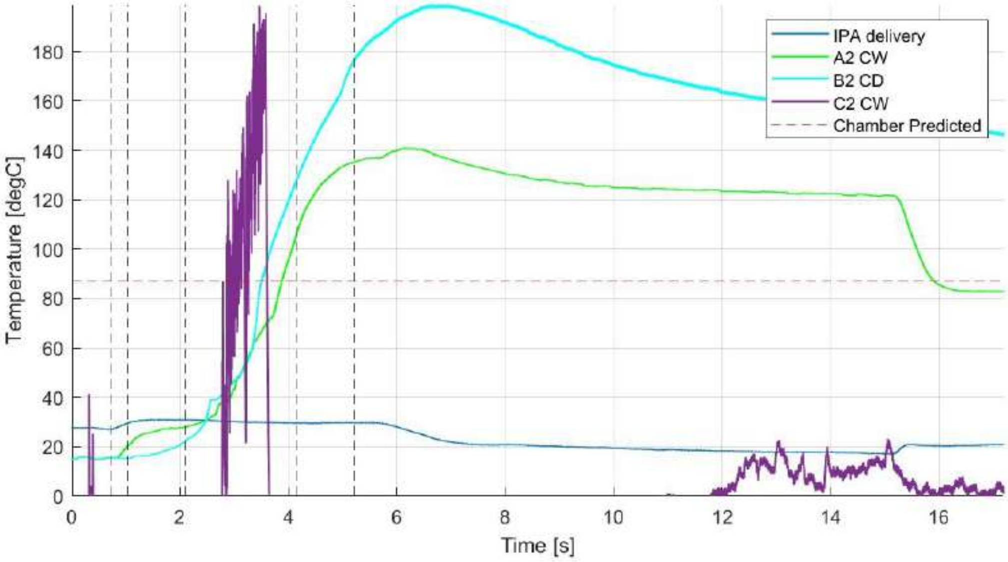

Figure 108, graph showing chamber thermocouple data. C2 will be ignored since it seems to have some sort of issue. A2 is directly reading the coolant temperature and by the end of the burn it is well above the predicted value. B2 also clearly demonstrates the Aluminium does not reach steady state even though it was assumed it would during a nominal burn.

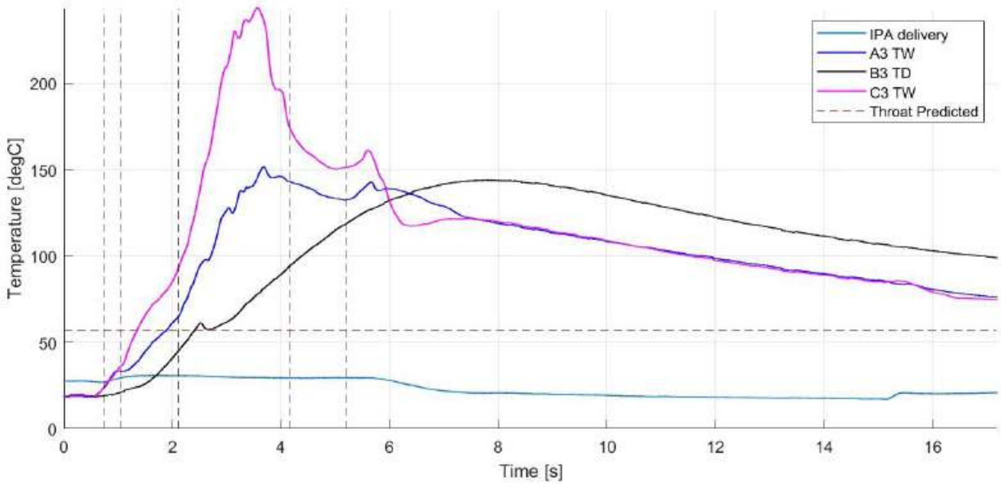

Figure 109, graph showing throat thermocouple data. It is immediately apparent that the throat coolant temperatures are higher than the chamber coolant temperatures. This is extremely disturbing since in our regen system it should always be the opposite, with more heat being added to the coolant as it moves past the throat. This further reinforces the fact that there was no coolant flow. The throat coolant temperatures during the burn also exceed the predicted value by almost 200 degrees and is almost certainly boiling. The C side also seems to be significantly hotter than the A side, which can also be seen in the damage itself. They do line up after the burn though as things cool down which is a good sign of their accuracy.

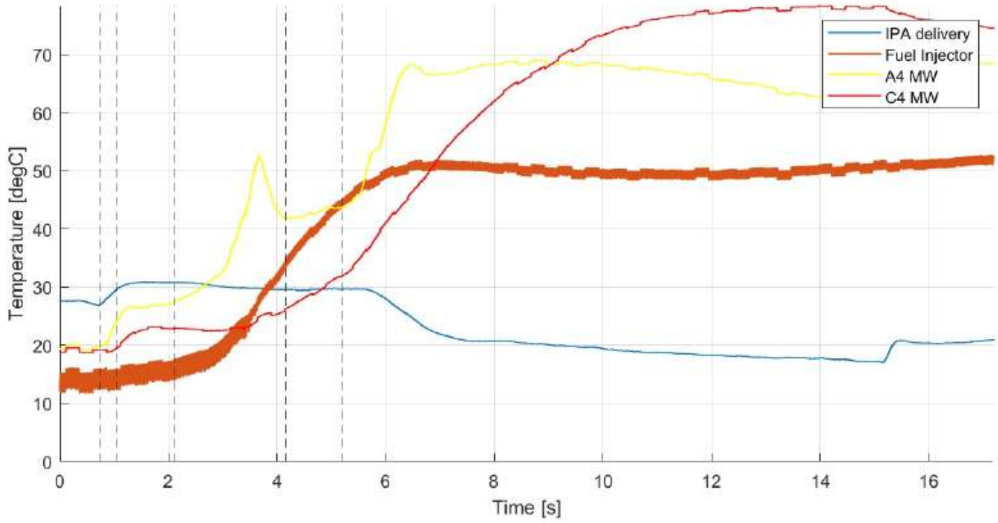

Figure 110, graph showing the chamber fuel manifold and injector fuel manifold thermocouple data. A4 and C4 should be identical but A4 seems to have some anomalies so no conclusions can be drawn from that.

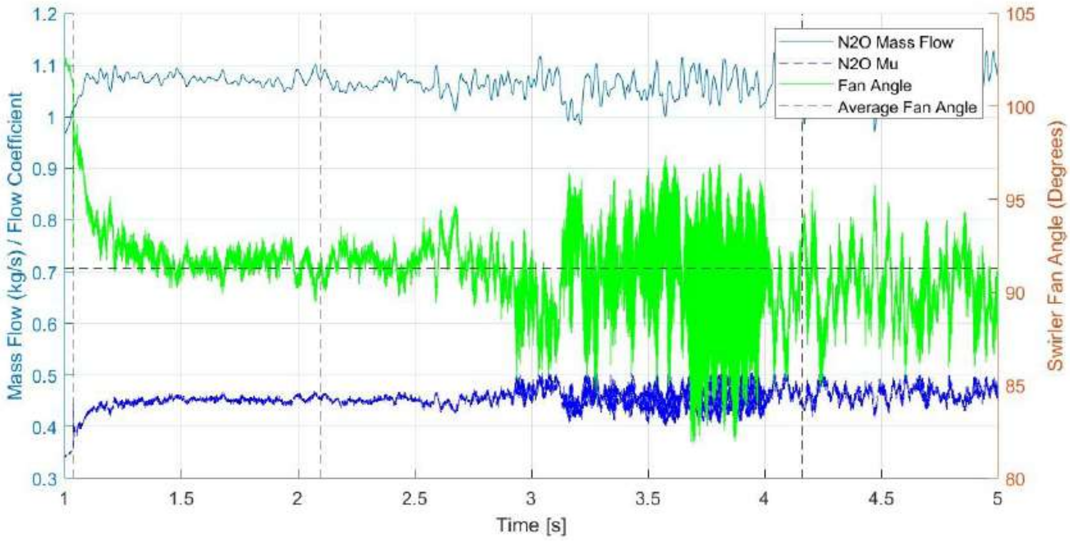

Figure 111, graph showing Injector fan angle against time. For a coaxial swirl Injector, one of the main performance factors is the fan angle (angle of swirled spray cone exiting swirler elements). Since IPA mass flow was unreliable, only the N2O flow was analysed. Originally, the fan angle was designed to be 90 degrees and initial 3d printed elements validated the design. However, due to manufacturing constraints, the angle was changed to 110 degrees and the efficacy of this new angle was only semi-validated during hasty 3d print tests. After processing the data, the average fan angle calculated was 93 degrees. This number is none-conclusive since N2O's 2-phase characteristics lead to a large error bar and the fuel was not accounted for. Nevertheless, if the fan angle was truly close to the calculated 93 degrees under these extremely arduous conditions, it is a good step in validating the coaxial swirl design.

Tear Down

Chamber

Clear bursts can be seen in the chamber. There are 5 major ones and a lot more smaller cracks. Almost every other channel has bulged significantly. This all happened at the same elevation inside the chamber. At first we thought this was where the oxidizer fan from the swirlers were hitting the wall, but the angle does not match. The "popping" of the channels is most likely a combination of the elevated inner wall temperature (due to lack of cooling and higher O/F ratio) degrading the strength of the Aluminium (see CP-1 strength graphs in BSEP 2025 CDR) and the increased pressure delta across the inner wall.

The throat is clearly melted due to the lack of cooling and elevated temperatures. Thin cracks and holes also appear throughout. Also noticeably no PDMS deposition is observed.

The major bursts are clustered and line up exactly where the swirl elements are located. So do the largest streaks of melting at the throat.

Figure 112 & 12, Swarf can be seen trying to escape through the burst channels

Figure 13 & 14, Channels are clearly filled with swarf. Popping and bursts clearly visible as well as throat melt streaks.

Figure 15, Close-up on throat.

Injector

Injector damage was much less significant. Lots of swarf was uncovered during removal, some O-rings were damaged, and some holes were blocked by swarf. After thorough cleaning it should be reusable.

We believe the swarf was introduced during chamber post-machining when the baseplate was machined away. It was not caught during low-pressure water flows since the water just flowed around the swarf instead of pushing it all out.

Figure 16, Injector plate immediately after it was taken off of the chamber. Swarf everywhere.

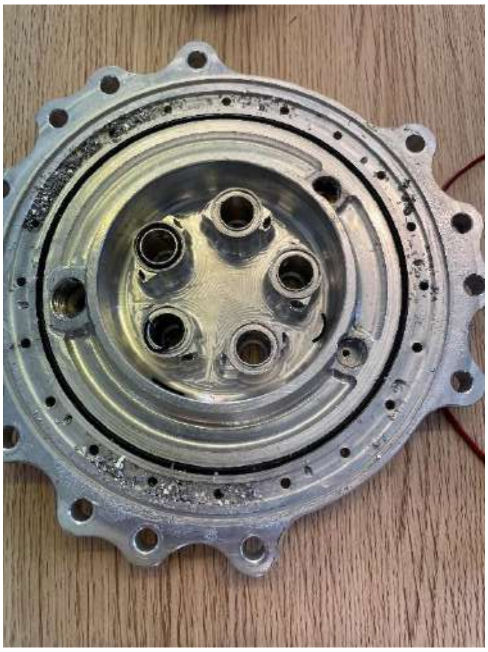

Figure 17, inside Injector. Swarf clearly visible in the fuel collection manifold. Swirl element O-rings broken and missing.

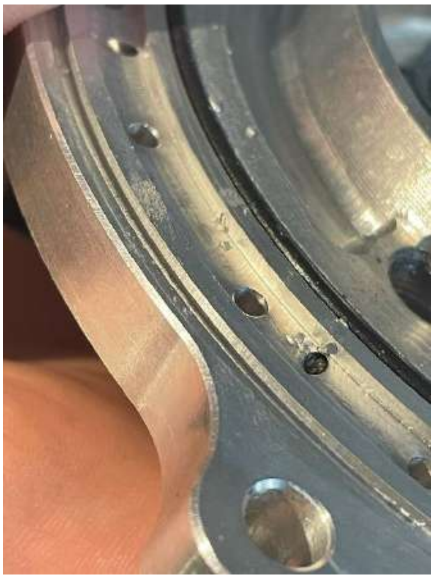

Figure 18, close-up of film cooling hole. Completely blocked by swarf.

Figure 18 & 19, Injector fuel cap and fuel manifold after removal. Massive amounts of swarf deposited inside.

Test Setup

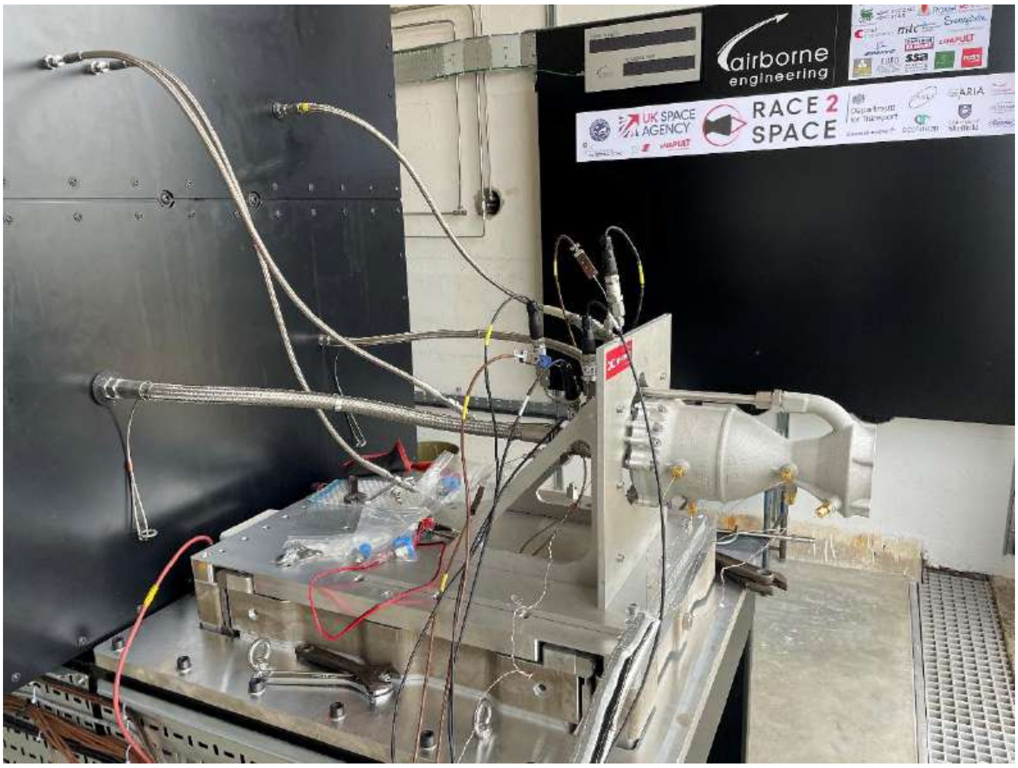

B.12 Oct 2024 Full Stack Testing Summary

In October 2024 we had the opportunity to test our integrated systems at Second Star Space over 4 days. This was our first experience testing our system hydrostatically, under water flows at rated pressure, propellant loading, cold flows with propellant and hot fires.

On the last day our fuel tank imploded, due to an electronics failure.

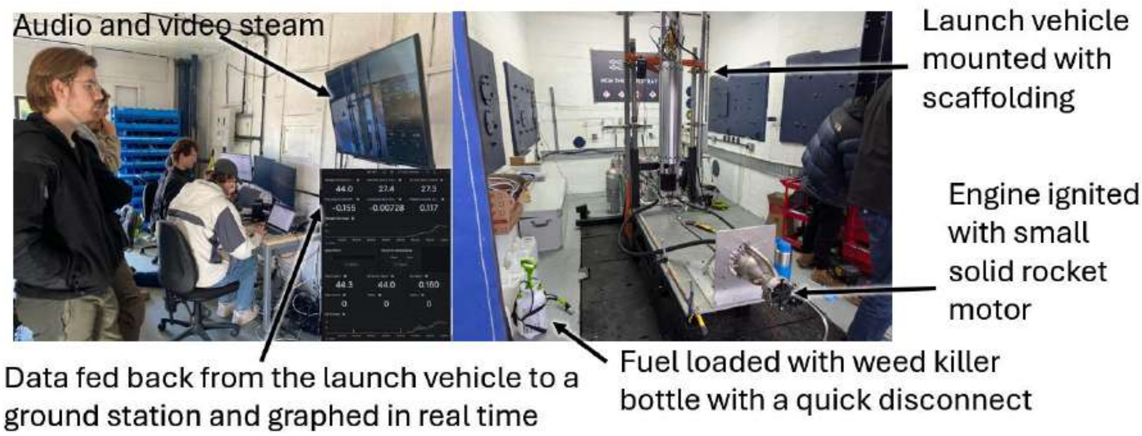

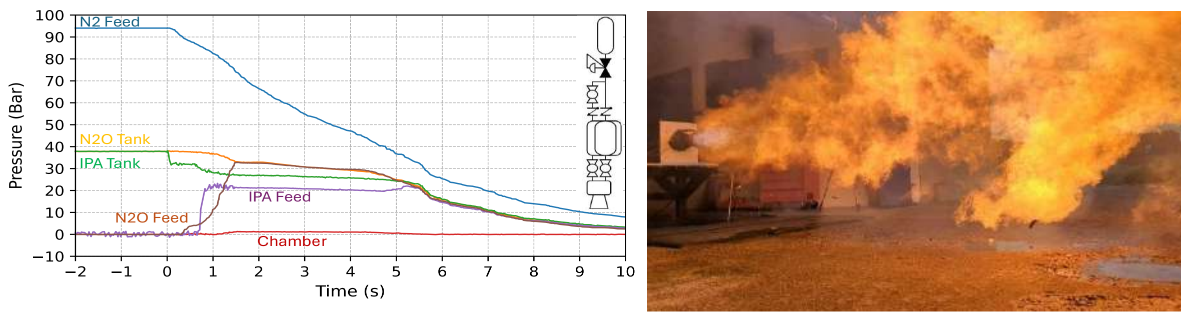

Figure 113 Hot fire data where the flame front was pushed out of the combustion chamber producing negligible chamber pressure.

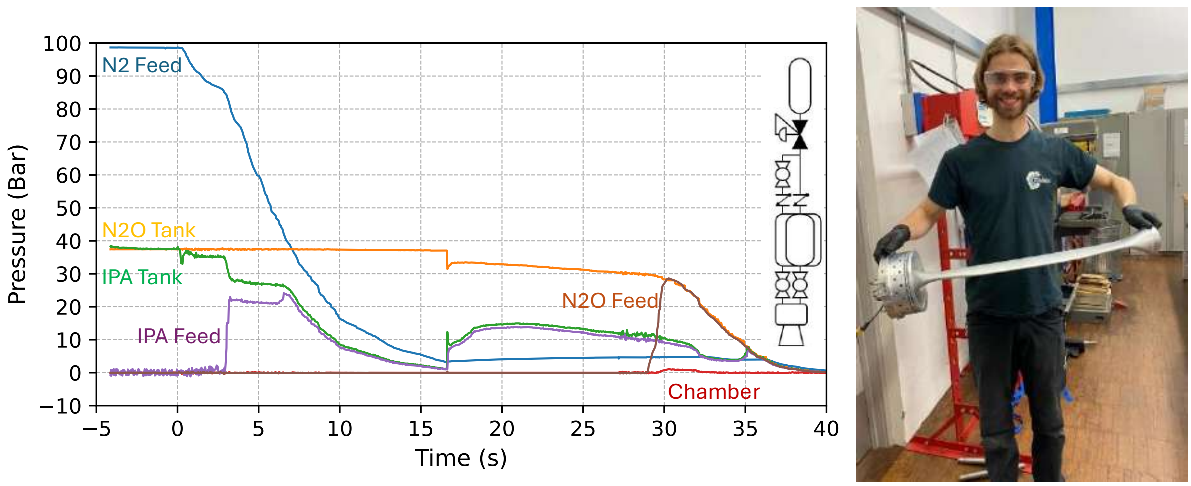

Figure 114 Tank implosion due to valve misfire

C. Hazard Analysis

Propulsion

Component	Hazard	Mitigation
Nitrous Oxide	Fire risk, severe poisoning due to fumes, chemical burns	Follow all instructions from trained professionals. There is to be no transport of Nitrous Oxide containers without explicit permission and instruction of a trained professional. Personnel are evacuated to a safe distance. Checklists are followed, under the supervision of a trained professional.
Ethanol	Fire risk, poisoning due to fumes, chemical burns	Require Personal Protective Equipment (PPE) at all times when handling chemicals, and emergency equipment is nearby and accessible. Ensure no ignition sources are nearby. Use in well-ventilated areas. Store chemicals properly in adequate containers.
High-Pressure Vessels	Explosion or implosion due to overpressure	Always require remote operation a vessel is pressurised. Follow safety guidelines from the manufacturer and range safety officers. Follow instructions of trained professionals. SRAD vessels to be designed ot withstand 3x Maximum Expected Operating Pressure (MEOP), and subjected to testing at 1.5 times MEOP.
Acetone cleaning	Chemical burns, fire risk, poisoning due to fumes	Require Personal Protective Equipment (PPE) at all times when handling chemicals, and emergency equipment is nearby and accessible. Ensure no ignition sources are nearby. Use in well-ventilated areas. Store chemicals properly in adequate containers.
Foreign Object Debris (FOD)	FOD blockage within propulsion system	Adequate checks and tests are carried out to ensure there is no FOD within plumbing system. When assembling, components are to be installed in a FOD-free, and preferably dust-free environment.
Solid motor/gerb ignitor	Unintended Combustion	To be stored in a fireproof container, far from potential ignition sources. To be only removed from container when the environment is adequately checked for ignition sources. Only certified and essential personnel are allowed to handle ignitor sources
E-match	Unintended Combustion	To be stored in a fireproof container, far from potential ignition sources. To be only removed from container when the environment is adequately checked for ignition sources. Only certified and essential personnel are allowed to handle ignitor sources

Launch Vehicle

Component	Hazard	Mitigation
Heavy Lifting/Manual handling	Damage to objects, injury to people	Always lift objects which are within your capability to do so and seek aid/use lifting apparatus if necessary.
Black Powder Handling	Explosion risk	To be stored in a fireproof container, far from potential ignition sources. To be only removed from container when the environment is adequately checked for ignition sources. Only certified and essential personnel are allowed to handle ignitor sources

Composite manufacture	Chemical risk, Chemical burns, fire risk, poisoning due to fumes	Require Personal Protective Equipment (PPE) at all times when handling chemicals, and emergency equipment is nearby and accessible. Ensure no ignition sources are nearby. Use in well-ventilated areas. Store chemicals properly in adequate containers.
Composite post-processing	Severe lung, eye and skin irritation	Require Personal Protective Equipment (PPE) at all times when handling chemicals, and emergency equipment is nearby and accessible. Ensure no ignition sources are nearby. Use in well-ventilated areas. Store chemicals properly in adequate containers.
Spray painting	Lung, eye and skin irritation	Require Personal Protective Equipment (PPE) at all times when handling chemicals, and emergency equipment is nearby and accessible. Ensure no ignition sources are nearby. Use in well-ventilated areas. Store chemicals properly in adequate containers.
Workshop use/using tools	Injury to persons and objects	Require the appropriate Personal Protective Equipment (PPE) at all times when utilising tools; communication to other team members/persons nearby of the work about to take place.

Electronics

Component	Hazard	Mitigation
High current/power electronics	Electrocution and shock	Ensure all working personnel have required competency around high current/power systems.
ESD protection	Damaging components	Ensure all personnel working on sensitive components are grounded.
Lithium-ion batteries	Unintended combustion, electrocution and shock	Battery charging must be balanced using a correctly specified charger. far from potential ignition sources. To be only removed from container when the environment is adequately checked for ignition sources.

D. Risk Assessments

10.4. Risk Assessment

The responsible persons are defined by the following acronyms.

M (Manufacturer)

HPB (HyPower Bristol)

BMS (Bristol Machine Shop)

EO (EuRoC Officials)

L – Likelihood of hazard occurring

S – Severity of hazard

R – Risk, Likelihood x Severity

		Likelihood				
		1	**2**	**3**	**4**	**5**
Severity	**1**	1	2	3	4	5
	2	2	4	6	8	10
	3	3	6	9	12	15
	4	4	8	12	16	20
	5	5	10	15	20	25

Risk Assessments.xlsx

No.	Feature / Hazard	Responsible Persons	Possible consequences without mitigation	Risk Level Before Mitigation			Design Options Available/Actions Taken to Mitigate Risk	Risk Level After Mitigation			Residual Risk
				L	S	R		L	S	R	
Section 1: Manufacturing and assembly											
1.01	Inconel material - dust	Manufactuer	Dust of material can be carcinogenic. Dust of material can be explosive if in strong combustion.	2	5	10	Manufacturer to rid print of dust as part of manufacturing process. HPB to scan and clean out channels again with pressurised water prior to hotfire.	1	3	3	Visual inpsection.
1.02	Inconel material - sharp edges	HPB / BMS	Cutting injury - 3D print may come back with sharp edges	1	2	2	Machine shop to ensure no edges sharp enough to cut.	1	1	1	Handle with care.
1.03	Stainless steel injector - sharp edges	HPB / BMS	Cutting injury on sharp edges.	1	2	2	Machine shop to ensure no edges sharp enough to cut.	1	1	1	Handle with care.
1.04	Plumbing system - swaged connections.	HPB	Trapping injury between connections. Connections at challenging angles to use spanners to swage. Risk of leaks	2	2	4	Consider constraining angles to re-swage items, and assemble system. Removeable panels around plumbing provide easier access. Leak testing to be conducted in lab setting prior to high pressure tests.	1	1	1	N/A
1.05	Valves - servo overheating	HPB	Electronical failure.	1	3	3	Servos to have good airflow around them.	1	2	2	Only power servos when required.
1.06	Valves - fail safe	HPB	Uncontrolled flow of propellant.	3	5	15	Fail safe boards with separate power bus to be used.	1	2	2	Area around rocket loaded with propellant to be kept clear.
1.07	Coaxial tank - design loads	HPB	Failure of tank under pressure.	2	5	10	Design values to use safety factors required from EuRoC DTEG. FEA simulations to verify before test. Construct using a homogenous material, aluminium.	1	2	2	Exclusion zone around fuelling rocket.
1.08	Coaxial tank - assembly	HPB	Injury from entrapment, lifting or sharp edges.	2	2	4	Care to be taken when moving and lifting, always having multiple people.	1	2	2	Tank to be transported in bubblewrap. Do not carry tank for long distances.
1.09						0				0	
Section 2: Testing											
2.01	Plumbing system	HPB	Failure of plumbing under pressure. Risk of leak.	1	3	3	All plumbing parts purchased to be able to withstand worst case scenarios. Leak testing to be conducted.	1	1	1	N/A
2.02	Valve actuation	HPB	No flow of propellant.	2	1	2		1	1	1	N/A
2.03	Chamber under pressurised tests	HPB	Failure of chamber under pressure	2	5	10	FEA simulations and hoop stress calculations results below yield strength	1	4	4	Area around rocket loaded with propellant to be kept clear.
2.04	Valve actuation under pressurised tests.	HPB	Uncontrolled flow of propellant.	3	5	15	Individual valves to be tested to ensure they can close under pressure	1	5	5	Area around rocket loaded with propellant to be kept clear.
2.05	Coaxial tank under pressurised tests.	HPB	Failure of tank under pressure.	2	5	10	Tank designed to beyond MEOP, Testing of tank capacity.	1	2	2	Exclusion zone around fuelling rocket.
2.06	Loading nitrous oxide into coaxial tank	HPB	Risk of leaks. Self pressurisation of propellant.	2	2	4	Leak testing to be conducted. Tank cavity designed and tested to take 1.5x MEOP of 55bar that Nitrous Oxide can self pressurise to.	1	2	2	Exclusion zone around fuelling rocket.
2.07	Loading 300bar nitrogen into pressurant tank	HPB	Failure of pressurant tank under pressure.	1	5	5	COTS tank designed to beyond MEOP, Testing of tank capacity. Burst Pressure is 1000bar.	1	2	2	Exclusion zone around fuelling rocket.
2.08	Sequencing of coaxial pressurisation.	HPB	Buckling of fuel tank.	2	3	6	Internal chamber to be pressurised using regulated pressurant before fuelling of nitrous oxide begins.	2	2	4	Exclusion zone around fuelling rocket.

2.09	Sealing face between injector and chamber	HPB	Risk of leak.	1	2	2	Smooth faces with industry guidance followed for O-ring specifications and groove depths. Leak testing to be conducted.	1	1	1	Exclusion zone around hotfire of engine.
2.1	Pressure regulator	HPB									
Section 3: Launch Operations											
3.01						0				0	
3.02	Over-pressurisation of tanks	HPB	Failure of tanks due to pressure	2	5	10	Tank designed to beyond MEOP, Testing of tank capacity.	1	2	2	Exclusion zone around fuelling rocket.
3.03	Debris in propellant lines	HPB	Blockage of propellant line. Failure due to increased pressure.	3	4	12	Propellant lines to be thoroughly cleaned before testing	1	1	1	N/A
3.04	Off-nominal valve actuation	HPB	Uncontrolled flow of propellant.	3	5	15	Exclusion zone, limited amount of propellant. Ignition lines to be unarmed.	1	2	2	N/A
3.05	Rocket motor for ignition	HPB	Dislodgement from launch vehicle Premature misfire of explosives	2	3	6	Igniter to be securely attached. Testing to be conducted of igniter electronics.	1	2	2	Residual match risk of explosives.
3.06	Ignition	HPB	Risk of engine not lighting	3	1	3	Abort sequence through feed system can be actuated. Following launch windows could be used.	1	2	2	Exclusion zone around rocket.
3.07	Hard start of rocket engine	HPB	Risk of over pressurization in chamber during ignition causing an explosion	1	5	5	Chamber designed to beyond MEOP, Testing of tank capacity.	1	2	2	Exclusion zone around rocket.
3.08	Blocked channels of regen cooling	HPB	Melting at throat due to loss of cooling. Loss of fuel pressure in injector.	3	2	6	Channels to be cleaned out prior to hot fire	1	1	1	Exclusion zone around rocket.

No.	Feature / Hazard	Responsible Persons	Possible consequences without mitigation	Risk Level Before Mitigation			Design Options Available/Actions Taken to Mitigate Risk	Risk Level After Mitigation			Residual Risk (action required on site)
				L	S	R		L	S	R	
Section 1: Manufacturing, Assembly and Test											
1.01	Composites and epoxy	HPB	Handling of COSHH items can be hazardous to health	2	3	6	Work in open/ventilated spaces. Wear gloves and lab coat.	1	2	2	First aid and handwashing stations available.
1.02	Demoulding composite parts	HPB	Sharp edges on composite parts. Some composite parts may need to be removed with force from mandrels.	2	2	4	Demoulding to take place in a safe area, with PPE and lab guidelines met.	1	2	2	First aid available, minimise number of persons present.
1.03	Thrust structure design loads	HPB	Thrust structure could buckle under force from engine.	3	5	15	Thrust structure to be able to withstand design loads of combined thrust and aerodynamic loads.	1	3	3	Eyes to be kept on the sky.
1.04	Stringer joints into bulkheads	HPB	Stiffness discontinuity found at joints could provide a weak point.	2	3	6	Bolted connection to be well seated to provide rigidity.	1	2	2	Eyes to be kept on the sky.
1.05	Connection of panels to stringers	HPB	Aerodynamic forces could cause lifting of panels from stringers.	3	3	9	Bolted connection to be at regular intervals, as well as providing good rigidity within the panel.	1	3	3	Eyes to be kept on the sky.
1.06	Stringer design loads	HPB	Stringers could buckle under thrust loads.	2	3	6	Stringers designed to be able to withstand flight loads with safety factor margin.	1	3	3	Eyes to be kept on the sky.
1.07	Stressed aeroshell	HPB	Loads need to be transferred through aeroshell, could experience cracking failure.	2	3	6	Top edge near recovery lines to be reinforced. Aeroshell designed to take thrust and bending loads.	1	3	3	Eyes to be kept on the sky.

1.08	Blast bulkhead	HPB	Under ejection charges, the blast bulkhead could fail. Tensile load from parachute could result in a pull-out failure of eyebolt or bulkhead.	2	5	10	Bulkhead is designed with a deep thread. Load testing of bulkhead. Ejection testing of system.	1	2	2	Eyes to be kept on the sky.
1.09	SRAD main parachute	HPB	Failure of parachute construction.	2	5	10	Industry standard material used. Researched construction techniques.	1	2	2	
1.1	Stability of rocket	HPB	An unstable rocket would lead to an uncontrolled flight.	2	5	10	RocketPy and Open Rocket simulations to confirm that rocket is stable.	1	3	3	Eyes to be kept on the sky.
1.11	Sharp edges on launch vehicle or payload	HPB / BMS	Injury from cutting.	2	2	4	Sharp edges to be filed down where possible.	1	1	1	Handle with care.
Section 2: Launch Operations											
	Surrounding area to the launch pad	HPB/EO	Trip hazards. Risk of misfiring pyrotechnics igniting something on the ground.	1	3	3	Make sure all combustible materials have been removed from the ground surrounding the launch pad.	1	1	1	N/A – Risk considered mitigated.
	Mis-ignition of any pyrotechnic	HPB/EO	Risk of ignition of live rocket, and injury to persons.	1	5	5	Igniter to only be installed once vehicle is on rail and as last step before people evacuate the area.	1	3	3	Persons in proximity to be made aware when rocket is made live.
	Dislodgement of launch button	HPB	Risk of launch button not taking stress of launch. Risk of launch button binding to the rail.	2	5	10	Launch button attachment to be able to support the full weight of the rocket. Plastic launch lug to be used to prevent binding.	1	3	3	N/A – Risk considered mitigated.
3.01	Shock cord breaking	HPB	Components of the rocket would freefall out of the sky, with a worst case of hitting persons.	1	5	5	Rated shock cord to be used.	1	3	3	Eyes to be kept on the sky.
3.02	Rocketry objects falling from sky	HPB	Risk that no parachutes deploy and descent is uncontrolled.	2	5	10	Flight computers to be bench tested. Redundant flight computers to be on board, to be live for the whole flight. Redundant ejection charges to be used, with different timing to the intended deployment. Launch to only occur in designated area, away from persons.	1	3	3	Eyes to be kept on the sky.
3.03	Weather takes rocket off course	HPB/EO	Danger of flight or decent being uncontrolled and rocket being out of range or descending near persons.	2	5	10	Do not launch if ground level winds exceed 20 mph or if any type of lightning is detected within 10 miles of the launch site No launch if the planned flight path will carry the vehicle through any clouds	1	2	2	Eyes to be kept on the sky.
3.04	Rocket lands in unsafe territory	HPB/EO	Rocket may drift of course and land in an unknown area.	2	3	6	GPS tracker to be onboard. RocketPy simulations with accurate weather to be done on the day.	1	1	1	EuRoC competition will communicate out of bounds areas.
3.05	Fit of launch vehicle sections	HPB	Risk of sections of launch vehicle separating in an unintended manner.	1	5	5	Sections of vehicle to be bolted together through metal bulkheads. Friction fit on joints to be able to support rocket self-weight, and additionally be fixed with nylon bolts.	1	1	1	Persons to clear the launch area.

3.06	Pressure build-up in launch vehicle chambers	HPB	Possible damage caused by rapid atmospheric changes on ascent. Possible damage caused by pressure impulse of ejection charges.	2	4	8	Use vent holes in all chambers as per EuRoC requirements. Amount of black powder to be tested. Redundant ejection charges to be set with different timings to control impulse.	1	2	2	Eyes to be kept on the sky.
3.07	Launch rail exit velocity.	HPB		2	5	10		1	2	2	
3.08	Needing to abort the mission	HPB	Risk that rocket sits on launch pad for an extended period of time, and batteries are depleted – risk of flight computers losing power.	2	5	10	Electronics systems to be rechargeable as per EuRoC requirements.	1	1	1	N/A – Risk considered mitigated.
3.09	Dislodgement of electronic components	HPB	Risk of electronic components to be dislodged by impulse.	2	3	6	Components to be screwed into a sled. Ejection/impact testing to confirm that they can withstand the loads.	1	2	2	Redundant flight computers and power buses
3.09	Recovery lines	HPB	Entanglement of lines	2	4	8	Revovery lines to be packed carefully as rehearsed, ensuring that they can slide past one another.	1	2	2	

E. Compliance Matrix

Requirement reference	Title	Text	Compliance
EuRoC-LV-RQT-0010	Non-toxic propellants	Launch vehicles entering EuRoC shall use non-toxic propellants	Fully Compliant
EuRoC-LV-RQT-0020	Air-start ignition circuit electronics	All upper stage and secondary ignition systems shall comply with the recovery systems redundant electronics and safety critical wiring requirements specified in Sections 5.1 (EuRoC-LV-RQT-0240 to EuRoC-LV-RQT-0280) and 5.4 respectively.	N/A
EuRoC-LV-RQT-0030	Ground-start ignition circuit arming distance	All ground-started propulsion system ignition circuits/sequences shall be capable of being armed and disarmed with no personnel within 15 m of the launch vehicle.	Fully Compliant
EuRoC-LV-RQT-0040	Clustered vehicle release system	All clustered vehicles shall have a launch release system ensuring lift-off only occurs if a minimum threshold force is met.	N/A
EuRoC-LV-RQT-0050	Clustered vehicle stability proof	All clustered vehicles shall be capable of performing a stable flight for any lift-off force above the minimum threshold value.	N/A
EuRoC-LV-RQT-0060	Clustered vehicle arming	For vehicles with a "main" and several "secondary" propulsion systems, the arming function of the secondary propulsion systems shall only be armed by launch detection (i.e., air-start).	N/A
EuRoC-LV-RQT-0070	Air-start ignition circuit arming	All upper stage and "secondary" (i.e., air-start) propulsion systems shall only be armed by launch detection.	N/A
EuRoC-LV-RQT-0080	COTS solid motors	All COTS solid motors shall be selected from the official EuRoC Motors List [RD02].	N/A
EuRoC-LV-RQT-0090	Ignition systems for solid motors	All solid motors shall use the electronic ignition system provided by EuRoC	N/A
EuRoC-LV-RQT-0100	Active pressurization	All gaseous and liquid propellant system shall be able to be externally pressurized with inert gas.	Fully Compliant
EuRoC-LV-RQT-0110	Loading lines disconnection	Systems employing any gaseous or liquid propellants shall perform propellant tank pressurization after all propellant and pressurant loading lines are disconnected.	Fully Compliant
EuRoC-LV-RQT-0120	Dissimilar connections	All loading lines, used for pressurization gases or propellants, shall feature dissimilar connectors.	Fully Compliant
EuRoC-LV-RQT-0130	Remote-controlled loading mechanism and respective emergency	Any remote-controlled loading mechanism for gases or liquid propellants shall feature a clearly marked and labelled, single action, hand actuated, "Emergency Release Mechanism".	Fully Compliant

	release mechanism		
EuRoC-LV-RQT-0140	Filling/loading/unloading connections	Any filling/loading/unloading connections for fluid propellants shall be readily accessible from the ground, when the rocket is in vertical launch position.	Fully Compliant
EuRoC-LV-RQT-0150	Filling/loading/unloading timing	Teams shall demonstrate that the filling/loading/unloading of the liquid fuels can be done to be ready for the launch window (maximum 90 minutes for liquid propellant loading, including pressurization).	Fully Compliant
EuRoC-LV-RQT-0160	Venting	For hybrid and liquid motors, teams shall facilitate oxidizer tank venting to prevent over-pressure situations.	Fully Compliant
EuRoC-LV-RQT-0170	Passive PRD in isolated sections of pressurized lines	All isolated sections of pressurized lines (including pressure vessels) shall incorporate a passive pressure relief device (PRD) with an opening set point below the maximum tested pressure of that line section.	Fully Compliant
EuRoC-LV-RQT-0180	PRD discharge coefficient	All pressure relief devices shall have a discharge coefficient equal to or higher than any other fluid interface on the respective pressurized section in which they are installed.	Fully Compliant
EuRoC-LV-RQT-0190	Propellant offloading after launch abort	Hybrid and liquid propulsion systems shall implement a means for remotely controlled venting or offloading of all liquid and gaseous propellants in the event of a launch abort.	Fully Compliant
EuRoC-LV-RQT-0200	Combustion chamber pressure test	SRAD and modified COTS propulsion system combustion chambers shall be designed and tested according to the SRAD pressure vessel requirements defined in Sections 0 and 6.3, respectively.	Fully Compliant
EuRoC-LV-RQT-0210	Combustion chamber leak proof	Combustion chambers shall be designed allowing to be closed off in a leak-tight manner for testing at any section between the throat and the exit section of the nozzle.	Fully Compliant
EuRoC-LV-RQT-0220	Hybrid and liquid tanking test	SRAD and modified COTS propulsion systems using liquid propellant(s) shall successfully (without significant anomalies) have completed a propellant loading and offloading test in "launchconfiguration", prior to the competition.	Fully Compliant

EuRoC-LV-RQT-0230	Static hot-fire test	SRAD propulsion systems shall successfully (without significant anomalies) complete an instrumented (chamber pressure and/or thrust), full scale (including system working time) static hotfire test prior to EuRoC.	Fully Compliant
EuRoC-LV-RQT-0240	Redundant recovery system electronics	Launch vehicles shall implement fully redundant recovery system electronics, including sensors/flight computers and "electric initiators", with a separate power supply (i.e., battery).	Fully Compliant
EuRoC-LV-RQT-0250	Redundant COTS recovery electronics	At least one redundant recovery system electronics subsystem shall implement a COTS flight computer.	Fully Compliant
EuRoC-LV-RQT-0260	Recovery electronics access panel	All electronics switches or connectors that need to be manually operated shall be accessible from outside the vehicle via either access panels or direct mounting on the outer skin.	Fully Compliant
EuRoC-LV-RQT-0270	Recovery electronics location	All electronics switches or connectors that need to be manually operated shall be readily accessible from the ground, when the rocket is in vertical launch position.	Fully Compliant
EuRoC-LV-RQT-0280	Recovery electronics access	All electronics switches or connectors that need to be manually operated shall be mounted on the vehicle side opposite to the launch rail.	Fully Compliant
EuRoC-LV-RQT-0290	Recovery system energetic devices	All stored-energy devices (i.e., energetics) used in recovery systems shall comply with the energetic device requirements defined in Section 6.1 of this document.	Fully Compliant
EuRoC-LV-RQT-0300	Onboard power systems	All onboard systems shall be free of batteries with either lithium-polymer or lithium (nonrechargeable) chemistry.	Fully Compliant
EuRoC-LV-RQT-0310	Onboard power systems access	Onboard batteries shall be readily accessible from the ground, when the rocket is in vertical launch position.	Partially Compliant
EuRoC-LV-RQT-0320	Launch rail standby time	Onboard power systems shall have at least six hours of battery lifetime on the launch rail.	Fully Compliant
EuRoC-LV-RQT-0330	Non-parachute/parafoil recovery systems	Teams exploring other recovery methods (i.e., non-parachute or parafoil based) shall mention it in the dedicated field of the Technical Questionnaire [RD04].	Fully Compliant
EuRoC-LV-RQT-0340	Dual deployment recovery	Each independently recovered launch vehicle body, anticipated to reach an apogee above 450 m	Fully Compliant

		above ground level (AGL), shall follow a dual deployment recovery operations concept.	
EuRoC-LV-RQT-0350	Initial deployment event altitude	The initial deployment event shall occur at or near apogee.	Fully Compliant
EuRoC-LV-RQT-0360	Initial deployment event descent velocity	The initial deployment event shall result in a descent velocity between 23 and 46 m/s.	Fully Compliant
EuRoC-LV-RQT-0370	Main deployment event altitude	The main deployment event shall occur at an altitude no higher than 450 m AGL.	Fully Compliant
EuRoC-LV-RQT-0380	Main deployment event descent velocity	The main deployment event shall result in a descent velocity of less than 9 m/s.	Fully Compliant
EuRoC-LV-RQT-0390	Ejection gas protection	The recovery system shall implement adequate protection (e.g., fire-resistant material, pistons, baffles etc.) to prevent hot ejection gases (if implemented) from causing burn damage to retaining chords, parachutes, and other vital components as the specific design demands.	Fully Compliant
EuRoC-LV-RQT-0400	Parachute swivel links	The recovery system rigging (e.g., parachute lines, risers, shock chords, etc.) shall implement swivel links at any connections including single-threaded anchors.	Fully Compliant
EuRoC-LV-RQT-0410	Dual deployment parachute coloration	Dual deployment parachutes shall be visually highly dissimilar from one another.	Fully Compliant
EuRoC-LV-RQT-0420	Parachute coloration	Utilised parachutes shall use colours providing a clear contrast to a blue sky, a grey/white cloud cover and ground vegetation (i.e. avoiding certain shades of green and brown, as well as black).	Fully Compliant
EuRoC-LV-RQT-0430	Mandatory system	Launch vehicle stages and deployable payloads shall feature a mandatory operational CATS Vega Flight Computer for official altitude logging and landing site tracking purposes.	Fully Compliant
EuRoC-LV-RQT-0440	CATS transmitter call-sign	Teams shall assign to each transmitter a "call-sign" (referred to in the CATS User Manual as the tele_link_phrase telecommand) respecting a specific string format to be found in Appendix D.	Fully Compliant

EuRoC-LV-RQT-0450	CATS Vega firmware update	Teams will be required to fly a specific firmware version in each mandatory CATS flight computer, mandated by the EuRoC organization.	Fully Compliant
EuRoC-LV-RQT-0460	CATS receiver	The CATS Ground Station shall be used for telemetry and tracking in conjunction with the mandatory system.	Fully Compliant
EuRoC-LV-RQT-0470	CATS electronics	CATS devices shall comply with the electronics general electronics requirements EuRoC-LV-RQT0260, EuRoC-LV-RQT-0270 and EuRoC-LV-RQT-0280.	Fully Compliant
EuRoC-LV-RQT-0480	Cable management	All safety critical wiring shall implement a cable management solution (e.g., wire ties, wiring, harnesses, cable raceways).	Fully Compliant
EuRoC-LV-RQT-0490	Secure connections	All safety critical wiring/cable connections shall be sufficiently secure as to prevent de-mating due to expected launch loads.	Fully Compliant
EuRoC-LV-RQT-0500	Cryo-compatible wire insulation	In case of propellants with a boiling point of less than -50°C any wiring or harness passing within close proximity of a cryogenic device (e.g., valve, piping, etc.) or a cryogenic tank (e.g., a cable tunnel next to a LOX tank) shall utilize safety critical wiring with cryo-compatible insulation (i.e., Teflon, PTFEvariants, etc.).	N/A
EuRoC-LV-RQT-0510	Electronics thermal testing	Teams shall thermally test the electronics to know the reliable operational temperature range, implement cooling or venting provisions and monitor at least one temperature sensor representative of the electronics temperature.	Fully Compliant
EuRoC-LV-RQT-0520	Recovery system ground test demonstration	All recovery system mechanisms shall be successfully (without significant anomalies) tested prior to EuRoC, either by flight testing, or through one or more ground tests of key subsystems.	Partially Compliant
EuRoC-LV-RQT-0530	Energetic device safing and arming	All energetics shall be “safed” until the rocket is in the launch position, at which point they may be "armed".	Fully Compliant
EuRoC-LV-RQT-0540	Arming device access	All energetic device arming features shall comply with the requirements EuRoC-LV-RQT-0260, EuRoC-LV-RQT-0270 and EuR	Fully Compliant

EuRoC-LV-RQT-0550	Arming device location	All energetic device arming features shall be located on the airframe	Fully Compliant
EuRoC-LV-RQT-0560	Burst discs	Each SRAD pressure vessel and every propellant tank shall implement an over-pressure safety measure, in the form of a (replaceable) burst disc, with a diaphragm orifice diameter of no less than 6 millimetres. The burst (or rupture) disc solution can be either COTS or SRAD.	Fully Compliant
EuRoC-LV-RQT-0570	Burst disc pressure	Burst discs (COTS or SRAD) shall be selected or calibrated to rupture at a pressure no higher than 1,25 times the nominal tank pressure.	Fully Compliant
EuRoC-LV-RQT-0580	Burst disc marking	Burst disc orifices (the body which determines the rupture pressure) shall be clearly and permanently marked with the average rupture pressure determined by testing, along with a unique identifier, tracing each burst disc orifice to an associated test report.	Fully Compliant
EuRoC-LV-RQT-0590	Burst discs material	All SRAD burst discs shall come from the same stock material sheet, both for flight, testing and rupture pressure characterization.	Fully Compliant
EuRoC-LV-RQT-0600	Relief device	SRAD pressure vessels shall implement an additional relief device, set to open in the range of 1,10 to 1,20 times the nominal operating pressure.	Fully Compliant
EuRoC-LV-RQT-0610	Designed burst pressure for metallic pressure vessels	SRAD and modified COTS pressure vessels constructed entirely from isotropic materials (e.g., metals) shall be designed to a burst pressure no less than 2 times the maximum expected operating pressure.	Fully Compliant
EuRoC-LV-RQT-0620	Designed burst pressure for composite pressure vessels	All SRAD and modified COTS pressure vessels either constructed entirely from non-isotropic materials (e.g., fibre reinforced plastics (FRP), composites) or implementing composite overwrap of a metallic vessel (i.e., composite overwrapped pressure vessels (COPV)), shall be designed to a burst pressure no less than 3 times the maximum expected operating pressure.	N/A
EuRoC-LV-RQT-0630	Burst discs testing	Individual test reports are required for each SRAD burst disc orifice, tied to its unique identifier or serial number. Each burst disc orifice test report must contain a minimum of five	N/A

		consecutive rupture tests, preferably using a data logging system and a pressure transducer for optimum rupture pressure documentation. The burst disc sheet metal must also be specified in detail.	
EuRoC-LV-RQT-0640	Proof pressure testing	SRAD and modified COTS pressure vessels shall be proof pressure tested successfully (without significant anomalies) to 1,5 times the maximum expected operating pressure for no less than twice the maximum expected system working time, using the intended flight article(s) (e.g., the pressure vessel(s) used in proof testing must be the same one(s) flown at EuRoC).	Fully Compliant
EuRoC-LV-RQT-0650	Restricted control functionality	Launch vehicle active flight control systems, if implemented, can only be implemented for pitch and/or roll stability augmentation, for aerodynamic "braking", guided recovery systems, precision landing or guided deployable loads.	Fully Compliant
EuRoC-LV-RQT-0660	Unnecessary for stable flight	Flight vehicles implementing active flight controls shall be naturally stable without these controls being implemented.	Fully Compliant
EuRoC-LV-RQT-0670	Designed to fail safe	Control Actuator Systems shall be designed to Fail Safe in any abnormal condition or during an active flight abort (if such functionality is implemented).	Fully Compliant
EuRoC-LV-RQT-0680	Boost phase dormancy	Control Actuator Systems shall be designed with a field adjustable boost dormancy capability, which will disable them in the initial period of the flight.	Fully Compliant
EuRoC-LV-RQT-0690	Active flight control system electronics	All electronics shall comply with the recovery systems redundant electronics and safety critical wiring specified in Sections 5.1 (EuRoC-LV-RQT-0240 and EuRoC-LV-RQT-0260 to EuRoC-LV-RQT-0280) and 5.4 respectively.	Fully Compliant
EuRoC-LV-RQT-0700	Active flight control system energetics	All stored-energy devices used in an active flight control system (i.e., energetics) shall comply with the energetic device requirements defined in Section 6.1 of this document.	Fully Compliant

EuRoC-LV-RQT-0710	Venting	All non-pressurized compartments of the airframe shall be vented in such a way that the pressures during flight are never above 1,05 times the atmospheric pressure at that point in the flight.	Fully Compliant
EuRoC-LV-RQT-0720	Material selection	PVC (and similar low-temperature polymers) Public Missiles Ltd. Quantum Tube components shall not be used in any structural (i.e., load bearing) capacity, most notably as load bearing eyebolts, launch vehicle airframes, or propulsion system combustion chambers.	Fully Compliant
EuRoC-LV-RQT-0730	Load bearing eyebolts type	All load bearing eyebolts shall be of the closed-eye, forged type	Fully Compliant
EuRoC-LV-RQT-0740	Load bearing eyebolts and U-bolts material	All load bearing eyebolts and U-Bolts shall be steel or stainless steel.	Fully Compliant
EuRoC-LV-RQT-0750	Coupling tubes	Airframe joints which implement "coupling tubes" shall be designed such that the coupling tube extends no less than one body calibre (1D) on either side of the joint — measured from the separation plane.	Fully Compliant
EuRoC-LV-RQT-0760	Launch lugs mechanical attachment	Launch lugs (i.e., rail guides) shall implement "hard points" for mechanical attachment to the launch vehicle airframe.	Fully Compliant
EuRoC-LV-RQT-0770	Aft launch lug support	The aft most launch lug shall support the launch vehicle's fully loaded launch weight while vertical.	Fully Compliant
EuRoC-LV-RQT-0780	RF transparency	Any internally mounted RF transmitter, receiver or transceiver, not having the applicable antenna(s) mounted externally on the airframe, shall employ “RF windows" in the airframe shell plating (typically glass fibre panels).	Fully Compliant
EuRoC-LV-RQT-0790	RF windows dimensioning	RF windows in the flight vehicle shell shall be a 360° circumference and be at least two body calibres in length.	Fully Compliant
EuRoC-LV-RQT-0800	RF windows material	RF windows shall be of a material other than carbon fibre	Fully Compliant
EuRoC-LV-RQT-0810	RF antennas’ location	RF antennas shall be kept as far away as possible from wiring and metallic structural element.	Fully Compliant

EuRoC-LV-RQT-0820	Internal RF antennas' location	The internally mounted RF antenna(s) shall be placed at the midpoint of the RF window section	Fully Compliant
EuRoC-LV-RQT-0830	Identifying markings	The Team ID shall be clearly and prominently displayed on the launch vehicle airframe, visible on all four quadrants of the vehicle, as well as fore and aft, and on all components that separate from the vehicle such as deployable payloads.	Fully Compliant
EuRoC-LV-RQT-0840	Payloads	Teams are required to carry payload(s) on the vehicle.	Fully Compliant
EuRoC-LV-RQT-0850	Payload form factor	Payloads shall fulfil one of following basic form factors: • CanSat: cylindrical shape with 115 mm height and 66 mm diameter; • CubeSat: cubic shape with one CubeSat Unit (1U) being defined as a 100 mm x 100 mm x 100 mm cubic structure; • PocketSat: cubic shape with 50 mm x 50 mm x 50 mm.	Fully Compliant
EuRoC-LV-RQT-0860	Payload minimum mass	The launch vehicle shall carry no less than 1000 g of payload, with no requirement applicable to the upper limit.	Fully Compliant
EuRoC-LV-RQT-0870	Payload mass factor	Payloads shall fulfil one of the following basic mass increments: • A single CanSat-type payload has a mass between 300 g and 350 g; • A single CubeSat-type payload has a mass between 1000 g and 1330 g; • A single PocketSat-type payload has a mass between 200 g and 250 g.	Fully Compliant
EuRoC-LV-RQT-0880	Independent payload functionality	The payload functionality must be completely independent of the launch vehicle and at the same time payloads cannot be a part of the launch vehicle functionality (e.g., a guidance and control system).	Fully Compliant
EuRoC-LV-RQT-0890	Payload removal for weigh-in	Teams must ensure that the payloads shall not be inextricably connected to other launch vehicle associated components (e.g., recovery system, internal structure, or airframe) while being weighed.	Fully Compliant
EuRoC-LV-RQT-0900	Payload materials	Payloads shall not contain significant quantities of lead or any other hazardous materials, and in case of payloads with potential biohazards such	Fully Compliant

		as seeds or living beings, those must not contain invasive species. The use of radioactive materials is not permitted.	
EuRoC-LV-RQT-0910	Payload energetic devices	All stored-energy devices (i.e., energetics) used in payload systems shall comply with the energetic device requirements defined in Section 6.1 of this document.	Fully Compliant
EuRoC-LV-RQT-0920	Recovery system	Deployable payloads shall have its own independent recovery system.	Fully Compliant
EuRoC-LV-RQT-0930	Unique recovery system	If teams plan to develop a deployable payload that requires a specific unique recovery system, they shall contact the EuRoC organization well in advance of the event to clarify if the payload satisfies all requirements.	Partially Compliant
EuRoC-LV-RQT-0940	Descent velocity	Deployable payloads shall incorporate an independent recovery system, reducing the payload's descent velocity to less than 9 m/s before it descends through an altitude of 450 m AGL.	Fully Compliant
EuRoC-LV-RQT-0950	Recovery system electronics	Payloads implementing independent recovery systems shall comply with the launch vehicle redundant electronics requirements defined in Section 5.1 (EuRoC-LV-RQT-0240 to EuRoC-LV-RQT0280).	Fully Compliant
EuRoC-LV-RQT-0960	Payload safety critical wiring	Payloads implementing independent recovery systems shall comply with the launch vehicle safety critical wiring requirements defined in Section 5.4.	Fully Compliant
EuRoC-LV-RQT-0970	Recovery system testing	Payloads implementing independent recovery systems shall comply with the launch vehicle recovery system testing requirements defined in Section 0.	Fully Compliant
EuRoC-LV-RQT-0980	Payload tracking	All deployable payloads shall feature the mandatory altitude logging and tracking system (see Section 5.3).	Fully Compliant
EuRoC-LV-RQT-0990	Payload tracking call-sign	Teams shall assign to each transmitter a call-sign respecting the format described in Appendix D	Fully Compliant
EuRoC-LV-RQT-1000	Launch azimuth and elevation	Launch vehicles shall nominally launch at an elevation angle of 84°±1° and a launch azimuth defined by the organisation at EuRoC.	Fully Compliant

EuRoC-LV-RQT-1100	Rail take-off velocity	The vehicle shall be capable of achieving a rail departure speed higher than 30 m/s on the intended launch rail's length.	Fully Compliant
EuRoC-LV-RQT-1020	Hold-down system	All vehicles using at least one liquid propellant shall employ a hold-down system that will release the rocket only after sufficient thrust for stable flight is achieved.	Fully Compliant
EuRoC-LV-RQT-1030	Stability margin	Launch vehicles shall maintain a static stability margin of at least 1,5 calibres throughout the whole flight phase (upon leaving the launch rail), regardless of CG movement due to depleting consumables and shifting CP location due to wave drag effects (which may become significant as low as 0,5 Mach).	Fully Compliant
EuRoC-SE-RQT-0010	Operational range	All team provided launch control systems shall be electronically operated and have a maximum operational range of no less than 750 metres from the launch rail.	Fully Compliant
EuRoC-SE-RQT-0020	Fault tolerance and arming	All team provided launch control systems shall be at least single fault tolerant by implementing a removable safety interlock (i.e., a jumper or key to be kept in possession of the arming crew during arming) in series with the launch switch.	Fully Compliant
EuRoC-SE-RQT-0030	Safety critical switches	All team provided launch control systems shall implement ignition switches of the momentary, normally open (also known as "dead man") type so that they will remove the signal when released.	Fully Compliant
EuRoC-SE-RQT-0040	Launch rail fit check	Teams using EuRoC launch rails shall perform a launch rail fit check as part of the Flight Readiness Review, before going to the launch range.	N/A
EuRoC-SE-RQT-0050	Launch rail bottom spacer	Teams shall provide their own bottom spacer to define their vehicles' vertical position on the rail.	Fully Compliant
EuRoC-SE-RQT-0060	Launch rail nominal elevation	Team provided launch rails shall be able to implement a nominal launch elevation of 84° ±1°.	N/A
EuRoC-SE-RQT-0070	Launch rail elevation range	Team provided launch rails with adjustable elevation shall only allow inclinations between 70° and 85°.	N/A

F. Checklists

F.1 Experimental Setup

Prior to any kind of testing the equipment must be set up for experiment, this includes the engine and bracket, the feed system and tanks, the ground station and supplemental equipment as well as finally the mission control laptop. Below outlines the expected steps to setup the experiment.

No.	Task	Operator	Time
1.	Secure commercial fluid bottles behind firing apron.		
2.	Attach brackets to firing bed and thrust cell.		
3.	Attach engine to firing bed brackets.		
4.	Attach run valves and hose to engine end.		
5.	Set up feed system rig at back of apron.		
6.	Attach run hoses between chamber and feed system.		
7.	Place ground station and activate brakes.		
8.	Set up ethernet connection.		
9.	Power on all electronics and ensure stable connection.		
10.	Ensure nominal sensor readings and valve operation.		
11.	Attach fueling lines between feed system and ground station.		
12.	Evacuate firing apron.		
13.	Ensure all gas bottle valves are closed.		
14.	Attach fueling lines from commercial fluid bottles to ground station.		

F.2 Leak Testing

Prior to any kind of testing the equipment must be set up for experiment, this includes the engine and bracket, the feed system and tanks, the ground station and supplemental equipment as well as finally the mission control laptop. Below outlines the expected steps to setup the experiment.

No.	Task	Operator	Time
1.	Observe nominal sensor readings.		
2.	Ensure all valves are closed (Including bottle, manual, and panel).		
3.	Open COTS N2 bottle valve to deliver pressure to GS intake.		
4.	Observe bottle pressure on GS intake.		
5.	Open GS N2 fill valve to deliver N2 to rocket pressurant tank.		
6.	Observe bottle pressure in rocket pressurant tank.		
7.	TEST 1: Nitrogen system. Wait 15 minutes, observing pressure readings.		
8.	Pass if <10 % pressure drop.		
9.	Open Fuel pressuring valve.		
10.	Observe regulator pressure in fuel tank.		
11.	Open Ox pressuring valve.		
12.	Observe regulator pressure in Ox tank.		
13.	Open N2O fill valve (pressuring N2O hose with N2).		
14.	Close COTS N2 bottle valve.		
15.	TEST 2: Full system. Wait 15 minutes, observing pressure readings.		
16.	Pass if < 10 % pressure drop.		
17.	Open Ox tank vent valve to vent Ox system and N2 system.		
18.	Observe atmospheric pressure in Ox and N2 system.		
19.	Open Fuel tank vent valve to vent Fuel system.		
20.	Observe atmospheric pressure in Fuel system.		
21.	Close all valves.		
	TROUBLESHOOTING:		
1.	Set N2 bottle regulator to 5 bar.		
2.	Repeat steps 1-6. Repeat steps 9-14.		
3.	Enter Apron with appropriate PPE and Leak detection fluid.		
4.	Apply Leak detection fluid to connections and observe for bubbles.		
5.	Tighten leaking fittings.		
6.	Evacuate Apron.		
7.	Repeat from step 1.		

F.3 Water Flow Test

Water flow tests will be used to measure the pressure drop across the fuel line and help set the fuel valve set point as well as provide a full system pressurized run though to ensure the system is safe to actuate for cold and hot testing.

No.	Task	Operator	Date
1.	Observe nominal sensor readings		
2.	Ensure all valves set to closed position.		
3.	Fill ground support fuel pump with water.		
4.	Attach ground support pump to fuel fill valve.		
5.	Open fuel vent valve.		
6.	Manually open fuel fill valve.		
7.	Fill fuel tank with water to full – (water drain from vent valve).		
8.	Manually close fuel fill valve.		
9.	Close fuel vent valve.		
10.	Disconnect ground support pump fuel.		
11.	Refill manual fuel pump with water.		
12.	Disconnect GS N_2O fill line.		
13.	Connect ground support pump to N_2O fill line.		
14.	Open N_2O vent valve.		
15.	Fill N_2O tank with water ~ 9L.		
16.	Close N_2O vent valve.		
17.	Remove the ground support pump.		
18.	Evacuate firing apron.		
19.	Open COTS N2 bottle valve to deliver pressure to GS intake.		
20.	Observe bottle pressure on GS intake.		
21.	Open GS N2 fill valve to deliver N2 to rocket pressurant tank.		
22.	Observe bottle pressure in rocket pressurant tank.		
23.	Open Fuel pressuring valve.		
24.	Observe regulator pressure in fuel tank.		
25.	Open Ox pressuring valve.		
26.	Observe regulator pressure in Ox tank.		
27.	Close GS N2 fill valve.		
28.	Close COTS N2 bottle valve.		
29.	Ensure Pressurant valves are open		
30.	PAUSE: Ensure system is nominal		
31.	TEST 1: (Run auto water flow sequence) Open N_2O and fuel run valve to 100% nominal.		
32.	Observe tank pressure drops to atmosphere.		

F.4 Cold Flow Test

A cold flow test will be conducted to gain an understanding of the system and set up for a hot fire attempt. Cold flow can be done with water to replace fuel.

Please note: timings in the auto sequence (steps 42-49) are subject to change.

No.	Task	Operator	Date
1.	Observe nominal sensor readings		
2.	Ensure all valves set to closed position.		
3.	Ensure ignitor circuit is isolated		
4.	Secure ignitor beside engine, within camera view, ensure ignitor is pointed **away** from engine output		
5.	Wire ignitor to circuit		
6.	Fill ground support fuel pump with IPA.		
7.	Mix in IPA additives.		
8.	Attach ground support pump to fuel fill valve.		
9.	Open fuel vent valve.		
10.	Manually open fuel fill valve.		
11.	Fill fuel tank with IPA to full – (IPA drain from vent valve).		
12.	Manually close fuel fill valve.		
13.	Close fuel vent valve.		
14.	Disconnect ground support pump fuel.		
15.	Evacuate firing apron area.		
16.	PAUSE: Ensure ground station fill valves, run valves, vent valves and N2O/IPA pressurant valves are closed.		
17.	Open COTS N2 bottle valve to deliver pressure to GS intake.		
18.	Observe bottle pressure on GS intake.		
19.	Open GS N2 fill valve to deliver N2 to rocket pressurant tank.		
20.	Observe bottle pressure in rocket pressurant tank.		
21.	Open Fuel pressuring valve.		
22.	Observe regulator pressure in fuel tank.		
23.	PAUSE: Ensure all pressure readings are nominal.		
24.	Open COTS N2O Bottle valve.		
26.	Observe N2O vapour pressure on GS N2O bottle side.		
27.	Open N2O Fill valve.		
28.	Observe N2O vapour pressure in N2O tank. (N2O liquid is now filling slowly)		
	Observe stabalisation of N2O tank pressure and COTS bottle pressure. (vessels are in equilibrium and no filling is occurring).		
29.	Open N2O vent valve for 3.5s **ONLY** to vent N2O gaseous phase (allowing more liquid phase to be filled). Observe N2O plume.		
29.	Repeat steps 26 and 27 until N2O vent plume is bright white and >40cm (correct N2O venting can be seen through binoculars 400m away from launch vehicle at EUROC).		
30.	Close N2O Fill valve.		
	PAUSE: Ensure all pressure readings are nominal.		
32.	Open N2O pressuring valve.		
33.	Observe regulator pressure in N2O tank.		
34.	Close N2O pressurant valve.		
35.	Close COTS N2 bottle valve.		
36.	Close COTS N_2O bottle valve.		
37.	Ensure ignitor electronics are not active.		

38.	Un-isolate ignitor to main circuit.		
39.	Evacuate the bottle storage.		
40.	PAUSE: Ensure all pressure readings are nominal.		
41.	TEST 1: (Run auto cold flow sequence) (these timings may be changed)		
42.	(Auto) Trigger Igniter at T-2s		
43.	(Auto) Open N_2O and Fuel run valve to 33% of nominal.		
44.	(Auto) Wait 0.5 seconds.		
45.	(Auto) Open N_2O Pressurant valve.		
46.	(Auto) Wait 1 second.		
47.	(Auto) Open N_2O and fuel run valve to 100% nominal.		
48.	(Auto) Wait 1 second or for full duration.		
49.	(Auto) Close N_2O and fuel run valves.		
50.	Open all vent valves.		
51.	Observe atmospheric tank pressures.		
52.	Ensure system is safe before approaching.		

F.5 Hot Fire Test

Hot fire test will ensure the successful ignition and thrust generation of the system, the procedure of water flow tests followed by cold flows should act to ensure that the safety and success of these attempts.

Please note: timings in the auto sequence (steps 42-49) are subject to change.

No.	Task	Operator	Date
1.	Observe nominal sensor readings		
2.	Ensure all valves set to closed position.		
3.	Ensure ignitor circuit is isolated		
4.	Secure ignitor **into** engine.		
5.	Wire ignitor to circuit		
6.	Fill ground support fuel pump with IPA.		
7.	Mix in IPA additives.		
8.	Attach ground support pump to fuel fill valve.		
9.	Open fuel vent valve.		
10.	Manually open fuel fill valve.		
11.	Fill fuel tank with IPA to full – (IPA drain from vent valve).		
12.	Manually close fuel fill valve.		
13.	Close fuel vent valve.		
14.	Disconnect ground support pump fuel.		
15.	Evacuate firing apron area.		
16.	PAUSE: Ensure ground station fill valves, run valves, vent valves and N2O/IPA pressurant valves are closed.		
17.	Open COTS N2 bottle valve to deliver pressure to GS intake.		
18.	Observe bottle pressure on GS intake.		
19.	Open GS N2 fill valve to deliver N2 to rocket pressurant tank.		
20.	Observe bottle pressure in rocket pressurant tank.		
21.	Open Fuel pressuring valve.		
22.	Observe regulator pressure in fuel tank.		
23.	PAUSE: Ensure all pressure readings are nominal.		
24.	Open COTS N2O Bottle valve.		
26.	Observe N2O vapour pressure on GS N2O bottle side.		
27.	Open N2O Fill valve.		
28.	Observe N2O vapour pressure in N2O tank. (N2O liquid is now filling slowly)		
	Observe stabalisation of N2O tank pressure and COTS bottle pressure. (vessels are in equilibrium and no filling is occurring).		
29.	Open N2O vent valve for 3.5s **ONLY** to vent N2O gaseous phase (allowing more liquid phase to be filled). Observe N2O plume.		
29.	Repeat steps 26 and 27 until N2O vent plume is bright white and >40cm (correct N2O venting can be seen through binoculars 400m away from launch vehicle at EUROC).		
30.	Close N2O Fill valve.		
	PAUSE: Ensure all pressure readings are nominal.		
32.	Open N2O pressuring valve.		
33.	Observe regulator pressure in N2O tank.		
34.	Close N2O pressurant valve.		
35.	Close COTS N2 bottle valve.		
36.	Close COTS N_2O bottle valve.		
37.	Ensure ignitor electronics are not active.		
38.	Un-isolate ignitor to main circuit.		

39.	Evacuate the bottle storage.		
40.	PAUSE: Ensure all pressure readings are nominal.		
41.	TEST 1: (Run auto cold flow sequence) (these timings may be changed)		
42.	(Auto) Trigger Igniter at T-2s		
43.	(Auto) Open N_2O and Fuel run valve to 33% of nominal.		
44.	(Auto) Wait 0.5 seconds.		
45.	(Auto) Open N_2O Pressurant valve.		
46.	(Auto) Wait 1 second.		
47.	(Auto) Open N_2O and fuel run valve to 100% nominal.		
48.	(Auto) Wait 1 second or for full duration.		
49.	(Auto) Close N_2O and fuel run valves.		
50.	Open all vent valves.		
51.	Observe atmospheric tank pressures.		
52.	Ensure system is safe before approaching.		

F.6 Cleaning of tank and plumbing

Check Number	6	**Asset**	Pre- Flight
Date		**Sub Team**	HyPower Bristol
Team ID:	16	**Location:**	Lab

	Items to be checked	Acceptance Criteria	Persons	
	List the action required to be performed	List the required outcome to pass the check	Two responsible persons; A checker and an observer	
1.0	Action	Acceptance	Checker	Observer
	1. Propulsion			
1.1	Disassemble all plumbing into small sub-runs	Plumbing disassembled		
1.2	Use a syringe to run acetone through the plumbing runs	Acetone clean complete.		
1.3	Place plumbing runs on an ox cleaned surface ready for assembly	Surface ox cleaned		
1.4	Wait for the acetone to evaporate out of the plumbing runs	Runs do not smell of acetone		
1.5	Take the ½” and ¾” plugs out of the lower tank bulkhead	Plugs removed		
1.6	Pour some warm soapy water into both tank chambers and reseal the tank	Tank resealed		
1..7	Rotate the tank to evenly clean the inside of the tank for any remaining oils.	Done for a period of no less than 5 minutes		
1.8	Take the ½” and ¾” plugs out of the lower tank bulkhead	Plugs removed		
1.9	Pour the water out of the tank and allow the remainder to evaporate	All water evaporated		
1.10	Pour some acetone in and reseal the tank	Tank resealed		
1.11	Rotate the tank to evenly clean the inside of the tank for any remaining oils (note that the tank was cleaned before assembly so this step is for cleaning the smallest amounts of dirt that may have accumulated over time)	Done for a period of no less than 5 minutes		
1.12	Take the ½” and ¾” plugs out of the lower tank bulkhead	Plugs removed		
1.13	Wait for the acetone to evaporate out of the tank	Waited for a period of no less than one hour		
1.14	Replace the ½” and ¾” plugs	Plugs replaced		
	Final Validation (Team Member Signature)			
	Total of Inspections Satisfactory / Not Satisfactory			

F.7 Pre-Flight Checks

Check Number	7	**Asset**	Pre-Flight
Date		**Sub Team**	HyPower Bristol
Team ID:	16	**Location:**	Tent/preparation area

Items to be checked		Acceptance Criteria	Persons	
List the action required to be performed		List the required outcome to pass the check	Two responsible persons; A checker and an observer	
1.0	Action	Acceptance	Checker	Observer
1.	Propulsion			
1.1	Check feed system is assembled as expected.	To be checked against parts list generated by CAD.		
1.2	Check all fittings on feed system.	Check against CAD drawings.		
1.3	Afix igniter mount to base of engine.			
2.0	Action	Acceptance	Checker	Observer
2.	Electronics Systems			
2.1	Check that all batteries are charged	Voltage readings of batteries are nominal		
2.2	Check condition of boards	No exposed connections, no damage, Multimeter probing validates no shorts or unconnected traces		
2.3	Assemble avionics bay	Ensure all connections and ejection charges are correctly wired		
2.4	Validate continuity of boards	Components switch on and function correctly.		
2.5	Ensure all boards are switched off	No LEDs are on, verified with a Multimeter.		
2.6	Connect bulkheads	Connectors to withstand a gentle pull-out tests.		
3.0	Action	Acceptance	Checker	Observer
3.	Launch Vehicle			
3.1	Check structure for damage.			
3.2	Ensure all bolts are tightened			
3.3	Check all eyebolt fixings			
3.4	Mount fincan to thrust structure. Ensure all bolts and fixture points are tightened.	Check that electronics and propulsion team are happy for aft of Coax to be covered.		
3.5	Check stiffness of connection to airbrakes.	Check all bolts are present and tightened.		
3.6	Check connection of airbrake mount to payload thrust structure.			
3.7	Check connection of avionics bay to airbrake structure			
3.8	Mount panels to stringer assembly	Check that electronics and propulsion team are happy for fore of Coax to be covered.		
4.0	Action	Acceptance	Checker	Observer
4.	Recovery and payload			
4.1	Fold main parachute	Diameter no higher than 190mm, length no greater than 200mm.		

4.2	Secure main parachute and lines into bag	Check that bag will unravel.		
4.3	Fold drogue parachute			
4.4	Check all batteries are charged			
4.5	Check condition of boards			
4.6	Assemble payload			
4.7	Validate continuity of boards and wiring			
4.8	Fold payload drogue parachute			
4.9	Assemble payload foam structure			
4.10	Pack chutes and payload into nosecone.	Do not pack chutes in too tight.		
4.11	Alert RSO launch vehicle is ready to add pyrotechnic charges.	Wait for RSO approval.		
Final Validation (Team Member Signature)				
Total of Inspections Satisfactory / Not Satisfactory				

F.8 Pyrotechnic Loading

Check Number	8	**Asset**	Pre-Flight
Date		**Sub Team**	HyPower Bristol
Team ID:	16	**Location:**	Pyrotechnic Tent

Items to be checked		Acceptance Criteria	Persons	
List the action required to be performed		List the required outcome to pass the check	Two responsible persons; A checker and an observer	
1.0	Action	Acceptance	Checker	Observer
1. Pyrotechnic Charges				
Ejection Charge Assembly – Separation event + Repeat for redundant				
1.1	Tape exposed points of igniters.			
1.2	Check continuity of ejection charge e-matches.	Must be 1-4Ohms. If off-nominal, discard and replace.		
1.3	Install ejection charges into cups.			
1.4	Affix the CO2 Cartridge mechanism to bulkhead	Must turned tightly. Ensure nylocks are used.		
1.5	Measure out black powder for ejection charge.	3g		
1.6	Load black powder and fill remaining space with wadding.			
1.7	Install tape cover over ejection charge canister.	No gaps.		
1.8	Cut charge wires to length			
1.9	Attach igniter wires to bulkhead connector. Test continuity.	1-4Ohms nominal, if not met, restart process.		
Ejection Charge Assembly – Tender Descender + Repeat for redundant				
1.10	Tape exposed points of igniters.			
1.11	Check continuity of ejection charge e-matches.	1-4Ohms if off-nominal, discard and replace.		
1.12	Install ejection charges into cups.			
1.13	Measure out black powder for ejection charge.	0.3g		
1.14	Load black powder and fill remaining space with wadding.			
1.15	Install tape cover over ejection charge canister.	No gaps.		
1.16	Attach igniter wires to bulkhead connector. Test continuity.	1-4Ohms nominal, if not met, restart process.		
2.0	Action	Acceptance	Checker	Observer
2. Final Launch Vehicle Assembly				
2.1	Seat nosecone onto main vehicle			
2.2	Insert shearpins to secure nosecone in place.			
2.4	External visual check on the launch vehicle	Inspect tubes for signs of fracture, unseated or missing bolts, unseated or msising shear pins, and ensure the ignitor is installed correcty.		

2.5	Alert RSO the rocket is ready to be carried to the pad and begin fuelling.	Wait for RSO approval		
Final Validation (Team Member Signature)				
Total of Inspections Satisfactory / Not Satisfactory				

F.9 Pad setup

Check Number	9	**Asset**	Pre-Flight
Date		**Sub Team**	HyPower Bristol
Team ID:	16	**Location:**	Launch Pad

Items to be checked		Acceptance Criteria	Persons	
List the action required to be performed		List the required outcome to pass the check	Two responsible persons; A checker and an observer	
1.0	Action	Acceptance	Checker	Observer
1. Launch pad sequence				
1.1	Install quick disconnect units to launch rail			
1.2	Install base stop on launch rail			
1.3	Test ignition continuity			
1.4	Place rocket on launch rail			
1.5	Enable electronics systems			
1.6	Start video recording			
1.7	Check that data is being transmitted	Video stream, valve positions, pressure readings.		
1.8	Remove igniter from ignition motor mount.			
1.9	Load igniter into D-class motor.			
1.10	Load motor into ignition motor mount.			
1.11	Arm ejection charge from CATS VEGA			
1.12	Arm ejection charge from Altus Metrum			
1.13	Arm igniter	Follow RSO instruction		
1.14	Move all persons away from launch site to begin remote fuelling	Follow RSO instruction		
Final Validation (Team Member Signature)				
Total of Inspections Satisfactory / Not Satisfactory				

HY-POWER Bristol SEDS

F.10 Propellant Loading Operation

Check Number	10	Asset	Pre-Flight
Date		Sub Team	HyPower Bristol
Team ID:	16	Location:	Mission Control

Items to be checked		Acceptance Criteria	Persons	
List the action required to be performed		List the required outcome to pass the check	Two responsible persons; A checker and an observer	
1.0	Action	Acceptance	Checker	Observer
1. Propulsion				
1.1	Ensure rocket is in nominal state vis a vis avionics	All valves functioning as expected		
1.2	At the requisite stage in the fuelling sequence connect the hand pump to the rocket using the QD	Hand pump connected		
1.3	Load the fuel (Ethanol) onto the rocket using the hand pump	All fuel loaded (A premeasured quantity shall be in the reservoir)		
.1.4	Disconnect the hand pump from the LV	Hand pump disconnected		
1.5	Connect LV quick disconnects for Nitrogen and Nitrous Oxide	QDs connected		
1.6	Connect the GS to high pressure Nitrogen and Nitrous Oxide bottles	GS Connected		
1.7	Retreat to a safe distance to allow the remaining stages of propellant loading to be completed	Retreat		
1.8	Close the N2 Vent Valve and open the GS N2 Fill Valve	Valves closed/open respectively		
1.9	Load N2 until the tank PT shows 300 bar	Tank PT shows 300 bar		
1.10	Close N2 Fill Valve	Valve closed		
1.11	Close all Valves	All valves closed		
1.12	Open the GS N2O Fill Valve	Valve open		
1.13	Load N2O whilst venting gaseous N2O when tank pressure exceeds 40 bar until the plume changes colour to “cloudy white”	Plume colour changes		
1.14	Close GS N2O Fill whilst still venting when tank pressure exceeds 40 bar	Valve closed		
1.15	Hold for launch authorisation	n/a		
1.16	Disconnect fuelling QDs	QDs are visibly disconnected		
1.17	Close all Valves	Plume disappears		
1.18	Open LV Pressurant Valves	Tank PTs read 40 bar		
1.19	Close all Valves	All valves closed		
1.20	Vent N2O tank down to 40 bar	Tank PT reads 40 bar		
1.21	Handover for launch	Wait for RSO approval		
Final Validation (Team Member Signature)				
Total of Inspections Satisfactory / Not Satisfactory				

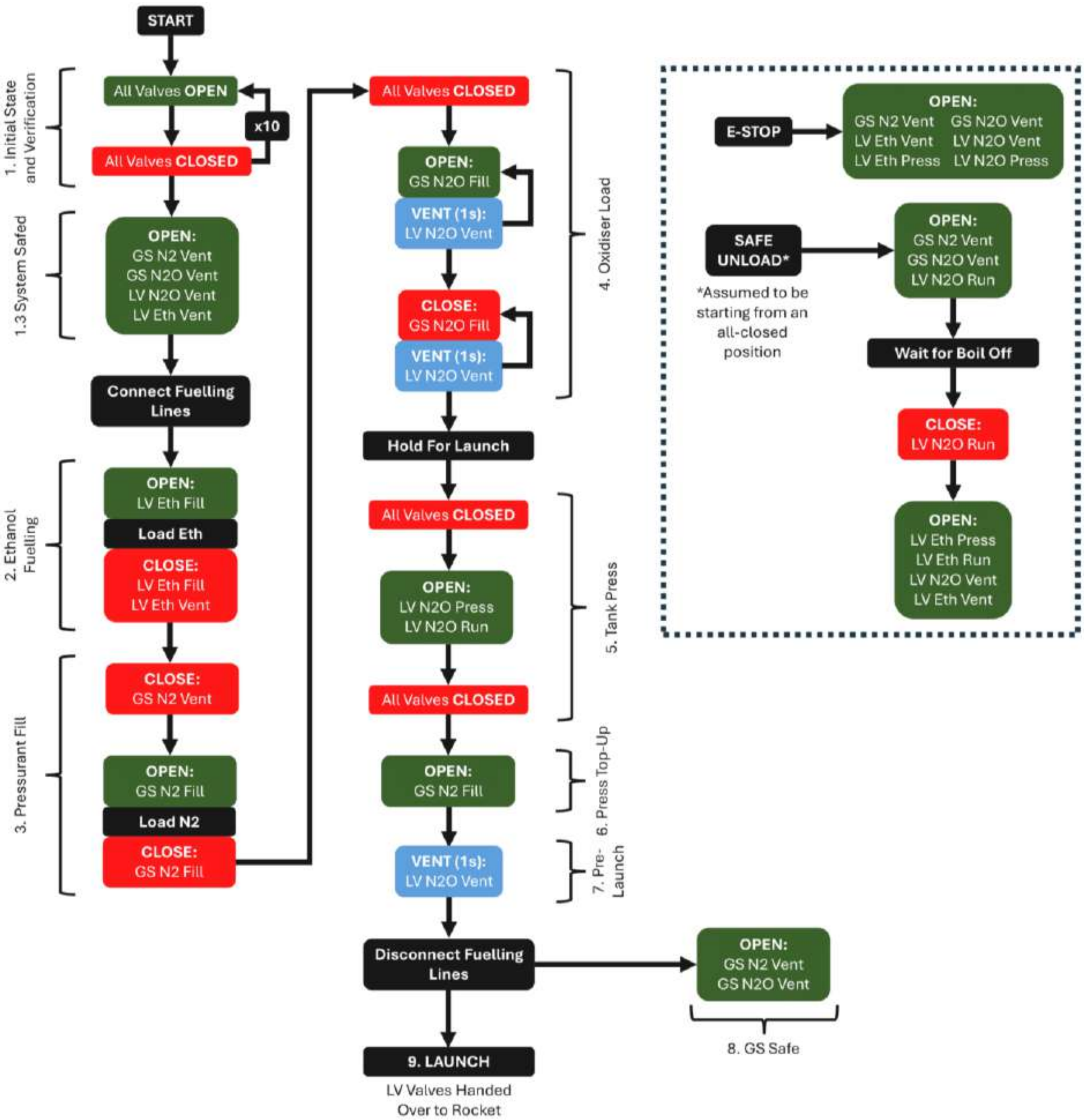
START
1. Initial State and Verification
All Valves OPEN
x10
All Valves CLOSED
1.3 System Safed
OPEN: GS N2 Vent GS N2O Vent LV N2O Vent LV Eth Vent
Connect Fuelling Lines
2. Ethanol Fuelling
OPEN: LV Eth Fill
Load Eth
CLOSE: LV Eth Fill LV Eth Vent
3. Pressurant Fill
CLOSE: GS N2 Vent
OPEN: GS N2 Fill
Load N2
CLOSE: GS N2 Fill
4. Oxidiser Load
All Valves CLOSED
OPEN: GS N2O Fill
VENT (1s): LV N2O Vent
CLOSE: GS N2O Fill
VENT (1s): LV N2O Vent
Hold For Launch
5. Tank Press
All Valves CLOSED
OPEN: LV N2O Press LV N2O Run
All Valves CLOSED
6. Press Top-Up
OPEN: GS N2 Fill
7. Pre-Launch
VENT (1s): LV N2O Vent
Disconnect Fuelling Lines
OPEN: GS N2 Vent GS N2O Vent
8. GS Safe
9. LAUNCH
LV Valves Handed Over to Rocket
E-STOP
OPEN: GS N2 Vent GS N2O Vent LV Eth Vent LV N2O Vent LV Eth Press LV N2O Press
SAFE UNLOAD*
*Assumed to be starting from an all-closed position
OPEN: GS N2 Vent GS N2O Vent LV N2O Run
Wait for Boil Off
CLOSE: LV N2O Run
OPEN: LV Eth Press LV Eth Run LV N2O Vent LV Eth Vent

F.11 Flight

Check Number	11	Asset	Flight
Date		Sub Team	HyPower Bristol
Team ID:	16	Location:	Mission Control

Items to be checked			Acceptance Criteria	Persons	
List the action required to be performed			List the required outcome to pass the check	Two responsible persons; A checker and an observer	
1.0	Action	Time to launch	Acceptance	Checker	Observer
1.	2. Flight checks				
1.1	Go/No GO from all subteams	00:10:00			
1.2	Mission Control Go/No Go				
1.3	Avionics Go/No Go				
.1.4	Recovery Go/No Go				
1.5	Propulsion Go/No Go				
1.6	Flight Go/No Go				
1.7	HOLD	00:02:00			
1.8	RSO Go/No Go				
1.9	Countdown starts	00:00:20			
1.10	Launch	00:00:00			
	Final Validation (Team Member Signature)				
	Total of Inspections Satisfactory / Not Satisfactory				

F.12 Shutdown Procedures

F.12.1 Nominal Shutdown Procedure

No.	Task	Operator	Date
1.	Ensure N_2O GS fill valve is closed.		
2.	Ensure Nitrogen GS fill valve is closed.		
3.	Open N_2O vehicle vent valve.		
4.	Measure N_2O tank pressure to atmosphere.		
5.	Open fuel vehicle vent valve.		
6.	Measure fuel tank pressure and Nitrogen tank pressure to atmosphere.		
7.	Check all pressures in system are ambient.		
8.	Approach cylinders.		
9.	Manually close nitrogen ground cylinder valve.		
10.	Manually close N_2O ground cylinder valve.		
11.	Evacuate area.		
12.	Open N_2O ground station vent valve.		
13.	Open N_2O ground station fill valve.		
14.	Ensure pressure reads 0 bar on N_2O ground station.		
15.	Open Nitrogen ground vent valve.		
16.	Open Nitrogen ground fill valve.		
17.	Ensure pressure reads 0 bar on nitrogen ground station.		
18.	Clear combustion chamber of excess pooled fuel.		

F.12.2 Failure Case 1: Failure to Ignite

Failure to ignite requires the venting of the entire system to safe it for a new ignitor. This is the same process as nominal shutdown with the expectation of a slower N_2O vent time based on a full tank rather than an empty tank.

Follow 7.1 nominal shutdown procedure

F.12.3 Failure Case 2: Failure to Actuate Run Valves

v

In the case of a failed valve actuation on the critical path the system must be vented to safe it for operation.

In the case of the **run valves**, the nominal shutdown procedure should be followed.

F.12.4 Failure Case 3: Failure to actuate N2O Vent Valves

In the case of a failed vent valve actuation, venting should be completed through the run valves as described below.

No.	Task	Operator	Date
1.	Ensure N_2O ground fill valve close.		
2.	Ensure Nitrogen ground fill valve closed.		
3.	Open N_2O ground vent valve.		
4.	Measure N_2O tank pressure to 0 bar.		
5.	Open fuel vent valve.		
6.	Measure fuel tank pressure and Nitrogen tank pressure to 0 bar.		
7.	Check all pressures in system are at 0 bar.		
8.	Approach cylinders.		
9.	Manually close nitrogen ground cylinder valve.		
10.	Manually close N_2O ground cylinder valve.		
11.	Evacuate area.		
12.	Open N_2O ground vent valve.		
13.	Open N_2O ground fill valve.		
14.	Ensure pressure reads 0 on N_2O ground station PT.		
15.	Open Nitrogen ground vent valve.		
16.	Open Nitrogen ground fill valve.		
17.	Ensure pressure reads 0 bar on nitrogen ground station PT.		
18.	Clear combustion chamber of excess pooled fuel.		

F.12.5 Failure Case 4: Failure to actuate fuel vent valve.

No.	Task	Operator	Date
1.	Ensure N_2O GS fill valve is closed.		
2.	Ensure Nitrogen GS fill valve is closed.		
3.	Open N_2O vent valve.		
4.	Measure N_2O tank pressure to 0 bar.		
5.	Open fuel run valve.		
6.	Measure fuel tank pressure and Nitrogen tank pressure to 0 bar.		
7.	Check all pressures in system are at 0 bar.		
8.	Approach cylinders.		
9.	Manually close nitrogen ground cylinder valve.		
10.	Manually close N_2O ground cylinder valve.		
11.	Evacuate area.		
12.	Open N_2O GS vent valve.		
13.	Open N_2O GS fill valve.		
14.	Ensure pressure reads 0 on N_2O ground station PT.		
15.	Open Nitrogen GS vent valve.		
16.	Open Nitrogen GS fill valve.		
17.	Ensure pressure reads 0 on nitrogen ground station PT.		
18.	Clear Combustion chamber of excess pooled fuel.		
19.	Clear Chamber are of expelled liquid fuel.		

F.12.6 Failure case 6: Failure to actuate ground station fill valves pre-fill

In the case of failed actuation of the ground station fill valves the ground station vent valves should be opened, and manual opening of these valves can then take place.

No.	Task	Operator	Date
1.	Ensure fueling lines are not loose and will not move in operation		
2.	Manually close N_2O cylinder valve		
3.	Manually close Nitrogen cylinder valve		
4.	Leave area		
5.	Actuate ground station and launch vehicle vent valves		
6.	Actuate working ground fill valves		
7.	Check all pressures read 0		
8.	Approach ground station with appropriate PPE		
9.	Using a socket, manually open stuck valve until venting sound heard		
10.	Wait until sound stops, ensuring cylinder valve closed		

F.12.7 Failure Case 7: Failure to actuate ground station fill valves post-fill

In this case the rocket is likely to be filled to flight pressure.

No.	Task	Operator	Date
1.	Approach ground cylinders and close their respective valves		
2.	Evacuate area		
3.	Open N_2O vent valve		
4.	Measure N_2O tank pressure to 0 bar		
5.	Open fuel vent valve		
6.	Measure fuel tank pressure and Nitrogen tank pressure to 0 bar.		
7.	Check all pressures in system are at 0 bar.		
8.	Open N_2O ground vent valve		
9.	Open N_2O ground fill valve if applicable		
10.	Ensure pressure reads 0 bar on N_2O ground station PT		
11.	Open Nitrogen ground vent valve		
12.	Open Nitrogen ground fill valve if applicable		
13.	Ensure pressure reads 0 bar on nitrogen ground station PT		
14.	Clear Combustion chamber of excess pooled fuel		

G. Engineering Drawings

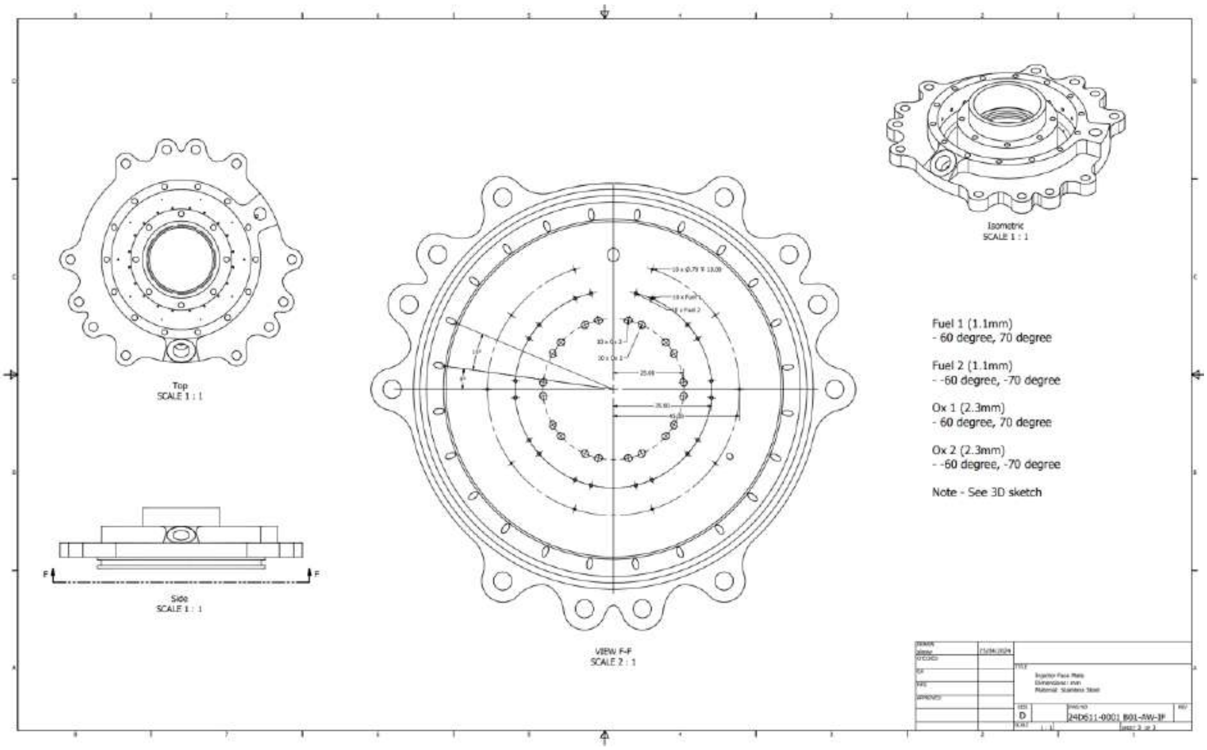

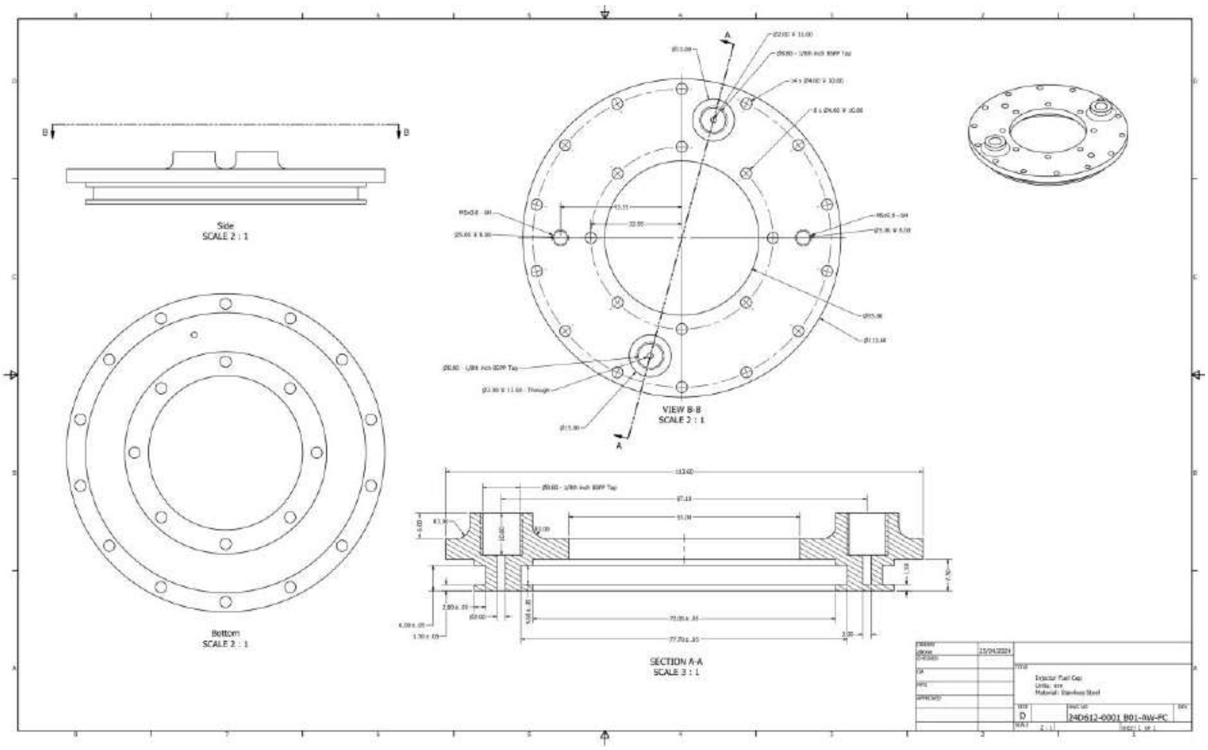

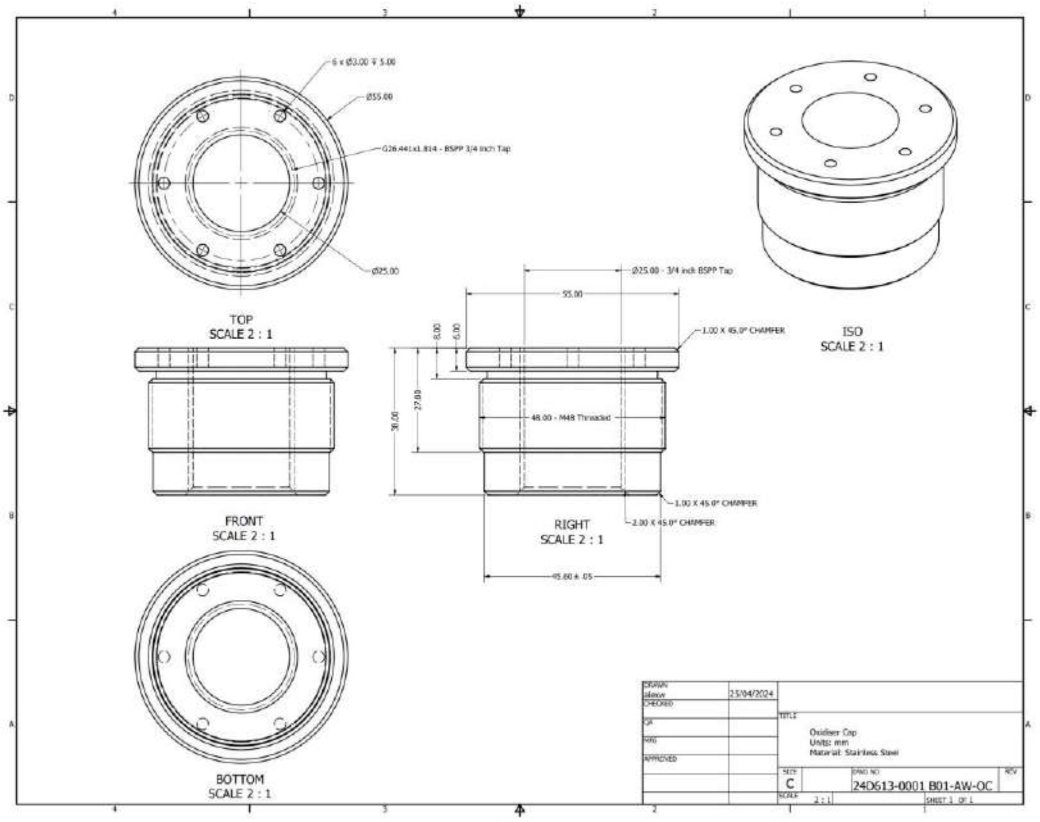
6 x Ø3.00 ↧ 5.00
Ø55.00
Ø25.00
Ø25.00 - 3/4 inch BSPP Tap
55.00
1.00 X 45.0° CHAMFER
48.00 - M48 Threaded
2.00 X 45.0° CHAMFER
TOP
SCALE 2 : 1
FRONT
SCALE 2 : 1
RIGHT
SCALE 2 : 1
BOTTOM
SCALE 2 : 1
ISO
SCALE 2 : 1
25/04/2024
Oxidiser Cap
Units: mm
Material: Stainless Steel
C
24D613-0001 B01-AW-OC
2 : 1

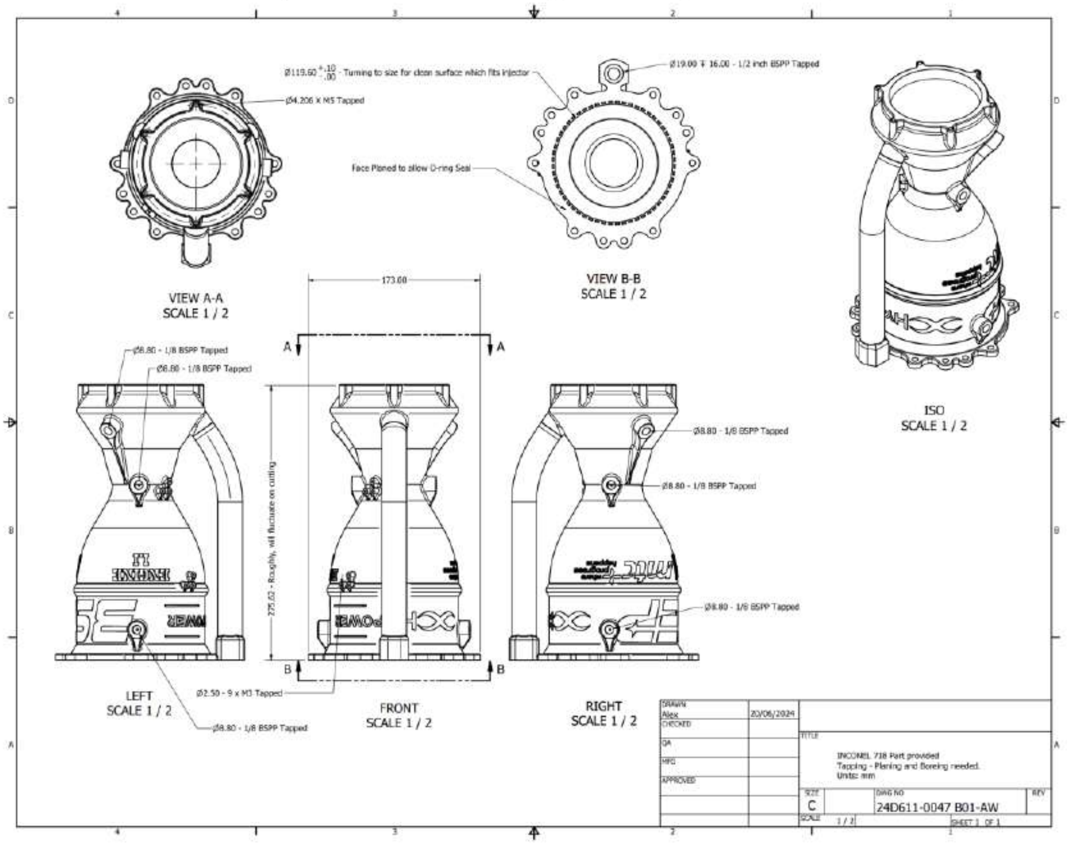
Turning to size for clean surface which fits injector
Ø19.00 ↧ 16.00 - 1/2 inch BSPP Tapped
Face Planed to allow O-ring Seal
VIEW A-A
SCALE 1 / 2
VIEW B-B
SCALE 1 / 2
173.00
Ø8.80 - 1/8 BSPP Tapped
275.02 - Roughly, will fluctuate on cutting
Ø2.50 - 9 x M3 Tapped
ISO
SCALE 1 / 2
LEFT
SCALE 1 / 2
FRONT
SCALE 1 / 2
RIGHT
SCALE 1 / 2
Alex
20/06/2024
INCONEL 718 Part provided
Tapping - Planing and Boreing needed.
Units: mm
C
24D611-0047 B01-AW
1 / 2

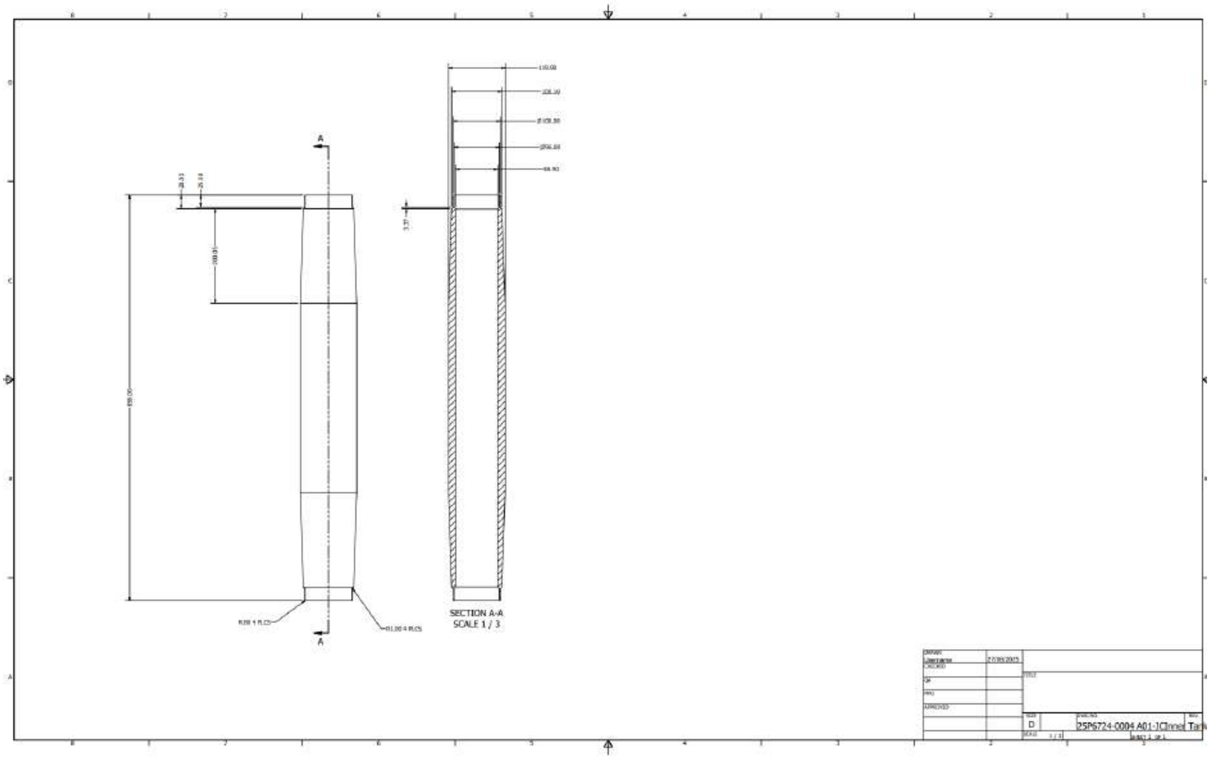
SECTION A-A
SCALE 1 / 3
2SP6724-0004 A01-1CInner Tank

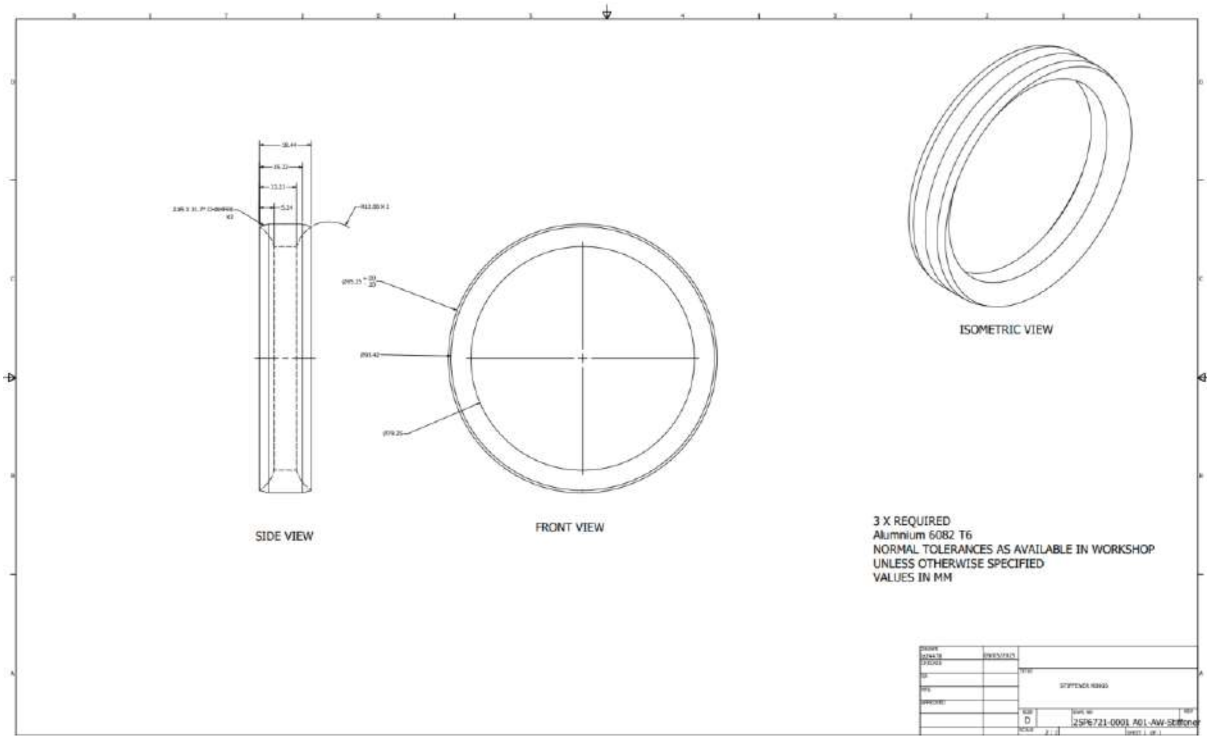
ISOMETRIC VIEW
SIDE VIEW
FRONT VIEW
3 X REQUIRED
Aluminium 6082 T6
NORMAL TOLERANCES AS AVAILABLE IN WORKSHOP
UNLESS OTHERWISE SPECIFIED
VALUES IN MM
2SP6721-0001 A01-AW-Stiffener

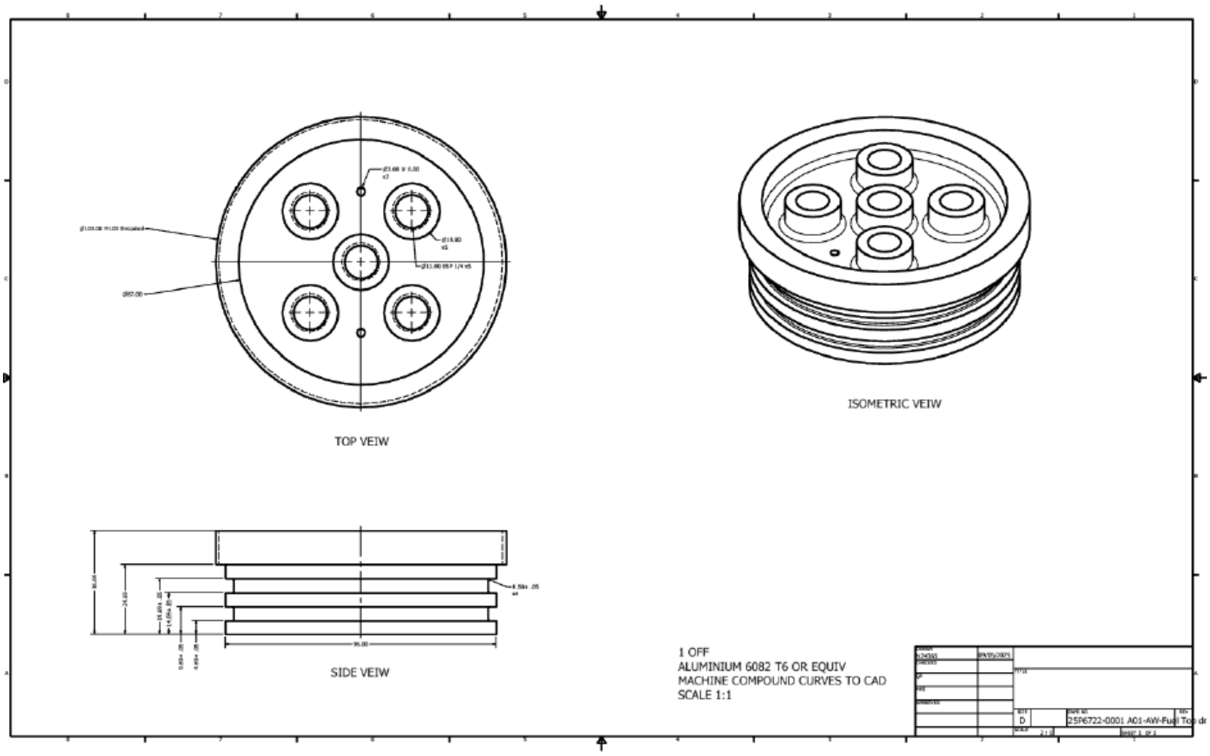
TOP VEIW
ISOMETRIC VEIW
SIDE VEIW
1 OFF
ALUMINIUM 6082 T6 OR EQUIV
MACHINE COMPOUND CURVES TO CAD
SCALE 1:1

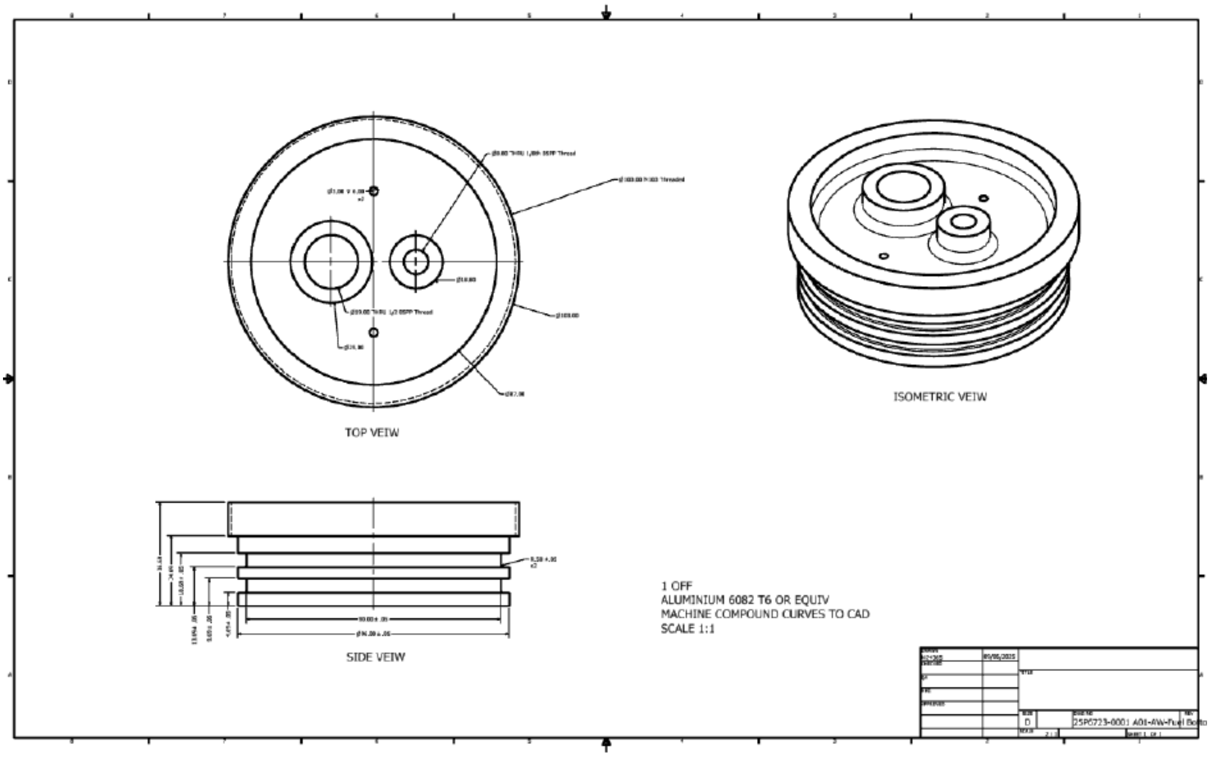
TOP VEIW
ISOMETRIC VEIW
SIDE VEIW
1 OFF
ALUMINIUM 6082 T6 OR EQUIV
MACHINE COMPOUND CURVES TO CAD
SCALE 1:1

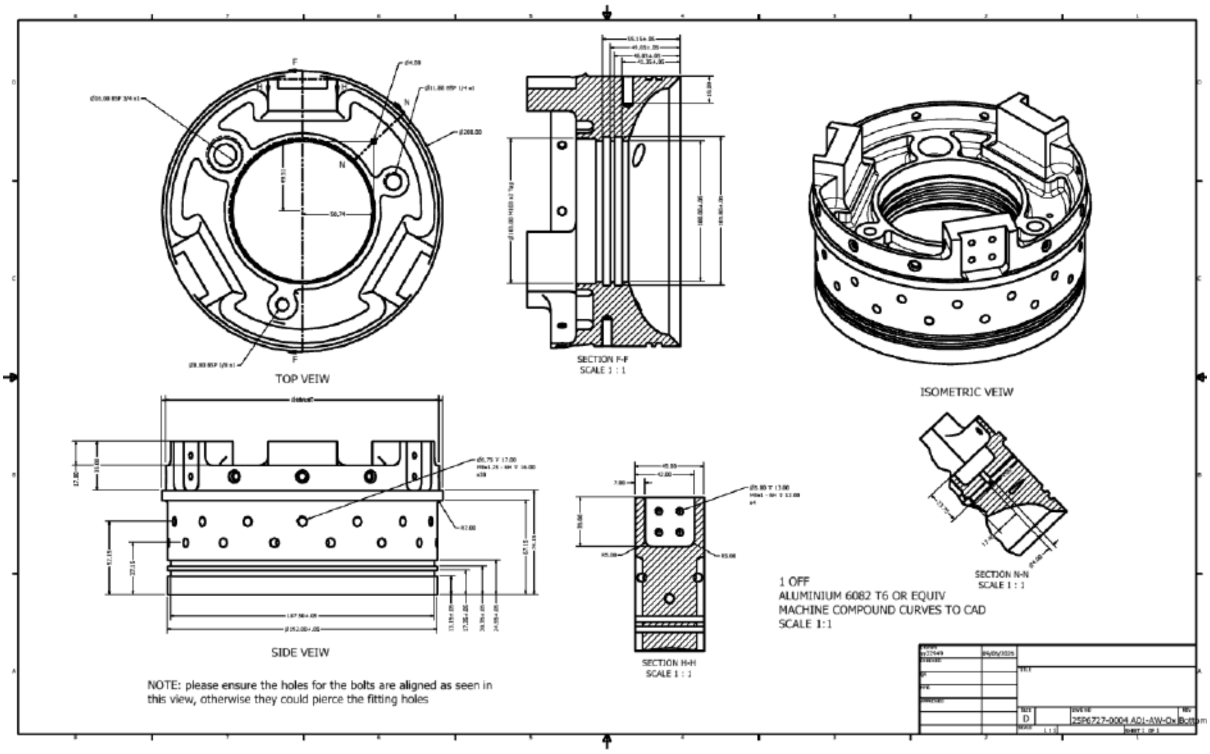
TOP VEIW
SECTION F-F
SCALE 1 : 1
ISOMETRIC VEIW
SIDE VEIW
SECTION H-H
SCALE 1 : 1
SECTION N-N
SCALE 1 : 1
1 OFF
ALUMINIUM 6082 T6 OR EQUIV
MACHINE COMPOUND CURVES TO CAD
SCALE 1:1
NOTE: please ensure the holes for the bolts are aligned as seen in
this view, otherwise they could pierce the fitting holes
25P6727-0004 A01-AW-Ox Bottom

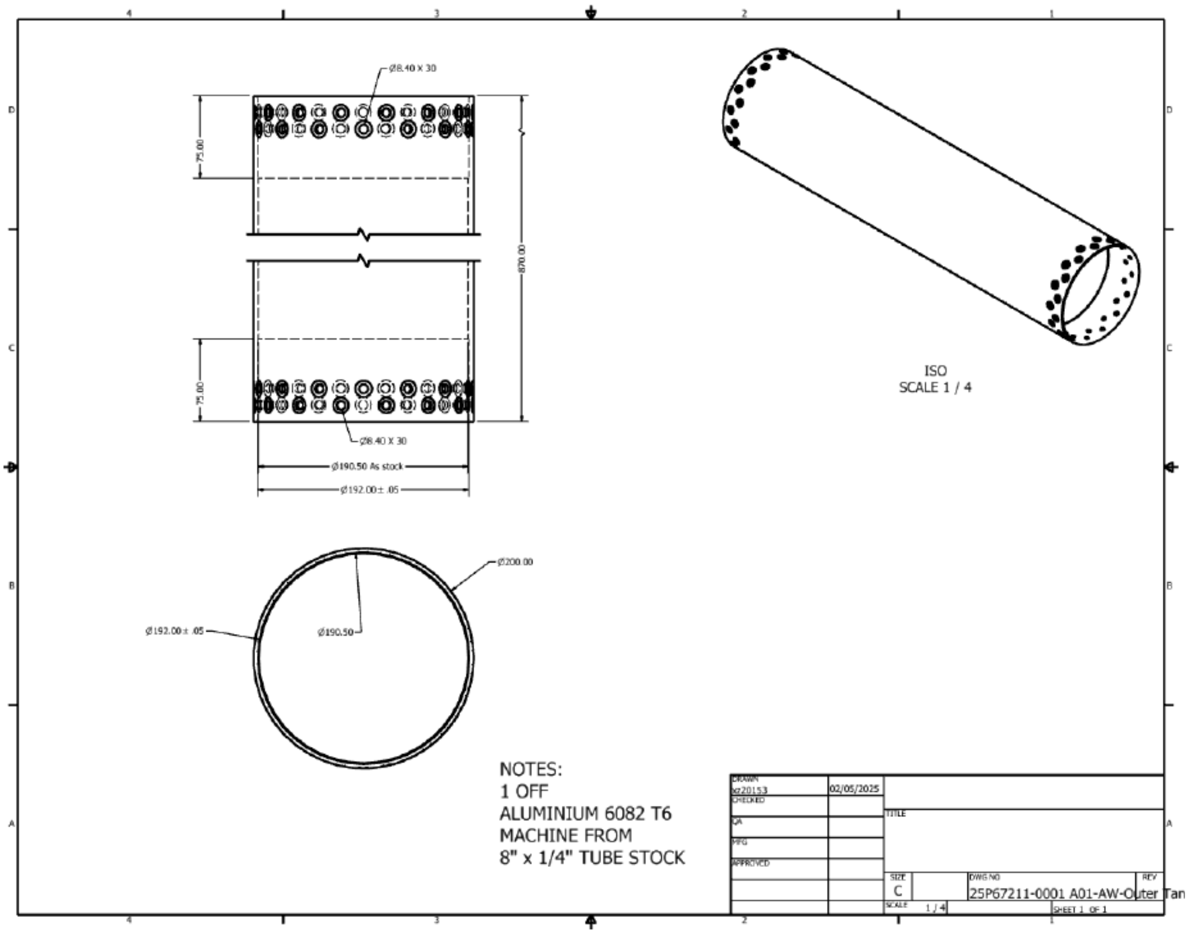
Ø8.40 X 30
75.00
870.00
Ø190.50 As stock
Ø192.00± .05
ISO
SCALE 1 / 4
Ø200.00
Ø192.00± .05
Ø190.50
NOTES:
1 OFF
ALUMINIUM 6082 T6
MACHINE FROM
8" x 1/4" TUBE STOCK
DRAWN
kz20153
02/05/2025
CHECKED
TITLE
QA
MFG
APPROVED
SIZE
C
DWG NO
25P67211-0001 A01-AW-Outer Tan
REV
SCALE
1 / 4
SHEET 1 OF 1

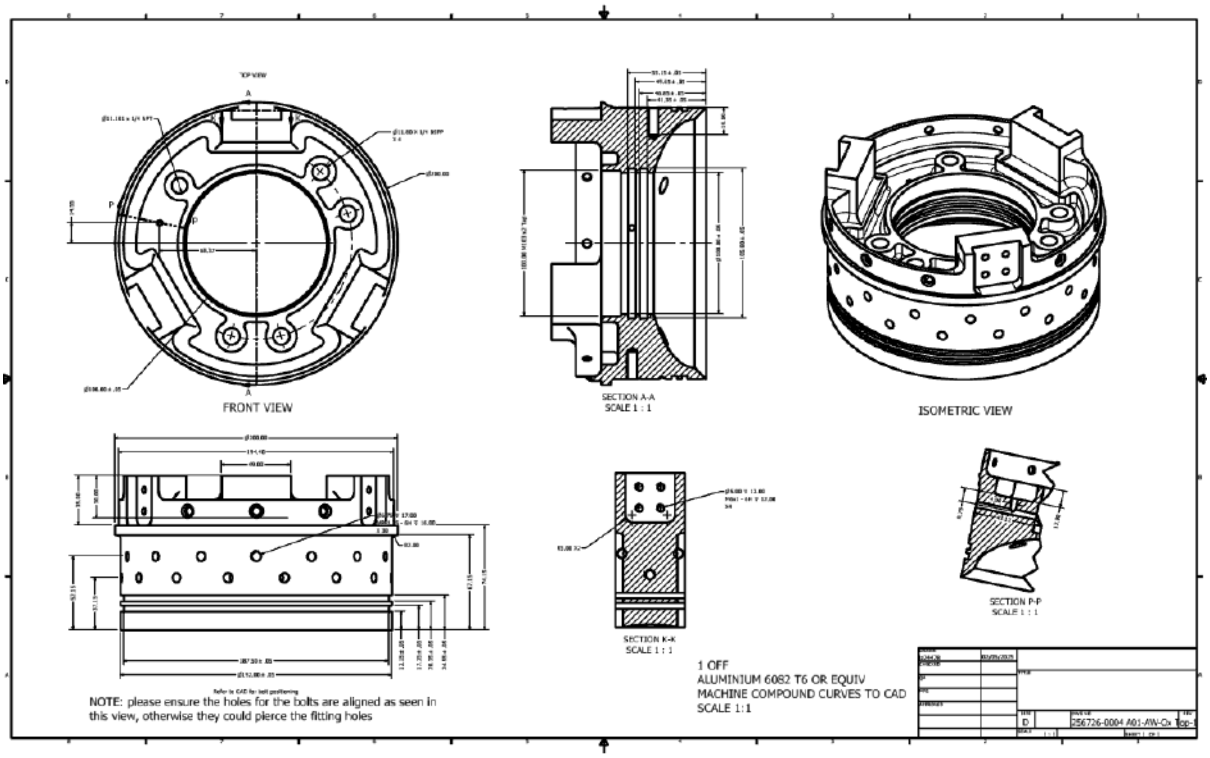

FRONT VIEW
SECTION A-A
SCALE 1 : 1
ISOMETRIC VIEW
SECTION K-K
SCALE 1 : 1
SECTION P-P
SCALE 1 : 1
NOTE: please ensure the holes for the bolts are aligned as seen in this view, otherwise they could pierce the fitting holes
1 OFF
ALUMINIUM 6082 T6 OR EQUIV
MACHINE COMPOUND CURVES TO CAD
SCALE 1:1

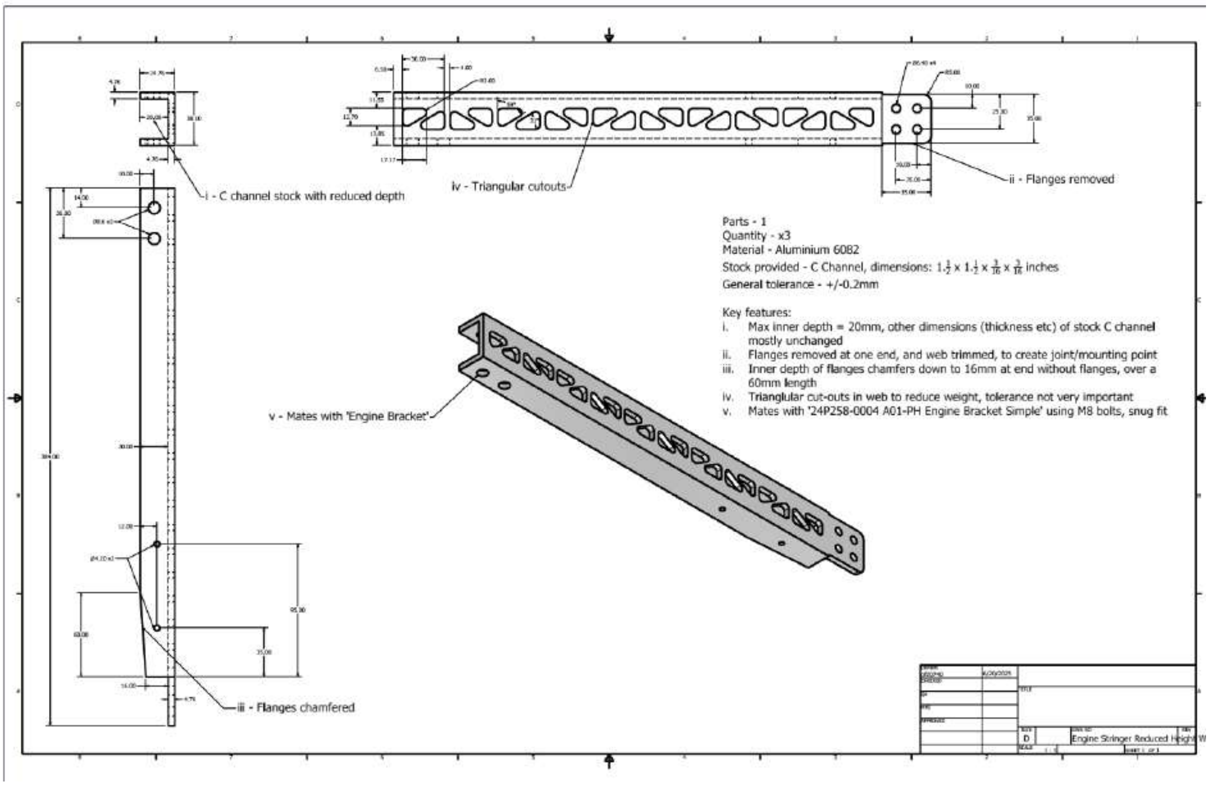

i - C channel stock with reduced depth
iv - Triangular cutouts
ii - Flanges removed
iii - Flanges chamfered
v - Mates with 'Engine Bracket'
Parts - 1
Quantity - x3
Material - Aluminium 6082
Stock provided - C Channel, dimensions: 1 1/2 x 1 1/2 x 3/16 x 3/16 inches
General tolerance - +/-0.2mm
Key features:
i. Max inner depth = 20mm, other dimensions (thickness etc) of stock C channel mostly unchanged
ii. Flanges removed at one end, and web trimmed, to create joint/mounting point
iii. Inner depth of flanges chamfers down to 16mm at end without flanges, over a 60mm length
iv. Triangular cut-outs in web to reduce weight, tolerance not very important
v. Mates with '24P258-0004 A01-PH Engine Bracket Simple' using M8 bolts, snug fit
Engine Stringer Reduced Height W

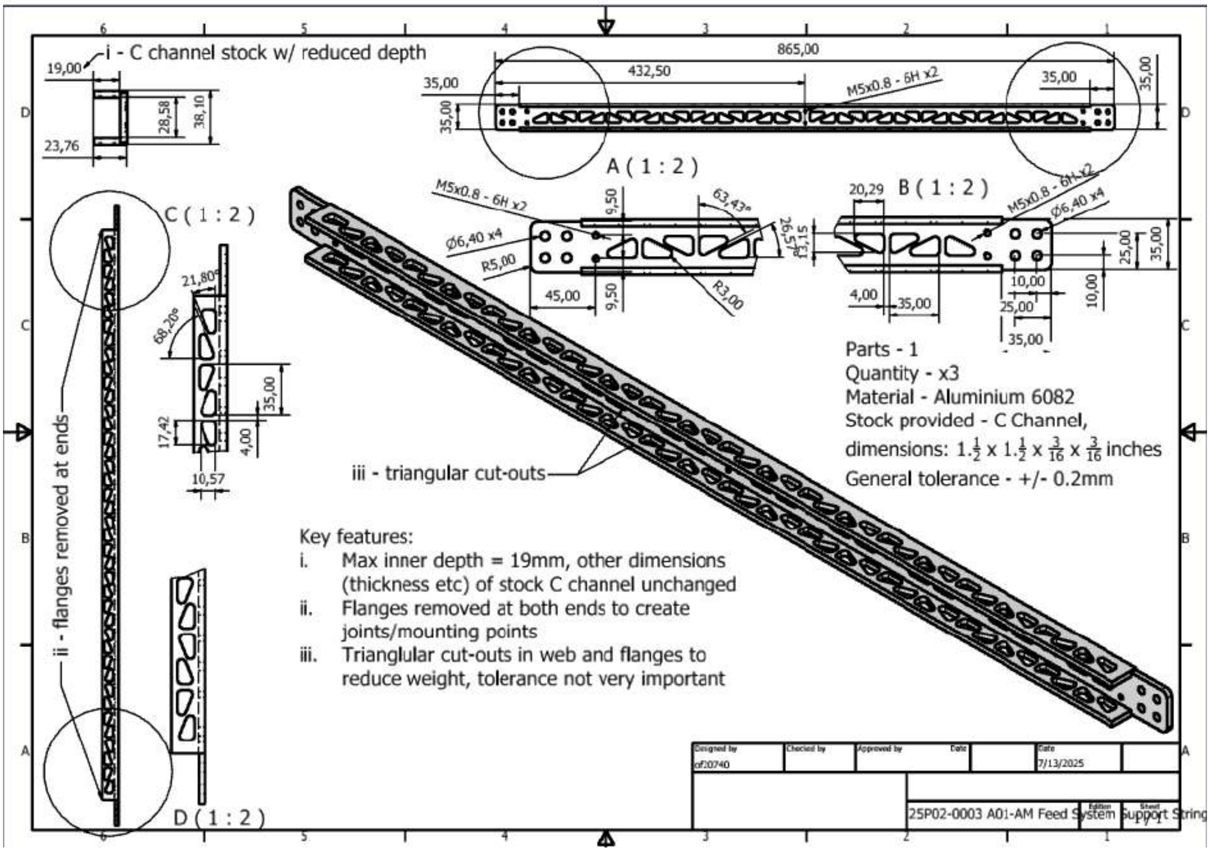
i - C channel stock w/ reduced depth
A (1 : 2)
B (1 : 2)
C (1 : 2)
D (1 : 2)
M5x0.8 - 6H x2
Ø6,40 x4
ii - flanges removed at ends
iii - triangular cut-outs
Parts - 1
Quantity - x3
Material - Aluminium 6082
Stock provided - C Channel,
dimensions: $1\frac{1}{2}$ x $1\frac{1}{2}$ x $\frac{3}{16}$ x $\frac{3}{16}$ inches
General tolerance - +/- 0.2mm
Key features:
i. Max inner depth = 19mm, other dimensions (thickness etc) of stock C channel unchanged
ii. Flanges removed at both ends to create joints/mounting points
iii. Trianglular cut-outs in web and flanges to reduce weight, tolerance not very important
7/13/2025
25P02-0003 A01-AM Feed System Support String

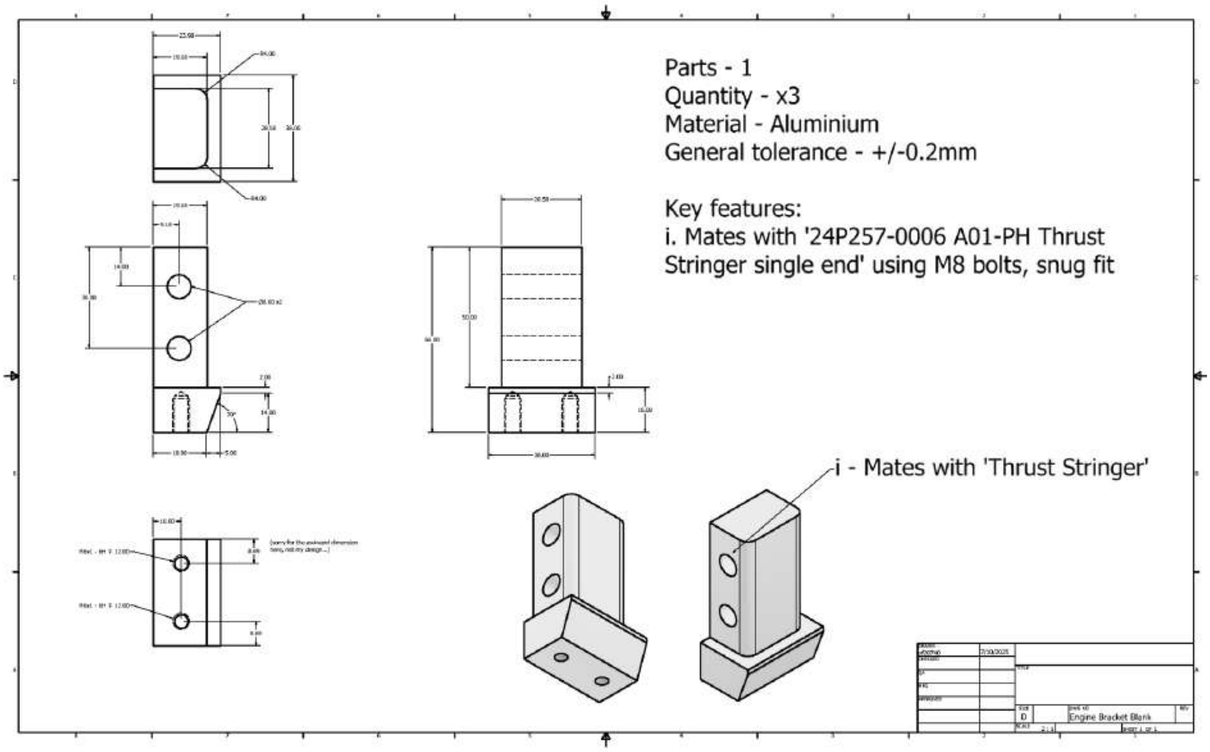
Parts - 1
Quantity - x3
Material - Aluminium
General tolerance - +/-0.2mm
Key features:
i. Mates with '24P257-0006 A01-PH Thrust Stringer single end' using M8 bolts, snug fit
i - Mates with 'Thrust Stringer'
Engine Bracket Blank

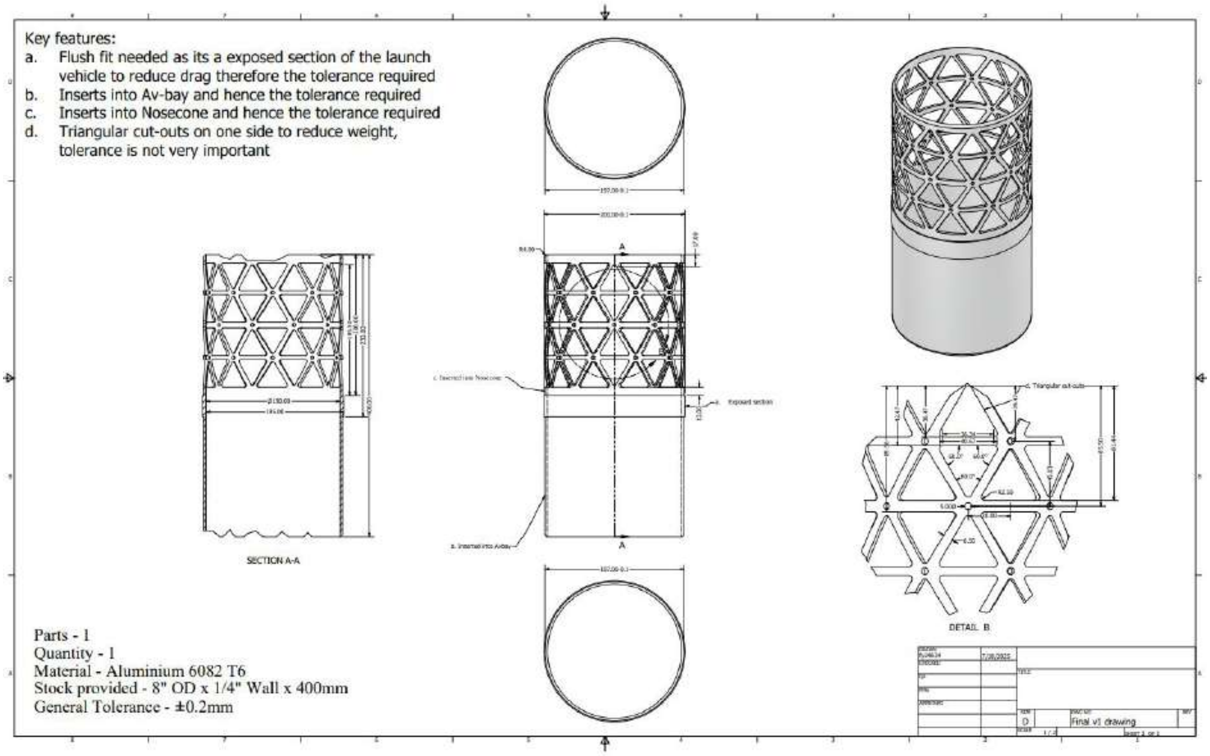
Key features:
a. Flush fit needed as its a exposed section of the launch vehicle to reduce drag therefore the tolerance required
b. Inserts into Av-bay and hence the tolerance required
c. Inserts into Nosecone and hence the tolerance required
d. Triangular cut-outs on one side to reduce weight, tolerance is not very important
SECTION A-A
DETAIL B
Parts - 1
Quantity - 1
Material - Aluminium 6082 T6
Stock provided - 8" OD x 1/4" Wall x 400mm
General Tolerance - ±0.2mm
Final v1 drawing

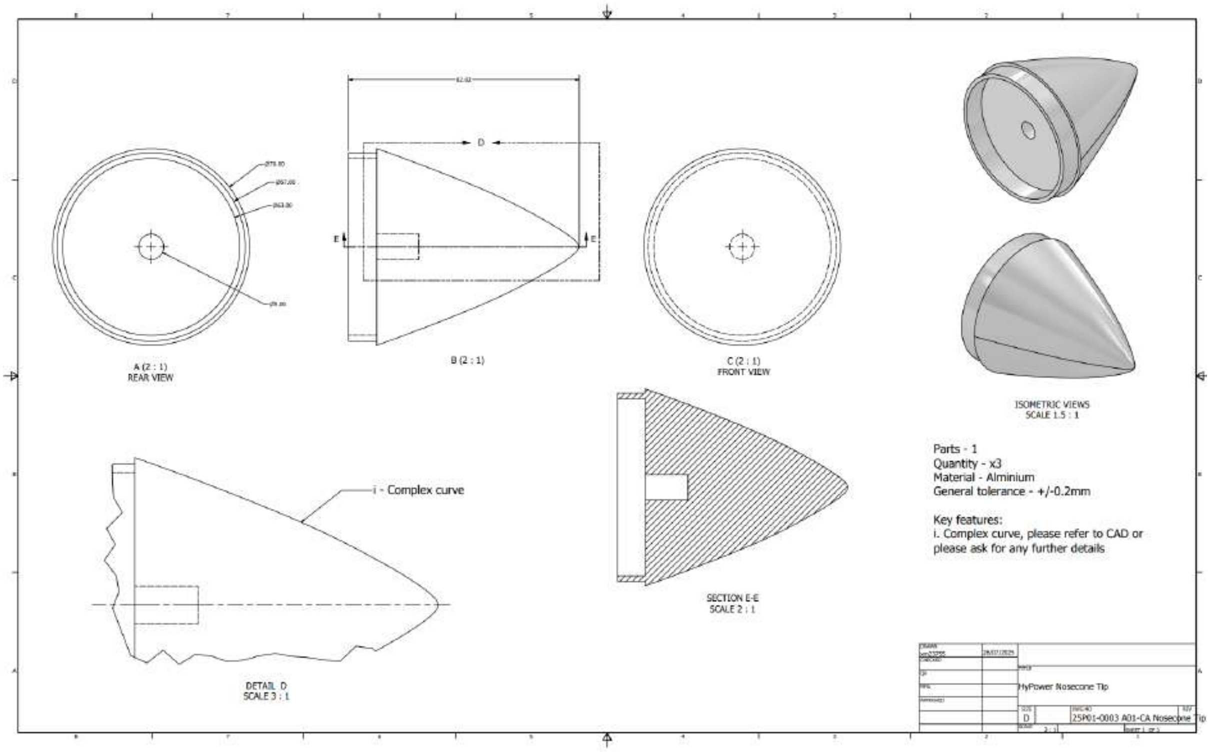
A (2 : 1)
REAR VIEW
B (2 : 1)
C (2 : 1)
FRONT VIEW
ISOMETRIC VIEWS
SCALE 1.5 : 1
i - Complex curve
DETAIL D
SCALE 3 : 1
SECTION E-E
SCALE 2 : 1
Parts - 1
Quantity - x3
Material - Alminium
General tolerance - +/-0.2mm
Key features:
i. Complex curve, please refer to CAD or please ask for any further details
HyPower Nosecone Tip

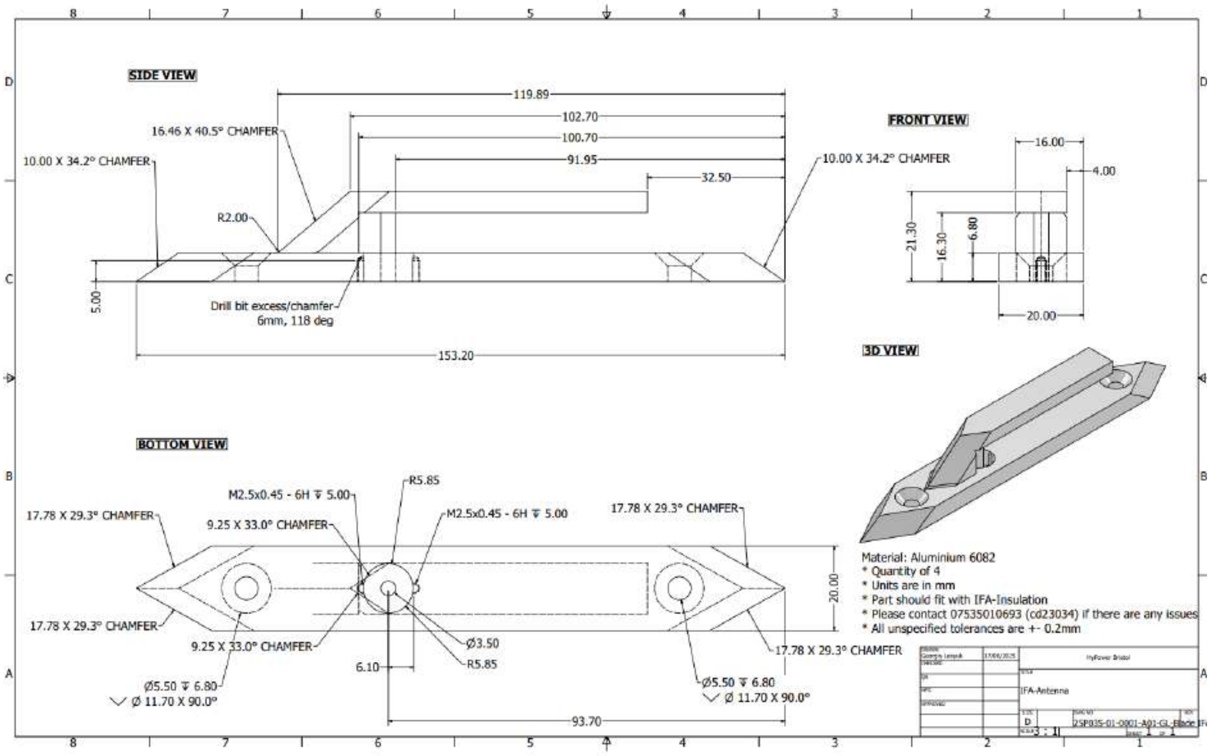
SIDE VIEW
119.89
102.70
100.70
91.95
32.50
16.46 X 40.5° CHAMFER
10.00 X 34.2° CHAMFER
R2.00
10.00 X 34.2° CHAMFER
5.00
Drill bit excess/chamfer
6mm, 118 deg
153.20
FRONT VIEW
16.00
4.00
21.30
16.30
6.80
20.00
3D VIEW
BOTTOM VIEW
M2.5x0.45 - 6H ⊽ 5.00
R5.85
M2.5x0.45 - 6H ⊽ 5.00
17.78 X 29.3° CHAMFER
9.25 X 33.0° CHAMFER
17.78 X 29.3° CHAMFER
20.00
17.78 X 29.3° CHAMFER
9.25 X 33.0° CHAMFER
Ø3.50
R5.85
6.10
17.78 X 29.3° CHAMFER
Ø5.50 ⊽ 6.80
⌵ Ø 11.70 X 90.0°
Ø5.50 ⊽ 6.80
⌵ Ø 11.70 X 90.0°
93.70
Material: Aluminium 6082
* Quantity of 4
* Units are in mm
* Part should fit with IFA-Insulation
* Please contact 07535010693 (cd23034) if there are any issues
* All unspecified tolerances are +- 0.2mm
HyPower Bristol
IFA-Antenna

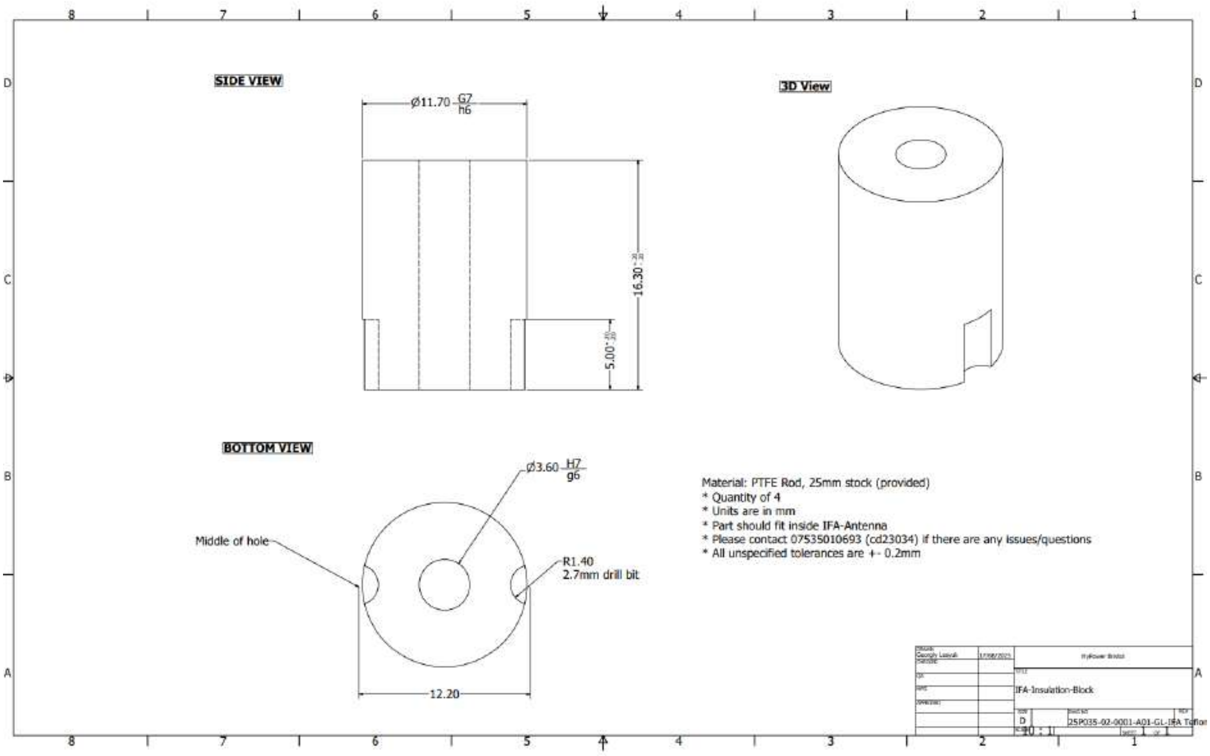
SIDE VIEW
Ø11.70 G7/h6
16.30
5.00
3D View
BOTTOM VIEW
Ø3.60 H7/g6
Middle of hole
R1.40
2.7mm drill bit
12.20
Material: PTFE Rod, 25mm stock (provided)
* Quantity of 4
* Units are in mm
* Part should fit inside IFA-Antenna
* Please contact 07535010693 (cd23034) if there are any issues/questions
* All unspecified tolerances are +- 0.2mm
HyPower Bristol
IFA-Insulation-Block

H. Propulsion Supporting Data

H.1 Combustion Chamber Supporting Figures

Table 3 Specific Impulse Efficiency - O/F = 1.9

INJECTOR	P_c PSIA	% Si 0	0.5	1.0	2.0
FUEL BARRIER	500	90.6	90.7	90.6	89.5
	750	92.4	92.5	92.3	91.5
	1000	93.4	93.3	93.1	92.1
FUEL/OX BARRIER	500	91.4	92.0	92.4	91.9
	750	92.8	93.0	93.5	93.3
	1000	93.7	93.7	94.0	93.4

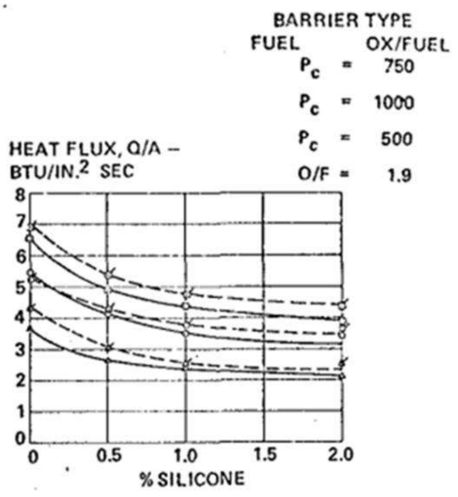

Fig. 11 Convergent Section Heat Transfer

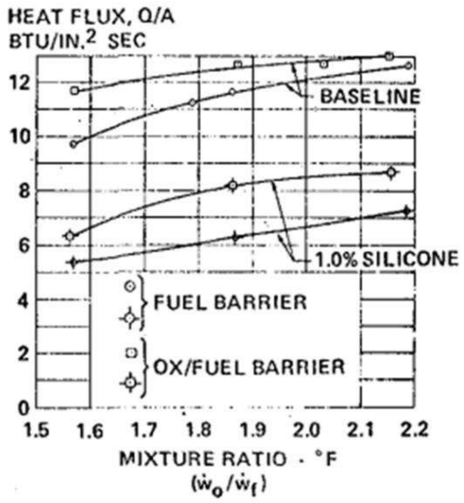

Fig. 9 Throat Section Heat Transfer - P_c = 750 psia

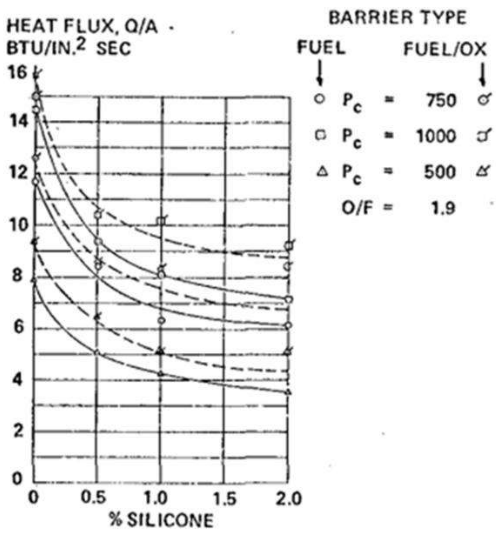

Fig. 12 Throat Section Heat Transfer

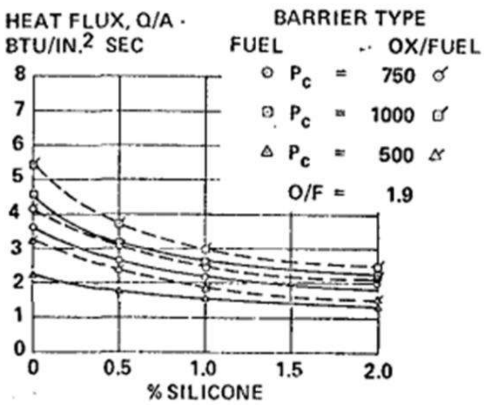

Fig. 10 Chamber Section Heat Transfer

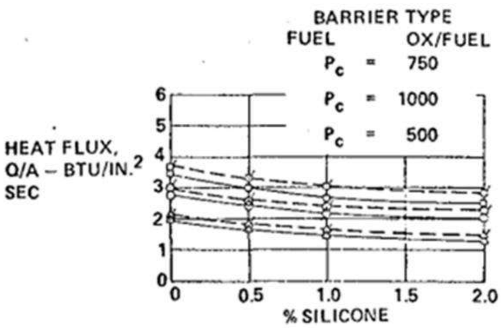

Fig. 13 Divergent Section Heat Transfer

Figure 115: Combustion Chamber - PDMS performance and total heat flux reduction Figures

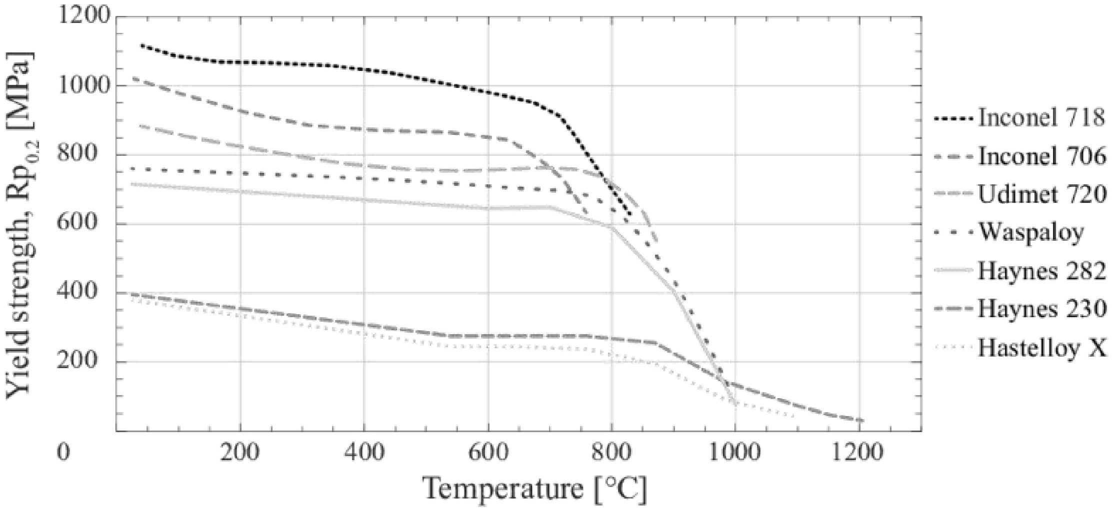

Figure 116: Combustion Chamber – Inconel 718 Yield Strength vs Temperature

A central challenge was reconciling incompressible WT testing with the compressible nature of launch flight. While subsonic tunnel testing captures fundamental aerodynamic trends, compressibility introduces nonlinear effects (e.g., shock formation, Mach-dependent drag rise, altered pressure distributions) that must be considered to ensure fidelity. Incorporating compressibility corrections—through Mach scaling, similarity parameters, and CFD extrapolation—was essential to extend WT data to launch conditions. This motivated the hybrid validation chain: leveraging the low-Re, incompressible insights from WT, embedding them into compressible CFD models, and thus improving predictive accuracy for launch performance. Overall, the project's strength lay in this layered validation strategy, where each dataset enhanced the reliability and transferability of the others, ensuring a robust aerodynamic foundation for design decisions.

H.2 Coaxial Swirl Injector Design

This appendix will focus on the design of our coaxial swirl injector, which was planned to be flown before the failure of the flight-weight engine at the Race2Space competition. We did not believe that the injector had sufficiently proved, during the one test that we did manage to complete, that it was capable of meeting the performance requirements.

A coaxial swirl injector plate has been designed and is machined from aluminium. The design features no inter-propellant seals. This is a requirement due to their difficulty to implement and associated risk of leakage. The injector plate consists of a "double decker" manifold, according to the swirler element manifold layout. The inner swirler is recessed according to Bazarov's procedure to allow for an internal mixing design. This is due to its better mixing and the fan angle sizing constraints imposed by an externally mixing design.

Fuel enters the injector plate from the combustion chamber's regenerative cooling channels via an intermediary manifold, and then through angled fuel passages to the upper manifold (detailed below). Oxidiser enters at the injector plate's centre directly through a ¾" BSPP thread. This arrangement is chosen to ensure that the lower mass flow propellant (fuel here) passes through the inner swirler elements. This limitation is because the analytical sizing procedure used scales with mass flow.

To be machinable, the injector is a three-part assembly. Due to space constraints, there is also a ¼” and two 1/8” NPT to BSPP adaptors to access the ignitor and pressure ports respectively.

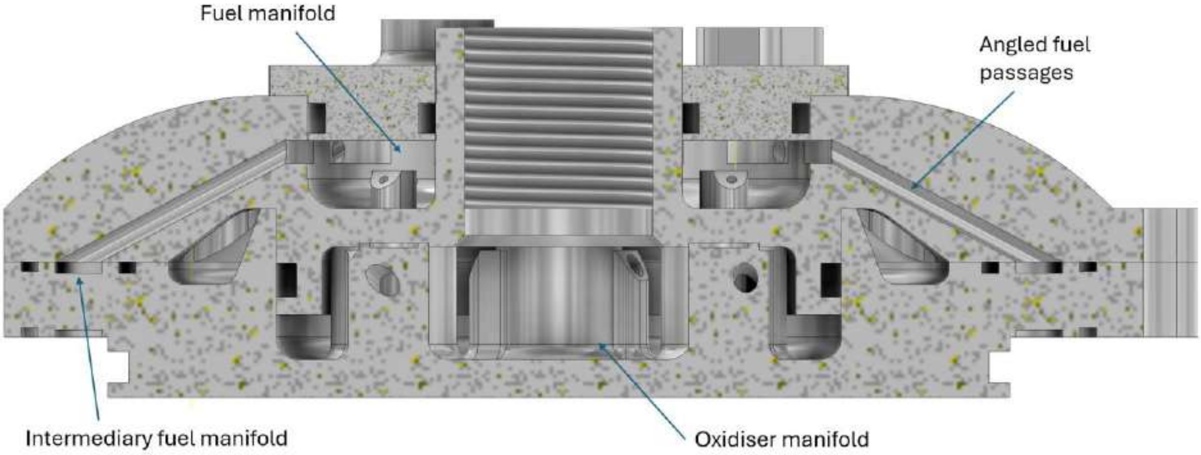

The base plate houses the oxidiser manifold and port threads for the pressure transducer and ignitor adaptors. It also interfaces with the chamber to channel the fuel flow into an intermediary (or ‘junction’) manifold. This is to redirect a portion of the flow to the film cooling orifices.

The central plate channels fuel from the intermediary manifold into the upper fuel manifold. It also features equally spaced cutouts in the radial space between the oxidiser and intermediary fuel manifolds. This is to create a “to-atmospheric” gap between the fuel face and main oxidiser piston seals, avoiding an inter-propellant seal.

Both the fuel and oxidiser swirlers are machined as one piece with their respective central and base plates. This is to further remove the need for any inter-propellant seals between the swirler elements.

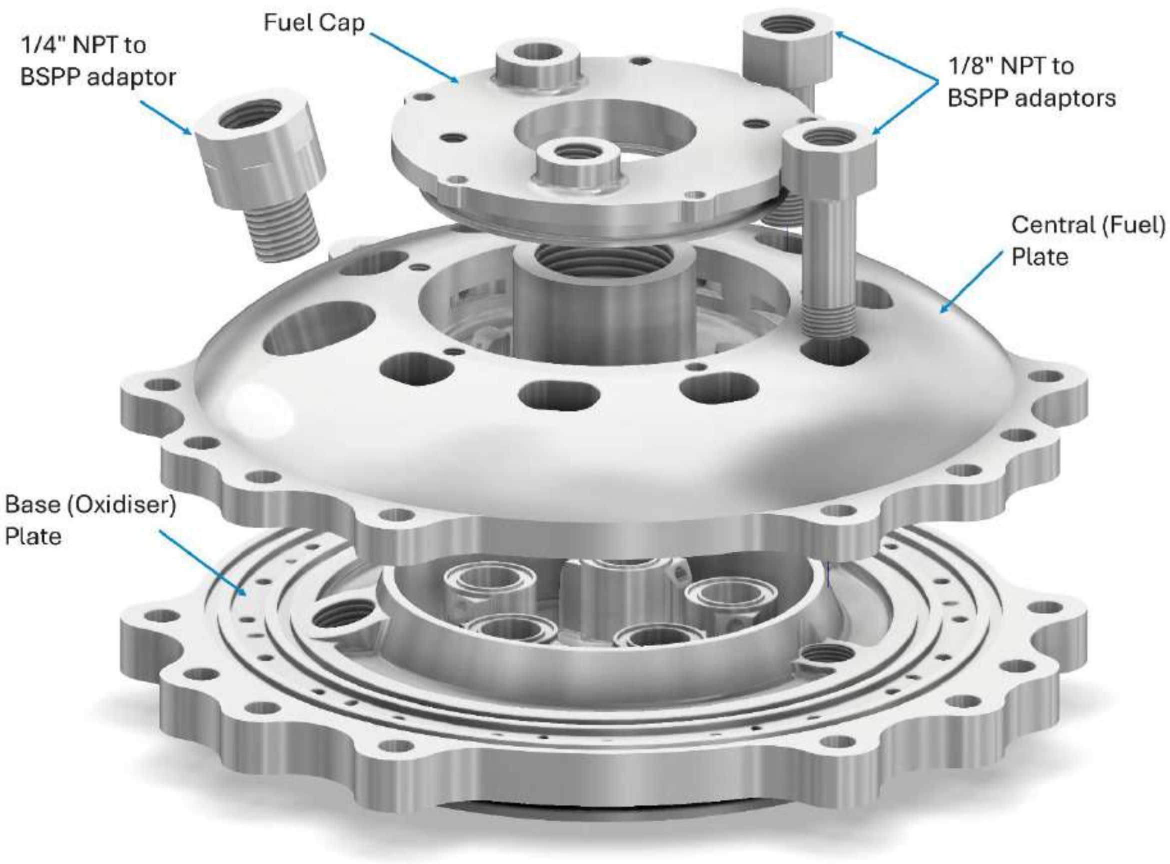

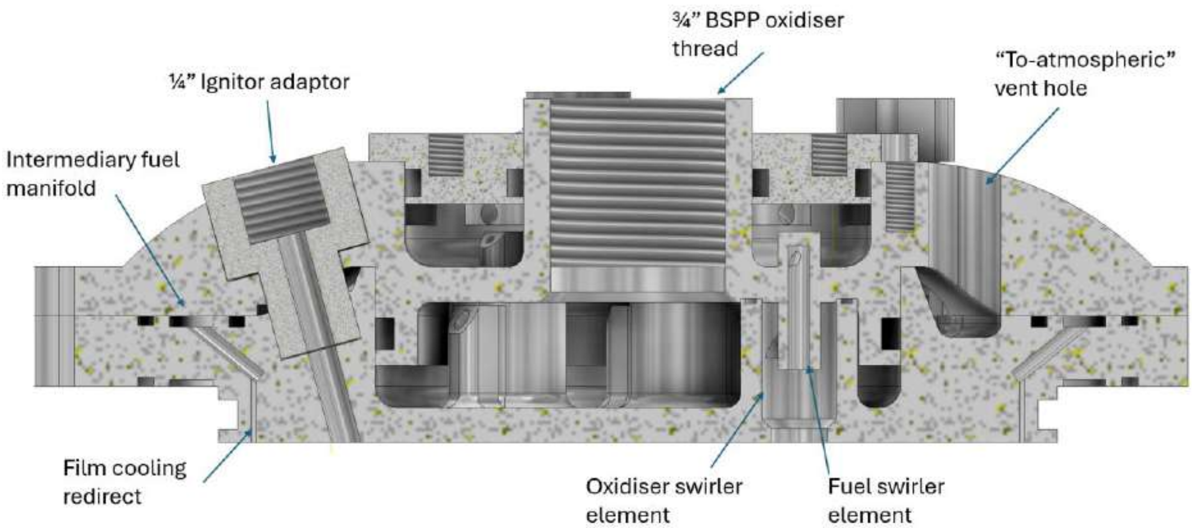

Swirler dimensions

Element type: Coaxial swirl elements, with inner and outer oxidiser swirlers, respectively

Property	Value	Unit
Fuel mass flow	0.64	kg/s
Oxidiser mass flow	1.922	kg/s
OF ratio	3	[--]

Fuel nozzle diameter	4.2	mm
Oxidiser nozzle diameter	8	mm
Fuel vortex chamber diameter	3	mm
Oxidiser vortex chamber diameter	10.7	mm
Fuel internal fan angle	60	°
Oxidiser fan angle	90	°
Film cooling orifice mass flow rate	0.06	kg/s

Injector Pressures

Property	Value	Unit
Fuel manifold pressure	30	bar
Oxidiser manifold pressure	30	bar
Fuel pressure drop across injector	10	bar
Oxidiser pressure drop across injector	10	bar

H.3 Plumbing Bill of Materials

Top Plumbing		
25A72 – Pressurant Line		
Item	**Supplier**	**Part Number**
Nitrogen Line		
3L Tank	Advanced Material Systems	XT00327
3L Tank M18X1.5 to NPT	Nero	
Sloc NPT branch tee	Swagelok	SS-400-3-4TTF
025 Check Valve	Swagelok	SS-4C-1
025 Sloc MBSPP	Swagelok	SS-400-1-4RS
025 QD	dnp	
025 Sloc tee	Swagelok	SS-400-3
025 Sloc to 0125 FBSPP	Swagelok	SS-400-1-2RS
Hi pressure transducer	Hefei Wnk Smart Technology Co.	WNK81MA
025 Sloc to 050 MNPT	Swagelok	SS-400-1-8
025 Sloc NPT	Swagelok	SS-400-1-4
Aqua Pressure Regulator	Aqua Environment	873-1500-NV-NA
025 Sloc tee	Swagelok	SS-400-3
Fuel Line		
025 Check Valve	Swagelok	SS-4C-1
025 Sloc MBSPP	Swagelok	SS-400-1-4RS
025 Actuated Valve	Delta-P	BV2-G1/4-06
025 Valve Actuator	SRAD	-
025 Sloc MBSPP	Swagelok	SS-400-1-4RS
025 Sloc MBSPP	Swagelok	SS-400-1-4RS
Ox Line		
025 Check Valve	Swagelok	SS-4C-1
025 Sloc MBSPP	Swagelok	SS-400-1-4RS
025 Actuated Valve	Delta-P	BV2-G1/4-06
025 Valve Actuator	SRAD	-
025 Sloc MBSPP	Swagelok	SS-400-1-4RS
025 Sloc MBSPP	Swagelok	SS-400-1-4RS

25A73 – Fuel Fill		
Item	**Supplier**	**Part Number**
025 Non-Actuating Valve	Delta-P	BV2-G1/4-06
025 Sloc MBSPP	Swagelok	SS-400-1-4RS
025 Sloc MBSPP	Swagelok	SS-400-1-4RS

25A76 – Fuel Vent		
Item	**Supplier**	**Part Number**
025 Slok MBSPP	Swagelok	SS-400-1-4RS
025 Actuating Valve	Delta-P	BV2-G1/4-06
025 Actuated Valve	Delta-P	BV2-G1/4-06
025 Slok MBSPP	Swagelok	SS-400-1-4RS
025 Slok MBSPP	Swagelok	SS-400-1-4RS

25A77 – Ox Vent		
Item	**Supplier**	**Part Number**
025 Slok MBSPP	Swagelok	SS-400-1-4RS

025 Actuating Valve	Delta-P	BV2-G1/4-06
025 Valve Actuator	SRAD	-
025 Slok MNPT	Swagelok	SS-400-1-8
025 Diptube	Swagelok	SS-DTM4-F4-104

Direct on Tank		
Item	**Supplier**	**Part Number**
Ox Burst disc (58.5-71.5 bar at 20degC)	Wehberg Safety	108954W
Ox transducer	Hefei Wnk Smart Technology Co.	WNK80MA
Fuel Burst Disc	Wehberg Safety	108954W
Fuel transducer	Hefei Wnk Smart Technology Co.	WNK80MA
025 0125 Ox Transducer adapter	Nero	RB0402P
025 0125 Fuel transducer adapter	Nero	RB0402P

Bottom Plumbing		
25A78 – Fuel Run		
Item	**Supplier**	**Part Number**
050 Sloc MBSPP	Swagelok	SS-810-1-8RS
050 Sloc 45 Elbow	Swagelok	SS-810-95
050 Sloc 45 Elbow	Swagelok	SS-810-96
050 Actuating Valve	Delta-P	BV2-G1/2-13
050 Valve Actuator	SRAD	-
050 Sloc BSPP	Swagelok	SS-810-1-8RS
050 Sloc BSPP	Swagelok	SS-810-1-8RS
25A74 – Ox Fill		
Item	**Supplier**	**Part Number**
025 Sloc MBSPP	Swagelok	SS-400-1-4RS
025 Check Valve	Swagelok	SS-4C-1
025 Sloc MBSPP	Swagelok	SS-400-1-4RS
025 QD	dnp	

H.4 Computational Model

Since aluminium itself has a much higher thermal conductivity compared to that of air or that of N2O liquid itself, the Biot number would be very low and the aluminium can be treated as having uniform temperature. Nusselt number of heat transfer between air and aluminium tank is unknown and depends on factors including wind speed, so a precise number is unknown. A parameter sweep study is conducted. Even with Nusselt numbers up to 20, the rocket can sit idle for more than 1000s before overpressure., therefore complying with EuRoC requirements.

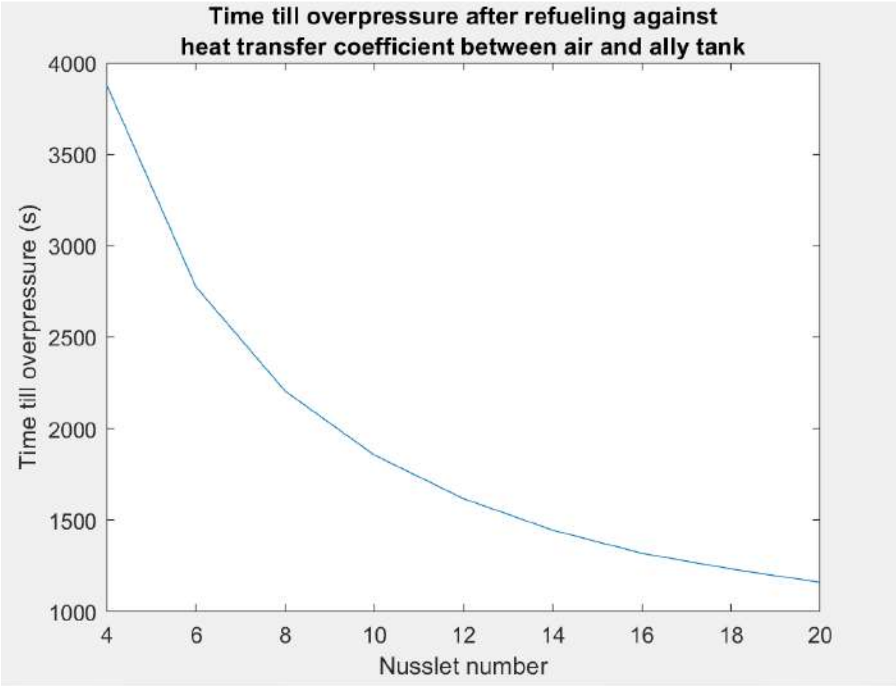

H.5 Initial Tank Design and Analysis

The primary aim of this year's tank was to prevent the failure case seen in the previous year's tank, while minimising the increase in mass. Shown below is a full CAD render of the final tank design.

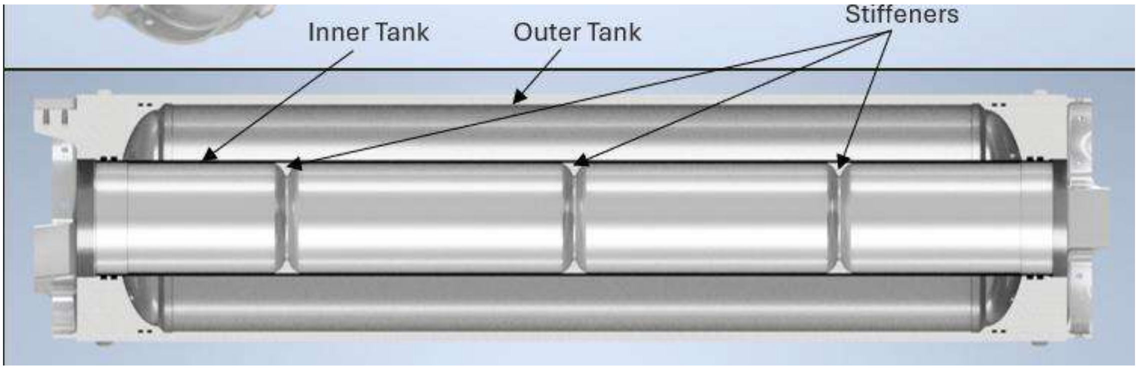

Figure 16: 3rd-Angle and Half-section view of the full tank assembly

The tank endcaps were the simplest part to redesign, as last year's caps were designed with multiple flaws, including:

- Varying fillet radii throughout the cap – changed to just a few radii, approved by the machine shop.
- Uneven, and inefficient weight-saving cutouts – improved by increasing the radius of cutouts, and cutting out more sections, saving mass.

Shown below is a comparison between the 2024 caps and the 2025 caps, demonstrating significant weight savings.

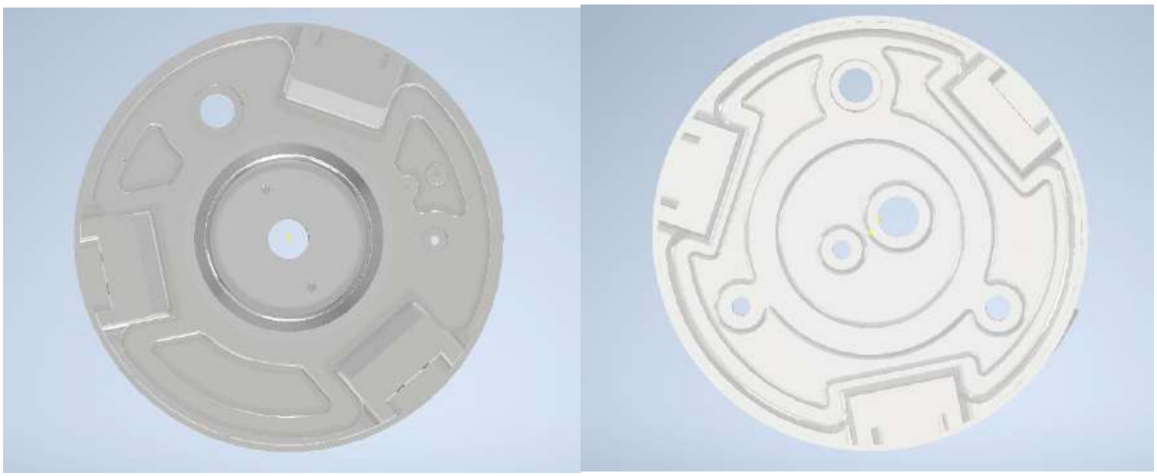

Figure 117: Bottom bulkhead comparison between 2024 (left) and 2025 (right)

Shown below are the fittings used on the bottom and top bulkheads, with the key shown.

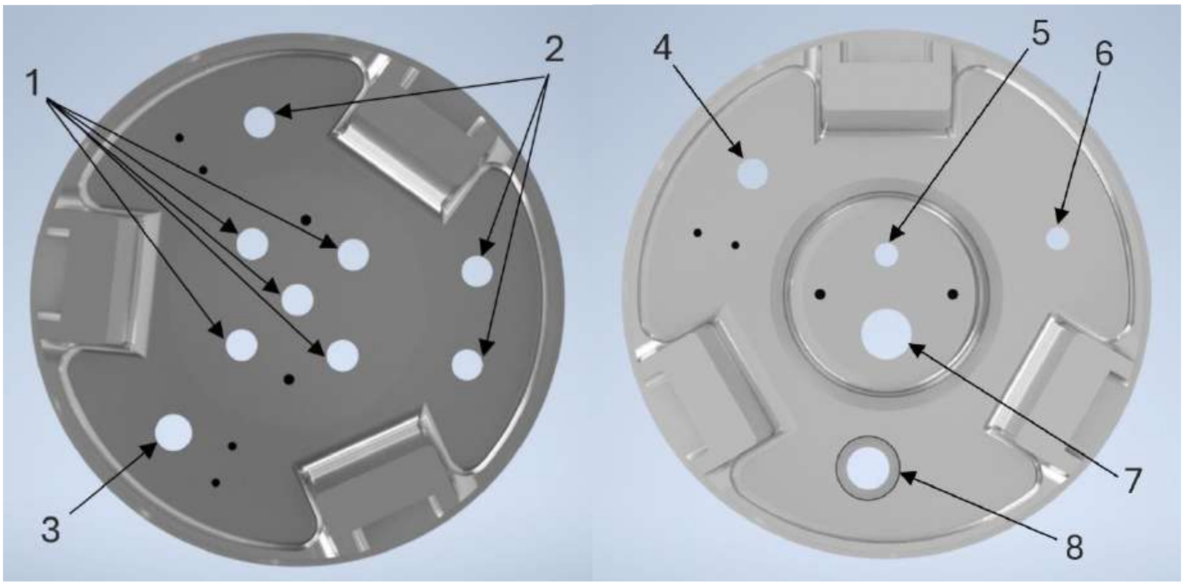

Figure 1187: CAD render showing tank endcaps

Label	Port size	Port function
1	5x1/4 BSPP	Pressure in, Fill, Transducer, Vent, Burst Disc
2	3x1/4 BSPP	Pressure In, Transducer
3	1x1/4 NPT	Diptube/Vent
4	1x1/4 BSPP	Fill
5	1x1/8 BSPP	Ignitor
6	1x1/8 BSPP	Ignitor
7	1x1/2 BSPP	Flow out
8	1x3/4 BSPP	Flow out

Table 32: Tank endcap label definitions

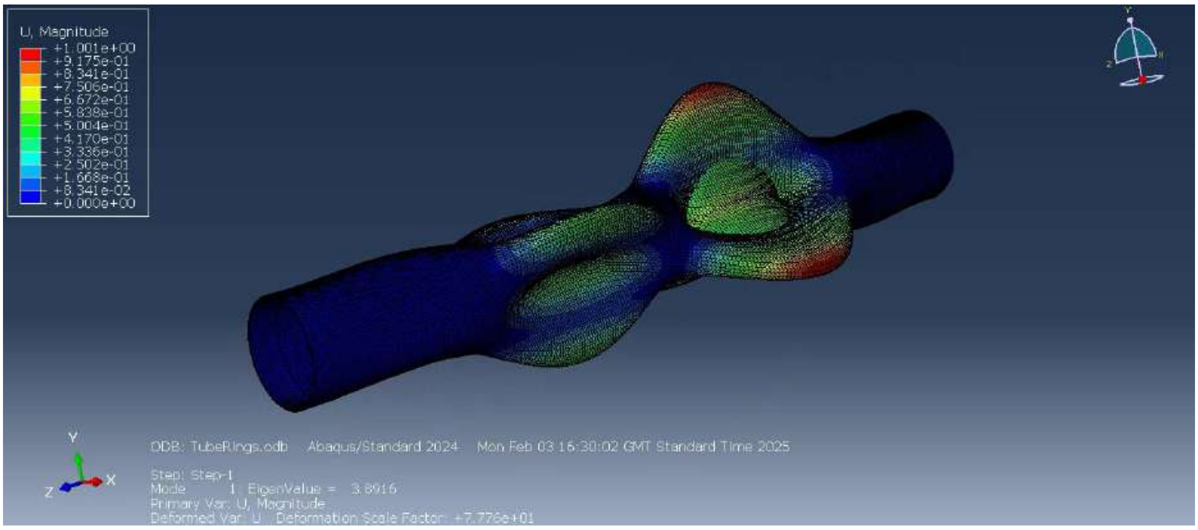

Figure 18: FEA simulation of inner tank buckling mode

To solve the issues of buckling encountered when only the oxidiser tank is filled, 3 stiffening rings have been added on the inside of the inner tank. The stiffening ring is shown on left and was designed with a highly filleted surface to ensure smooth fuel flow. Using the same methods as in non-stiffened FEA an eigenvalue of 3.89 was observed, giving a pressure of 116.7 bar, as shown in stiffened FEA This is well within the range of 2xMEOP (100 bar) using the current design.

Figure 19 – CAD render of stiffening ring

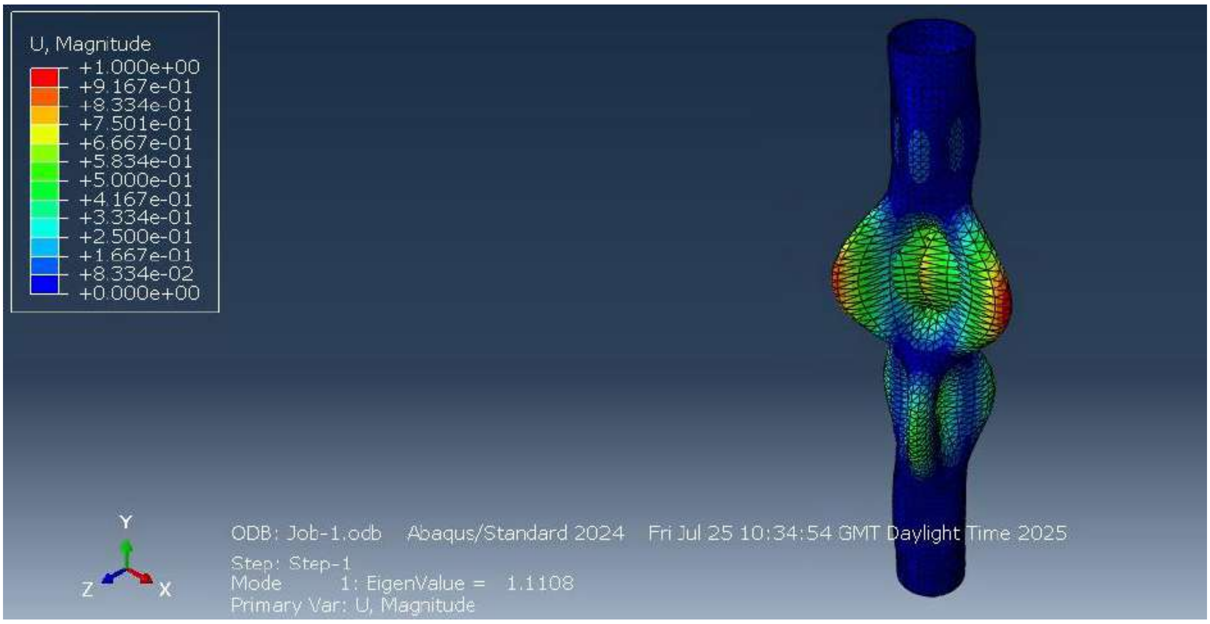

Figure 119: FEA simulation with a 100 bar pressure on the outer surface of the inner tank

As seen in the figures above, the new inner tank with the stiffening rings would not buckle in the event of inner tank depressurisation, which was caused last year by a faulty valve. Even in this worse-case scenario this year, the tank would not fail.

Following the first hydrostatic testing campaign, the inner tank was redesigned to prevent the buckling failure that the initial design suffered. The stiffening rings were most likely detached from the inner walls of the tube, due to insufficient adhesive application or human error. This led to the pressure acting solely on the wall thickness, which was not enough to resist the pressures, which went up to 85 bar.

To eliminate this failure mode, the tank was redesigned with a significantly greater wall thickness; the stiffening rings were removed, meaning any human error in applying the adhesive was removed entirely. FEA simulations in ABAQUS were carried out for inner wall thicknesses of 6.5mm, 7.5mm, and 8.5mm, which can be found in the appendix. These were carried out using a non-linear buckling step, and solved using the Lanczos method, with 25 eigenvalues requested, with the force applied a uniform pressure of 50 bar. Finally, to ensure that the tank did not fail by this buckling mode, the tank design was altered to have a higher thickness near the centre of the tank.

From the pressure of 50 bar applied, this had an eigenvalue of 44.258, which meant the inner tank could withstand 514.6, over 10x the MEOP.

H.6 R2S 2025 Critical Design Report

Overview of a 5 kN Aluminium Regeneratively Cooled Engine

A regeneratively cooled bi-propellant liquid rocket engine has been designed with capability to produce 5 kN thrust for 5 seconds. We aim to hot fire our engine at nominal thrust and burn duration to validate our design and evaluate the engine's capability for use in launch vehicle with 3 km target apogee.

Table 33: Engine Summary

Property	Value
Engine type	Bi-propellant
Fuel	IPA (15% film cooling) + 1% PDMS
Oxidiser	N_2O
Chamber pressure	20 bar
Thrust	5 kN
Cooling	Regenerative cooling, film cooling, additive cooling

The combustion chamber is designed as a lightweight flight version of Project Feynman's engine.last year's engine. To reduce the mass the chamber is designed to be additively manufactured with CP1 aluminium, instead of Inconel 718. The change in material results in a threefold mass reduction as well as increasing the cooling capabilities that an enhanced thermal conductivity. However, the tensile strength of aluminium degrades rapidly with temperature, therefore a careful thermal design is required.

The figure below shows a quarter section view of the engine assembly. The injector plate is a co-axial swirl design. Fuel enters the engine via a spout in the bottom right. The fuel then enters a manifold to evenly distribute across the nozzles circumference before entering straight regenerative cooling channels that run axially to the injector plate on the left. The fuel inlet tube is tapped to take a BSPP fitting, to allow integration into the full system.

Figure 120, Quarter section view of full engine assembly CAD

Fuel and oxidiser fittings consist of stainless steel BSPP ½ inch and ¾ inch fittings respectively. These will be sealed using dowty washers against the combustion chamber and injector. Thermocouples are attached to the engine using 1/8 inch BSPP to 1.5mm brass compression fittings. The thermocouples are not subject to a pressure seal, so there is no requirement here to include dowty washers. The injector plate features 1/8th inch BSPP fitting ports for the combustion chamber, nitrous oxide and ethanol manifold pressure transducers.

Table 34: Further particular details for engine design.

Property	Value	Unit
Fuel mass flow rate	0.64	kg/s
Oxidiser mass flow rate	1.93	kg/s
OF ratio	3	[--]
Chamber diameter	119.6	mm
Engine length	274.35	mm
Contraction ratio	6	[--]
Throat diameter	48.54	mm
Nozzle diameter	88.6	mm
L*	843.21	mm
Expansion ratio	3.36	[--]
Inner wall thickness	0.8	mm
Outer wall thickness	2	mm

Multiple thermocouple ports are built into the chamber and pressure transducer ports are built into the injector to allow collection of sensor data. A series of dry thermocouples are used to monitor the temperature of coolant along the channel walls, and a pair of pressure transducers are present on the injector to log the incoming pressure of the fuel and as well as the chamber pressure in the engine.

Table 3: Key instrumentation properties

Type	Value	Range	Part	Connection
Temperature	T(XX)	198 - 523	T type thermocouple	Type T Connection
Pressure	P(XX)	0 – 60 Bar	GPT200 Universal	4 pin M12

Figure 2, *Instrumentation Diagram*

Coaxial swirl injector plate

Two injector plate designs are to be machined. Both injectors adhere to the same chamber interface dimensions, this is to allow for interchangeable injector and combustion chamber combinations.

The first of these is an aluminium version of last cycle's like-like impinging design. This is to provide a lighter flight version of the existing chamber and injector plate assembly. All geometric dimensions are to be kept the same, so as not to unexpectedly introduce any combustion instabilities.

For the second, a coaxial swirl injector plate has been designed and is to be machined from aluminium. The design features no inter-propellant seals. This is a requirement due to their difficulty to implement and associated risk of leakage **Error! Bookmark not defined.**. The injector plate consists of a "double decker" manifold, according to the swirler element manifold layout (see). The inner swirler is recessed according to Bazarov's procedure to allow for an internal mixing design. This is due to its better mixing and the fan angle sizing constraints imposed by an externally mixing design.

Fuel enters the injector plate from the combustion chamber's regenerative cooling channels via an intermediary manifold, and then through angled fuel passages to the upper manifold (detailed below). Oxidiser enters at the injector plate's centre directly through a ¾" BSPP thread. This arrangement is chosen to ensure that the lower mass flow propellant (fuel here) passes through the inner swirler elements. This limitation is because the analytical sizing procedure used scales with mass flow.

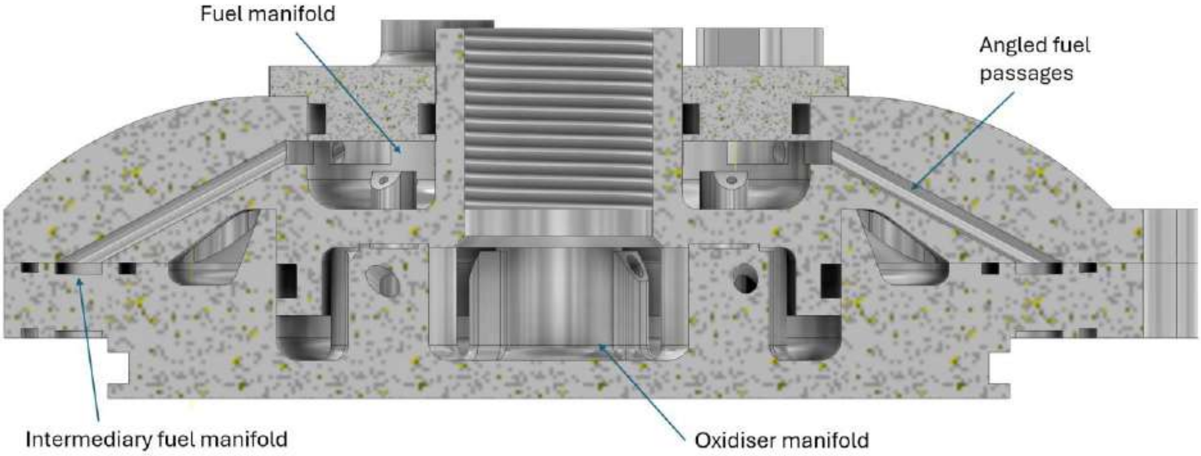

Figure 121 — "Double Decker" manifold layout

To be machinable, the injector is a three part assembly. Due to space constraints, there is also a ¼" and two 1/8" NPT to BSPP adaptors to access the ignitor and pressure ports respectively.

The base plate houses the oxidiser manifold and port threads for the pressure transducer and ignitor adaptors. It also interfaces with the chamber to channel the fuel flow into an intermediary (or 'junction') manifold. This is to redirect a portion of the flow to the film cooling orifices (see above).

The central plate channels fuel from the intermediary manifold into the upper fuel manifold. It also features equally spaced cutouts in the radial space between the oxidiser and intermediary fuel manifolds. This is to create a "to-atmospheric" gap between the fuel face and main oxidiser piston seals, avoiding an inter-propellant seal.

Both the fuel and oxidiser swirlers are machined as one piece with their respective central and base plates. This is to further remove the need for any inter-propellant seals between the swirler elements.

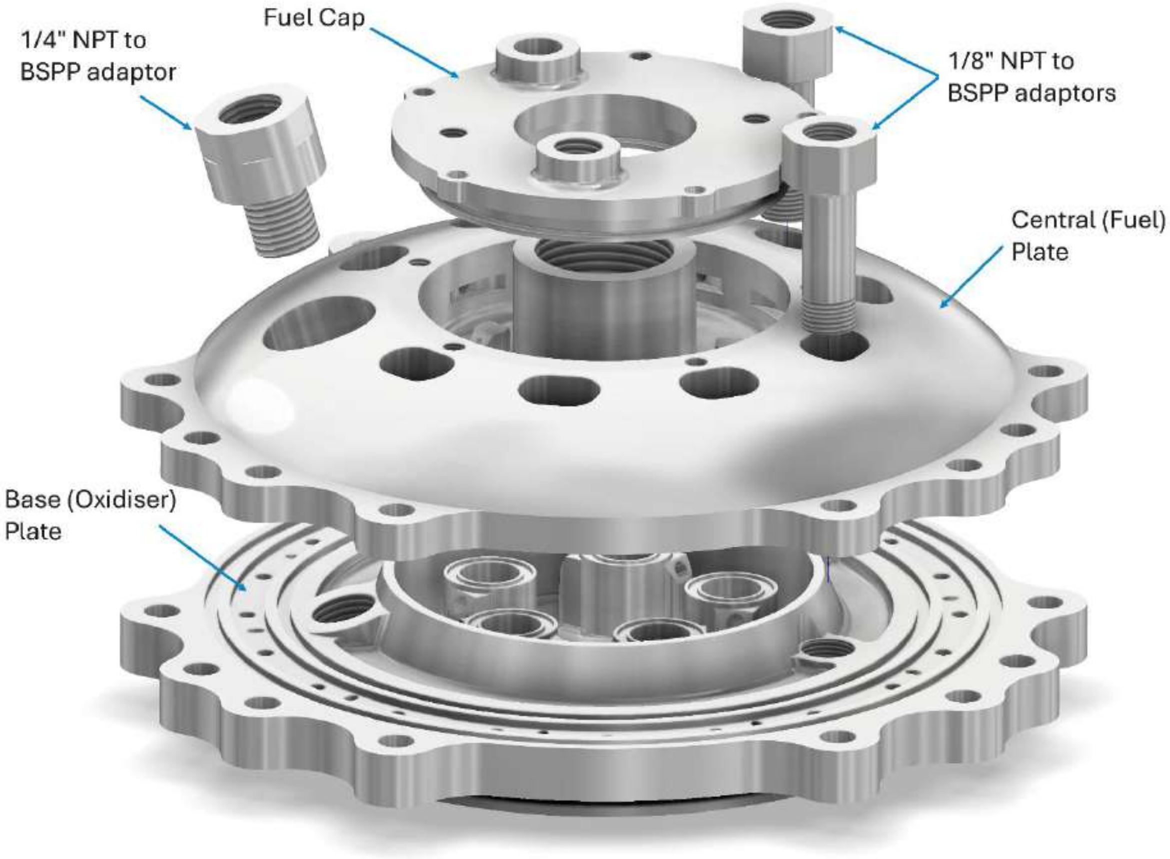

Figure 122 — Coaxial swirl injector components

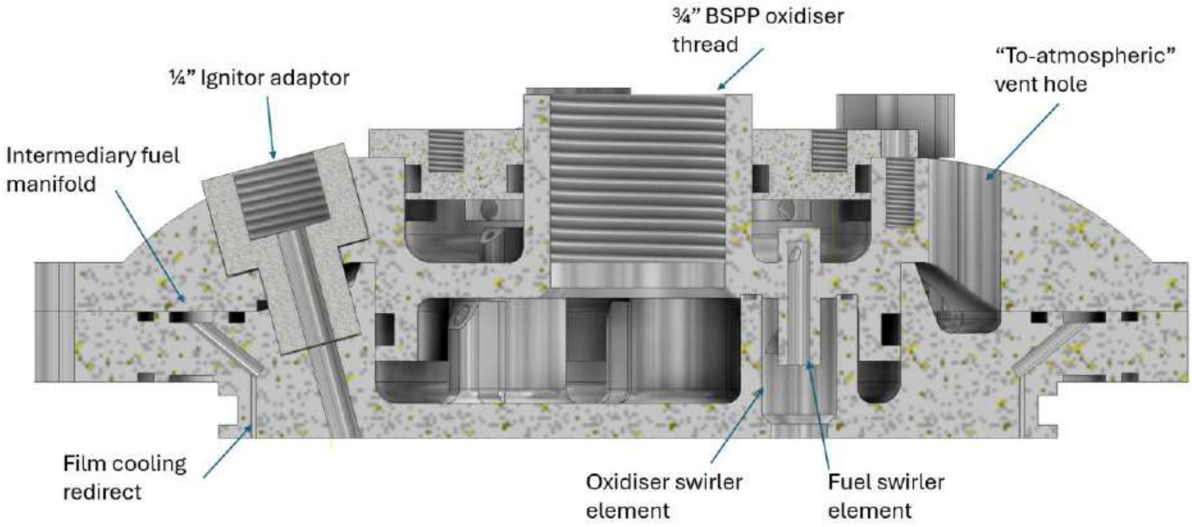

Figure 123 — Coaxial Swirl cross section

Swirler dimensions

Element type: Coaxial swirl elements, with inner and outer oxidiser swirlers, respectively

Table 4: Key properties for coaxial swirl injector design

Property	Value	Unit
Fuel mass flow	0.64	kg/s
Oxidiser mass flow	1.922	kg/s
OF ratio	3	[--]
Fuel nozzle diameter	4.2	mm
Oxidiser nozzle diameter	8	mm
Fuel vortex chamber diameter	3	mm
Oxidiser vortex chamber diameter	10.7	mm
Fuel internal fan angle	60	°
Oxidiser fan angle	90	°
Film cooling orifice mass flow rate	0.06	kg/s

Injector Pressures

Table 5: Key pressures for injector design

Property	Value	Unit
Fuel manifold pressure	30	bar
Oxidiser manifold pressure	30	bar
Fuel pressure drop across injector	10	bar
Oxidiser pressure drop across injector	10	bar

Design of a Compact Flame Torch Igniter

A compact, electrically controlled flame torch has been designed to utilise the existing IPA and N2O propellants to ignite the main engine.

In previous integrated hot fires, ignition has been a key challenge for the team. In contrast, isolated engine testing at the Airborne test site demonstrated reliable ignition using a flame torch igniter. Therefore, the team is trialling an SRAD version that can be used in integrated hot fire and is compact enough to fit within a launch vehicle.

The propellants are mixed through a pair of unlike impinging elements and ignited via a spark plug. The flame torch is inserted into an angle port at the edge of the injector plates.

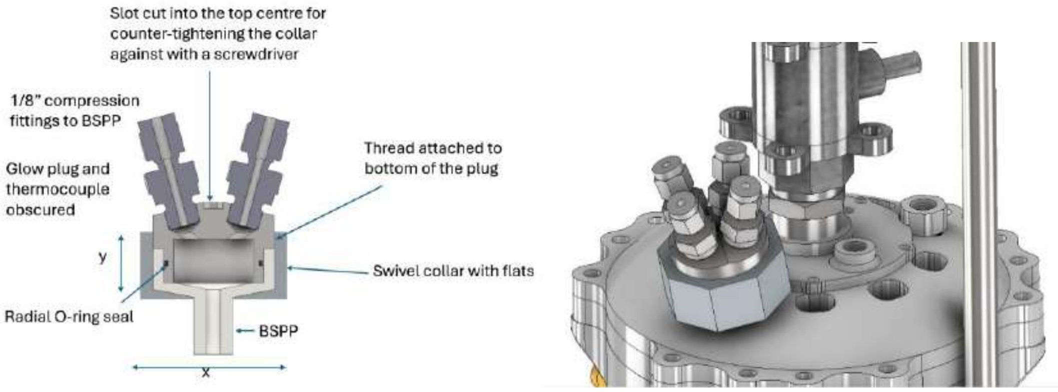

Figure 124 Left: section view of the ignitor. Right: assembly of the ignitor.

The igniter is screwed into the injector plate via a ¼” BSPP thread and seals on a copper gasket, this arrangement is compatible with our two injector plate designs (coaxial swirl and like-like impinging). The top of the igniter contains 4 x 1/8” BSPP fittings for fuel, oxidiser, spark plug and thermocouple. Within a launch vehicle these will be hard lined in and unable to rotate during assembly. To allow the bottom half of the igniter to be screwed into the injector plate and the top half remain fixed, a sealing arrangement using a radial O-ring seal has been used. The top and bottom half of the igniter are retained via a threaded collar, which threads from the bottom onto male threads on the top half. This arrangement allows more space to fit the compression fittings on the top. Tension to tighten the collar against is provided via a machined slot in the top for a screwdriver.

The 3-part assembly will be machined out of stainless steel, due to the harsh operating temperatures, small size and hope to service multiple engines.

Table 6: Ignitor parameters

Property	Value	Units
Oxidiser flow rate	0.062	kg/s
Fuel flow rate	0.062	kg/s
OF ratio	1	
Operating temperature	400	K
Operating pressure	45	bar
Chamber volume	6000	ml

Stress calculations

A series of analytical and computational simulations were performed to validate the stress experienced by each part of the system.

Engine

Material Properties

The combustion chamber is to be 3D printed out of a single heat-treated piece of CP1 Aluminium, an Aluminium-Iron-Zirconium powder alloy for additive manufacture that is faster and easier to print, lighter and has superior thermal conductivity to Inconel 718 (the material of BSEP's previous engine) and higher high temperature performance than other Aluminium alloys such as $AlMgSi_{10}$. [4]

The tabulated material properties are taken from datasheets from the powder manufacturer, Constellium, and the printing company, the MTC.

Table 7: Material properties of CP1 Aluminium

Property	Value	Units
Melting Point	~900	K
Maximum Operating Temp (MOT)	600	K
Ultimate Tensile Strength	342	MPa
Yield Tensile Strength	323	MPa
Yield Strength at MOT	~72	MPa
Ultimate Tensile Strength at MOT	~78	MPa
Thermal Conductivity	187	W/m-k
Thermal Conductivity at MOT	208	W/m-k
Young's Modulus	71	GPa
Poisson Ratio	0.31	[--]
Thermal Expansion Coefficient	25.19e-6	C^{-1}

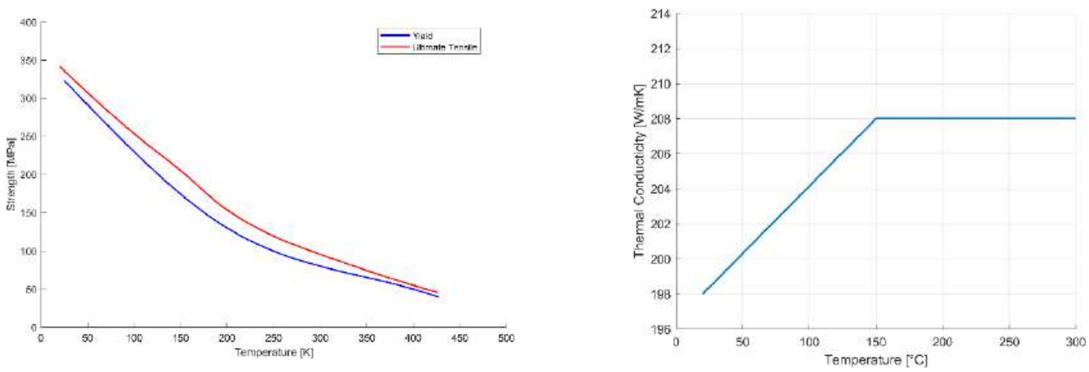

(a) (b)

Figure 125: Material data for the CP1 Al alloy: (a) Yield Strength and UTS data provided by Constellium; (b) Thermal conductivity data collected by the MTC

As seen in the graphs above, the yield strength and ultimate tensile strength of CP1 fall off quite hard with temperature. This is something that must accounted for in any stress calculations and why the peak temperature should be designed to stay below 650K. The thermal conductivity increases with temperature and levels off around 208W/mK2 so this is the value chosen for later simulations.

A series of analytical and computational simulations were performed to validate the stress experienced by each part of the system.

Hoop Stresses

A series of cases were looked at to determine the hoop stresses experienced by the engine. These simulations verify that the chamber and cooling channel walls will not burst under the pressures they will be subjected to.

Thick-Walled Hoop Stress

$$\sigma_\theta = \frac{P_a a^2 - P_b b^2}{b^2 - a^2} + \frac{a^2 b^2 (P_a - P_b)}{(b^2 - a^2) r^2}$$

Lame's equation for thick-walled hoop stress where σ_θ is the hoop stress, P_a is the pressure at the inner surface, P_b is the pressure at the outer surface, a is the inner diameter, b is the outer diameter, and r is the diameter inside the hoop at which the hoop stress is measured. [5]

Multiple cases were evaluated with different combinations of the 20 bar chamber pressure, 30 bar coolant pressure and 1atm exterior pressure at different thicknesses of the material and point of the engine.

Table 8: Results for hoop stress calculations.

Position	Inner – Outer Pressure [bar]	Analytical Value [MPa]	Safety Factor
Chamber – Channel	20 – 30	77.8	4.1
Chamber – Wall	20 – 1 atm	24.4	13.1
Throat – Channel	20 – 30	33.8	9.5
Throat – Wall	20 – 1 atm	10.5	30.5
Chamber – Channel	1 atm – 30	224	1.4
Chamber – Channel	20 – 1 atm	150	2.1

Thin wall hoop stress was also used and found to give similar values.

Thermal Stresses

Multiple types of thermal stress equations were used as seen below to ensure no cracks or "doghouse effect," which will be described later, occur. Many of the equations were taken from Stephen D. Heister's "Rocket Propulsion."

Tangential Thermal Stress

Two equations were used to determine tangential thermal stresses.

$$\sigma_{t1} = \frac{(P_{co} - P_g)D}{2t} + \frac{E\alpha qt}{2(1-v)k}$$

$$\sigma_{t2} = \frac{\left(P_{co} - P_g\right)}{2}\left(\frac{w}{t}\right)^2 + \frac{E\alpha qt}{2(1-v)k}$$

Where σ_t is the tangential stress, P_{co} is the coolant pressure, P_g is the combustion gas pressure, D is the chamber diameter, t is the inner wall thickness, E is the Young's Modulus, α is the thermal expansion coefficient, v is the Poisson's ratio, k is the thermal conductivity, and w is the internal width of the cooling channel. [7] Tangential stresses are created by the internal pressure in the coolant passage and its relationship to the local gas pressure as well as due to thermal growth of the material on the heated side of the passage The first half of both equation takes into account the hoop stresses, the first equation calculating it for the inner wall and the second for the channels. The second half of the equations is the tangential thermal stress induced by heat transfer.

Longitudinal Thermal Stress

$$\sigma_l = E\alpha(T_w - T_{ow})$$

Where σ_l is the longitudinal stress, T_w is the hot wall temperature, and T_{ow} is the cold wall temperature. [7] The longitudinal stresses result from the tendency of the heated side of the passages to grow in length. Due to the superior ductility and thermal conductivity of CP1, the likelihood of failure from these stresses is quite low.

Thermal Buckling Stress

$$\sigma_b = \frac{EE_c\frac{t}{D}}{\left(\sqrt{E} + \sqrt{E_c}\right)^2 \sqrt{3(1-v^2)}}$$

Where σ_b is the buckling stress and E_c is the compression modulus.[7] For Aluminum the compression modulus is equal to the Young's Modulus.

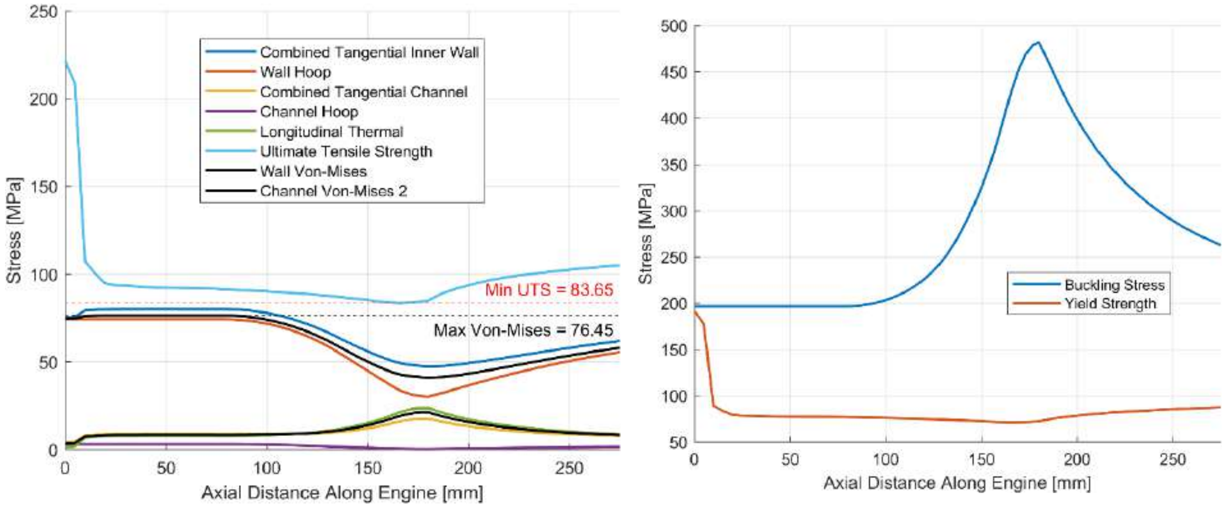

Figure 126, calculated stresses experienced by the chamber under pressure and thermal loads(left) and buckling stress (right)

The above graphs show the stress results at every points along the engine contour. The tangential stresses were split into their hoop and thermal parts as well as combined. The yield strength values were extrapolated from the graph in the previous section to accurately model when they will yield in each location at the operating temperature that location will experience. It can be seen from the left graph that all stresses remain below the local Ultimate Tensile Strength, hence the engine will survive these stresses at steady-state. The right graph shows that buckling stress remains comfortably above the Yield strength throughout the engine, which is ideal since if yield strength is over the buckling stress at any point, that point will buckling.

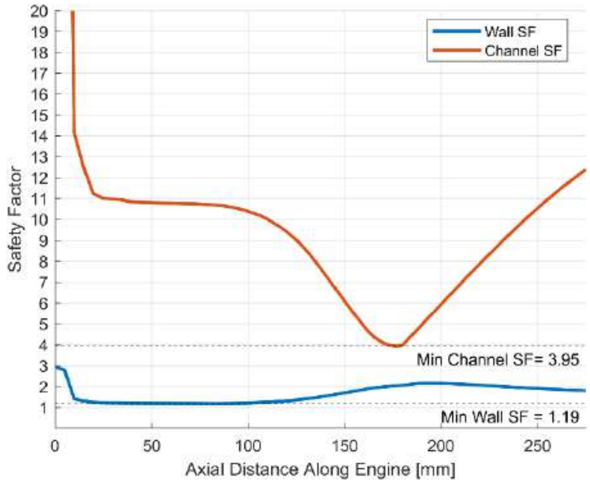

Figure 127, safety factor

Some engine designers opt not to model the wall hoop stresses due to the inner wall being reinforced by the channel ribs, thus only modelling the pressures the channels experience themselves. This approach would therefore reduce the maximum stress from ~80MPa to ~30MPa and would no longer be dominated by hoop stresses at the chamber, instead by longitudinal thermal stresses at the throat.

FEA

A series of FEA models were completed to further model any potential failure points.

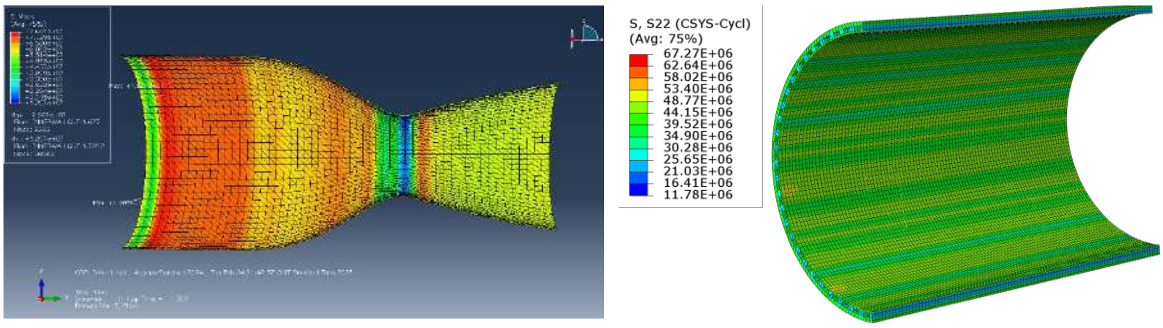

(a) (b)

Figure 128: Abaqus FE simulations of the hoop stresses on the: (a) Engine; (b) Chamber

The simulation above, Fig 128 (a), consisted of a simplified version of the engine geometry, isolating the inner wall. The expected 20bar chamber pressure was applied to the inner surface and a 30bar was applied to the outer surface to act as the inwards acting pressure of the channel coolant. As seen above, the maximum stress of 76.7MPa occurred at the chamber and the stress reduced heavily at the throat. This lines up near perfectly with the results from the previous equations, with 77.8MPa equated from this case from the thick-walled hoop stress equations and 74.3MPa equated from the pressure component of the inner wall tangential stress. This is the first step in validating the models and further analysis will be undertaken.

The second simulation, Fig 128 (b), demonstrates a simplified hoop stress analysis of the chamber and cooling channels. In this scenario, only the expected 20bar chamber pressure was applied to the inner surface. A resulting consistent 40 to 50MPa of hoop stress was present across the chamber, with some peaks of 60MPa along the inner surfaces of the channel walls.

Stress Considerations

Stress considerations

The above simulations offer a worst-case scenario of the performance of the combustion chamber. Considerations should be made for the fact a list of positive factors have not been included in this modelling due to the difficulties involved in integrating these features. These factors which will act to positively affect the stress loads are as follows:

- The Bartz equation has been used which is known to overestimate when compared to other sources such as the Ievlev equation and truth data.
- Material properties of CP-1 Aluminium vary at high temperatures so the assumed Yield Strength and Ultimate Tensile Strength may not be exact although attempts where made to model it.
- Addition of 1% Polydimethylsiloxane (PDMS) to the fuel will act to considerably decrease wall temperatures at hotspots such as the throat as will be discussed in the next section.

Failure Modes

The most likely failure mode of this engine according to the above simulations is the inner wall failing due to hoop stresses at the chamber due to the high temperatures degrading the Aluminium's strength. This has been mitigated by ensuring the temperatures remain as low as possible and, as seen above, the thicker channel walls at the chamber should help reinforce the inner wall and make it less likely to fail.

A second likely failure mode is that of dog-housing in the coolant lines. This is a phenomenon where the stress experienced by the material between the cooling channels and combustion chamber exceeds the yield strength of the material. At this point a breakdown between the coolant and the chamber occurs resulting in a flooding of fuel into the combustion chamber causing a pressure spike. Should this occur, the engine will be shut down and further testing cancelled.

Bolt calculations

A pattern of 12 M6 bolts has been included to secure the injector into the combustion chamber as well as to mount the chamber to the rocket itself. Half of the 12 bolts will be used for mounting the injector plate to the combustion chamber. The expected load on each bolt can be computed with the following equation

$$P_b = \frac{P_c * A_I}{N_b * A_b}$$

Where P_b is the pressure on each bolt, P_c Is the nominal combustion chamber pressure, A_I is the cross-sectional area of the injector exposed to the combustion chamber pressure, N_b is the number of bolts in use and A_b is the area of each bolt. Using the above each bolt will experience 130MPa of stress each. We can now choose the grade of bolt to choose the safety factor on the combustion chamber. Depending on the test we might want the injector bolts to fail first before the combustion chamber. Using low grade 4.6 bolts we can get a SF of 1.8 however using high grade 10.9 bolts we can achieve a SF of 8.3.

L-bracket

Mounting is achieved using an aluminium mounting plate. This will transfer loads from the engine to the test stand. The same setup was used in a previous test with similar loads and it handled it perfectly. The full setup is seen below, see Section 4.3 for further details.

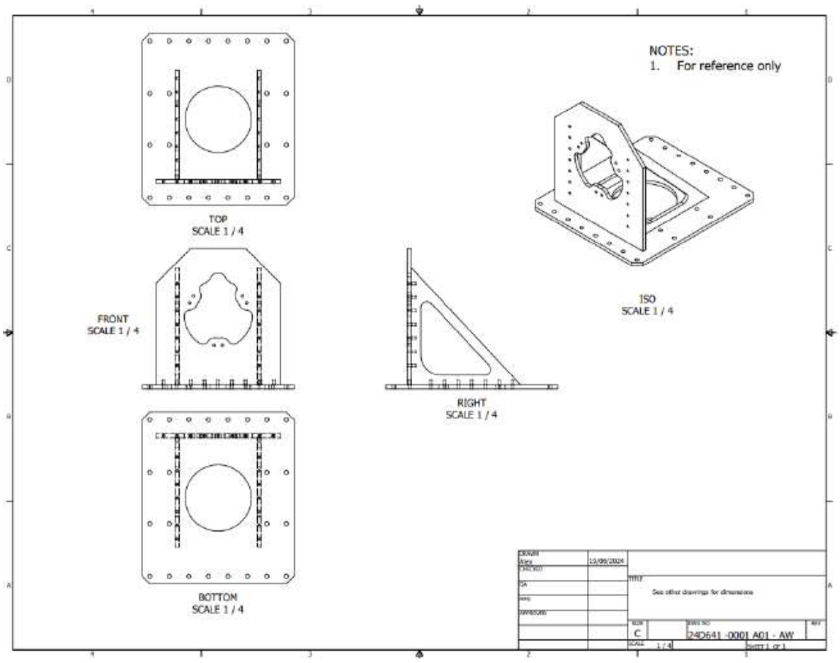

Figure 129: Drawings for fabrication of L-bracket used to support engine during testing.

The engine mount, which interfaces with the test stand, is constructed out of 10mm plate aluminium and has a safety factor of 6 at the weakest point under a nominal 5 kN load. The construction is bolted for ease of assembly and disassembly. The bottom face mounting plate can be drilled to fit the requirements of the test stand in question.

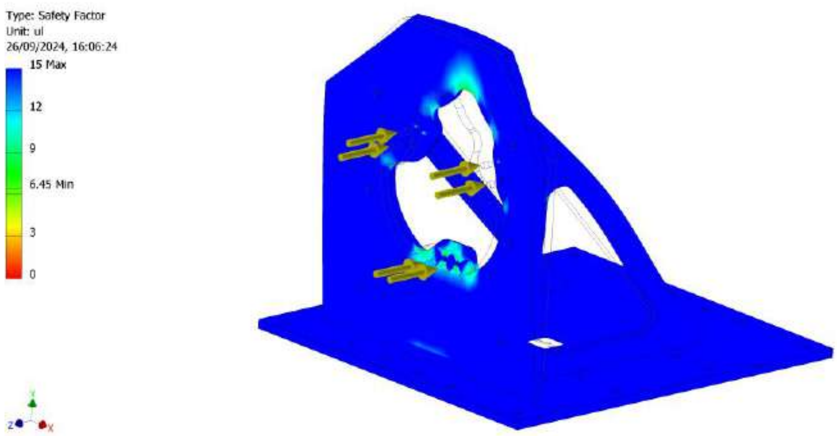

Figure 130: Finite Element Analysis of the L-bracket.

This engine mount is to be fastened to the available thrust plate as specified by the Airborne Engineering Ltd J1 test site via 16xM10 and the BSEP engine via 6xM6 bolts.

This design proved effective in previous hotfireshot-fires of similar thrust.

L-Bracket Bolt Calculations

The peak force from the engine is predicted to be 8KN and given the maximum stress of the L-Bracket is 23.321MPa, we can calculate the maximum shear stress per bolt on the bolts holding the L-Bracket to the thrust plate:

$$\tau_{bolt} = \frac{F_{engine}}{NA_{bolt}}$$

Here, τ_{bolt} is the maximum shear stress on a single bolt, F_{engine}, N is the number of bolts and A_{bolt} is the cross-sectional area of the bolt. Evaluating this equation gives a maximum shear stress of 6.37MPa (3.s.f). If this value is compared to an existing bolt such as the 12.9 grade Socket Cap heads from Trident Racing Supplies, we find they have a shear strength of 517MPa (Trident Racing Supplies, n.d.). Therefore, the bolts should be sufficient to hold the L-bracket in place. Additionally, the stress would be distributed across the L-bracket so it is unlikely that the bolts will experience the maximum stress anyway, which gives an added layer of confidence that the bolts will survive.

Engine Mount Bolts

The following bolt pattern was chosen to hold the engine in the mount:

Figure 131: Bolthole locations within L-bracket

Three sets of two bolts were chosen to hold the engine in the L-bracket at equal intervals. Slots would also be cut to account for the pipes to attach to the mount. The bolts will go through the holes in the engine, injector plate and L-Bracket as shown in the top view CAD below:

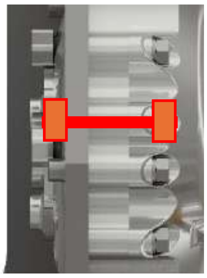

Figure 132: Bolt location highlighted on CAD.

Engine Mount Bolt Calculations

To verify if bolts will be suitable to hold the engine in place before ignition, a calculation was made with the following simplified diagram, where "1/6 Engine" is a sixth of the lumped mass on the end of a single bolt, since there are six bolts to distribute the load.

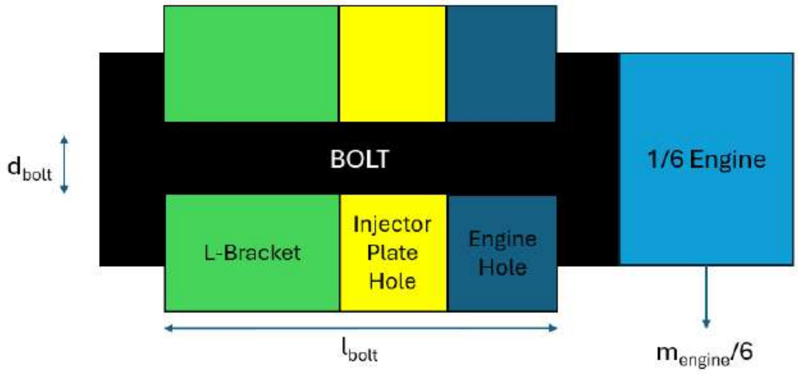

Figure 133: Schematic to describe assemble around bolt.

Then we can use the bearing stress equation to approximate the load on the bolt:

$$\sigma_{bearing,bolt} = \frac{m_{engine}}{6d_{bolt}l_{bolt}}$$

Assuming the engine mass is 6kg, this will give the bearing stress of 3.7KPa (2.s.f). Comparing the to the Trident Racing bolt, which has a tensile strength of 1206MPa (Trident Racing Supplies, n.d.), this design would be sufficient. In reality, there would be distributed load along the bolt with considerably more force at the bottom of the bolt towards the engine and the top of the bolt towards on the other side. However, given that the bearing stress is several orders of magnitude below the yield strength, we can conclude it is not necessary to evaluate this stress distribution.

Thermal Analysis

To define the cooling solution a series of requirements were first imposed. The combustion chamber will be constructed out of the aluminium alloy ‘Aheadd® CP1 20/63’ due to its improved thermal conductivity and reduced density relative to the previous manufactured Inconel 718 engine.

Figure 134 - CAD render of aluminium 2025 engine

Minimum cooling channel dimensions would be 2mm to avoid any issues in post manufacturing powder clearing. Wall temperature should not ever exceed a maximum value of the thermal operating limit of Aheadd® CP1 20/63, ~650K. [4]

Cooling strategies were converged upon though a series of thermal and mechanical stress simulations. Rocket Propulsion Analysis (RPA) was used to implement the Bartz equation for heat transfer coefficient through the chamber and nozzle boundary layer. Hot wall temperatures were then inserted into a thermal hoop stress calculation to derive stress values which fed redesign of thermal solutions until a final solution was converged upon. Additionally, a 15% film cooling solution was added to further reduce the thermals reached by the engine and a 1% addition of the additive PDMS will further minimal gains are seen past 1%. Additionally, a 15% film cooling solution was added to further reduce the thermals reached by the engine and a 1% addition of the additive PDMS will further reduce temperatures at hotspots. This percentage was chosen since, as seen in the graph below, minimal gains are seen past 1%.

Figure 135, Heat flux reduction as a function of PDMS addition [1]

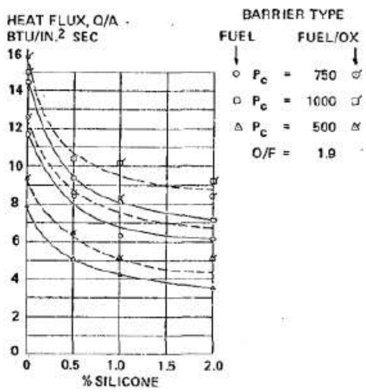

PDMS reduces the total heat flux across the entire engine by creating silicon dioxide upon combustion which is deposited along the engine’s inner walls and acts as an ablative thermal coating. At 1% PDMS, the expected heat flux reductions are within the range of 25-60% with negligible effects on the performance of the engine [2][3]. The PDMS additive has been modelled in the thermal analysis of the combustion chamber as approximately a 20% reduction in total heat flux at the throat. This acts as a conservative thermal estimate and does not accurately represent the potential heat flux reductions elsewhere in the engine.

Table 9: Channel Geometry

Property	Value [mm]
Wall thickness	0.8
Rib thickness (Chamber – Throat - Manifold)	2.9 - 0.9 – 1.1
Channel width (Chamber – Throat - Manifold)	5 – 2 – 3
Channel Height (Chamber – Throat - Manifold)	2 – 2 – 2

Table 10: Results of thermal simulations

Property	**Value**
Maximum chamber-side wall temperature	600 K
Maximum coolant-side wall temperature	590 K
Maximum coolant temperature	367 K
Minimum velocity of coolant	3.73 m/s
Maximum heat flux	3455 kW/m^2
Increase in coolant temperature	69K

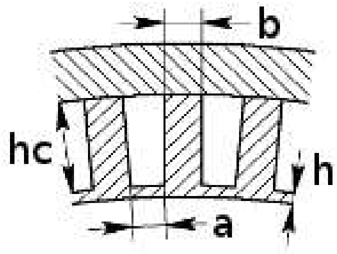

Figure 1235: Channel Geometry (Figure taken from RPA)

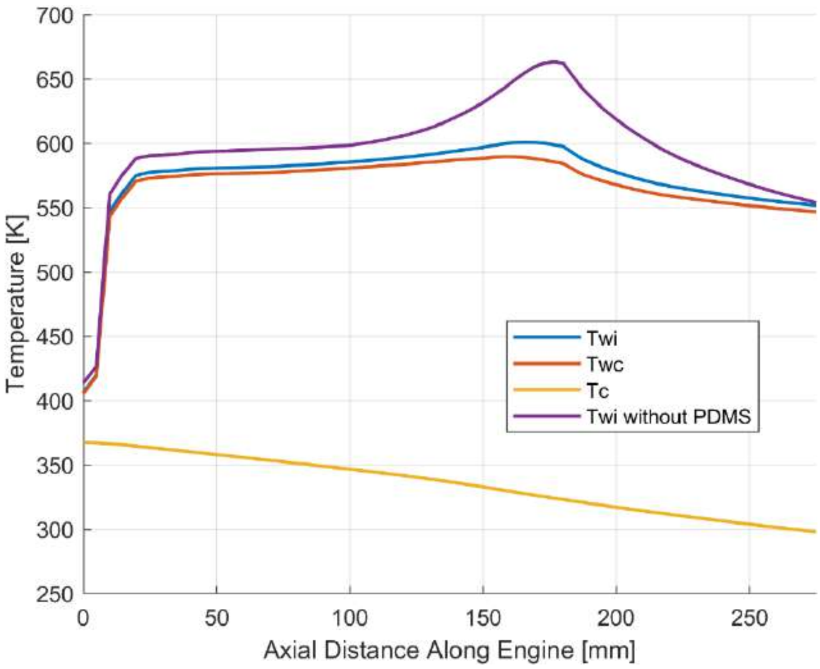

Figure 136, Results from thermal simulations

The graph and table above display the results of the thermal simulations. Twi is the inner wall temperature chamber and Twc is the inner wall temperature of the cooling channels. Tc is the temperature of the coolant and Twi without PDMS is the results of the simulations without factoring in the 20% heat flux reduction at the throat from the PDMS. Even without factoring in the PDMS, the temperatures are just above the 650K limit.

Test plan

The test outlines below are preliminary and subject to change following input from test facility. Integration with the test facility at Airborne Engineering Ltd is facilitated by the ICD provided by the Race to Space competition.

Test 1: Full duration Burn 1

A full burn to provide a complete test to collect thrust and chamber pressure.

Table 11: Test parameters for full duration burn hotfire

c	Test Value	Unit
Oxidiser injector feed pressure	30	bar
Fuel injector feed pressure	30	bar
IPA mass flow	0.64	kg/s
N2O mass flow	1.93	kg/s
OF ratio	3	[--]
Chamber pressure	20	bar
Thrust	5	kN
Run time	5	s
IPA consumed	3.2	kg
N2O consumed	9.65	kg

Potential issues

Leak: A leak may be observed by footage of test. In the event of a leak, examine and reassemble. Discuss with AEL suitable next steps.

Ignition: Failure to ignite observed by no burn. Consult with AEL of suitable next steps

Unexpected readout: Discuss with AEL potential causes and how they might be addressed. Repeat test or terminate testing if necessary.

Channel burn through: Thermal management no longer possible. Terminate testing.

Reattempts

Failure to ignite: Discuss with AEL for advice.

Unexpected readout: Check connections

Insights

Nominal thrust.

Nominal chamber pressure.

Thermal management solution outcome.

Test 2: Full duration Burn 2

A second burn to optimize from Test 1 and achieve the nominal values by increasing/decreasing mass flows and pressures as needed.

Table 12: Test parameters for full duration burn hotfire

Property	Test Value	Unit
Oxidiser injector feed pressure	30 (subject to change)	bar
Fuel injector feed pressure	30 (subject to change)	bar
IPA mass flow	0.64 (subject to change)	kg/s
N2O mass flow	1.93 (subject to change)	kg/s
OF ratio	3	[--]
Chamber pressure	20 (subject to change)	bar
Thrust	5	kN
Run time	5	s
IPA consumed	3.2 (subject to change)	kg
N2O consumed	9.65 (subject to change)	kg

Potential issues

Leak: A leak may be observed by footage of test. In the event of a leak, examine and reassemble. Discuss with AEL suitable next steps.

Ignition: Failure to ignite observed by no burn. Consult with AEL of suitable next steps

Unexpected readout: Discuss with AEL potential causes and how they might be addressed. Repeat test or terminate testing if necessary.

Channel burn through: Thermal management no longer possible. Terminate testing.

Reattempts

Failure to ignite: Discuss with AEL for advice.

Unexpected readout: Check connections

Insights

Nominal thrust.

Nominal chamber pressure.

Thermal management solution outcome.

Test 3: Re-Light

A short duration burn followed immediately by a second short duration burn

Table 13: Test parameters for Test 3

Property	Test Value	Unit
Oxidiser injector feed pressure	30	bar
Fuel injector feed pressure	30	bar
IPA mass flow	0.64	kg/s
N2O mass flow	1.93	kg/s
OF ratio	3	[--]
Chamber pressure	20	bar
Thrust	5	kN
Run time	1.5, 1.5	s
IPA consumed	1.92	kg
N2O consumed	5.79	kg

Potential issues

Leak: A leak may be observed by footage of test. In the event of a leak, examine and reassemble. Discuss with AEL suitable next steps.

Ignition: Failure to ignite observed by no burn. Consult with AEL of suitable next steps

Unexpected readout: Discuss with AEL potential causes and how they might be addressed. Repeat test or terminate testing if necessary.

Channel burn through: Thermal management no longer possible. Terminate testing.

Reattempts

Failure to ignite: Discuss with AEL for advice.

Unexpected readout: Check connections

Insights

Nominal thrust.

Nominal chamber pressure.

Thermal management solution outcome.

Test 4: Depth of Throttle

A long burn starting at half throttle and gradually throttling down in order to determine the depth of throttle of the injector

Table 14: Test parameters for Test 4

Property	Test Value	Unit
Oxidiser injector feed pressure	30	bar
Fuel injector feed pressure	30	bar
IPA mass flow	0.32 -	kg/s
N2O mass flow	0.965 -	kg/s
OF ratio	3	[--]
Chamber pressure	20	bar
Thrust	2.5 - 0	kN
Run time	-	s
IPA consumed	-	kg
N2O consumed	-	kg

Potential issues

Leak: A leak may be observed by footage of test. In the event of a leak, examine and reassemble. Discuss with AEL suitable next steps.

Ignition: Failure to ignite observed by no burn. Consult with AEL of suitable next steps

Unexpected readout: Discuss with AEL potential causes and how they might be addressed. Repeat test or terminate testing if necessary.

Channel burn through: Thermal management no longer possible. Terminate testing.

Reattempts

Failure to ignite: Discuss with AEL for advice.

Unexpected readout: Check connections

Insights

Nominal thrust.

Nominal chamber pressure.

Thermal management solution outcome.

References

[1] Bazarov, V., Yang, V. and Puri, P. (2004). Design and Dynamics of Jet and Swirl Injectors. American Institute of Aeronautics and Astronautics.

[2] Hyde, S. and Okninski, A. (2016). Silicon Oil Thermal Barrier System for in Space Applications. Space Propulsion 2016.

[3] Additives for heat flux reduction | Joint Propulsion Conferences. (2025). Joint Propulsion Conferences.

[4] Shahani, R. and Bechir, S. (2021). Constellium Aheadd ®: Aluminium Alloys Designed for Laser Powder Bed AM to Improve Properties and Processing Performance Formnext 2021. [online] Available at: https://assets.foleon.com/eu-central-1/de-uploads-7e3kk3/41170/2021-11-8_constellium_aheadd_formnext_final.a0a8c4307e76.pdf [Accessed 30 Dec. 2024].

[5] Huzal and Hueng (1967). NASA SP-125: DESIGN OF LIQUID PROPELLANT ROCKET ENGINES. NASA.

[6] Constellium (n.d.). Aheadd ® CP1: ALUMINIUM POWDERS FOR ADDITIVE MANUFACTURING. [online]

[7] Heister, S.D. (2019). Rocket Propulsion.

[8] Richard Nakka, Experimental Rocketry Website [online]

[9] OpenRocket [application]: https://openrocket.info/

H.7 2024 Tank Technical Report

A coaxial propellant tank approach with concentric fuel and oxidiser tanks was seen to offer the greatest efficiency as fore and aft plumbing of the coaxial can be made in parallel which was projected to save 300mm of length and 2.7kg of structural mass compared to separate SRAD fuel and oxidiser tanks, Figure 16.

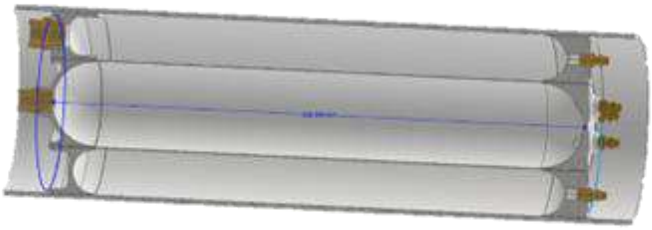

Figure 16: Initial Coaxial design

The coaxial strategy also offers major packaging improvements if it uses the full diameter available, with the outer tank wall supporting the vehicles structural loads in addition to its internal pressure. Wiring across the full diameter tank was decided to be achieved with an external “raceway”, a common strategy in commercial launch vehicles. Radial bolts were deemed the easiest to manufacture approach to secure the end caps to the tank wall.

1. Sizing Calculations

The Half Cat Rocketry Pressure Vessel Design Manual [4] was initially used to guide the analysis, with a MATLAB script implemented to predict the recommended set of basic stresses. The script was further developed to output the optimum tank length/ inner tank diameter for a given oxidiser to fuel ratio. After discussion with stock material suppliers' aluminium 6082 T6 was chosen, and the tank was sized as follows:

Stress Type	MEOP s.f. (5.5MPa)	1.5x Proof test s.f.	2x MEOP DTEG criteria
Outer wall hoop	5.0	3.3	2.5
Inner wall hoop	3.3	2.2	1.7
Wall tensile	8.5	5.7	4.3
Bolt shear	4.7	3.1	2.4
Bolt tear out	3.7	2.4	1.8
Bolt bearing	4.5	2.8	2.2
Detail		**Value**	
Outer wall thickness		7.95mm	
Inner wall thickness		3mm	
Bolt pattern		30x M8 per end	

Table 5: Tank sizing results

Safety factors were calculated with the 0.2% proof yield strength of the material. This value was experimentally determined as 328MPa through BS EN ISO 6892-1:2019 [5] tensile testing by NDT Services Ltd (/f 10.9). This represents a very high performing batch of 6082T6 used in the tank construction, with an excellent failure elongation of 13.5%. Button head socket screw bolts were supplied by Unbrako LLC and are property class 12.9 and rated to a shear stress of 660MPa. The safety factors represent high confidence of the integrity of the tank under handling and testing, and meet the DTEG 4.2.4 requirement [6] with a designed burst pressure above 2x MEOP.

2. Finite Element Correlation

Finite element static stress simulations were conducted in Autodesk Inventor Nastran 2024.

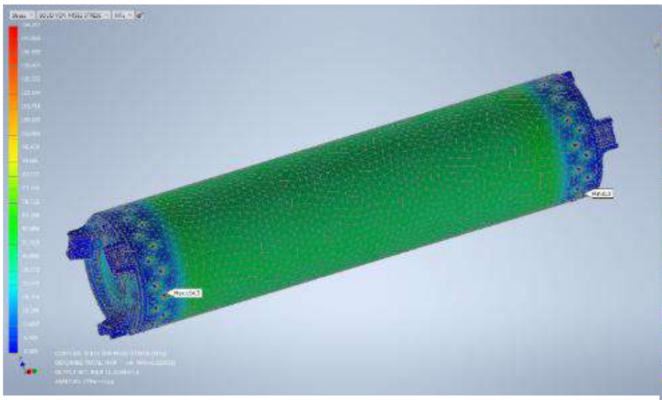

Figure 17: Stress distribution under MEOP

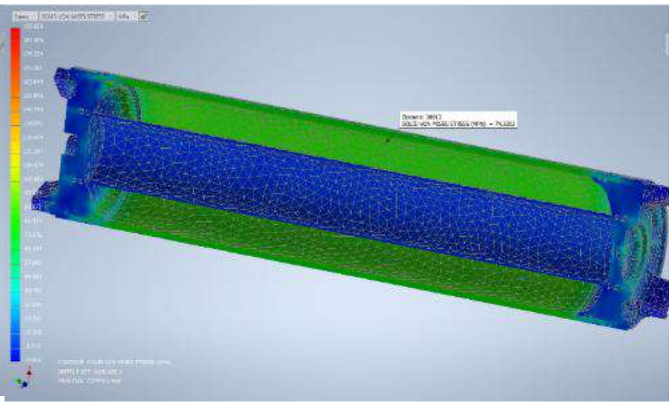

Figure 18: Stress distribution for proof test

For 5.5MPa internal pressure in both tanks, Nastran gives a wall stress of 58MPa, in line with the MATLAB hoop stress result of 66Mpa, *Figure 17*. Similarly, for 7.5MPa internal pressure Nastran predicts 74MPa, while hoop stress gives 91MPa, *Figure 18*. This lower stress prediction from FE results is believed to be caused by a thicker wall section in the model, which accounts for the true shape of the tank wall. While the MATLAB calculations use only the minimum thickness which occurs at the machined mating surface. It is therefore likely that the true safety factors are greater than stated in *Table 5*.
A notable result is that the inner wall is unstressed when an equal pressure is applied to the internal and external tanks, as the inner wall is allowed to “float” longitudinally in order to prevent build up of tensile stresses. During the filling procedure the internal tank will be pressurised first, creating a pressure differential of up to 55bar with respect to the outer tank, this situation was also analysed, Figure 19.

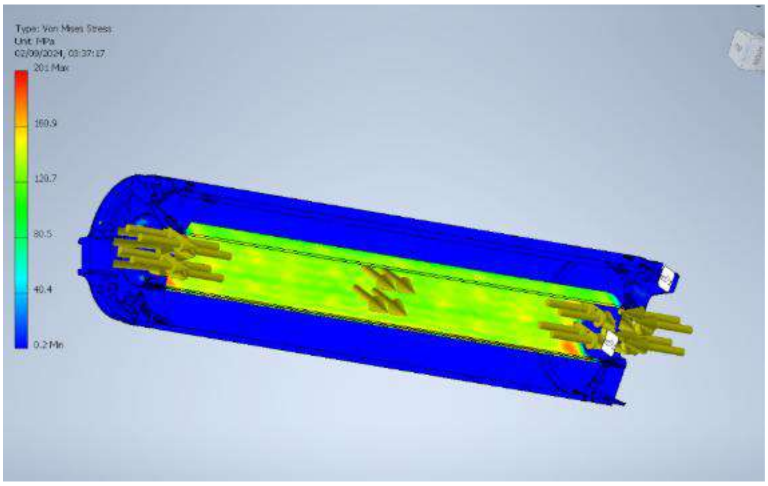

Figure 19: Internal wall stress distribution for proof test

Autodesk Inventor FE Static analysis was used to correlated against MATLAB hoop stress results. Good agreement is again observed, FE predicting 120MPa compared to 140MPa with hoop stress for the 1.5x MEOP proof pressure case. This agreement follows the same hand calculation overprediction due to the geometric difference from the machined sealing face.
Special attention was given to the bolt hole design in this analysis as initial FE results predicted extreme stress concentrations on the bolt bearing faces of greater than 2000MPa, *Figure 20*.

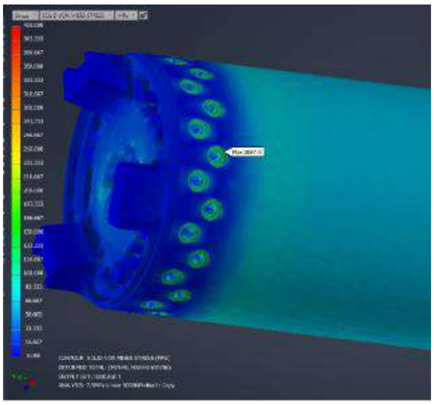

Figure 20: Non-physical bolt hole FE prediction

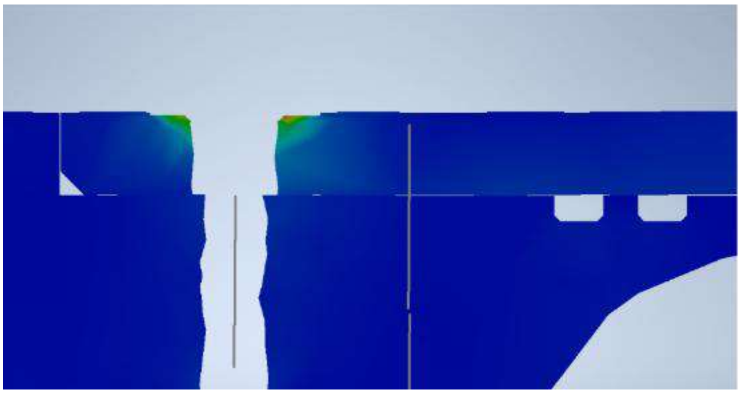

Figure 21: Bolt face stress distibution

This result was intuitively nonphysical and believed to be due to the mesh implementation, *Figure 21*. Following discussion FE researchers and academic advisors, mesh refinements were implemented and a nonlinear solver applied, which more accurately characterised these concentrations as well within design limits. Although the compression from inertial loading acts to reduce tensile stress in the tank wall, analysis must be undertaken to understand the effect of bending, this is discussed in section 4.1.3.2 Coaxial tank

3. Detail design

Resistance against failure was the driving design objective of the tank, with design constraints as mass and volume, Figure 22. This approach is not just reflected in the high gross stress safety factors but also in the detailed implementation. The tank features back up O-rings at each sealing location, requiring 4 seal failures for fuel/oxidiser mixing. These seals were appropriately sized using the Parker O-Ring calculator with the results found Appendix 10.10 These O-rings are nitrile rubber type for chemical compatibility with both propellants [7]. A high elongation alloy was also chosen for the inner wall to improve its toughness in the event of an anomaly. Furthermore, an ellipsoid end cap profile was utilised to provide a balanced stress distribution through the end caps and create space for 2 radial bolt patterns which reduce stress concentrations.

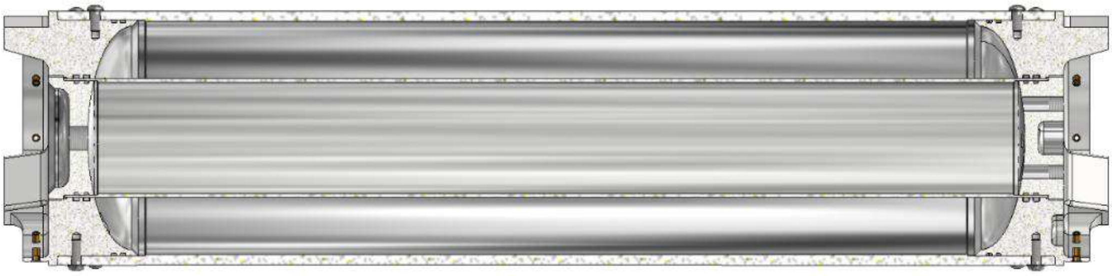

Figure 22: Flight coaxial design

The radial bolts feature a counterbore to facilitate proper contact between the bolt and the curved outer surface of the aluminium, this counterbore is of minimum depth and broken with a radius to minimise stress concentrations. The bolt through hole also features a countersink as described in the Unbrako Engineering Guide to fit the non-standard head radius of Unbrako bolts [8], *Figure 25*,. The design affords great flexibility in port configurations, with 10 ports total across the tanks, *Figure 23*, *Figure 24*. This greatly improves ease of the plumbing configuration by eliminating the need for features like tee junctions to attach a tank pressure transducer as seen on single port COTS COPVs. This parallelisation of lines saves 300mm from the vehicle length. Additional space on the tank faces is utilised with electronic mounting points and weight saving cutouts. The central aft port has also been set into the centre of the tank to save a further 16mm of vehicle length.

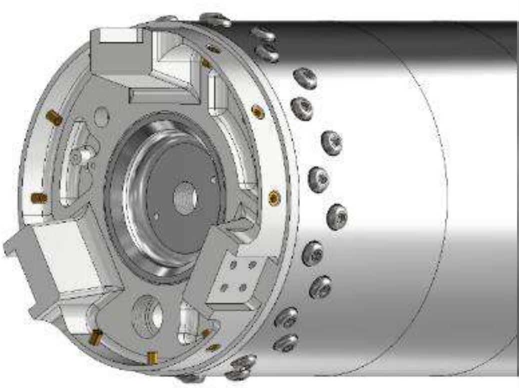

Figure 23: Aft end caps

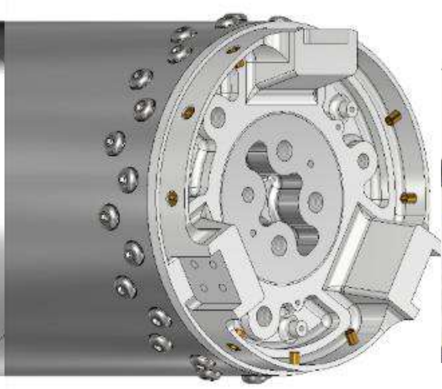

Figure 24: Fore end caps

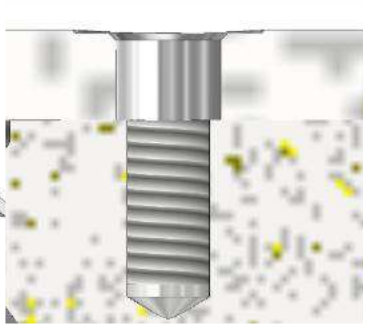

Figure 25: Radial bolt details

The design choices have created a heavy tank, with a total mass of 18kg. Future designs will look to reduce this, especially by making use of composite materials and integrating the end caps without the use of bolts.

4. Manufacture and Assembly

Parts were machined by the University of Bristol Engineering Mechanical Workshop with a Colchester Lathe and Hass CNC centre, *Figure 26*.

Figure 26: End cap machining

Figure 27: Dividing head for radial features

A dividing head was employed to add radial features such as the end cap bolt holes, *Figure 27*. Critical tolerances such as the O-ring grooves and the shaft fits for the end caps were post inspected and cross referenced to ensure proper sealing.

Tank parts were first degreased using Swarfega Jizer and water to remove large debris and cutting oils. The next degreasing step used sodium lauryl sulphate anionic surfactants and water. Final contamination was removed through isopropanol wash. Next, O-ring seals and sealing surfaces were coated with the oxygen safe [9] and nitrile rubber compatible lubricant Brit-Lube Crystal Lube [9]. Tank parts were finally integrated together, with the radial bolts torqued to 18.5Nm according to NASA/TM—2017-219475 specification for assembly torques [10].

5. Testing

The tank was transported to Roxel UK to undergo leak and hydrostatic testing as discussed in Appendix 10.2.6 and is summarised here:

Test type	Chambers	Pressure (bar)	Time (mins)	Result
Leak	Inner	4	5	Pass
Leak	Outer	4	5	Pass
Hydrostatic	Inner & Outer	82.5	30	Pass
Hydrostatic	Inner	82.5	30	Pass

Table 6: Coaxial tank testing steps

Hydrostatic testing was conducted in a shielded hydrostatic test chamber for safety. Due to overshoot in the pressure test control loop, the tanks saw a transient of >85bar. The pressure was increased up to the 82.5bar control set points in 10bar increments with a pause at each to observe for leakage, *Figure 29*. When the test pressure of 82.5bar was achieved, the 30-minute timer was started.

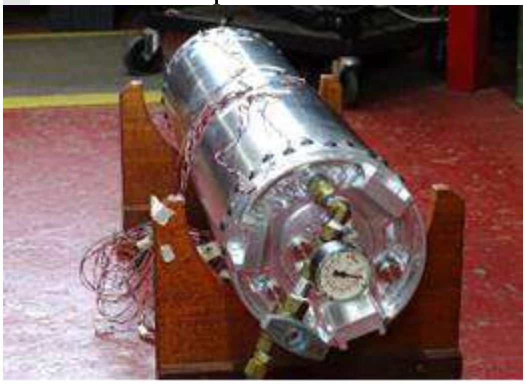

Figure 28: Leak testing

Figure 29: Post hydrostatic test inspection

The tank was instrumented with strain gauges for this testing, points of interest included the hoop and radial strain in the bulk of the outer wall, and strain between the holes in the bolt pattern to identify a possible failure situation, Figure 28. Some difficulty was experienced with gauge debonding and ADC glitches, the data can be found in Appendix 10.8.

H.8 Fluid system modelling

A 1D, lumped parameter model of the whole refuelling and feed system was created in Simulink using the Simscape Fluids library and CoolProp (Bell, Ian H. , Wronski, Jorrit , & Quoilin, Sylv, 2014) as the source of fluidic information. This model predicts that the total refuelling time to be around 10-15 minutes based on the ground station design. Furthermore, it predicts that the N2O will be at a temperature of 260K at the end of N2O tank fill. This is backed up by this paper of a rocket sled test (Yasuda, K, et al., 2018). After refuelling, the N2O will slowly heat back up to ambient temperature.

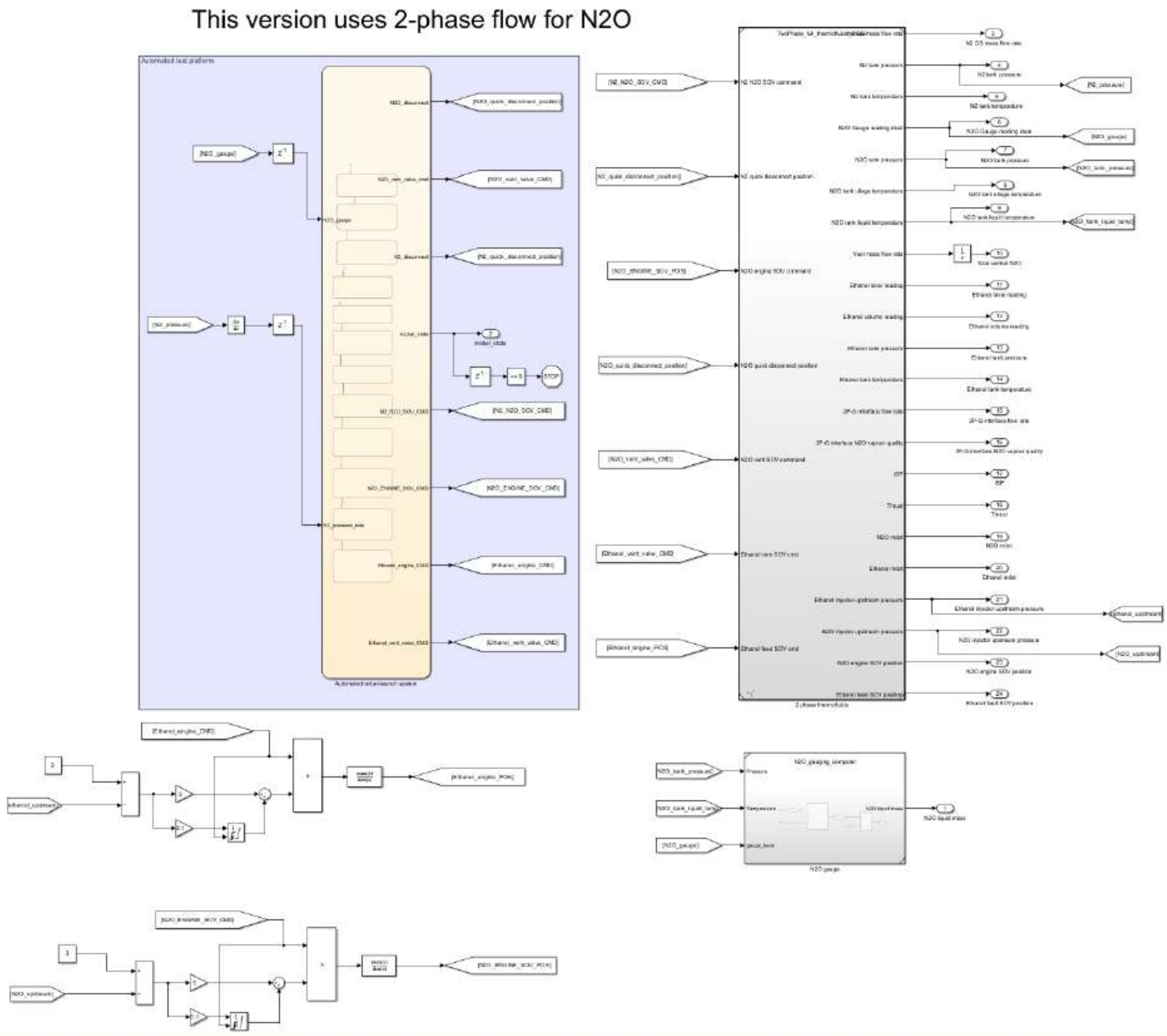

Figure 137. A screenshot of the model

According to the model, the remote refueling process takes about 10 minutes to complete.

The model also predicts that the tank can sit on the pad fully fuelled for more than 10 minutes without triggering the overpressure protection. Detailed calculations are in the Appendix.

Another form of modelling that was investigated was a first-principles MATLAB script that simulates the drain of a nitrous oxide (N_2O) tank pressurised with nitrogen (N_2) as it feeds through an injector through intermediary piping and valves. The geometry and loss coefficients of the tanks, piping, valves, and injector are defined as constants whilst initial N_2O and N_2 properties are obtained from CoolProp (a thermophysical property library for a variety of propellant fluids) at a stated initial temperature. The ullage volume of each part of the mixture is then calculated, which then allows us to closely estimate the N_2 partial pressure within the N_2O tank to meet the stated initial tank pressures. Then, a differential-algebraic equation based on 3 states (N_2O mass, N_2 mass, and total internal energy) can be formulated using all the constants and variables so far, solved using ode23s, resulting in temperature, vapour quality, and partial pressure outputs. Finally, mass flow (and the resulting N_2O mass and energy decreases) is obtained by using Bernoulli 's orifice equation that accounts for flashing pressure, assuming for quasi-steady flow and injector, valve, and pipe losses applied are as effective areas. This process generates the tank pressure, masses of the phases of each component of the mixture, N_2O vapour quality, and injector pressure losses over time, which can be displayed in graphical form.

A 1D, lumped parameter model of the whole refuelling and feed system was created in Simulink using the Simscape Fluids library and CoolProp (Bell, Ian H. , Wronski, Jorrit , & Quoilin, Sylv, 2014) as the source of fluidic information. This model predicts that the total refuelling time to be around 10-15 minutes based on the ground station design. Furthermore, it predicts that the N2O will be at a temperature of 260K at the end of N2O tank fill. This is backed up by this paper of a rocket sled test (Yasuda, K, et al., 2018). After refuelling, the N2O will slowly heat back up to ambient temperature.

The model also predicts that the tank can sit on the pad fully fuelled for more than 10 minutes without triggering the overpressure protection. Detailed calculations are in the Appendix.

Another form of modelling that was investigated was a first-principles MATLAB script that simulates the drain of a nitrous oxide (N_2O) tank pressurised with nitrogen (N_2) as it feeds through an injector through intermediary piping and valves. The geometry and loss coefficients of the tanks, piping, valves, and injector are defined as constants whilst initial N_2O and N_2 properties are obtained from CoolProp (a thermophysical property library for a variety of propellant fluids) at a stated initial temperature. The ullage volume of each part of the mixture is then calculated, which then allows us to closely estimate the N_2 partial pressure within the N_2O tank to meet the stated initial tank pressures. Then, a differential-algebraic equation based on 3 states (N_2O mass, N_2 mass, and total internal energy) can be formulated using all the constants and variables so far, solved using ode23s, resulting in temperature, vapour quality, and partial pressure outputs. Finally, mass flow (and the resulting N_2O mass and energy decreases) is obtained by using Bernoulli 's orifice equation that accounts for flashing pressure, assuming for quasi-steady flow and injector, valve, and pipe losses applied are as effective areas. This process generates the tank pressure, masses of the phases of each component of the mixture, N_2O vapour quality, and injector pressure losses over time, which can be displayed in graphical form.

According to the model, the remote refuelling process (N2 and N2O filling) takes about 10 minutes to complete.

I. Launch Vehicle Supporting Data

I.1 Wind Tunnel Motivation and Design

This appendix will expand on the aerodynamic and experimental side of the Wind Tunnel test. The validation chain mentioned in the report was designed to build reliability in computational and experimental predictions. The process begins by assuming both the CFD and WT test as incomplete and potentially biased, then improving them through several stages of iterative correlation. Launch vehicle (LV) CFD simulations are created under idealised conditions, which establish preliminary aerodynamic characteristics such as pressure distribution and drag. These simulations, however, are inherently wrong initially due to incorrect meshing and simulation setup as there is no data to validate against, plus they neglect manufacturing imperfections, surface roughness, and tunnel interference effects. Wind tunnel (WT) testing therefore provides an essential experimental dataset against which CFD can be benchmarked.

To ensure proper comparability, WT-specific CFD simulations are conducted. This mirrors the geometry (tunnel sting and walls) and boundary conditions of the tunnel experiment, enabling the introduction of compressibility corrections for Cl and Cd. Finally, launch data collected via accelerometers and strain gauges during flight provides a realistic reference point for the original CFD.

Both CFD and WT results are initially regarded as imperfect. Agreement in global aerodynamic behaviour, such as pressure distribution trends of similar order of magnitude, is a positive indicator but not definitive proof of accuracy. Discrepancies are carefully analysed to identify their origins, where CFD uncertainties may arise from grid resolution, turbulence modelling, or solver schemes while WT uncertainties may stem from surface imperfections in the model, support interference, or wall effects. These can often be mitigated by model refinements, applying wall corrections, or conducting delta-testing between configurations. Notably, CFD could be incorrect even if properly correlated in case the simulation was done incorrectly from the start, making it more prone to error.Notably, CFD can inherently be wrong even if the correlation is correct in case the

By applying correlation factors to key coefficients (e.g. drag and lift), WT data can be used to systematically adjust CFD predictions. The WT-specific CFD plays a pivotal role here by reproducing the exact tunnel geometry at 40 m/s, providing a yardstick to calibrate compressibility corrections, refine the mesh and ensure solver is setup correctly before extrapolation to LV Mach regimes.

The primary feasibility challenge lies in the mismatch of operating conditions. The WT test is constrained to a maximum velocity of 40 m/s (0.12 Mach) while LV simulations extend to 0.8 Mach. Subsonic and transonic CFD at tunnel conditions therefore acts as a bridging step through agreement at low Mach validates the physical modelling, while compressibility runs (e.g. Mach sweeps at 0.3, 0.5, 0.8) reveal whether corrections are consistent with experimental evidence.

This approach is justified by boundary-layer scaling arguments. The Reynolds number for the WT test can be calculated as:

$$Re = \frac{\rho U L}{\mu} = \frac{1.225 \times 40 \times 0.5}{1.8 \times 10^{-5}} \approx 1.36 \times 10^{6}$$

This value is within the turbulent regime according to the Strouhal–Reynolds relationship (Figure 36). Since the boundary layer is turbulent, testing at lower speeds is unnecessary as the flow physics are already representative of full-scale conditions. The critical requirement is to allow the tunnel flow to stabilise at the target velocity before taking measurements, ensuring reliable parametric data.

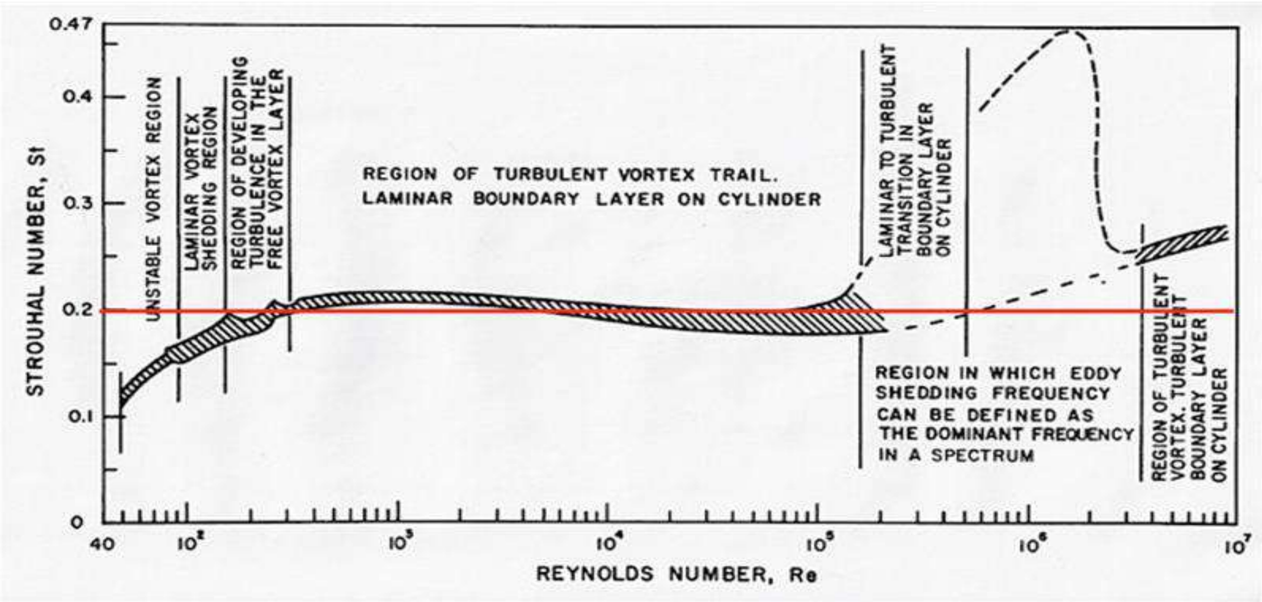

Figure 138 – Boundary Layer behaviour regime

Once the WT to CFD correlation has been established and compressibility corrections applied, the improved CFD model is validated further against launch flight data. Accelerometers and strain gauges provide time-resolved aerodynamic loading, which can be processed into effective Cd and Cl values. Discrepancies at this stage are critical, as they may reveal unmodelled effects such as aeroelastic deflections or transient separation phenomena.

The iterative strategy is therefore:

1. CFD defines aerodynamic baseline under idealised conditions.
2. WT validates gross behaviour and identifies discrepancies.
3. WT-specific CFD applies compressibility corrections and calibrates coefficients.
4. Corrected CFD extrapolates to Mach 0.8 and beyond.
5. Launch data provides final validation, closing the loop.

The ultimate goal is to establish a CFD framework that is reliable across subsonic and transonic conditions, reducing reliance on repeated experimental campaigns. With a well-validated CFD toolchain, interpolation across operating envelopes and rapid scenario testing become feasible without the cost of additional tunnel models or launches.

The next section will focus on the WT test plan. The first two days of Week 1 will be dedicated to model setup and validation within the tunnel. The model will be assembled, inspected, and sealed to eliminate gaps or surface imperfections that could affect data quality. All instrumentation, including the Chell MicroDAQ-3 16-channel pressure scanner, will be calibrated and verified for operational readiness. Surface flow features will be visualised using tufts, allowing qualitative assessment of separation and reattachment behaviour.

Initial runs will be carried out in the baseline configuration to provide a reference dataset and to characterise the influence of the tunnel strut. Each run will include both wind-off and wind-on measurements to correctly tare the force balance. During the first week, priority will also be given to tuning airbrake PID control gains in collaboration with the control and electronics group. The second week will focus on systematic aerodynamic testing, assessing the effect of airbrake deployment, fin-airbrake interactions, and yaw offsets.

Table 36 - Wind Tunnel testing procedure

Test Configuration	Fins	Air brakes	Tufts	Yaw	Extra features
1	off	stowed	no	no	-
2	off	stowed	yes	no	-
3	on	stowed	no	no	-
4	on	stowed	yes	no	-
5	on	stowed	yes	1 degrees	-
6	on	stowed	yes	2 degrees	-
7	on	stowed	yes	3 degrees	-
8	on	stowed	yes	4 degrees	-
9	on	deployed	yes	no	Vary airbrake deployment extent
9	on	deployed	yes	no	Fins aligned with airbrakes
10	on	deployed	yes	no	Fin/airbrake alignment setting 1
11	on	deployed	yes	no	Fin/airbrake alignment setting 2

Test No.	3	**Asset**	Feed Systems
Risk Assessment No.	n/a	**Sub Team**	Propulsion
ITP No.	2	**Date**	28/08/2025

Item 3: 1.5x MEOP Testing of Coaxial Tank			Initial	Time	Pass
3.1	Ensure that systems are as expected.	No damage to SRAD system in transport. No dismantling of system. Confirmation from Astron that system is nominal.	GL	10:49	Yes

<table>
<tr><td>3.2</td><td>Integrate systems.</td><td>Ensure that fittings are flush, no threads have been crossed.</td><td>GL</td><td>10:49</td><td>Yes</td></tr>
<tr><td>3.4</td><td>Depressurise system.</td><td></td><td>GL</td><td>10:50</td><td>Yes</td></tr>
<tr><td>3.5</td><td>Inspect tank and system for signs of fatigue.</td><td></td><td>GL</td><td>10:50</td><td>Yes</td></tr>
<tr><td>3.6</td><td>Bring vessel and outer tank to 1.5x MEOP in 10 bar increments, holding at each interval of 10 bar for 2 minutes.</td><td><table><tr><th>Pressure</th><th>No Pressure Drop for 2 min</th></tr><tr><td>15</td><td>pass</td></tr><tr><td>25</td><td>pass</td></tr><tr><td>35</td><td>Pass</td></tr><tr><td>45</td><td>pass</td></tr><tr><td>55</td><td>pass</td></tr><tr><td>65</td><td>pass</td></tr><tr><td>75</td><td>pass</td></tr></table></td><td>GL</td><td>11:00
Start</td><td>Pass</td></tr>
<tr><td>3.7</td><td>Hold 1.5x MEOP for 15 minutes.</td><td>Less than 10% pressure drop seen.</td><td>GL</td><td>11:20</td><td>Pass</td></tr>
<tr><td>3.8</td><td>Depressurise system.</td><td></td><td>GL</td><td>11:37</td><td>Pass</td></tr>
<tr><td>3.9</td><td>Inspect tank and system for signs of fatigue.</td><td></td><td>GL</td><td>11:50</td><td>Pass</td></tr>
<tr><td>3.10</td><td>Bring inner coaxial tank to 1.5x MEOP in 10 bar increments, holding at each interval of 10 bar for 2 minutes.</td><td><table><tr><th>Pressure</th><th>No Pressure Drop for 2 min</th></tr><tr><td>15</td><td>Pass</td></tr><tr><td>25</td><td>Pass</td></tr><tr><td>35</td><td>Pass</td></tr><tr><td>45</td><td>Pass</td></tr><tr><td>55</td><td>Pass</td></tr><tr><td>65</td><td>Pass</td></tr><tr><td>75</td><td>Pass</td></tr></table></td><td>GL</td><td>11:55</td><td>Pass</td></tr>
<tr><td>3.11</td><td>Hold 1.5x MEOP for 15 minutes</td><td>Less than 10% pressure drop seen.</td><td>GL</td><td>12:26</td><td>Pass</td></tr>
<tr><td>3.12</td><td>Bring both inner and outer coaxial tank to 1.5x MEOP in 10 bar increments, holding at each interval of 10 bar for 2 minutes.</td><td><table><tr><th>Pressure</th><th>No Pressure Drop for 2 min</th></tr><tr><td>15</td><td>Pass</td></tr><tr><td>25</td><td>Pass</td></tr><tr><td>35</td><td>Pass</td></tr><tr><td>45</td><td>Pass</td></tr><tr><td>55</td><td>Pass</td></tr><tr><td>65</td><td>Pass</td></tr><tr><td>75</td><td>Pass</td></tr></table></td><td>GL</td><td>12:48</td><td>Pass</td></tr>
</table>

3.13	Hold 1.5x MEOP for 60 minutes.	Less than 10% pressure drop seen.	GL	13:05	Pass
3.14	Depressurise system.		GL	13:35	Pass
3.15	inspect tank and system for signs of fatigue.				Pass

1.2 3D CFD for Airbrake Controller

To enhance the data set used to tune the gains for the air brake controller, Computational Fluid Dynamics (CFD) simulations were used to quantify the drag at different deployment angles and speeds of the air brakes. These simulations were run using StarCCM+. Due to the air brakes lying out of plane with the direction of motion, a fully 3D simulation is necessary. The airbrakes are to be deployed at velocities up to 150 m/s which correspond to a maximum Mach number 0.5, as shown by fig []. However, after Mach 0.3 (which corresponds to a velocity of 100 m/s), compressibility becomes significant. For the purposes of these simulations only velocities up to 100 m/s were modelled.

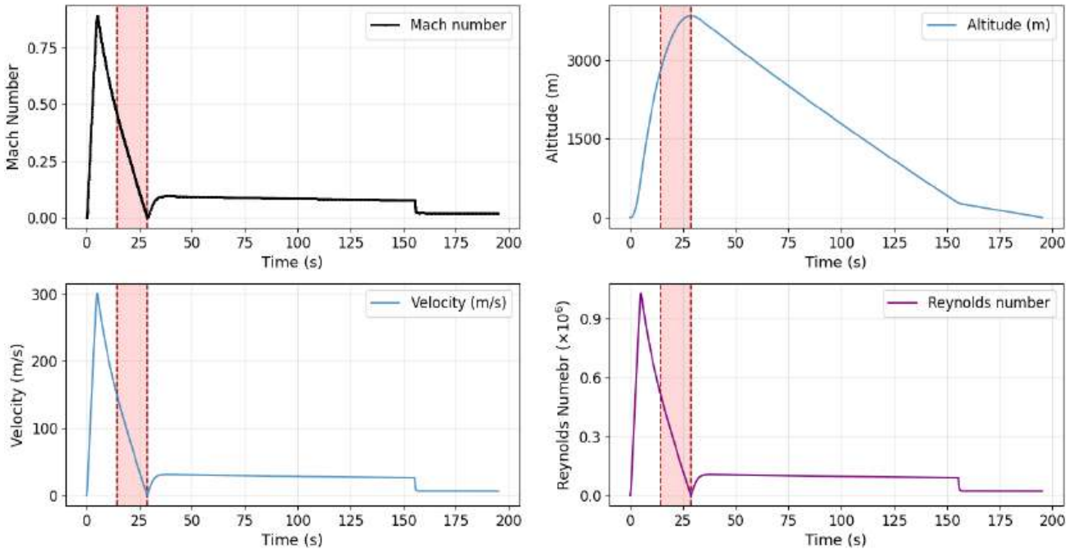

Figure 139: Graphs of Mach Number, Velocity, Altitude and Reynolds number.

Simulation Setup

Geometry and Domain

Autodesk Inventor was used to generate the CAD geometry, however certain simplifications needed to be made. Firstly, in the physical rocket there will be certain gaps or discontinuities between panels due to minor manufacturing defects. At high Reynolds numbers, these may cause disturbances in the boundary layer or cause recirculation. However, including these features are beyond the scope of an initial model and will aim to be included in after correlation studies with the wind tunnel model.

Also note that there is a gap between the petals and their housing as shown in figure. This gap may marginally change the results of the CFD however their of error is assumed insignificant compared to the absolute values of drag and therefore were not included in the simulation.

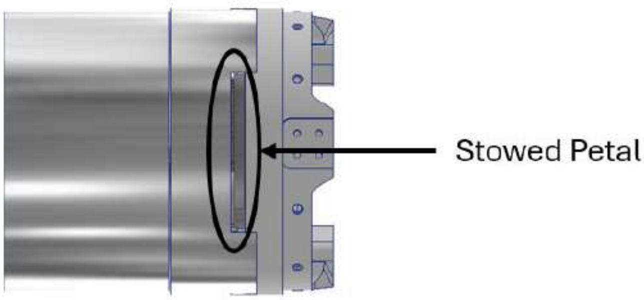

Figure: Side view of Airbrake showing gap between the petal and airbrake

Additionally, it is planned for the final rocket that tri-tangent tips will be added to the ends of each fin as they reduce the strength and concentration of vortices at the fin tips, which reduce drag. However, Autodesk Inventor does not have the capabilities of producing this geometry so instead they will be produced by hand. Therefore, the simulation may marginally overpredict drag due to the lack of this feature.

The exhaust hole at the bottom of the rocket was not included as the aim for these simulations was to create a simple physically correct model and an exit hole would introduce complex flow behaviour such as vortices and internal flow inside the exhaust hole. This feature will be added once the CFD is validated against wind tunnel data.

Finally, since carbon fibre will be the main material used on the rocket's surface, the CFD simulation modelled this surface as smooth. However, the fin tips are made of 3D printed PLA, which has a higher surface roughness than carbon fibre, thus it may increase the turbulence and therefore slightly increase the drag at the fin tip, despite it being tri-tangent.

Autodesk inventor was used to create the CAD file which was imported into Star CCM+. Since the petals in the airbrakes are out of phase with the fins, the rocket becomes asymmetrical when the airbrakes are deployed. Therefore, a symmetry plane simulation could not be used to save computational time, so the full geometry was simulated. To reduce computational expense, whilst gathering a sweep of all the different deployment angles, 5 geometries were exported from Autodesk Inventor, with different deployment angles as shown in figure [].

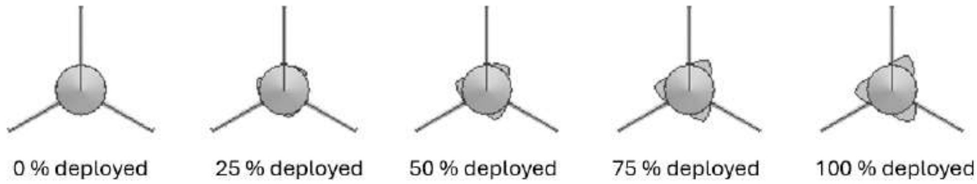

Figure: Front views of rocket at different deployment angles

Once the CAD geometries were imported into Star CCM+, the following cuboid domain shown in figure () was generated. Note that the unit "rocket radii" refers to the radius of the rocket from the fore-aft centreline of the rocket to the fin tip. This distance is 0.03m.

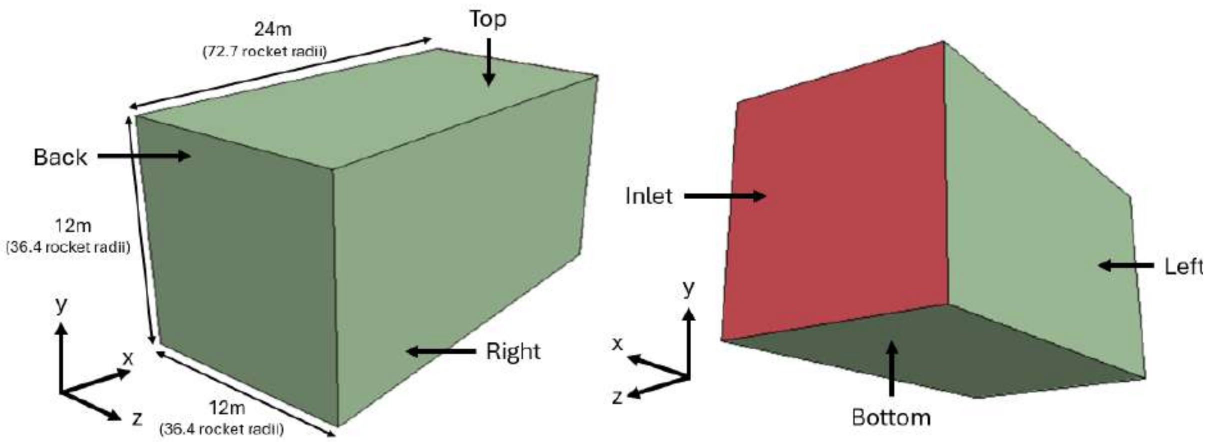

Figure: Domain with boundary labels, dimensions.

The distance between the base of the rocket was positioned at 48.5 Rocket Radii (16m) form the outlet as shown in figure ()

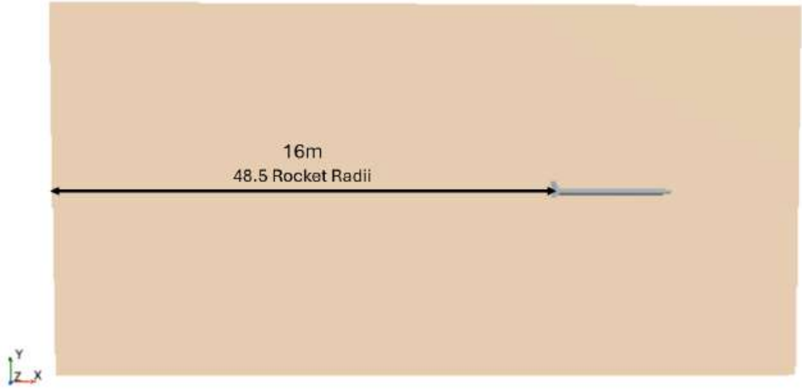

Figure: Position of rocket within the domain

The volume of each rocket was subtracted from the domain, leaving the exterior flow domain that was meshed.

Mesh

The mesh was generated automatically to save time in manually remeshing each CAD surface for the different deployment levels. A trimmed cell mesher was used to mesh the outer flow domain and was used alongside a prism layer mesher which more finely resolve the boundary layer and a surface remesher was used to more finely resolve the CAD surface.

This means an accurate resolution of near wall gradients is essential, since the velocity gradient directly controls the laminar viscous stress and, therefore, the dominant component of drag. A well-refined prism layer mesh provides sufficient resolution in the wall-normal direction to capture these the viscous sublayer, which is the part of the boundary layer in contact with the wall. This is also why the mesh needs to be more resolved at the nose cone as the simulation must capture the upstream laminar flow accurately, to provide a stable and accurate inputs to the developing turbulent boundary layer downstream.

The trimmed cell mesher generates a hex-dominant mesh with hexahedral cells in the outer flow domain and trimmed polyhedral cells near the rocket. The polyhedral cells are formed by clipping the corners and edges of hex cells to better conform to the underlying geometry, which in this case would be the prism layer subsurface. The core mesh in the outer flow domain is aligned orthogonally to the inlet velocity, thereby minimising numerical diffusion and improving accuracy for wall-bounded flows aligned with the freestream, such as the cylindrical section of a rocket. This setup allows for accurate resolution of turbulent boundary-layer growth while maintaining lower computational cost than a fully polyhedral mesh.

The prism layer mesher produces refined orthogonal prismatic cells, adjacent to the surface of the rocket, in order to capture the effects of the turbulent boundary layer. A high resolution of the turbulent boundary layer is required as it has a significant impact on the predicted drag coefficients. To generate the prism layer, a subsurface offset from the wall by the total prism-layer thickness is defined. This layer is the interface at which the core volume mesh begins and within the subsurface, the prism layer mesh will be generated.

Finally, the surface remesher is used to remesh the rocket surface, which aids the subsurface generator for the prism layer mesher. Most of the surface remeshing parameters have been kept the same as the trimmed cell mesher, however the parameters that have been changed are highlighted table []. Star CCM+ has the option to project the volume mesh vertices onto the CAD surface during the surface remesh step, which makes the surface mesh more accurate to the original CAD. However, this is very computationally expensive (an expected 300% increase in CPU time is expected) and the surface mesh already closely matches the CAD without this feature, so it wasn't done.

To determine appropriate prism layer meshing parameters, the maximum boundary layer length was estimated from the Prandtl–Schlichting empirical formula $\delta \approx 0.37xRe_x{}^{1/5}$. Here δ is the boundary layer thickness in meters, x is the distance along the plate and Re_x is the Reynolds number based on distance from the leading edge of the flat plate. Considering the highest free stream velocity of 100m/s and a kinematic viscosity of 1.460e-5 PaS, the maximum height of the boundary layer will be at the end of the simplified 2D flat plate (i.e. the length of the rocket). This gives a maximum boundary layer thickness of 47.2 mm in the regime. Therefore, the prism layer thickness of 250mm, defined in table (), is sufficient to capture the entire boundary layer height.

Table : Meshing Parameters

Trimmed Cell Mesher	
Meshing Parameter	Value
Base Size	4.0 m
Target Surface Size	6.25 % of Base Size
Minimum Surface Size	1.5625 % of Base Size
Surface Curvature	36.0 point/circle
Surface Proximity	2 points in gap,
Surface Growth Rate	1.3
Prism Layer Mesher	
Meshing Parameter	Value
Number of Prism Layers	16
Prism Layer Stretching	1.5
Prism Layer Total Thickness	0.1953125 % of Base Size
Maximum Cell Size	10000.0 % of Base Size
Volume Growth Rate	Default: 1 layer of each cell size for each transition
	Surface: 2 layer of each cell next to surfaces.
Custom Surface Controls	
Meshing Parameter	Value
Target Surface Size	0.1953125 % of Base Size
Minimum Surface Size	0.048828125 % of Base Size
Surface Curvature	200 points/circle
Surface Growth Rate	1.3
Number of Prism Layers	2
Prism Layer Total Thickness	0.1953125 % of Base Size

The mesh shown in figure () is a half section showing the 2D mesh refinement of the entire domain.

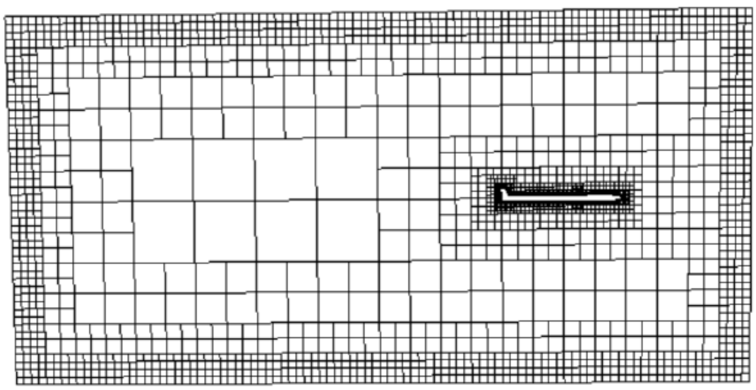

Figure: Half-section showing the mesh

Although the mesh is coarser in the region aft of the rocket, which may lead to poor wake refinement, the coarsening helps prevent pressure perturbations from reflecting off the boundary conditions and propagating back towards the rocket. Additionally, since the rocket is a streamlined body, the majority of the drag will come from skin friction as supposed to drag from pressure difference and flow separation. Therefore, it is more critical to resolve the region around the rocket than resolving the wake, which meant this precaution had to be taken so the flow around the rocket was undisturbed by the boundary conditions.

Figure [] shows the mesh refinement of the volume mesh key features of the geometry. This was achieved by refining the surface mesh of the rocket CAD, as supposed to refining the volume mesh around the fins and airbrakes. As the surface connects to the volume mesh, refining the entire surface mesh, will refine the volume mesh in the regions close to the rocket. The mesh is more refined at the leading edge of the fin and the nosecone. Since the largest pressure and velocity gradients will be present in these regions, it was important resolve them further.

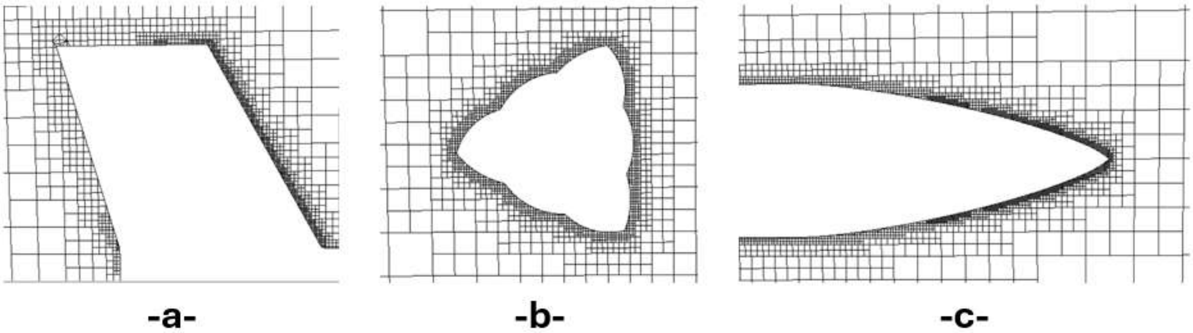

Figure: a) Mesh refinement of fin. b) Mesh refinement of airbrake. c) Mesh refinement of nosecone

In terms of the surface mesh figure [] shows the key features of the surface mesh in the 100% deployed configuration. As can be seen the surface mesh is sufficiently refined to capture the geometry at the tips of the airbrake petal and the nosecone. However, the mesh around the root of trailing edge introduced a sharp edge which does not smoothly blend with the base of the rocket. Additionally, the tip of the nosecone is slightly clipped from the bottom and the fin fillet at the root, is not entirely smooth. While these deviations from the true geometry are in significant regions, they are not large enough or frequent enough to invalidate the simulations.

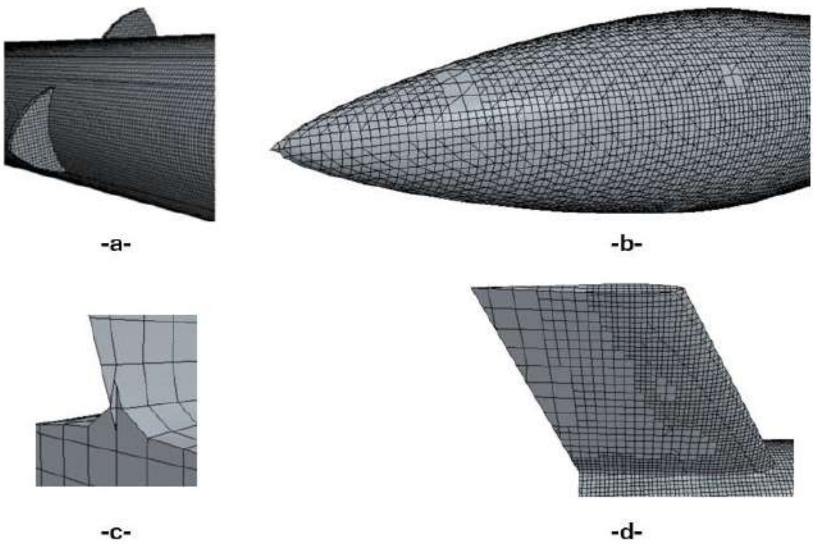

Figure: Surface mesh at a) airbrake, b) nosecone, c) fin trailing edge, d) fin.

Turbulence Model

The Reynolds Averaged Navier Stokes (RANS) model was used with a realisable 2-layer k-ε (RKE 2L) turbulence model to run the CFD simulation. This model was chosen for its abilities to model fully turbulent flows. The overall Reynolds number throughout the flight and during deployment is show in graph in figure (). While the maximum Reynolds number during airbrake deployment is below $6x10^5$ and the laminar to turbulent transition takes place at approximately $5x10^5$, the local Reynolds number will change along the length of the rocket. For example, figure () plots the local Reynolds number at 100m/s across the length of the Rocket if it was modelled at s 2D flat plate:

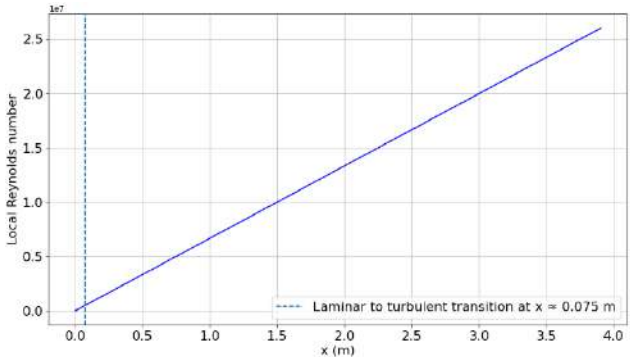

Figure: Plot showing predicted local Reynolds number along rocket length

This clearly shows the flow becomes turbulent very quickly along the length of the rocket and at high Reynold numbers on the order of $x10^7$, thereby justifying the use of the k-ε model. Additionally, the k-ε model is less computationally expensive than other turbulence models like k-ω and since several simulations need to be run, it was critical to minimise computational cost.

Another advantage of the RKE 2L model is that it can adapt to the dimensionless wall distance to the first cell centre, y^+. This allows the inner boundary layer to be modelled, regardless of the y^+ value. If $y^+ \leq 1$ a low wall function is used, which will model the viscous sublayer. The log-layer is resolved by simply solving the turbulence transport equations directly. If $y^+ \geq 30$ a high wall function is used, and a log-law is used to model the log layer of the inner boundary layer, ignoring the viscous sublayer. For intermediate values, $1 \geq y^+ \geq 30$, a blending function is used to smoothly transition between the two approaches, ensuring consistent treatment across the viscous sublayer, buffer layer, and log layer. Therefore, the mesh did not need to be specifically refined to match a particular y^+ value. As skin friction is the dominant contributor to drag for a streamlined body, this setup gives drag predictions that are comparatively insensitive to variations in y^+. This allows the same meshing parameters to be kept across all deployment angles and inlet velocities while maintaining repeatability.

The RKE 2L model solves the turbulent kinetic energy's, k, transport equation can be solved throughout the entire, however the transport equation for the turbulent dissipation rate ε cannot explicitly be solved close to a wall. Therefore, at the layer closest to the wall, the dissipation rate is approximated is approximated by equation ()

$$\varepsilon = \frac{k^{2/3}}{l_\varepsilon} \qquad ()$$

Where $l_\varepsilon$is is the length scale function which is given by equation (). Note that this equation was taken from the Star CCM+ documentation.

$$l_\varepsilon = 0.42C_\mu{}^{-0.75}d\left(1 - \exp\left(-\frac{Re_d}{0.84C_\mu{}^{-0.75}}\right)\right) \quad ()$$

where C_μ is a model coefficient, d is the distance from the wall and ν the kinematic viscosity and Re_d is the wall-distance Reynolds number, given by equation ().

$$Re_d = \frac{\sqrt{k}d}{\nu} \quad ()$$

The blending function then smoothly combines the turbulent viscosity μ_t obtained from the high-Re formulation with the two-layer Wolfstein formulation, ensuring a continuous and physically consistent prediction of near-wall turbulence quantities across all y^+ values.

Fluid Properties

As air is the fluid being simulated for the regime, it was modelled as an ideal gas. The material properties of the air are displayed in table [], and were the default settings in star CCM+, apart from the dynamic viscosity term.

Table : Material Properties

Parameter	Value
Dynamic Viscosity	1.7x10^-5 Pa.s
Molecular Weight	28.9664 kg/kmol
Specific Heat	1003.62 J/kg-K
Thermal Conductivity	0.0260305 W/m-K
Turbulent Prandtl Number	0.9

Initial Conditions

The initial conditions of the air given in table (). These conditions define the level of turbulence at each cell in the domain and were set to the default parameters given by Star CCM+.

Table : Initial Conditions

Parameter	Value
Pressure	0.0 Pa (Reference pressure: 101325.0 Pa)
Static Temperature	300.0 K
Turbulence Intensity, *I*	0.01
Turbulence Viscosity Scale, v	1 m/s
Turbulence Viscosity Ratio, $\left(\frac{\mu_t}{\mu}\right)$	10.0

The turbulence values define the initial k and ε values through equations ()

$$k = \frac{3}{2}(Iv)^2 \quad ()$$

$$\varepsilon = \left(\frac{\rho C_\mu k^2}{\left(\frac{\mu_t}{\mu}\right)\mu}\right) \quad ()$$

Where ρ is the density, C_μ is a model coefficient set at 0.09, μ is the dynamic viscosity and ρ (1.225 kg/m^3) is the density. This gives the initial k value as 0.00015 m^2/s^2 and ε as 0.000015 m^2/s^3

Boundary Conditions

The boundary conditions at each surface were carefully chosen to model the real conditions of the rocket during airbrake deployment whilst minimising computational cost.

Outlet boundary conditions were given to all faces of the domain, apart from the inlet boundary face, as the flow was assumed to be fully developed at the outlet faces, since they were far from the rocket. The field variables of static pressure and temperature at the outlet are computed by extrapolating from adjacent cells. However, the mass flow rate at the outlet face is calculated using a split ratio. This is done by first considering equation () for the velocity at the outlet boundary, $\boldsymbol{v}$.

$$\boldsymbol{v} = \boldsymbol{v}^{ext} + \frac{x_i}{\rho}\boldsymbol{n} \qquad ()$$

Here $\boldsymbol{v}^{ext}$ is the extrapolated velocity at the adjacent cell, ρ is the density at the boundary face and $\boldsymbol{n}$ is the normal vector to the outlet face. The boundary mass flux correction factor, x_i is calculated via equation ():

$$x_i = -\frac{f_{i,spec}}{\sum_{j=1}^{n\ outlets} f_{j,spec}} \frac{(\dot{m}_{in} - \dot{m}_{in,out}{}^{*})}{\sum_{outlet\ i\ faces}|\boldsymbol{a}|} \qquad ()$$

Where $f_{i,spec}$ is the split ratio which informs the solver what fraction of the total inlet mass flow rate should leave through a given outlet. For all outlet boundaries, $f_{i,spec}$ was set to 1, in order to minimise the risk of pressure perturbations from reflecting off the boundary conditions, which would cause recirculation and inaccurate flow behaviour. The total inlet and outlet mass flow rates $\dot{m}_{in}$ and $\dot{m}_{in,out}$ are defined by equations () and ():

$$\dot{m}_{in} = \sum_{non-outlet\ faces} \rho(\boldsymbol{v}\cdot\boldsymbol{a}) \qquad () \qquad \dot{m}_{in,out} = \sum_{outlet\ faces} \rho max(\boldsymbol{v}^{ext}\cdot\boldsymbol{a}, \boldsymbol{0}) \qquad ()$$

In terms of the wall boundary condition, it was defined as a smooth, adiabatic, no-slip wall. The inlet boundary conditions simply described the velocity the rocket would be travelling at and kept the same initial turbulence conditions.

Results

The simulation was run using a segregated flow solver which solves the pressure and momentum equations sequentially rather than simultaneously. As for the turbulence model the k and ε are also solved separately with an algebraic multigrid (AMG) linear solver. This is much more computationally efficient than a coupled solver which solves the pressure–momentum system as a single matrix. However the segregated solver it may need more iterations to converge, which is why, each simulation was run till 1000 iterations. This was sufficient allow the residual values of continuity, energy and momentum to drop between 10^{-7} and $10^{-10.}$

Star CCM+ calculates the drag coefficient by summing the pressure force $\boldsymbol{f}_f^{pressure}$ and shear force $\boldsymbol{f}_f^{shear}$ vectors over each cell of the surface mesh. Since the rocket is streamlined, the contribution from $\boldsymbol{f}_f^{shear}$, is much larger than that of $\boldsymbol{f}_f^{pressure}$, so accurate refinement of the boundary layer was necessary to obtain reliable results. The equations for the pressure and shear forces are given in equation () and ().

$$\boldsymbol{f}_f^{shear} = -\boldsymbol{T}_f\boldsymbol{a}_f \qquad () \qquad \boldsymbol{f}_f^{pressure} = (p_f - p_{ref})\boldsymbol{a}_f \qquad ()$$

Where $\boldsymbol{T_f}$ is the stress tensor at face f, $\boldsymbol{a_f}$ is the face area vector, p_f is the static pressure the face and p_{ref} is the reference pressure. The drag coefficient, C_D is then calculated using equation ().

$$C_D = \frac{\sum_f \left(\boldsymbol{f}_f^{shear} + \boldsymbol{f}_f^{pressure}\right) \cdot \boldsymbol{n}_{\mathrm{D}}}{\frac{1}{2}\left(\boldsymbol{\rho}_{ref} v_{ref} \boldsymbol{a}_{ref}\right)} \qquad ()$$

Where $\boldsymbol{n}_{\mathrm{D}}$ is the direction vector which is in the direction of drag and $\boldsymbol{\rho}_{ref}$, v_{ref} ,$\boldsymbol{a}_{ref}$ are the reference density, velocity, and area. The stress tensor, $\boldsymbol{T_f}$, which contributes to $\boldsymbol{f}_f^{shear}$ is a function of the laminar stress tensor and modelled turbulent shear stress tensor. In the RKE 2L turbulence model, the near wall stress tensor is resolved by damping the eddy viscosity contribution to zero at the wall. Therefore, the wall shear stress only depends on the molecular viscosity and the velocity gradient normal to the wall. As a 2-layer all y+ wall condition was applied, Star CCM+ will always adapt the wall function to determine the velocity gradient based on y+, so at no point along the rocket's surface there will be an inappropriate velocity gradient. This ensures the $\boldsymbol{f}_f^{shear}$ term is accurately calculated along the entire length of the rocket, leading to a more reliable C_D values.

The results of all simulations are presented in Figure (). They show the expected pattern of the drag coefficient increasing with both deployment angle and velocity and the effect the drag coefficient becoming more pronounced at higher deployment angles.

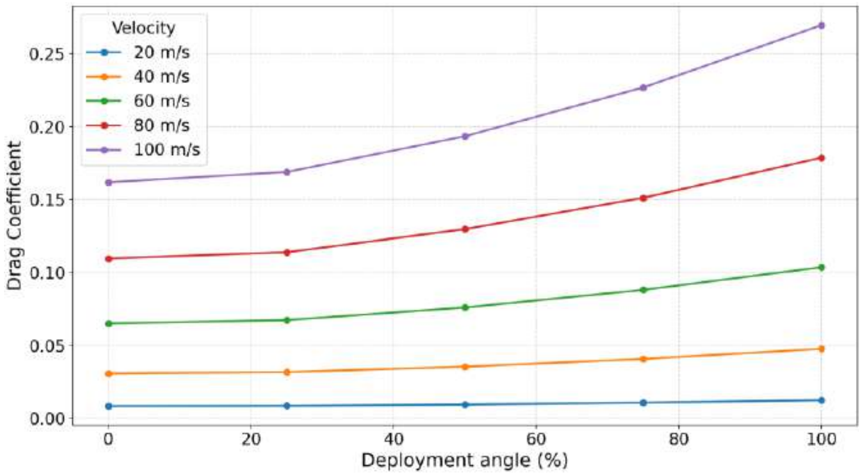

Figure: Results of drag coefficients at different deployment angles and velocities.

Other key findings include the y^+ value along the body of the rocket. For example, in the 80 m/s 100% deployed simulation the y^+ value was found to be predominantly around 10 as shown by figure:

Figure: y+ value along rocket length at 100% deployment at 80 m/s

This indicates that the prism layers were sufficiently refined such that the blending function was used to model the boundary layer, with certain regions around the airbrake and fins using the log-law wall treatment. While either wall treatment is sufficient to capture the boundary layer, it would be preferred to capture the viscous sublayer as it more closely matches the real flow.

In terms of the boundary layer, the simulation matches the predicted boundary layer height for the 100m/s, 0% deployed simulation, thereby validating the prism layer height, as illustrated by figure ().

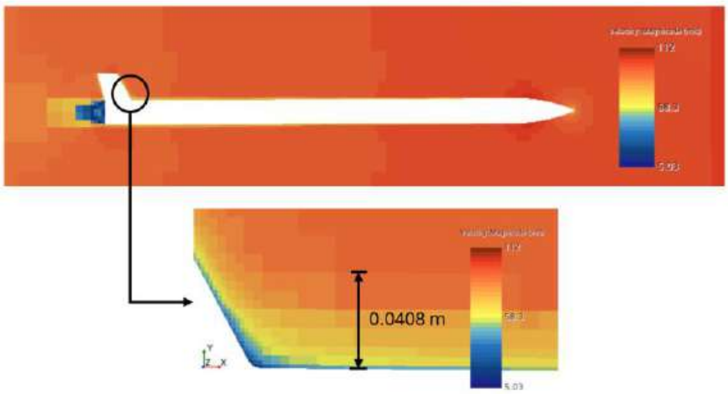

Figure: Boundary layer height at 100m/s & 0% deployed

The simulation also provided insight into key flow features that the rocket would experience during braking in the low Mach number regime. It was found that when the rocket is travelling at 80m/s at with fully deployed airbrakes two recirculation regions developed as shown in figure {}

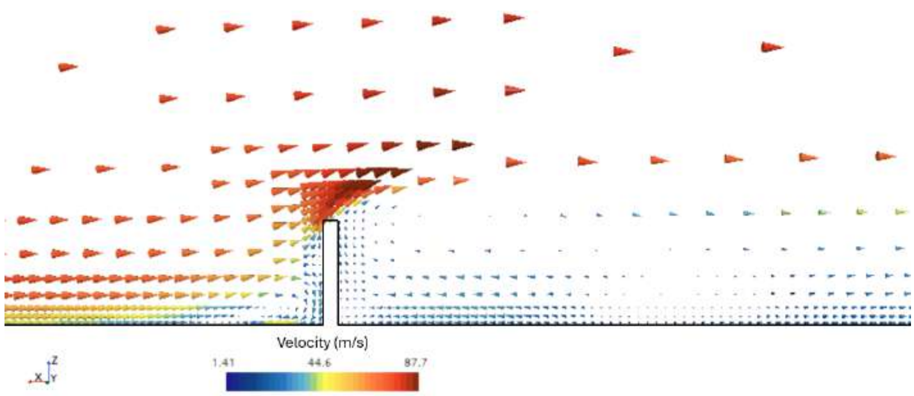

Figure: Velocity profile of 100% out 80m/s simulation at airbrake

However, beyond these recirculation regions, the flow attached quickly meaning there was no interference with the fins, which meant the flow remained attached as it passed the fins as illustrated by figure (). Note that the recirculation region in (a) will not be present in the real rocket due to the nozzle exit.

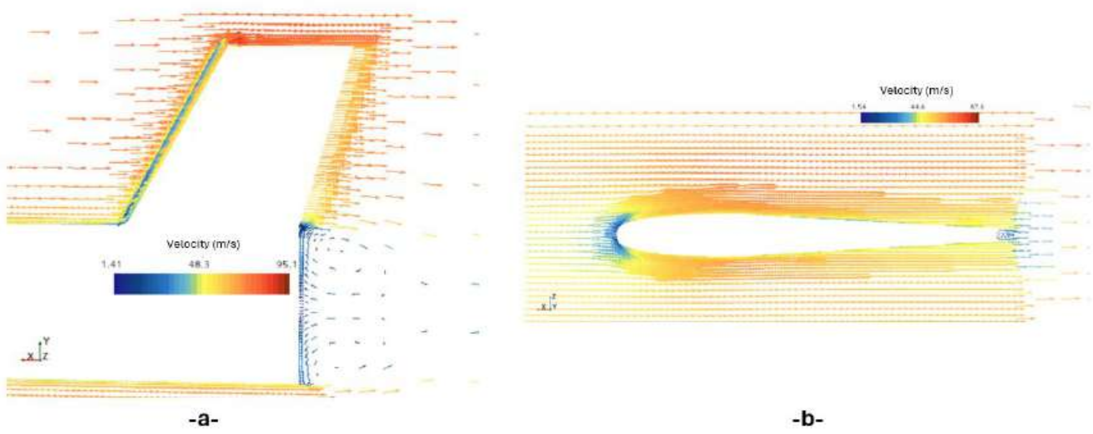

Figure: Velocity profile of 100% out 80m/s simulation at a) half-section showing fin b) 10cm above centreline showing aerofoil.

I.3 Selection Process for Fin Configuration

Table [] describes the requirements for the fin design, table [] is a pairwise comparison matrix which determines the importance of each requirement and table [] is a MCDA matrix which ultimately decides which fin configuration is to be used.

Table 37:Requirements table for fin.

Feature or requirement for comparison	Details about that requirement
Static Stability Across Flight	Keep CP behind CG with margin through subsonic to transonic.
Transonic Drag Rise Minimization	M≈0.8–1.0 brings wave/pressure-drag spike
Flutter & Aeroelastic Margin	Thin fins at high q risk bending–torsion flutter.
Structural Strength & Stiffness at q_max	Structural Strength & Stiffness at q_max
Roll Behaviour & Alignment Tolerance	Unwanted roll increases drag and stresses; desired spin must be predictable.
Manufacturability & Surface Quality	Transonic drag and flutter are very sensitive to surface finish

Table 38:Pairwise comparison matrix to obtain weightings for MCDA matrix

***Much* More Important**	***More* Important**	**The *Same***	***Less* Important**	***Much Less* Important**
9	3	1	0.33333333	0.111111111

#		Static Stability Across Flight	Transonic Drag Rise Minimization	Flutter & Aeroelastic Margin	Structural Strength & Stiffness at q_max	Roll Behaviour & Alignment Tolerance	Manufacturability & Surface Quality	Cost of Materials		
	X	1	2	3	4	5	6	7	Total	%
Static Stability Across Flight	1	X	3	1	1	3	3	9	20.00	25
Transonic Drag Rise Minimization	2	0.333333333	X	0.33333333	0.333333333	1	1	3	6.00	7
Flutter & Aeroelastic Margin	3	1	3	X	0.333333333	3	3	9	19.33	24
Structural Strength & Stiffness at q_max	4	1	3	3	X	3	3	9	22.00	27
Roll Behaviour & Alignment Tolerance	5	0.333333333	1	0.33333333	0.333333333	X	1	3	6.00	7
Manufactura bility & Surface Quality	6	0.333333333	1	0.33333333	0.333333333	1	X	3	6.00	7
Cost of Materials	7	0.111111111	0.333333333	0.11111111	0.111111111	0.33333333	0.333333333	X	1.33	2
Total		3.11	11.33	5.11	2.44	11.33	11.33	36.00	80.67	100
%		3.9	14.0	6.3	3.0	14.0	14.0	44.6	100	80.67

1.4 Aerodynamics & Airbrake controller validation

Down selection for Aerodynamic components

Table 439:Requirements table for fin.

Feature or requirement for comparison	Details about that requirement
Static Stability Across Flight	Keep CP behind CG with margin through subsonic to transonic.
Transonic Drag Rise Minimization	M≈0.8–1.0 brings wave/pressure-drag spike
Flutter & Aeroelastic Margin	Thin fins at high q risk bending–torsion flutter.
Structural Strength & Stiffness at q_max	Structural Strength & Stiffness at q_max
Roll Behaviour & Alignment Tolerance	Unwanted roll increases drag and stresses; desired spin must be predictable.
Manufacturability & Surface Quality	Transonic drag and flutter are very sensitive to surface finish

Table 540:Pairwise comparison matrix to obtain weightings for MCDA matrix

			***Much* More Important**	***More* Important**	**The *Same***	***Less* Important**	***Much Less* Important**			
			9	3	1	0.33333333	0.111111111			
#		**Static Stability Across Flight**	**Transonic Drag Rise Minimization**	**Flutter & Aeroelastic Margin**	**Structural Strength & Stiffness at q_max**	**Roll Behaviour & Alignment Tolerance**	**Manufacturability & Surface Quality**	**Cost of Materials**		
	X	**1**	**2**	**3**	**4**	**5**	**6**	**7**	Total	%
Static Stability Across Flight	**1**	**X**	3	1	1	3	3	9	20.00	25
Transonic Drag Rise Minimization	**2**	0.333333333	**X**	0.33333333	0.333333333	1	1	3	6.00	7
Flutter & Aeroelastic Margin	**3**	1	3	**X**	0.333333333	3	3	9	19.33	24
Structural Strength & Stiffness at q_max	**4**	1	3	3	**X**	3	3	9	22.00	27
Roll Behaviour & Alignment Tolerance	**5**	0.333333333	1	0.33333333	0.333333333	**X**	1	3	6.00	7
Manufacturability & Surface Quality	**6**	0.333333333	1	0.33333333	0.333333333	1	**X**	3	6.00	7
Cost of Materials	**7**	0.111111111	0.333333333	0.11111111	0.111111111	0.33333333	0.333333333	**X**	1.33	2
Total		3.11	11.33	5.11	2.44	11.33	11.33	36.00	80.67	100
%		3.9	14.0	6.3	3.0	14.0	14.0	44.6	100	80.67

Table 641: MCDA matrix used to select the design

	Weightings	**Low-AR Swept Trapezoid**		**Highly Swept Clipped Delta**		**Swept Trapezoidal**		**Cross-section upgrade: Biconvex**		**Elliptical Planform Fin**	
		score	**weighted score**	**score**	**weighted score**	**score**	**weighted score**	**score**	**weighted score**	**score**	**weighted score**
Static Stability Across Flight	0.250	4	1.0	4	1.0	5	1.3	4	1.0	4	1.0
Transonic Drag Rise Minimization	0.070	4	0.3	3	0.2	4	0.3	5	0.4	2	0.1
Flutter & Aeroelastic Margin	0.240	3	0.7	3	0.7	3	0.7	3	0.7	2	0.5
Structural Strength & Stiffness at q_max	0.270	3	0.8	3	0.8	3	0.8	3	0.8	2	0.5
Roll Behaviour & Alignment Tolerance	0.070	3	0.2	3	0.2	3	0.2	3	0.2	3	0.2
Manufacturability & Surface Quality	0.070	4	0.3	4	0.3	5	0.4	3	0.2	2	0.1
Cost of Materials	0.030	4	0.1	3	0.1	4	0.1	3	0.1	3	0.1
Total score for design →		**3.4**		**3.3**		**3.7**		**3.4**		**2.6**	

Considering these requirements, an MCDA matrix was used to select the fin type. Table 37. details the requirements that are to be met when selecting the fin.

Table 38 is a pairwise comparison matrix, which outlines the weightings for the MCDA selection matrix.

As can be seen, the Swept Trapezoidal fin was chosen due to its high stability across flight and transonic drag rise minimisation. Additionally, swept fins reduce the intensity of oblique shocks that may form at transonic speeds [ref].

J. Electronics Supporting Data

J.1 Avionics and Schematics

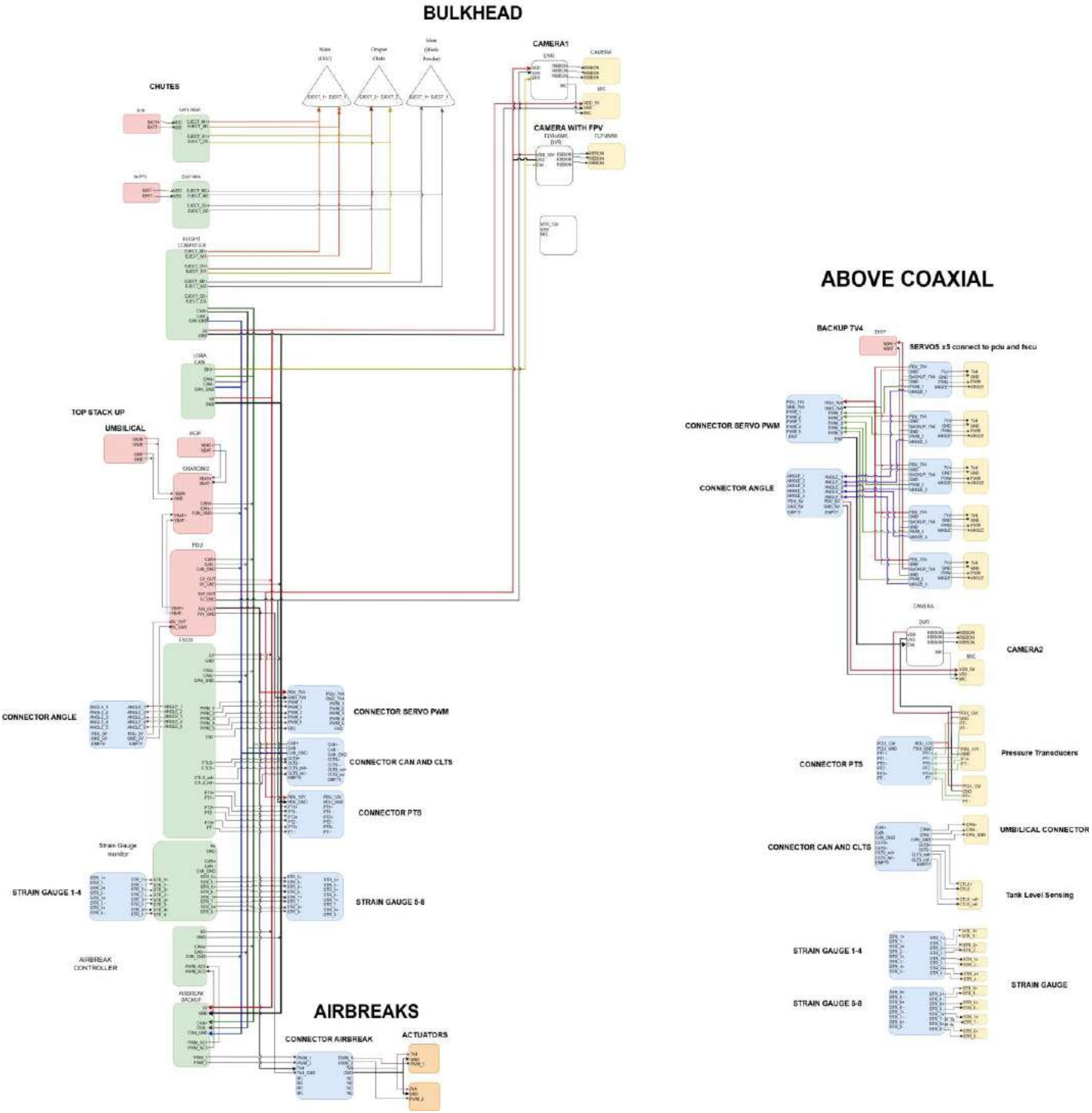

Figure 140:Top Stack Harness

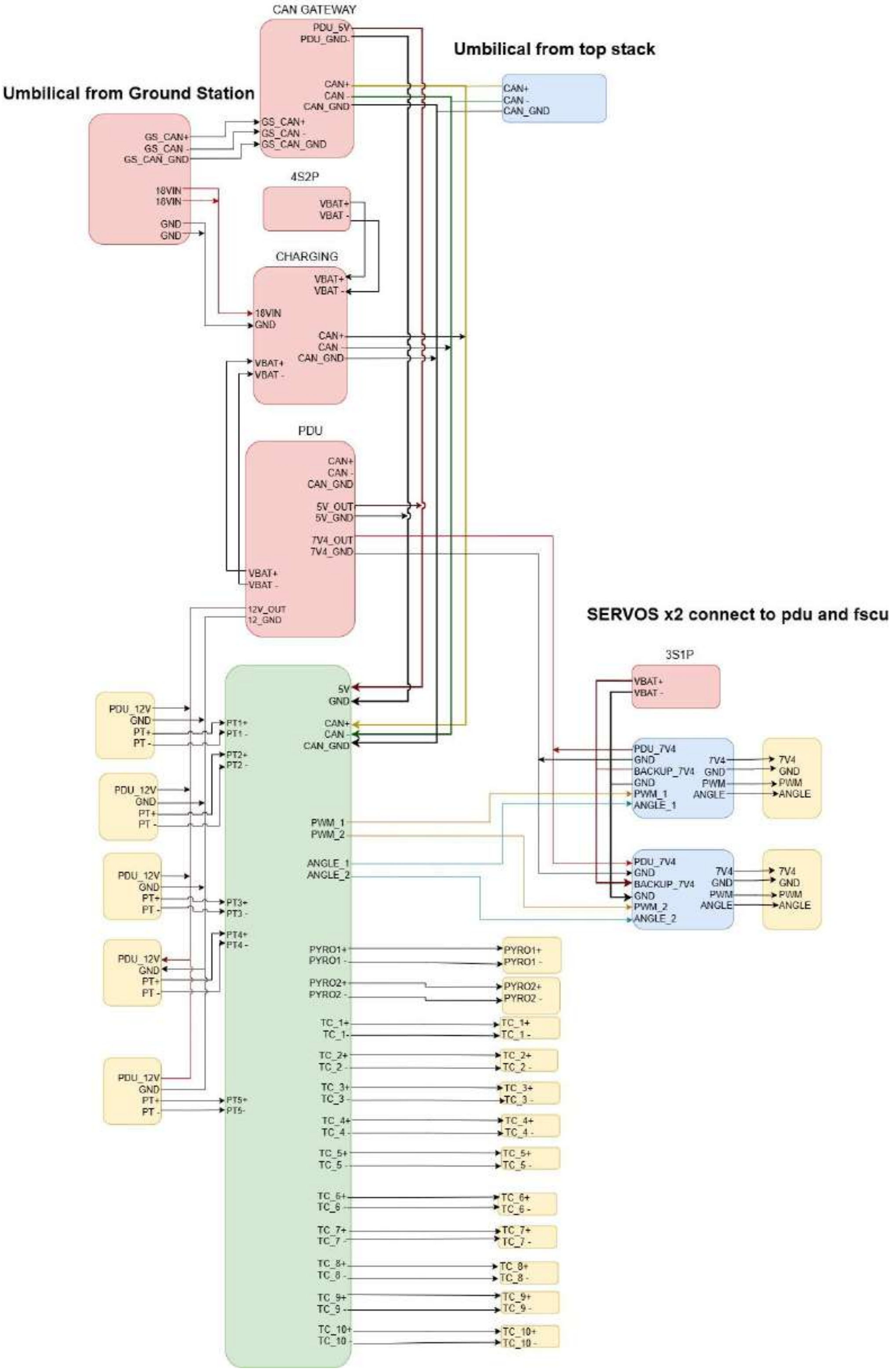

Figure 141: Aft Stack Harness

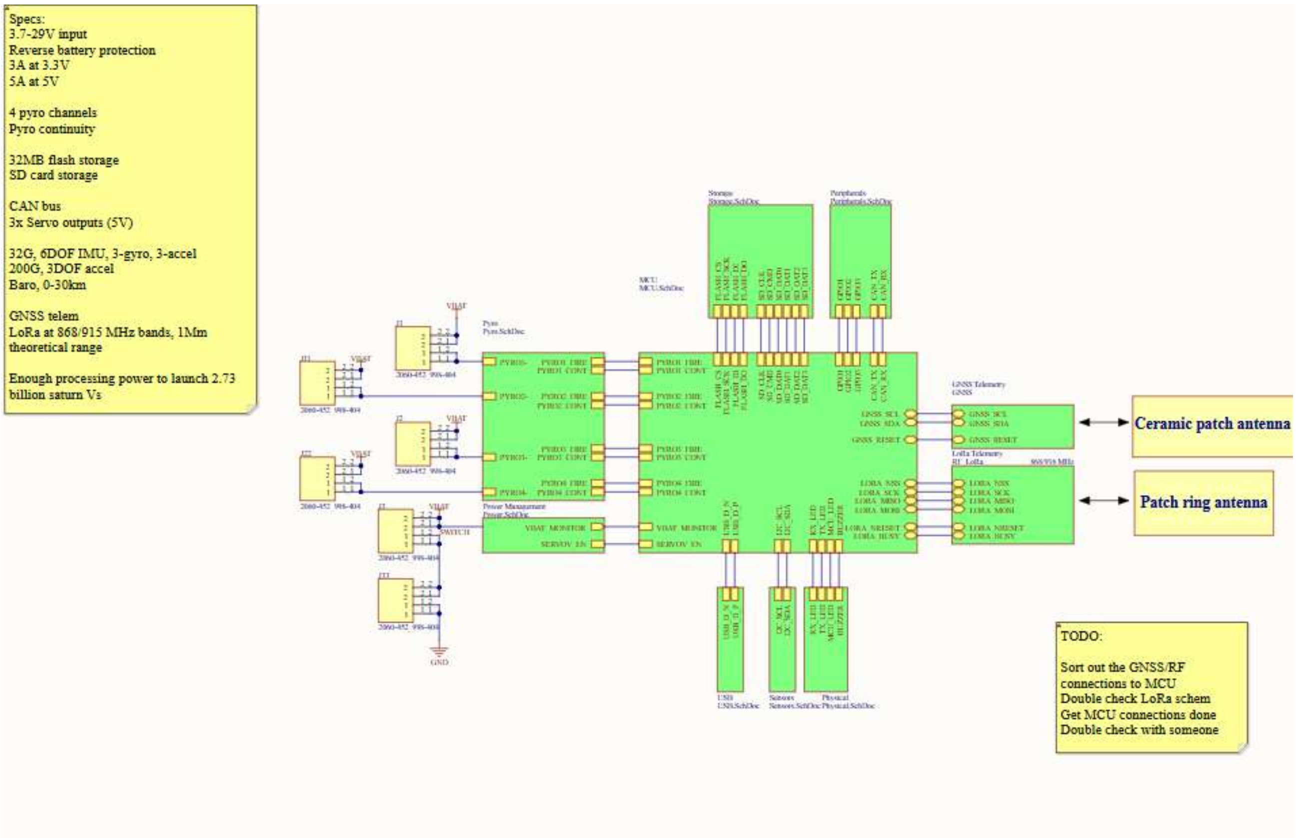

Figure: Flight Controller Schematic

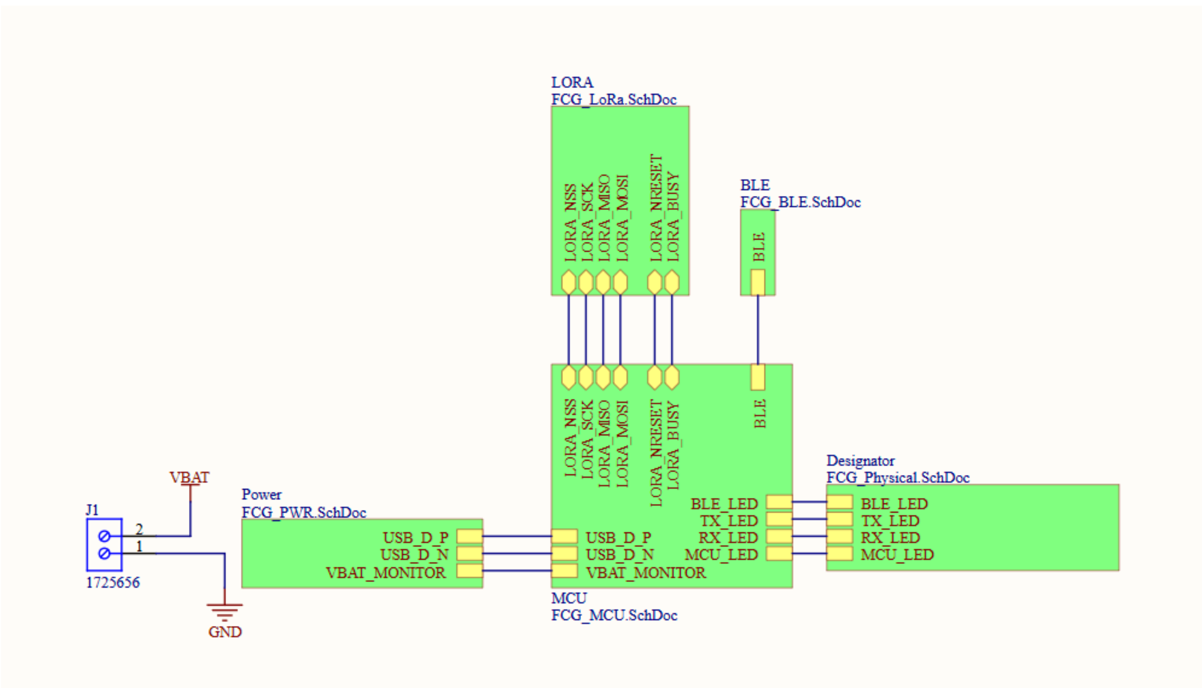

Figure 142: Ground Station Flight Controller

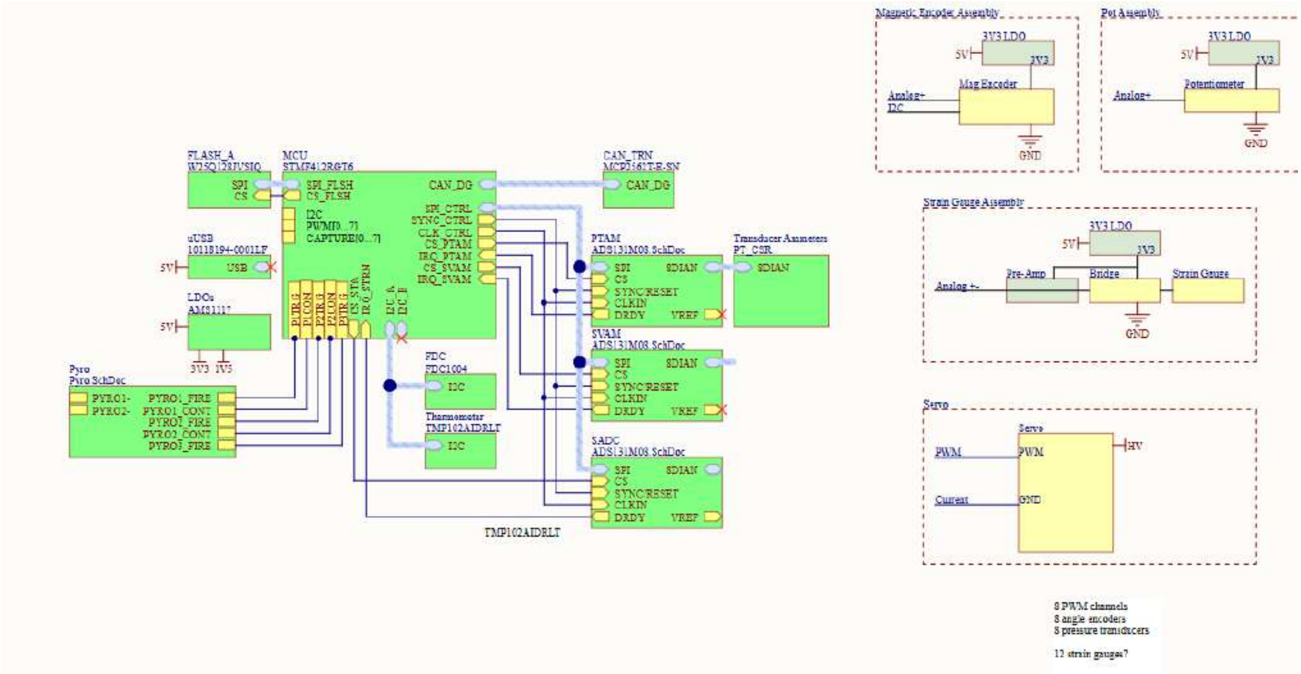

Figure 143: Feed Systems Control Unit Schematic

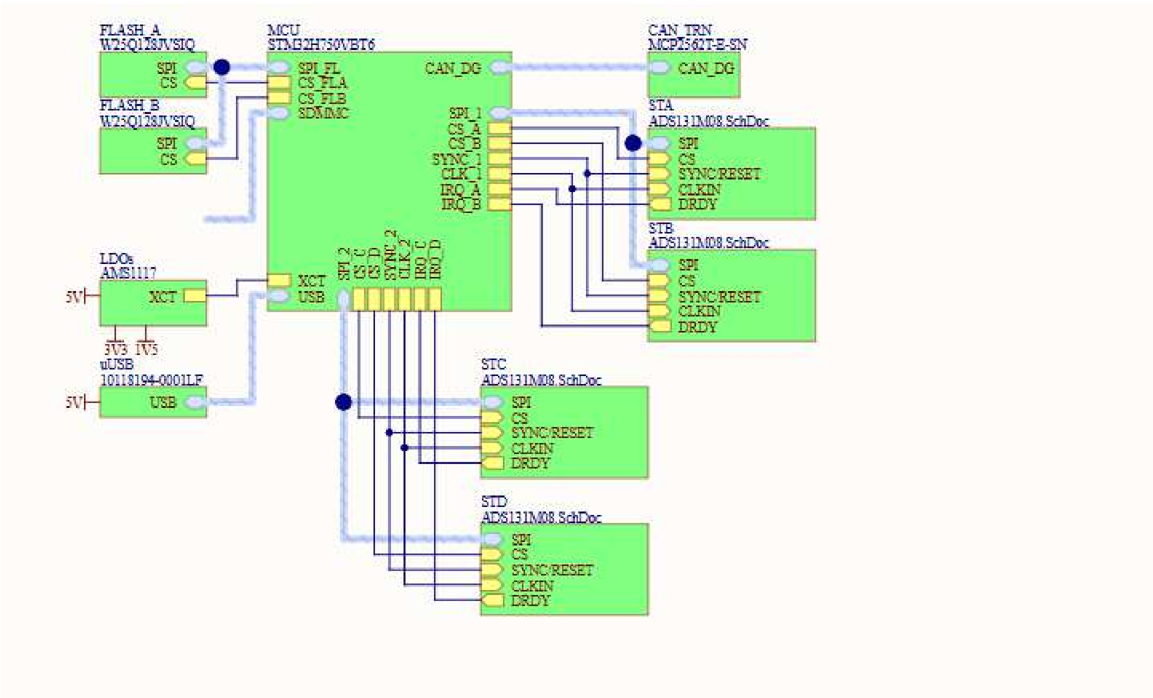

Figure 144: Strain Gauge Monitor Schematic

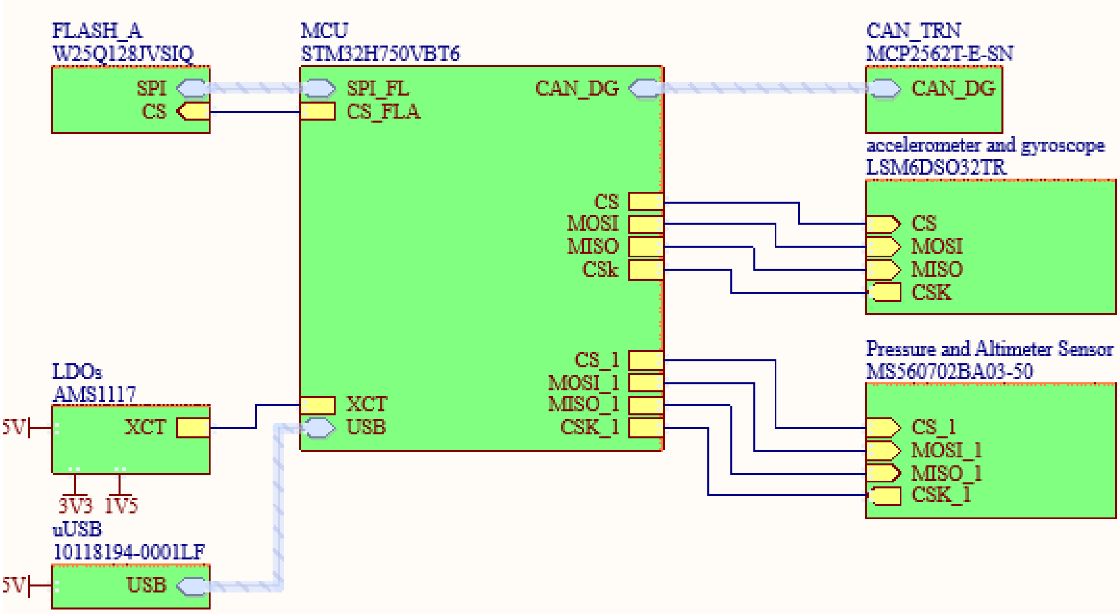

Figure 145: Airbrake Controller Schematic

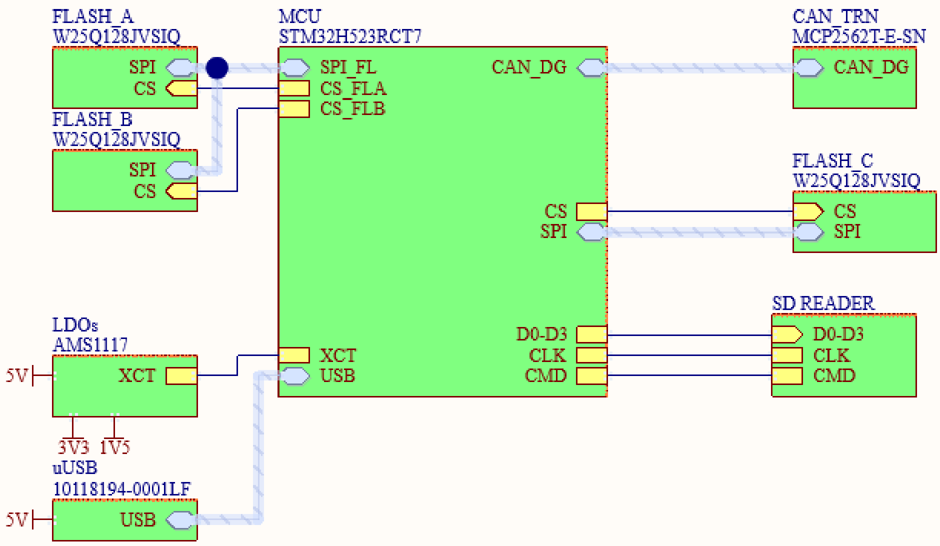

Figure 146: CAN Gateway Schematic

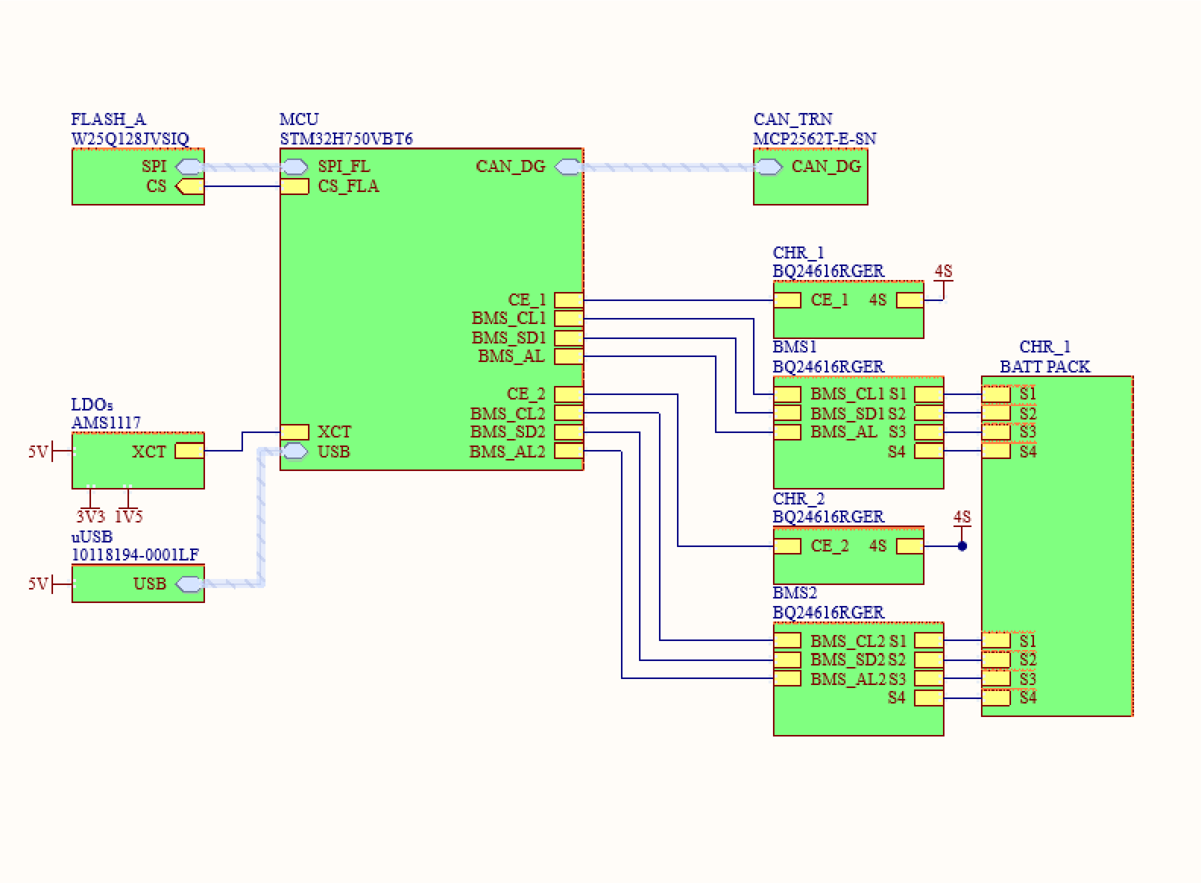

Figure 147: Charging Board Schematic

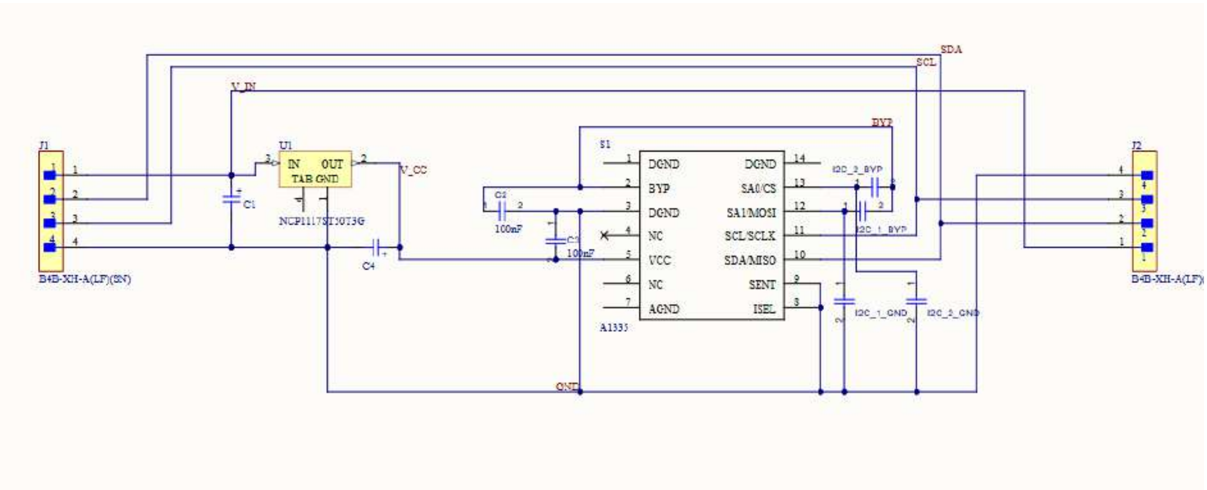

Figure 148: 3/4-inch Valve Angle Sensor

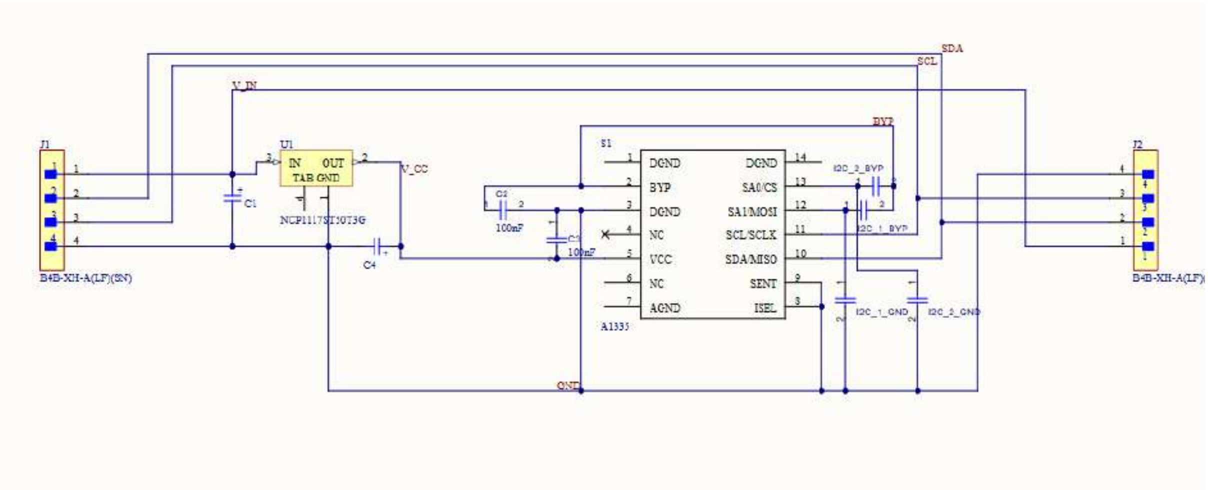

Figure 149: 1/2-inch Valve Angle Sensor

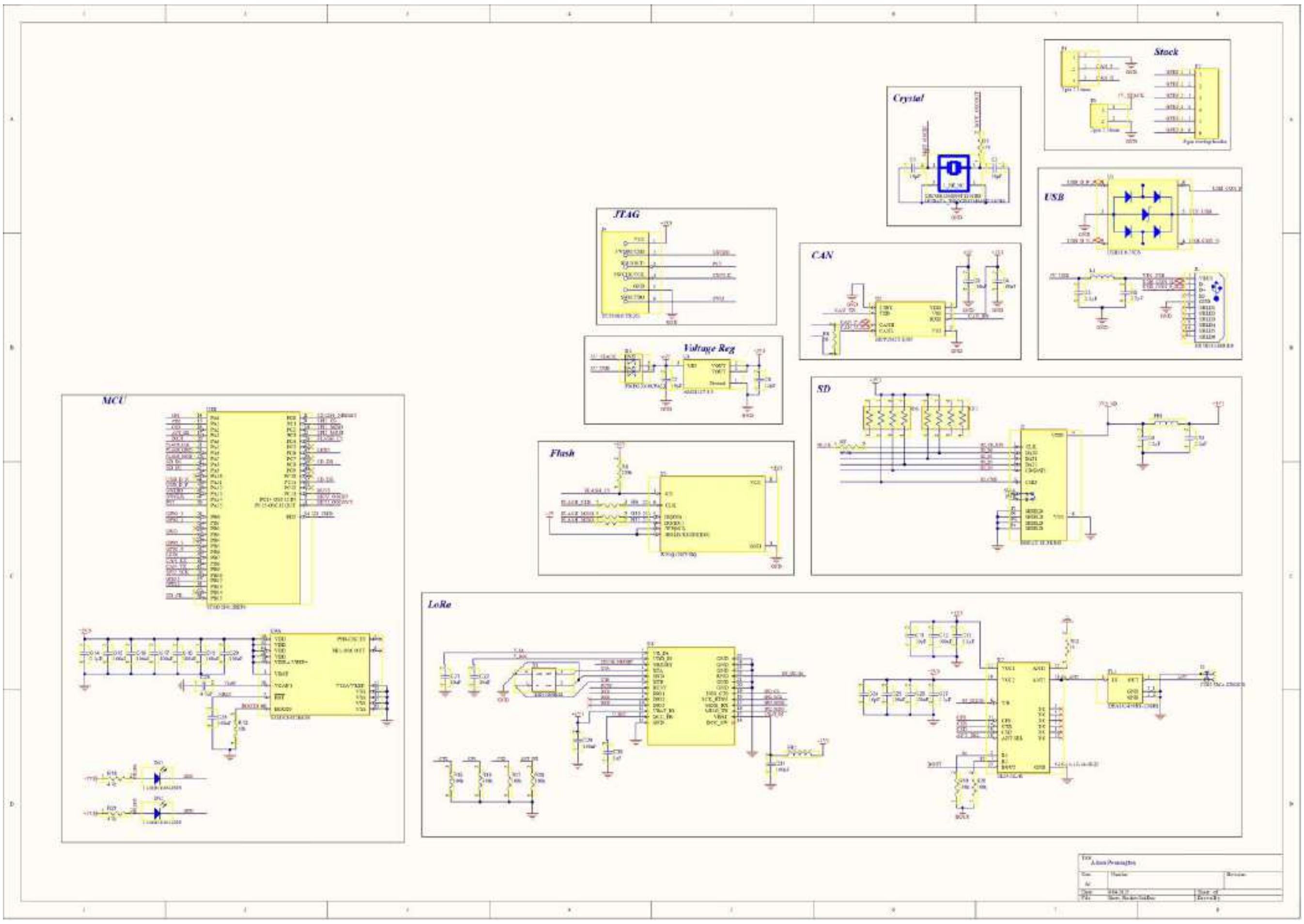

Figure 150: LoRa Board Schematic

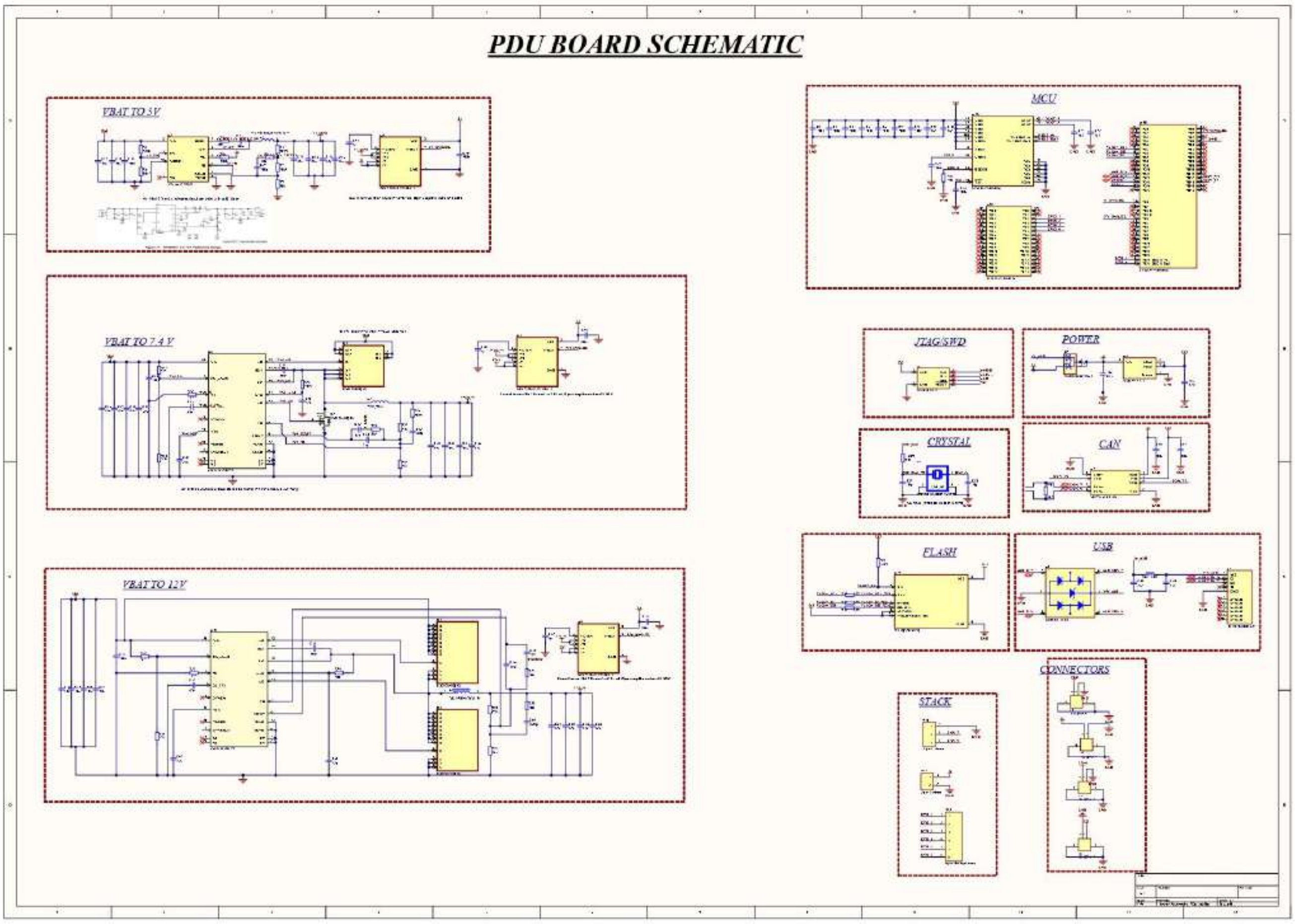

Figure 151: Power Distribution Unit Schematic

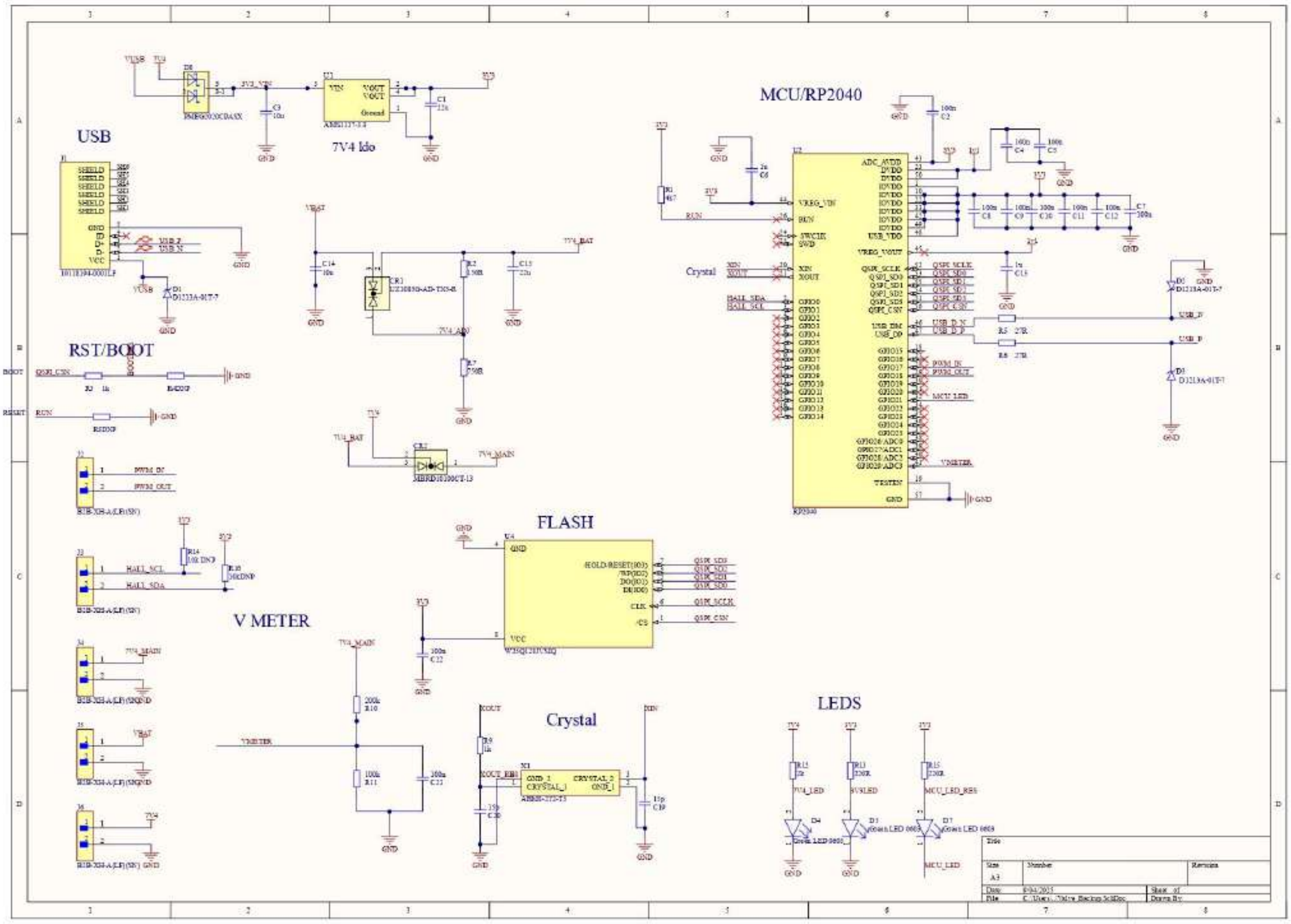

Figure 152: Valve Backup Board Schematic